Universidad de Córdoba

Departamento de Química Analítica

CONTRIBUCIONES DEL GRAFENO A LA NANOCIENCIA Y NANOTECNOLOGÍA ANALÍTICAS

Tesis Doctoral

Sandra Benítez Martínez

Córdoba, Febrero 2015

TITULO: *Contribuciones del grafeno a la Nanociencia y Nanotecnología analíticas*

AUTOR: *Sandra Benítez Martínez*

Campus de Rabanales
Ctra. Nacional IV, Km. 396 A
14071 Córdoba

www.uco.es/publicaciones
publicaciones@uco.es

CONTRIBUCIONES DEL GRAFENO A LA NANOCIENCIA Y NANOTECNOLOGÍA ANALÍTICAS

EL DIRECTOR,

Fdo. **Miguel Valcárcel Cases**
Catedrático del Departamento
de Química Analítica de la
Universidad de Córdoba

Trabajo presentado para aspirar al grado de Doctor en Ciencias

LA DOCTORANDA,

Fdo. **Sandra Benítez Martínez**
Licenciada en Ciencias Ambientales

Miguel Valcárcel Cases, Catedrático del Departamento de Química Analítica de la Universidad de Córdoba,

EN CALIDAD DE:

Director de la Tesis Doctoral presentada por la Licenciada en Ciencias

Ambientales SANDRA BENÍTEZ MARTÍNEZ, titulada "Contribuciones del Grafeno a la Nanociencia y Nanotecnología Analíticas",

CERTIFICA:

1) Que el trabajo experimental de la Tesis Doctoral ha sido desarrollado en los laboratorios del Departamento de Química Analítica de la Universidad de

Córdoba (España).

2) A mi juicio, reúne todos los requisitos exigidos a este tipo de trabajo.

3) Sandra Benítez Martínez es la primera autora de todos los trabajos científicos desarrollados durante la fase experimental de la Tesis. De acuerdo a la normativa de la Universidad y los acuerdos internos de nuestro grupo de investigación, el primer autor es el responsable por completo de la implementación del trabajo experimental y de la producción de la primera versión del artículo. Además, ella ha participado activamente en las reuniones con el director para comprobar y discutir el progreso del trabajo doctoral.

Córdoba, a 4 de febrero de 2015.

Fdo. **Miguel Valcárcel Cases**

TÍTULO DE LA TESIS: CONTRIBUCIONES DEL GRAFENO A LA NANOCIENCIA Y NANOTECNOLOGÍA ANALÍTICAS

DOCTORANDO/A: SANDRA BENÍTEZ MARTÍNEZ

INFORME RAZONADO DEL/DE LOS DIRECTOR/ES DE LA TESIS

La doctoranda Sandra Benítez Martínez cursó brillantemente los estudios de Máster en Química Fina Avanzada, obteniendo excelentes calificaciones en las materias del mismo. El trabajo Fin de Máster se publicó en la revista Electrophoresis, situada en el primer cuartil del área de conocimiento.

La temática de la tesis se encuadra en la línea de investigación "Nanociencia y Nanotecnología Analíticas" (NNA), que es puntera en el grupo FQM-215 de la Junta de Andalucía. La tesis está dedicada a las nanopartículas del grafeno y su familia. Teniendo en cuenta que esta familia fue descrita hace 10 años, la tesis supone una clara apuesta por las fronteras del conocimiento. Tiene el mérito adicional de que ningún miembro del grupo de investigación ha trabajado con el grafeno y derivados, siendo la doctoranda, por tanto, la que ha abierto camino en una temática de gran repercusión futura.

En la tesis se han abordado las dos líneas clásicas de la NNA, es decir, la consideración de las nanopartículas como herramientas analíticas y como analitos. Además, incluye un enfoque avanzado, que es considerado como la "tercera vía" de potencial impacto en el futuro, como es la búsqueda de sinergias cuando se combinan en un mismo proceso analítico las nanopartículas, tanto como herramientas como analitos.

La realización de la investigación recogida en esta Memoria ha permitido a la doctoranda adquirir una sólida formación científica adiestrándose en el manejo de una amplia serie de tecnologías analíticas, así como en la gestión de una gran variedad de problemáticas analíticas nanotecnológicas. La Memoria ha dado lugar a la publicación de 7 artículos (4 de los cuales enviados a publicar), así como a la presentación de 7 comunicaciones científicas en congresos nacionales e internacionales.

Por todo ello, considero que la investigación desarrollada y recogida fielmente en esta Memoria reúne todos los requisitos necesarios en cuanto a originalidad, innovación y calidad y autorizo, pues, la presentación de la Tesis Doctoral de Sandra Benítez Martínez.

Por todo ello, se autoriza la presentación de la tesis doctoral.

Córdoba, 4 de febrero de 2015

Fdo.: Miguel Valcárcel Cases

Agradezco a la Junta de Andalucía la concesión de una beca de excelencia para la Formación de Personal Investigador (FPI) que ha hecho posible mi dedicación a este trabajo durante los últimos cuatro años

ÍNDICE

ACRÓNIMOS

ADN	Ácido desoxirribonucleico
AFM	Microscopia de fuerza atómica
AINEs	Aintiinflamatorios no esteroideos
ATP	Adenosin trifosfato
AuNPs	Nanopartículas de oro
CDs	Carbon dots
CG	Cromatografía de gases
CL	Quimioluminiscencia
CM	Mecanismo químico
CMC	Concentración micelar crítica
CNPs	Nanopartículas de carbono
CNTs	Nanotubos de carbono
CVD	Deposición química en fase vapor
DCC	N,N-diciclohexilcarbodiimida
DMF	N,N-Dimetilformamida
DWCNT	Nanotubos de carbono de pared doble
EDC	l-etil-3-(3-dimetilaminopropil)-carbodiimida
EM	Mecanismo electromagnético
EOF	Flujo electrosmótico
EVOO	Aceite de oliva virgen extra

FDA	Administración de Medicamentos y Alimentos / Food and Drug Administration, U.S.
FL	Fluorescencia
FRET	Transferencia de energía por resonancia de Föster
GAE	Equivalentes al ácido gálico
Gly	Glicina
Gly–GQDs	Puntos cuánticos de grafeno funcionalizados con glicina
GNP	Nanoplaquetas de grafeno
GNRs	Nanocintas de grafeno
GO	Óxido de grafeno
GQDs	Puntos cuánticos de grafeno
HATU	2-(7-aza-1H-benzotriazol-1-il)-1,1,3,3-tetrametiluronio hexafluorofosfato
HPLC	Cromatografía líquida de alta resolución
HRTEM	Microscopía de transmisión electrónica de alta resolución
IARC	Agencia Internacional de Investigación contra el Cáncer
LLE	Extracción líquido–líquido
LOO	Aceite de oliva lampante
MWCNT	Nanotubos de carbono de pared múltiple
N&NA	Nanociencia y Nanotecnología Analíticas
NMP	N-metil-2-pirrolidona

NPs	Nanopartículas
P3HT	Poli(3-hexiltiofeno)
PAHs	Hidrocarburos aromáticos policíclicos
PL	Fotoluminiscencia
PSS	Poli(sodio 4-estirenosulfonato
QDs	puntos cuánticos
QY	Rendimiento cuántico
rGO	Óxido de grafeno reducido
SAX	Intercambio aniónico fuerte
SC	Colato sódico
SDBS	Dodecilsulfonato sódico
SERS	Espectroscopia Raman amplificada por superficies
SPE	Extracción en fase solida
SPME	Microextracción en fase solida
SWCNT	Nanotubos de carbono de pared simple
TEM	Microscopia electrónica de transmisión
THF	Tetrahidrofurano
TiO_2NPs	Nanopartículas de óxido de titanio
VOO	Aceite de oliva virgen

OBJETO

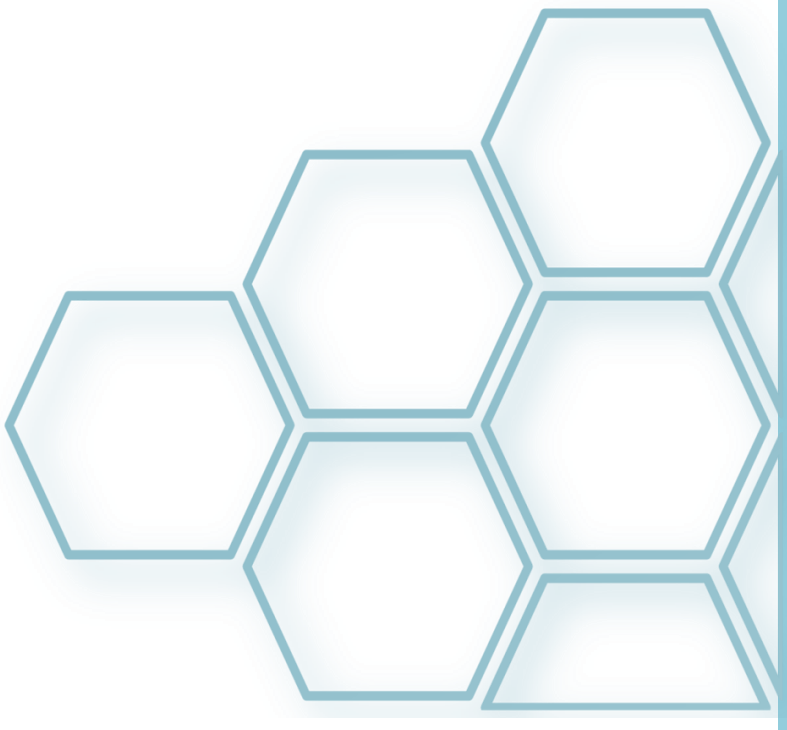

Hace solo poco más de diez años (2004) que se pudo sintetizar el grafeno en el contexto de las nanoestructuras de carbono. Es pues un nuevo material del siglo XXI. En esta década, el crecimiento de artículos científicos relacionados con la síntesis del grafeno en sí y de sus derivados ha crecido manera espectacular, por las extraordinarias propiedades físicas y químicas de los mismos así como por su amplísima variedad de aplicaciones científico-técnicas todas ellas de gran relevancia. Este crecimiento atípico ha demostrado que actualmente se trata una de las nanoestructuras de carbono más prometedoras. Incluso ha generado la aparición de empresas basadas exclusivamente en la obtención de grafeno y sus derivados. La Química Analítica no ha sido ajena a este *trending topic* y el número de artículos con fines analíticos también ha crecido exponencialmente.

En la línea de investigación *Nanociencia y Nanotecnologías Analíticas* del Grupo FQM-215 de la Junta de Andalucía al que pertenece la doctoranda, las nanoestructuras de carbono (ej. fulerenos, nanotubos de carbono, nanodiamantes, carbon dots, etc.) han sido unas de las primeras nanopartículas que se han explotado desde dos facetas distintas, es decir, como herramientas para el desarrollo de nuevas metodologías y el enriquecimiento y mejora de procesos ya establecidos, y considerándolas objetos de análisis.

En el inicio de esta Tesis Doctoral, nos propusimos iniciar por primera vez el estudio y aplicación del grafeno con una o varias láminas tanto como herramienta en procesos analíticos como analito en sí. En el trascurso de la misma han surgido dos temáticas que han ampliado el enfoque inicial:

- La importancia y la aplicabilidad de sus derivados simples como el óxido de grafeno y los puntos cuánticos del mismo (*Graphene Quantum Dots*) así como derivados más complejos como los puntos cuánticos de grafeno funcionalizados con glicina, han propiciado su incorporación al enfoque inicial.
- La consideración sistemática de la "tercera vía" de la Nanociencia y Nanotecnología Analíticas. Se trata de la involucración simultanea de nanopartículas como herramientas y analitos en el mismo proceso analítico. Con ello se buscan efectos sinérgicos al explotar simultáneamente las extraordinarias propiedades físico-químicas de ambas nanopartículas.

Para diseñar y optimizar los procesos analíticos correspondientes se han empleado, por una parte, una amplia variedad de técnicas analíticas instrumentales, tales como la electroforesis capilar, la espectroscopia Raman(SERS), la espectroscopia de fluorescencia molecular, además de las técnicas microscópicas de caracterización tales como, HRTEM y SEM. Por otra

parte se han utilizado técnicas previas de tratamiento de muestra clásicas como la extracción liquido-liquido y sólido-líquido (cartuchos y membranas).

Estos procesos analíticos optimizados sistemáticamente se han empleado para la determinación de analitos en una amplia variedad de muestras (ej. ambientales, agroalimentarias, cosméticas) para determinar una amplia variedad de analitos como antiinflamatorios, antibióticos, polifenoles, óxido de grafeno, nanopartículas de titanio y GQDs. Los resultados obtenidos han permitido validar las metodologías propuestas.

BLOQUE I

Introducción

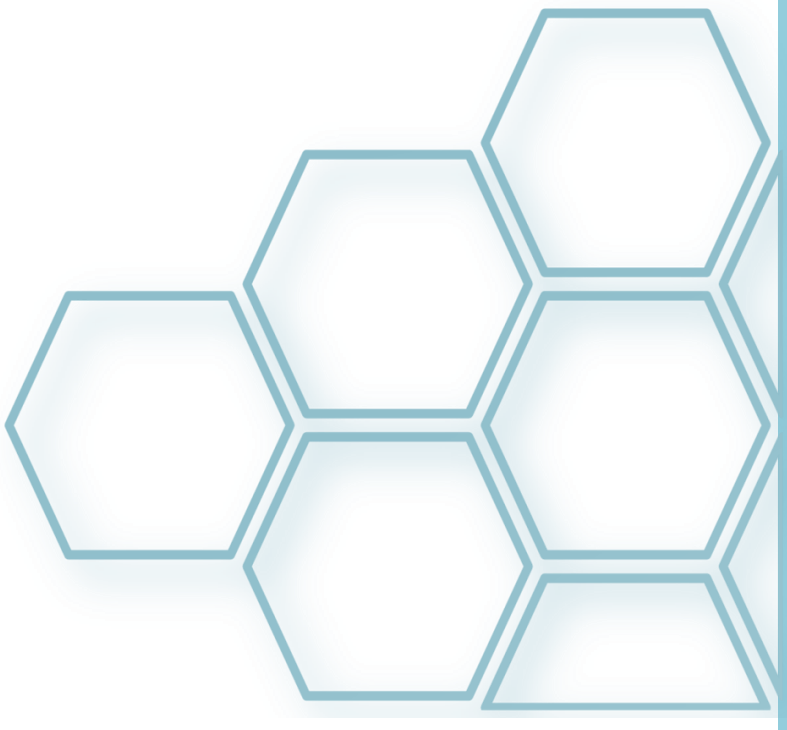

I.1. NANOMATERIALES DE CARBONO

La aparición, en los últimos años, de numerosos tipos de los nanomateriales ha supuesto un gran avance científico y tecnológico que ha permitido el desarrollo exponencial de lo que se conoce como **Nanotecnología**. Esta puede definirse como la ciencia que "aborda el diseño, caracterización y el uso de estructuras, dispositivos y sistemas, cuya forma y tamaño son controlados en la nanoescala[1]".

Ligada a ella podemos definir la **Nanociencia** como la "ciencia de la síntesis, el análisis y la manipulación de materiales a escala atómica o molecular nivel, donde las características o propiedades físicas o químicas son sustancialmente diferentes a los mostrados por el mismo material a una escala mayor (micro o macro)"

La Nanociencia y Nanotecnología se caracterizan por centrarse en el estudio de objetos de reducidas dimensiones, comprendidos entre 1 y 100 nm, dimensiones entre las cuales se define la nanoescala.

[1] M. Valcárcel. Las nanoestructuras de carbono en la Nanociencia y nanotecnología analíticas. Discurso de recepción como académico de número de la Real Academia de Ciencias (2010)

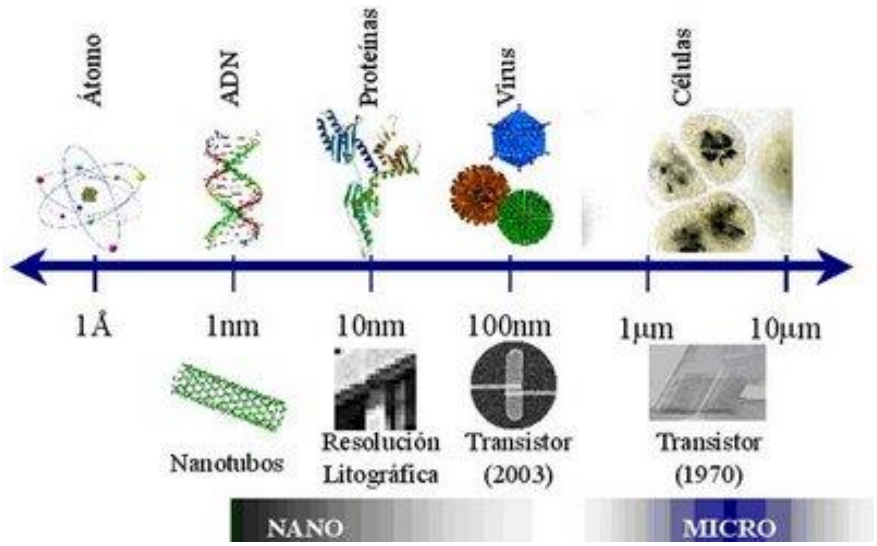

Figura I.1.1. *Unidades de medida de diversos sistemas y escala en la que se incluyen.*

Ambas poseen un carácter multidisciplinar que se expande hacia otras áreas de conocimiento como la física, la química, la biotecnología y la ingeniería, pudiendo converger en ellas.

En el contexto de la Química Analítica, pueden definirse dos facetas clave de la Nanociencia y Nanotecnología. Por una parte, la consideración de los materiales nanoestructurados como herramienta para la creación de nuevos métodos analíticos o mejora e innovación de procesos, métodos o técnicas bien establecidos previamente, faceta que ha alcanzado mayor grado de desarrollo hasta el momento. Por otra parte, la consideración de las

nanopartículas y nanoestructuras como objeto de análisis, con el fin de extraer información físico–química de calidad, para lo cual se hacen necesarios métodos analíticos capaces de detectar y cuantificar estos nanomateriales presentes, a nivel de trazas, en muestras de naturaleza variada y complejidad diversa, como son matrices ambientales y biológicas. Sin embargo, esta rama de la Nanociencia y Nanotecnología Analíticas (N&NA) se encuentra actualmente en su fase de desarrollo más temprana, existiendo escasas metodologías que permitan una determinación sensible, rápida y fiable de estas nanoestructuras. Como consecuencia del crecimiento exponencial de la producción de nanopartículas y la incorporación de éstas en la industria, así como su utilización en productos comerciales, como cosméticos, cremas solares y productos alimenticios, la liberación y acumulación de éstas en el medio ambiente es cada vez un hecho más probable, con los consiguientes posibles efectos sobre la salud humana y de los ecosistemas acuáticos y terrestres, haciéndose cada vez más necesario el desarrollo de esta faceta.

Los materiales nanoestructurados son aquellos cuyas dimensiones caen en el rango de los nanómetros. Pueden definirse como "nanoestructuras ultra finas que poseen un tamaño medio de grano o fase del orden de los nanómetros (10^{-9}m)". Atendiendo a un significado más amplio del término, "cualquier material que contenga granos o clústeres de tamaño inferior a 100nm, capas o filamentos de esa dimensión puede ser considerado

nanoestructurado"[2]. Pueden ser clasificados en función de su naturaleza y propiedades, pero lo más usual es encontrarlos clasificados en función de sus dimensiones. Según este último criterio, las nanoestructuras pueden ser clasificadas de dos formas distintas. La Real Academia de Ingeniería[3] (Royal Academy of Engineering) clasifica los materiales nanoestructurados en tres tipos de estructuras fundamentales, en función del número de dimensiones de dichos materiales que se encuentran comprendidas dentro de la nanoescala. De este modo podemos encontrar (i) nanomateriales de una dimensión (1D) como láminas de espesor nanométrico, (ii) nanoestructuras bidimensionales (2D) como los nanoalambres y los nanotubos, (iii) tridimensionales (3D) como nanopartículas metálicas y sus óxidos. Sin embargo, otros autores[4] han realizado una clasificación de las nanoestructuras en función de las dimensiones que exceden los 100 nm, siendo categorizadas en: (0D) materiales con dimensiones cero, si todas sus dimensiones están comprendidas en la nanoescala, como nanopartículas metálicas y puntos cuánticos (QDs). (1D) nanoestructuras con una dimensión micro o macrométrica, como nanoalambres y nanotubos. (2D) aquellos que tienen dos dimensiones por debajo de 100 nm y una tercera excede los límites de la nanoescala, como monocapas y capas finas. (3D) materiales cuyas

[2] H.S. Nalwa, Hanbook of Nanostrucutred Materials and Nanotechnology: concise edition. Gulf Professional Publishing, 2001.
[3] http://www.raeng.org.uk/publications/reports/nanoscience-and-nanotechnologies-opportunities (acceso el 16/01/2015)
[4] V.V. Pokropivny, V.V. Skorokhod, Materials Science and Engineering C 27 (2007) 990–993.

dimensiones quedan todas por encima de la nanoescala, pero se trata de un material formado por un set de nanopartículas comprimidas que forman un micro o macro bloque. Estas son materiales nanoporosos y pulverizados.

Las nanopartículas de carbono (CNPs), entre las que se encuentran los fulerenos (0D), nanotubos de carbono (1D), el grafito (3D) y el grafeno (2D), son muy empleadas en la Química Analítica actual debido a las excepcionales propiedades físicas, químicas, magnéticas, térmicas, electrónicas y ópticas que exhiben, como consecuencia de su nanotamaño.

La historia de las nanoestructuras de carbono comenzó en 1985 cuando el fulereno fue descubierto por Kroto[5]. Los fulerenos son moléculas de carbono que presentan una estructura en forma de icosaedro truncado, que contiene anillos pentagonales y hexagonales. Entre ellos pueden encontrarse una amplia gama de isómeros y homólogos, siendo los más estudiados el fulereno C60 (Figura I.1.2a) y el C70. Los fulerenos poseen superficie hidrófoba y una relación superficie/volumen elevada.

Desde entonces, varias nanoestructuras de carbono han sido descubiertas. Ejemplo de ello son los nanotubos (CNTs), descubiertos por Ijima[6] en 1991, momento desde el cual han recibido una especial atención. Se trata de nanoestructuras de carbono en las que los átomos se unen

[5] H.W. Kroto, J.H. Heath, S.C. OBrian, R.F. Carl, R.E. Smalley, Nature 318 (1985) 162-163.
[6] S. Iijima, Nature 354 (1991) 56-58.

covalentemente formando anillos hexagonales, que a su vez forman una estructura tubular abierta y hueca que puede estar compuesta por una sola capa (nanotubos de pared simple o SWCNT, Figura I.1.2f), dos capas (nanotubos de pared doble o DWCNT) o más capas (nanotubos de carbono multicapa o MWCNT, Figura I.1.2b) dispuestas de forma concéntrica a la capa mas externa. En teoría, cada capa puede ser considerada una lámina de grafeno enrollada. Los CNTs son considerados nanomateriales a pesar de que, en la mayoría de los casos, solamente su diámetro cae dentro de la nanoescala pues suelen ser estructuras tubulares muy largas. Al igual que los fulerenos, poseen carácter hidrófobo que los hacen insolubles en agua facilitando su agregación.

Los nanoconos de carbono, descritos por primera vez en 1994 por Ge y Sattler[7] se definen como una hoja de grafeno enrollada con un ápice cónico definido por la presencia de uno a cinco anillos pentagonales, que a su vez condicionan el ángulo del nanocono. Resultan ser una estructura abierta por un extremo y cerrada por el extremo opuesto (Figura I.1.2g).

En 1999, Ijima[8] descubrió una estructura tubular abierta, de pared única similar a los SWCNT pero con un diámetro superior (2-5 nm) y una longitud de 50 nm. La diferencia estructural más notable es su punta en forma

[7] M. Ge, K. Sattler, Chem. Phys. Lett. 220 (1994)192-196.
[8] S. Iijima, M. Yudasaka, R. Yamada, S. Bandow, K. Suenaga, F. Kokai, K.Takahashi, Chem. Phys. Lett. 309 (1999) 165-170.

de cuerno, que resulta de la presencia de cinco de pentágonos en la hoja de grafeno, lo cual, evidentemente, también afecta a sus propiedades. Estas nanopartículas se conocen con el nombre de nanocuernos (Figura I.1.2c).

El grafeno fue aislado por primera vez en 2004 por Geim y Novoselov[9] a partir de la exfoliación micromecánica de grafito, empleando cinta Scotch. Se trata de una estructura abierta, bidimensional y plana de un átomo de espesor en la que los átomos de carbono, que presentan hibridación sp^2, se organizan en una red de hexágonos en forma de panal de abeja (Figura I.1.2h). El grafeno ha suscitado gran interés desde su aparición debido a su gran área superficial y a sus propiedades únicas. Debido a que esta nanopartícula es el objeto central de esta Tesis Doctoral, sus propiedades y características serán detalladas más extensamente en los siguientes apartados de esta Introducción.

Otros ejemplos de nanopartículas 0D son los nanodiamantes[10] y los puntos de carbono o *carbon dots* (CDs). Los nanodiamantes (Figura I.1.2e) son nanopartículas de carbono que presentan una estructura de octaedro truncado con un diámetro de 2 a 8 nm. Están compuestos en un 98% por carbono, y el 2% restante está constituido por hidrógeno, oxígeno y nitrógeno

[9] K. S. Novoselov, A.K. Geim, S.V. Morozov, D. Jiang, Y. Zhang, S. V. Dubonos, I. V. Grigorieva,A. A. Firsov, Science 306 (2004) 666–669.
[10] R. A. Shimkunas, E. Robinson, R. Lam, S. Lu, X. Xu, X.-Q. Zhang, H. Huang, E. Osawa, D. Ho, Biomaterials 30 (2009) 5720–5728.

residuales. Poseen un núcleo con hibridación sp^3 y carbono amorfo en su superficie.

Los puntos de carbono o CDs son nanopartículas luminiscentes cuasi esféricas con tamaños por debajo de los 10 nm y presentan también carbono amorfo en su composición.

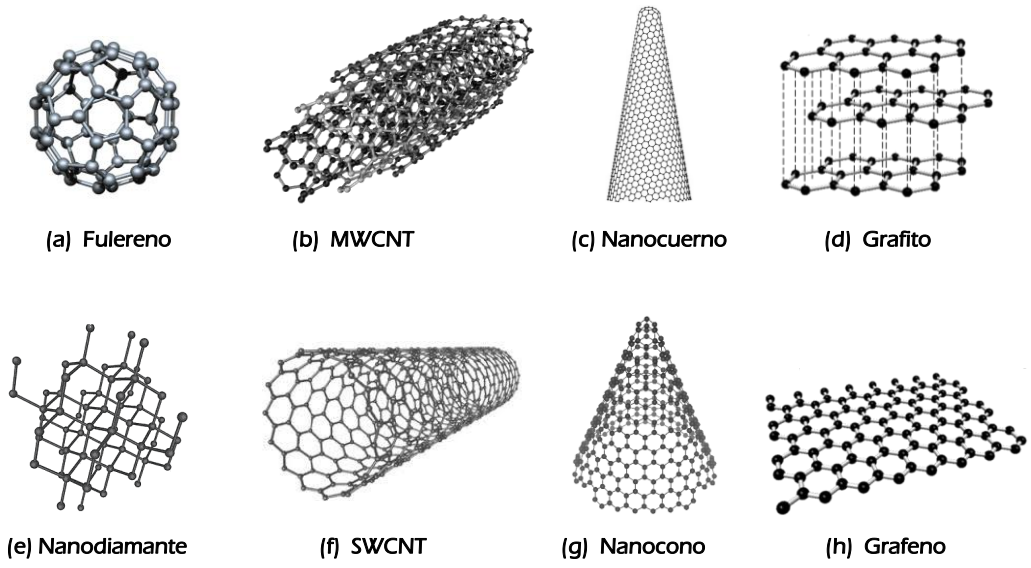

Figura I.1.2. Representación de las principales nanoestructuras de carbono.

Las excepcionales propiedades que presentan todas las nanoestructuras de carbono mencionadas anteriormente han propiciado el interés de la comunidad científica por explotarlas

Las nanopartículas de carbono han sido muy bien aceptadas en el campo de la Química Analítica. Su empleo se ha centrado tradicionalmente en el desarrollo de nuevas metodologías para la determinación de analitos de interés en muestras complejas[11], pudiendo ser empleadas en las distintas etapas del proceso analítico (tratamiento de muestra, separación instrumental y detección). El estudio de estas nanopartículas como analito diana está poco desarrollado, como bien comentábamos anteriormente, existiendo una clara falta de metodologías analíticas que permitan extraer y preconcentrar nanopartículas de carbono de muestras reales. La tendencia futura de la Química Analítica está encaminada a la implementación de esta faceta.

[11] M. Valcárcel, B.M. Simonet, S. Cárdenas, Anal. Bioanal. Chem. 391 (2008) 1881-1887.

I.2. EL GRAFENO, CARACTERIZACIÓN Y PROPIEDADES

Durante muchos años el grafeno ha sido considerado un mero concepto usado para la aproximación descriptiva de otras formas complejas de carbono aromático.

Muy pocos investigadores consideraron al grafeno como especie de interés per se hasta 2004[6]. Sin embargo, la observación directa de monocapas de grafeno aisladas provocó un gran aumento del interés por este nanomaterial y solo unos pocos años fueron necesarios para que la comunidad científica investigara las propiedades de este nuevo material bidimensional. La evolución en los últimos diez años en cuanto al número de publicaciones científicas bajo el tópico "grafeno", en buscadores científicos como Scopus o Scifinder, describe una clara tendencia exponencial que indica que se ha abierto un nuevo campo en la Nanociencia y Nanotecnología de los nanomateriales bidimensionales.

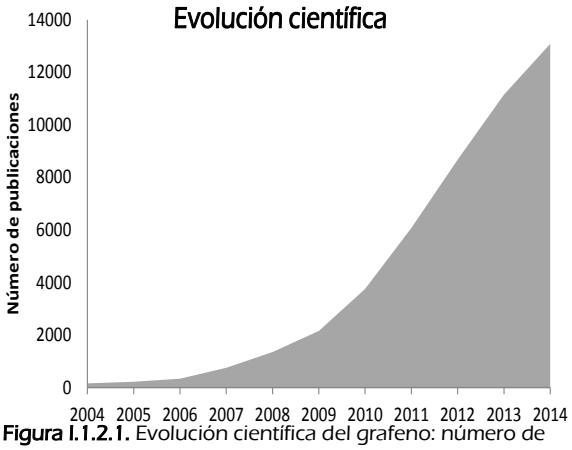

Figura I.1.2.1. Evolución científica del grafeno: número de publicaciones por año.

I.2.1. El grafeno

El grafeno está compuesto por átomos de carbono con hibridación sp^2 organizados en una red en forma de panal de abeja[12], como se muestra en la Figura I.2.1. Puede poseer una, dos, o varias capas, pero no más de 10[13].

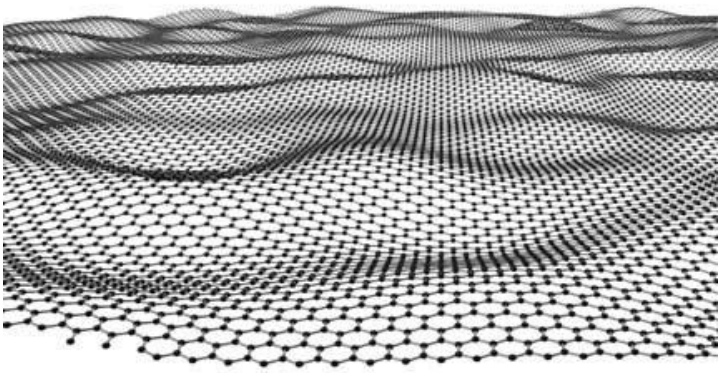

Figura I.2.1. Estructura ideal de grafeno.

La red puede considerarse como dos subredes triangulares interpenetradas, en la que el átomo de una subred es el centro de los triángulos definidos por la otra subred con una longitud entre los enlaces de carbono, C–C, de 1.42 Å. La celda unidad comprende dos átomos de carbono y no varía si se produce una rotación de 120º alrededor de algún átomo.

[12] C. Soldano, A. Mahmood, E. Dujardin, Carbon 48 (2010) 2127–2150.
[13] S. Guo, Chem. Soc. Rev 40 (2011) 2644–2672.

Cada átomo tiene un orbital *s* y dos orbitales *p* en el mismo plano, contribuyendo a la estabilidad mecánica de la lámina de carbono. El orbital *p* restante está orientado perpendicularmente hacia el plano molecular e hibrida para formar las bandas π*(conducción –en color claro) y π (valencia – en color oscuro), las cuales determinan el fenómeno de conducción.

En el régimen de baja energía, estas dos bandas se encuentran la una a la otra produciendo valles en forma cónica, como se muestra en la Figura I.2.2.

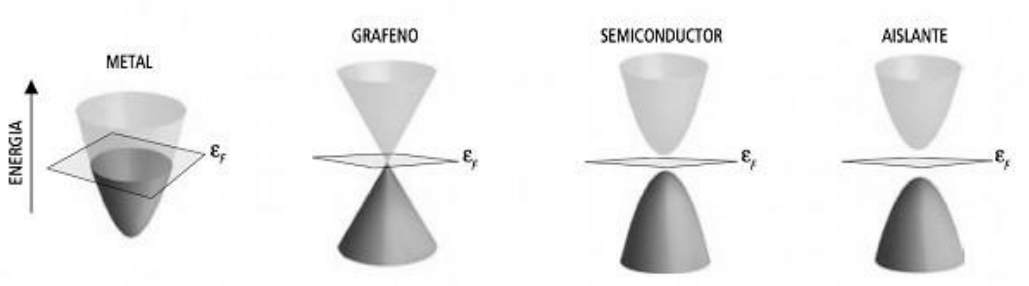

Figura I.2.2. Estructura en bandas del grafeno.

La hibridación sp^2 es la que mejor explica los ángulos de enlace, a 120°, de la estructura hexagonal. Como cada uno de los carbonos tiene cuatro electrones de valencia, en el estado hibridado, tres de esos electrones se alojarán en los híbridos sp^2, formando el esqueleto de enlaces covalentes

simples de la estructura y el electrón sobrante, se alojará en un orbital atómico de tipo *p* perpendicular al plano de los híbridos. La solapación lateral de dichos orbitales es lo que da lugar a la formación de orbitales de tipo π. Algunas de estas combinaciones dan lugar a un gigantesco orbital molecular deslocalizado entre todos los átomos de carbono que constituyen la capa de grafeno.

En el régimen de alta energía, la relación entre momento y energía deja de ser lineal y las bandas están sometidas a una distorsión que conduce a la anisotropía, también conocida como deformación trigonal. Al producirse el apilamiento de capas, se obtiene primero dos capas de grafeno, presentando un conjunto de propiedades muy específicas. El centro de los anillos aromáticos de la lámina de grafeno superior se encuentra en la parte superior de un átomo de la lámina inferior, de modo que la simetría es trigonal en vez de hexagonal (Figura I.2.3) Con la interacción interplanar, los portadores de carga adquieren masa y la dispersión produce de forma parabólica, pudiendo ser descrita por el formalismo de Shrödinger. Sin embargo, el grafeno bicapa se mantiene sin interrupciones si se omite a la deformación trigonal. La interacción de las bandas π y π* de cada lámina de grafeno produce otras dos bandas. Generalizando, el apilamiento perfecto del grafito en capas alternas (ABAB, tipo Bernal) o de forma escalonada (ABCABC, tipo romboédrico) es función de

si el átomo de carbono lateral cambia de dirección de una capa a la siguiente, o no. La distancia interplanar de un grafeno ideal es 3.45 Å, pero si se produce la rotación de planos sucesivos, uno con respecto del otro, este espacio puede aumentar.

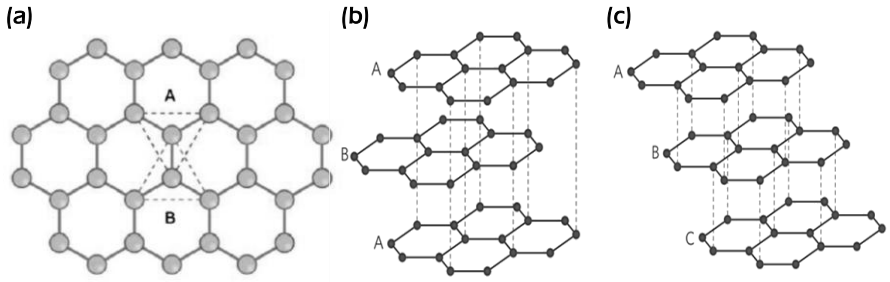

Figura I.2.3. a) Distribución de los átomos de carbono en la red hexagonal de grafeno. b) Apilamiento de grafeno tipo Bernal. c) Apilamiento de grafeno tipo romboédrico.

I.2.2 Caracterización del grafeno

La caracterización física y química de los nanomateriales es un aspecto muy importante pues nos permite conocer propiedades intrínsecas de las nanopartículas como son sus dimensiones y topografía así como su

composición, reactividad y quiralidad[14]. En lo que a grafeno se refiere, la caracterización se ha basado en el empleo de numerosas técnicas que se resumen a continuación.

- *Microscopía óptica*

El microscopio óptico fue usado en las primeras fases de la caracterización de grafeno debido a que es una técnica no destructiva de bajo coste que se encuentra fácilmente en la mayoría de laboratorios. Sin embargo, mediante esta técnica, solamente es posible observar varias capas de grafeno. Además es necesario emplear un sustrato adecuado que permita potenciar la visibilidad de las delgadas hojas. SiO_2 y Si_3N_4 son los sustratos más usados comúnmente para la amplificación del contraste de las capas de grafeno. La longitud de onda de la luz incidente es otro factor clave para mejorar el contraste[15].

- *Técnicas basadas en la atenuación de la fluorescencia*

Gracias al empleo de técnicas como la Microscopia de Fluorescencia ha sido posible observar el grafeno. Esta técnica se basa en el empleo de colorantes que recubren las nanoláminas de grafeno y su mecanismo de acción se centra en interacción química entre las moléculas del colorante y el grafeno, produciéndose una transferencia electrónica desde el fluoróforo

[14] R. Lucena, B.M. Simonet, S. Cárdenas, M. Valcárcel, J. Chromatogr. A 1218 (2011) 620–637.
[15] I. Jung, M. Pelton, R. Piner, D. A. Dikin, S. Stankovich, S.Watcharotone, Nano Lett, 7 (2007)3569–3575.

hasta el grafeno que hace que la fluorescencia que se observa a través del microscopio sea atenuada mediante un proceso de *quenching*[16]. El empleo de esta técnica de visualización permite, en este caso, el empleo de diferentes sustratos para la deposición de grafeno, como con cuarzo, vidrio e incluso plástico. La técnica se circunscribe solo a la observación de láminas de grafeno de gran tamaño debido a que la resolución lateral se encuentra limitada por la difracción de la luz.

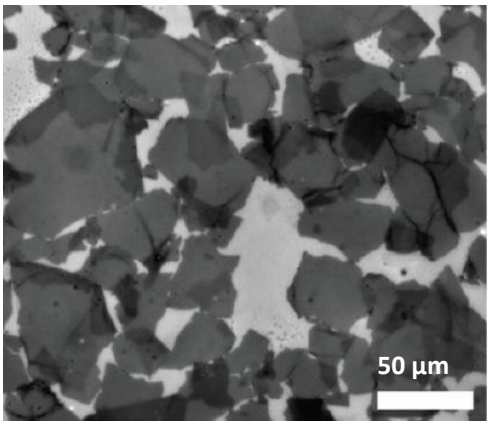

Imagen I.2.4. Imagen de láminas de grafeno obtenida con la técnica de microscopía de fluorescencia. Adaptada de la referencia[17]

- *Microscopia de fuerza atómica (AFM)*

El microscopio de fuerza atómica permite el análisis superficial de muestras con resolución nanométrica o incluso atómica. El empleo de esta

[16] E. Treossi, M. Melucci, A. Liscio, M. Gazzano, P. Samori, V. J. Am. Chem. Soc. 131 (2009) 15576–15577.
[17] J. Kim , L.J. Cote , F. Kim, J. Huang, J. Am. Chem. Soc., 2010, 132, 260–267.

técnica para la caracterización de grafeno permite obtener información sobre su topografía y sobre el número de láminas que lo forman. La técnica no permite distinguir entre grafeno y alguna forma de grafeno funcionalizada, si se trabaja en modo de operación normal. Sin embargo, el modo de contacto intermitente permite establecer diferencias en cuanto al espesor de la muestra que varían en función de si se trata de grafeno que contiene grupos funcionales ricos en oxigeno o no. Además la técnica permite la caracterización mecánica de este nanomaterial puesto que es capaz de resolver las fuerzas atómicas involucradas en el proceso de deformación del grafeno. Los tres modos principales de operación de AFM (sin contacto, contacto y contacto intermitente) ofrecen la posibilidad de estudiar diferentes propiedades como son las mecánicas, eléctricas, magnéticas y elásticas[18].

- *Microscopia electrónica de transmisión (TEM)*

De forma general, la microscopia de transmisión electrónica se emplea para la observación de nanomateriales con el fin de obtener una resolución a escala atómica. El haz de electrones incidente atraviesa la ultrafina capa de muestra, alcanzando las lentes y el detector. Esta técnica parece ser la única herramienta que permite la observación de la estructura atómica del grafeno, sin embargo, se encuentra limitada por su baja resolución cuando se opera a

[18] J.I. Paredes, S. Villar-Rodil, P. Solis-Fernandez, A. Martinez-Alonso, J.M.D. Tascon. Langmuir 25(2009) 5957–5968.

bajos voltajes. El empleo de altos voltajes podría ocasionar daños en la monocapa.

- *Espectroscopia Raman.*

La espectroscopia Raman es una técnica fotónica de gran resolución que proporciona información química y estructural de compuestos orgánicos e inorgánicos permitiendo así su identificación, en unos pocos segundos, gracias al conocido efecto de "huella dactilar". En los últimos años se ha convertido en una técnica muy usada para la caracterización de nanopartículas de carbono dado que proporciona información acerca de su estructura y propiedades electrónicas de una forma simple, no destructiva ni invasiva, en condiciones de temperatura ambiente y presión atmosférica. Los alótropos del carbono muestran, de forma general, unas bandas características designadas como D, G y 2D que suelen aparecer alrededor de los 1350 cm^{-1}, 1580 cm^{-1}, y 2700 cm^{-1}[19], respectivamente. La banda G, o tangencial, está asociada a la vibración en el plano de los átomos de carbono con hibridación sp^2, la banda D aparecen en presencia de desorden en la estructura atómica, que origina la aparición de defectos. También se relaciona con el efecto de borde, aparición de ondulaciones topográficas y falta de homogeneidad en la densidad electrónica, en el caso del grafeno. La banda 2D o G' corresponde

[19] C. Qiu, H. Zhou, H. Yang ,M. Chen, Y. Guo, L. Sun, J. Phys. Chem. C 115 (2011) 10019–10025.

con el sobretono de la banda G y está relacionada con vibraciones de tipo acústico.

La identificación de estas características en el grafeno permite obtener información en cuanto al número de láminas que lo conforman, espesor, dopaje, efecto de la temperatura y presencia de defectos, entre otros. Los espectros Raman en los que no aparece La banda D indican claramente la presencia de una sola lámina de grafeno perfecto. El incremento en el número de láminas de grafeno reduce la intensidad relativa de la banda 2D, incrementando su anchura a mitad de pico y provocando un desplazamiento hacia el azul en el número de onda[20]. Desplazamientos en la banda G indican efectos de la temperatura (desplazamiento hacia el rojo) y dopaje (desplazamientos hacia el azul). Debido a que las propiedades del grafeno están relacionadas directamente con su número de láminas y su pureza, algunos investigadores han hecho de la espectroscopia Raman una herramienta para el control de calidad del grafeno monocapa y del grafeno de pocas capas.

[20] J.S. Park, A. Reina, R. Saito, J. Kong J, G. Dresselhaus, M.S. Dresselhaus, Carbon 47 (2009) 1303–1310.

I.2.3 Propiedades del grafeno

Tras la aparición del grafeno la mayoría de las investigaciones se enfocaron en el estudio de las propiedades de este nanomaterial bidimensional. El grafeno posee un elevado número de propiedades excepcionales entre las que destacan las electrónicas, ópticas, térmicas y mecánicas, y por tanto este nanomaterial alberga gran potencial para la transformación de las futuras tecnologías, incluyendo dispositivos electrónicos, células solares, optoelectrónica, materiales compuestos, y aplicaciones biotecnológicas. En el sector privado, la industria, inversores privados y organizaciones gubernamentales financian la investigación de grafeno con el fin de acelerar su incorporación al mercado comercial.

Entre sus excepcionales propiedades se pueden resaltar la alta movilidad de carga (a través del par electrón/hueco, 230.000 cm2/Vs)[21], una gran conductividad térmica (5000 W/mK), enorme resistencia (130GPa), una elevada área superficial especifica (2600 m^2/g)[22], efecto de Hall cuántico a temperatura ambiente. Otras propiedades y efectos observados en este nanomaterial son: Comportamiento entre conductor metálico y semiconductor, dado que el nivel de Fermi se encuentra justo en la unión entre las capas de valencia y conducción. Esto implica que la banda *gap* sea

[21] C. Lee, X. Wei, J. W. Kysar, J. Hone, Science 321 (2008) 385–388.
[22] C. N. R. Rao, A. K. Sood, K. S. Subrahmanyam , A. Govindaraj, Angew. Chem. 48 (2009) 7752–7777.

cero y los electrones pueden saltar sin problema de de una capa a otra facilitando la conducción eléctrica. También muestra un elevado módulo de Young (aprox. 1100 GPa)[23], una gran estabilidad química, elevada transmitancia óptica, efecto de campo eléctrico ambipolar y una fuerte naturaleza hidrofóbica, lo que se traduce en una fuerte tendencia a la aglomeración. Esta última es una propiedad importante ya que algunas de las propiedades excepcionales que exhibe este material se deben al fenómeno de la agregación.

Propiedades de transporte electrónico

El grafeno, material bidimensional, es un semiconductor con banda gap cero. En él los átomos se unen formando anillos hexagonales. En un anillo simple ideal, que podría asemejarse al benceno, cada átomo de carbono tiene tres orbitales híbridos sp^2 colocados en un mismo plano y un orbital p perpendicular al plano de los híbridos, formando de este modo un sistema de enlaces π deslocalizados en el que la densidad electrónica se distribuye de forma simétrica por encima y por debajo del plano.

Como ya se avanzaba en la breve introducción de esta sección, el grafeno presenta un inusual comportamiento de los portadores de carga que se propagan como fermiones de Dirac, es decir, como partículas sin masa, que

[23] A. A. Balandin, S. Ghosh, W. Bao, I. Calizo et al., Nano Lett. 8 (2008) 902–907.

se comportan de una forma anormal y muy distinta a los electrones bajo un campo magnético, dando lugar a la observación del efecto de Hall cuántico a temperatura ambiente[24]. La estructura de bandas del grafeno de una única lámina muestra dos bandas que se cortan en dos en un punto equivalente, K y K_0 en el espacio reciproco. La dispersión electrónica se asemeja a los electrones de Dirac en la cercanía a ambos puntos, que pueden ser referidos como puntos donde las bandas de conducción y de valencia se degeneran, haciendo del grafeno un semiconductor con banda gap cero. La alta conductividad electrónica de las láminas simples se debe a la ausencia de defectos en la red, defectos que generalmente actúan como sitios de dispersión inhibiendo el transporte de la carga.

El carácter ambipolar del grafeno a temperatura ambiente, es otra importante característica que puede ser observada gracias a que los portadores de carga pueden pasar de electrones a huecos aplicando un determinado voltaje.

Propiedades ópticas

El grafeno, bien sea en forma de nanolámina o con varias capas, es capaz de absorber una pequeña fracción de la luz incidente en un amplio rango de longitud de onda, encontrándose que la absorción de la luz es

[24] A.K. Geim, K.S. Novoselov, Nat. Mater. 6 (2007)183–191.

proporcional al número de capas que conformen el grafeno, de modo que la a mayor numero de láminas, mayor absorción de la luz. Además, su transición óptica puede ser modificada alterando la energía de Fermi. La absorción de la luz en su superficie genera pares del tipo electrón–hueco que pueden recombinarse en cuestión de picosegundos, dependiendo de la temperatura y de la densidad de electrones y huecos[25]. Si se aplica un campo eléctrico, interno o externo, los huecos y electrones pueden separase y generarse corriente[26]. Otra propiedad del grafeno es la fotoluminiscencia (PL) que si bien no es observada directamente, puede inducirse a través de una adecuado gap. Para ello se han propuesto dos rutas: la primera transformar las nanocintas de grafeno o *graphene nanoribbons* (GNRs) en puntos cuánticos. El segundo método es el tratamiento físico o químico con gases para reducir la conectividad de la red de electrones π[27].

Propiedades mecánicas

La aplicación de fuerzas externas a materiales cristalinos suele afectar a su estructura, alterando distancias interatómicas, que se traduce en la redistribución de la carga electrónica. Al igual que los CNTs, el grafeno posee un gran modulo elástico y una elevada resistencia que ha sido estudiada en

[25] F. Rana, P.A. George, J.H. Strait, J. Dawlaty, S. Shivaraman, M. Chandrashekhar, et al., Phys. Rev. B 79 (2009) 115447.
[26] F .Xia, T. Mueller, R. Golizadeh-Mojarad, M. Freitag, Y.M. Lin, T.J. Sang, et al., Nano Lett. 9 (2009) 1039–1044.
[27] D.C. Elias, R.R. Nair, T.M.G. Mohiuddin, S.V. Morozov, P. Blake, M.P. Halsall, et al. Science 323 (2009) 610–613.

muestras con diferente número de láminas. De estas investigaciones se puede concluir que el grafeno monocapa presenta una gran resistencia a la tracción interna mostrando una rigidez similar a la del grafito[28]. La espectroscopia Raman ha sido la técnica más usada para estudiar estas propiedades puesto que permite monitorizar la frecuencia de vibración de los fonones (cuasipartículas asociada con ondas de compresión tales como el sonido o, en nuestro caso, vibración de una red cristalina). Se ha podido observar que los esfuerzos de tensión provocan el debilitamiento de los fonones debido a la disminución del modo de frecuencia vibracional, mientras que los esfuerzos de compresión causan un fortalecimiento en los fonones haciendo que aumente la frecuencia vibracional. Ambos esfuerzos, tracción y compresión pueden ser observados a través de cambios en las bandas G y 2D del grafeno, poniéndose de manifiesto a través de desplazamientos en el número de onda, hacia el rojo[29] o el azul[30], y desdoblamientos de estos picos característicos. Se ha demostrado que la aplicación de una fuerza de tensión uniformemente aplicada sobre la estructura de grafeno (tensión uniaxial) puede afectar de forma más significativa a la estructura electrónica y provocar la ruptura de los enlaces C–C de la red hexagonal.

[28] T. Yu, Z. Ni, C. Du, Y. You, Y. Wang, Z. Shen., J Phys Chem C 112 (2008) 12602–12605.
[29] T.M.G. Mohiuddin, A. Lombardo, R.R. Nair, A. Bonetti, G. Savini, et al., Phys. Rev. B. 79 (2009) 205433.
[30] Z.H. Ni, W. Chen, X.F. Fan, J.L. Kuo, T. Yu, A.T.S. Wee, et al. Phys Rev B 77 (2008) 115416.

Propiedades térmicas

Los alótropos del carbono, como grafito y nanotubos de carbono han mostrado una gran conductividad térmica debido a los fuertes enlaces covalentes y a la dispersión de los fonones[31]. El grafeno, en forma de lámina única, presenta una conductividad térmica de 5000W/mK[32] gracias a la ausencia de defectos, mientras que si este es depositado sobre un sustrato, esta conductividad térmica disminuye hasta los 600W/mK. Estos cambios pueden registrarse empleando técnicas como la espectroscopia confocal Raman, capaz de detectar cambios de temperatura midiendo el desplazamiento que se produce en la banda G. la conductividad térmica se ve afectada por factores como el dopaje de las nanoestructuras y la dispersión que producen los defectos de los bordes de las láminas.

[31] E. Pop, D. Mann, Q. Wang, K. Goodson, H. Dai., Nano Lett. 6 (2005) 96–100.
[32] A.A. Balandin, S. Ghosh, W. Bao, I. Calizo, D. Teweldebrhan, F. Miao, et al., Nano Lett. 8 (2008) 902.907.

I.3. NANOMATERIALES DE LA FAMILIA DEL GRAFENO

El grafeno y las nanoestructuras relacionados con él han sido ampliamente estudiados en la última década. Dentro de esta familia de nanomateriales podemos encontrar, a demás de la lámina aislada de grafito con naturaleza análoga a un hidrocarburo aromático policíclico de tamaño infinito (grafeno), al óxido de grafeno (GO) y al óxido de grafeno reducido (rGO). Asimismo pueden considerarse, en función de sus dimensiones, las nanocintas de grafeno (*graphene nanoribons*, GNR), las nanoláminas, las nanoplaquetas (*graphene platelets, GNP*) y los puntos cuánticos de grafeno (*graphene quantum dots*, GQDs). En esta memoria se presentan las características y propiedades más importantes del grafeno (sección I.2. de este bloque), de los GQDs y del GO, por haber sido los nanomateriales implicados en el desarrollo de la misma.

I.3.1 Puntos cuánticos de grafeno

Los puntos cuánticos de grafeno, conocidos como *graphene quantum dots* (GQDs) en inglés, han surgido muy recientemente dentro de la familia del

grafeno. Al igual que grafeno y óxido de grafeno, los GQDs muestran unas propiedades excelentes y únicas que han conseguido atraer la atención de numerosas investigaciones en varios campos de aplicación.

Los GQDs son estructuras cero dimensionales, con una distribución de átomos carbono en forma de anillos hexagonales, al igual que el grafeno. Se caracterizan por ser nanopartículas fotoluminiscentes que consisten en láminas de grafeno con geometría circular plana de un tamaño muy pequeño, típicamente entre 3–20 nm, aunque pueden alcanzar tamaños laterales de hasta 80 nm. La Figura I.3.1.1 muestra imágenes de GQDs de distinto tamaño obtenidas por HRTEM.

Los GQDs muestran confinamiento de los excitones y efecto de tamaño cuántico. Este efecto se produce cuando se reduce considerablemente el tamaño de una red formada por átomos, alcanzando unas dimensiones en las que las superficies de las partículas se encuentran separadas por distancias del orden de longitudes de onda de los electrones. En esta situación se pueden modelar los niveles de energía mediante el tratamiento mecánico cuántico de una partícula en una caja. Esto es lo que se denomina efecto de tamaño cuántico[33].

[33] P.P. Charles, J. Frank, Owens, Introducción a la Nanotecnología, Reverte, 2007.

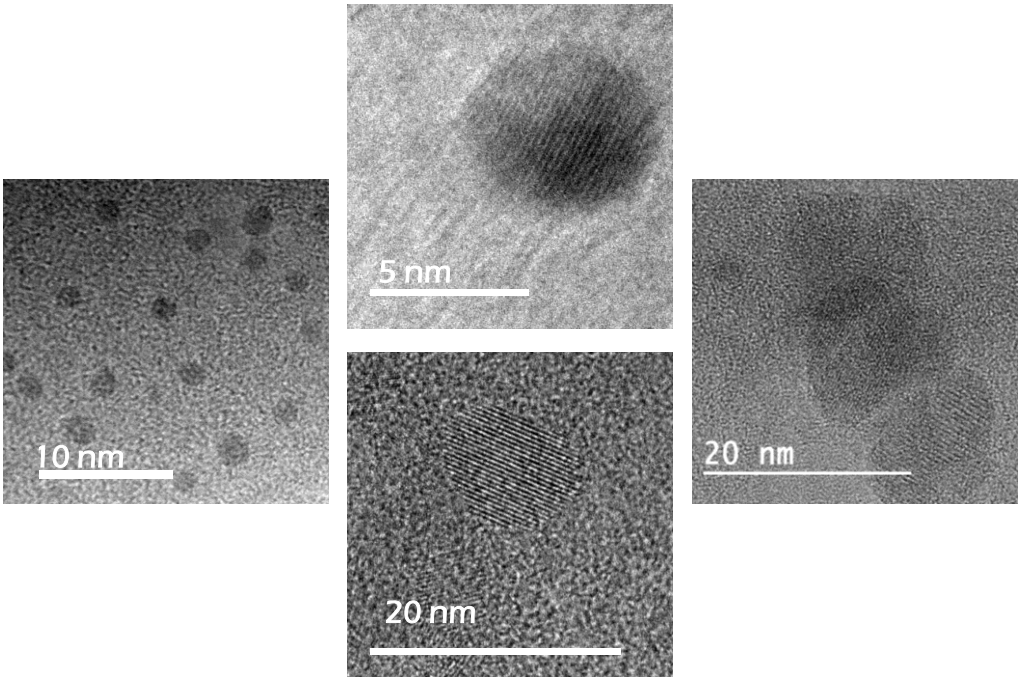

Figura I.3.1.1, *Imágenes HRTEM de GQDs de distinto tamaño.*

El grafeno, como vimos anteriormente, es un nanomaterial con *gap* cero, por lo que no es posible observar su fluorescencia. Sin embargo, muestra un radio de excitón de Bohr infinito que hace que el confinamiento cuántico aparezca en láminas de grafeno de un tamaño reducido[34]. En los GQDs la

[34] X.Yan, X. Cui, L.S. Li, J. Am. Chem. Soc. 132 (2010) 5944–5945.

banda *gap* es distinta de cero y puede ser ajustada modificando el tamaño y la química superficial de estas nanopartículas[35].

GQDs pueden encontrarse como láminas aisladas, dobles o múltiples[36]. El confinamiento cuántico y el efecto de borde hacen que los GQDs presenten propiedades muy interesantes y atractivas como la actividad fluorescente, una robusta inercia química, una excelente fotoestabilidad, gran biocompatibilidad y baja toxicidad. También merecen ser mencionados su gran solubilidad en varios disolventes, su fotoluminiscencia estable y su resistencia al fotoblanqueo, más conocido por su nombre en inglés, *photobleaching*, es decir, la destrucción fotoquímica de un fluoróforo.

Los puntos cuánticos de carbono (CDs) también han surgido recientemente. Se trata de nanopartículas cuasi–esféricas con diámetros por debajo de los 10 nm que presentan unas propiedades muy similares a las mostradas por los GQDs a pesar de contener carbono amorfo en su estructura.

Volviendo a los GQDs, estos pueden presentar grupos funcionales en sus extremos o superficie. Los grupos funcionales más comúnmente descritos son los mismos que se pueden encontrar en el óxido de grafeno, grupos

[35] S. Kim, S.W. Hwang, M.K. Kim, D.Y. Shin, D.H. Shin, et al., ACS Nano 6 (2012) 8203–8208.
[36] Y. Dong, C. Chen, X. Zheng, L. Gao, Z. Cui, et al., J. Mater. Chem. 22 (2012) 8764–8766.

carboxílicos, hidroxílicos, carbonilo y epóxido. Estos grupos actúan como sitios reactivos para el anclaje o reacción con otras moléculas, induciendo cambios en la fotoluminiscencia emitida debido a perturbaciones de la densidad electrónica[37].

El rendimiento cuántico (QY) es un factor clave cuando se habla de materiales fluorescentes. Los GQDs pueden tener QYs comprendidos entre el 2% y el 46%, dependiendo en gran medida estos valores del método de síntesis y su química superficial, es decir, si ésta se encuentra pasivada, funcionalizada, dopada, reducida u oxidada.

Pueden seguirse dos estrategias para la obtención de GQDs, las rutas descendentes o *Top–down* en inglés, o las síntesis ascendentes o *Bottom–up*. Bajo el marco de estas dos estrategias se engloban una gran cantidad de métodos y técnicas que permiten sintetizar GQDs empleando una amplia variedad de precursores como fibras de carbono, grafito, nanotubos de carbono y grafeno (en las rutas *Top–Down*) y ácido cítrico, glucosa y ácido L–glutámico (en las síntesis de tipo *Bottom–up*).

Sus magníficas propiedades hacen que sean una herramienta muy útil en el desarrollo de aplicaciones en diversos sectores, permitiendo el desarrollo de nuevos y mejorados dispositivos eléctricos, optoelectrónicos,

[37] S. H. Jin, D. H. Kim, G. H. Jun, S. H. Hong, S. Jeon, ACS Nano 7 (2012) 1239–1245.

fotovoltaicos[38], de almacenamiento de energía y su aplicación se extiende hasta el ámbito de la biomedicina, y la monitorización ambiental, aplicándose a sensores y biosensores y utilizándose como agente de contraste para la obtención de bioimágenes. Tanto los métodos de obtención de GQDs como las sus aplicaciones en el contexto de la Química Analítica serán comentados extensamente en el Capítulo 1 de la Sección I.4 del presente Bloque.

I.3.2 Óxido de grafeno

El óxido de grafeno (GO) puede considerarse como un derivado modificado del grafeno, por lo tanto sus propiedades y comportamiento diferirán de los esperados para el grafeno. El GO posee una estructura única compuesta of carbonos con hibridación sp^2 rodeados de otros carbonos con hibridación sp^3 y grupos funcionales ricos en oxígeno, principalmente, hidroxilos, carboxilos, carbonilos y epóxidos[39]. La presencia de estos grupos funcionales confiere al GO una excelente solubilidad, facilidad para ser funcionalizado superficialmente y habilidad para atenuar la fluorescencia de otras sustancias.

[38] Z. Zhu, J. Ma, Z. Wang, C. Mu, Z. Fan,.et al., J. Am. Chem. Soc. 136 (2014) 3760–3763.
[39] K.P. Loh, Q. Bao, G. Eda, M. Chhowalla, Nat. Chem. 2 (2010) 1015–1024.

De forma general y resumida, el GO puede obtenerse por tres métodos diferentes: siguiendo el método descrito por Brodie[40], empleando el de Staudenmaier [41]o aplicando el de Hummers[42], o alguna ligera modificación de alguno de ellos. Los tres métodos consiguen la oxidación del grafeno hasta distintos niveles, de modo que los tres métodos emplean como material de partida el grafito. Los métodos de Brodie y Staudenmaier aplican una combinación de clorato potásico ($KClO_3$) y ácido nítrico (HNO_3) para oxidar grafito y el método de Hummers consigue la oxidación mediante el empleo de permanganato potásico ($KMnO_4$) y ácido sulfúrico (H_2SO_4).

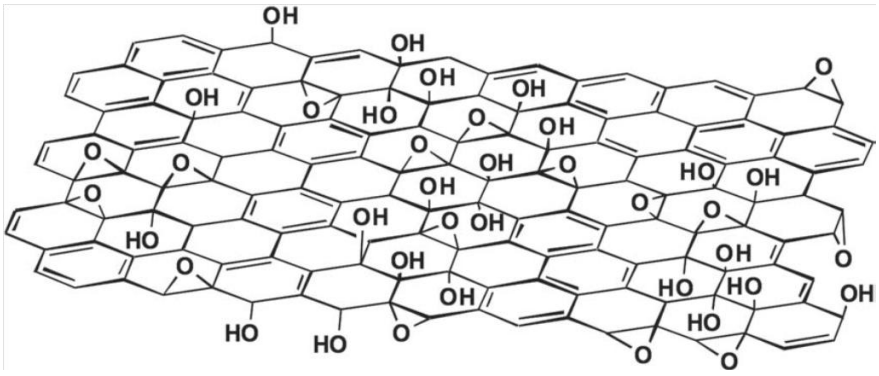

Figura I.2.4. Estructura de óxido de grafeno

[40] B.C. Brodie, Ann. Chim. Phys. 59 (1860) 466–472.
[41] L. Staudenmaier, Ber. Deut. Chem.. Ges. 31 (1898) 1481–1487.
[42] W.S. Hummers, R.E. Offeman, J. Am. Chem. Soc. 80 (1958) 1339–1339.

La transformación de grafito en GO se ha convertido en una ruta que permite la obtención de cantidades considerables de monocapas de grafeno[43]. El óxido de grafito se obtiene principalmente, como ya avanzábamos antes, mediante el método descrito por Hummers. El material obtenido posee átomos de carbono con hibridación sp^3 en el plano basal y presenta una gran cantidad de grupos hidroxilo y epóxido anclados a estos carbonos. Los grupos carbonilo y carboxilo aparecen en los bordes, enlazados a carbonos sp^2. Dichos grupos funcionales (de carácter polar), anclados a la superficie del GO después de su obtención, le confieren un marcado carácter hidrofílico que le permite ser exfoliado e dispersado en distintos disolventes y agua, con ayuda de mecanismos de agitación y ultrasonicación, obteneniéndose dispersiones estables de GO. Óxido de grafito y GO difieren en cuanto a estructura, grupos funcionales y propiedades químicas. La exfoliación de oxido de grafito también puede obtenerse de forma satisfactoria en otros disolventes distintos del agua como N, N–dimetilformamida (DMF), tetrahidrofurano (THF), N–metil–2–pirrolidona (NMP) y etilenglicol[44]. El GO presenta carga negativa cuando se encuentra disperso agua debido a la ionización de los ácidos carboxílicos y de los grupos fenólicos hidroxilos[45]. De hecho, la obtención de dispersiones

[43] C. Gomez-Navarro, R.T. Weitz, A.M. Bittner, M. Scolari, A. Mews, et al., Nano Lett. 7 (2007) 3499–3503.
[44] J.I. Paredes, S. Villar-Rodil, A. Martinez-Alonso, J.M.D. Tascon, Langmuir 24 (2008) 10560–10564.
[45] D. Li, M.B. Muller, S. Gilje, R.B. Kaner, G.G. Wallace, Nat Nanotechnol. 3 (2008) 101–105.

estables de GO en agua se debe a la hidrofobicidad que le confiere la presencia de estos grupos junto a las repulsiones electrostáticas.

El estudio de la estructura química de GO, como tipo y distribución de grupos funcionales ricos en oxígeno, ha revelado que los grupos hidroxilo y epóxido se sitúan en el plano basal, mientras que los grupos lactol, éster, ácidos, cetonas y carbonilos se encuentran en los bordes de la nanoestructura[46]. Dichos grupos funcionales dotan al GO de sitios reactivos para la modificación de la superficie con el fin de obtener materiales basados en grafeno funcionalizados. Sin embargo, estos grupos distorsionan la estructura electrónica del GO y esto hace que disminuya su conductividad y que contenga gran cantidad de defectos y desordenes estructurales irreversibles. La reducción química del GO puede recuperar su conductividad sin llegar a alcanzar la del grafeno[47].

Funcionalización de GO

La funcionalización de GO supone modificar las propiedades químicas de este nanomaterial y, por tanto, abrir un amplio abanico de posibles aplicaciones. La funcionalización superficial puede conseguirse de dos formas principalmente: mediante funcionalización covalente o a través de estrategias no covalentes.

[46] W.W. Cai, R.D. Piner, F.J. Stademann, S. Park, M.A. Shaibat, Y. Ishii, et al., Science 321 (2008) 1815–1817.
[47] S. Stankovich, R.D. Piner, X.Q. Chen, N.Q. Wu, S.T. Nguyen, R.S. Ruoff., J Mater Chem 16 (2006) 155–158.

En la funcionalización covalente, los grupos carboxílicos en el borde, y los grupos hidroxilo y epóxido en el plano basal son utilizados para modificar la funcionalidad del GO. Puede tratarse con isocianato formando amidas, a partir de los grupos carboxilo, y carbamatos, a partir de los hidroxilos, disminuyendo su hidrofobidad y aumentando su afinidad hacia disolventes polares apróticos[48]. Otras sustancias empleadas para la funcionalización de GO han sido el cloruro de tionilo ($SOCl_2$)[49], 1-etil-3-(3-dimetilaminopropil)-carbodiimida (EDC)[50], N,N-diciclohexilcarbodiimida (DCC)[51], o 2-(7-aza-1H-benzotriazol-1-il)-1,1,3,3-tetrametiluronio hexafluorofosfate (HATU)[52]. La adición de aminas y alcoholes produce la unión covalente de los grupos funcionales al GO mediante la formación de amidas y ésteres. La funcionalización con polímeros tiene lugar a través de la reacción con los grupos hidroxilos, presentes en el plano basal, y los grupos epóxido pueden albergar líquidos iónicos[53] y otras moléculas que contengan un grupo amino terminal. La Figura I.2.5 muestra una representación esquemática de las posibles rutas de funcionalización de grafeno.

[48] S. Stankovich, R.D. Piner, S.T. Nguyen, R.S. Ruoff., Carbon 44 (2006) 3342–3347.
[49] Y. Xu, Z. Liu, X. Zhang, Y. Wang, J. Tian, Y. Huang, et al., Adv Mater 21 (2009) 1275–1279.
[50] Z. Liu, J.T. Robinson, X. Sun, H. Dai., J Am Chem Soc 130 (2008) 10876–10877.
[51] L.M. Veca, F. Lu, M.J. Meziani, L. Cao, P. Zhang, G. Qi, et al., Chem Commun (2009) 2565–2567.
[52] N. Mohanty, V. Berry., Nano Lett 8 (2008) 4469–4476
[53] H. Yang, C. Shan, F. Li, D. Han, Q. Zhang, L. Niu., Chem Commun (2009) 3880–3882.

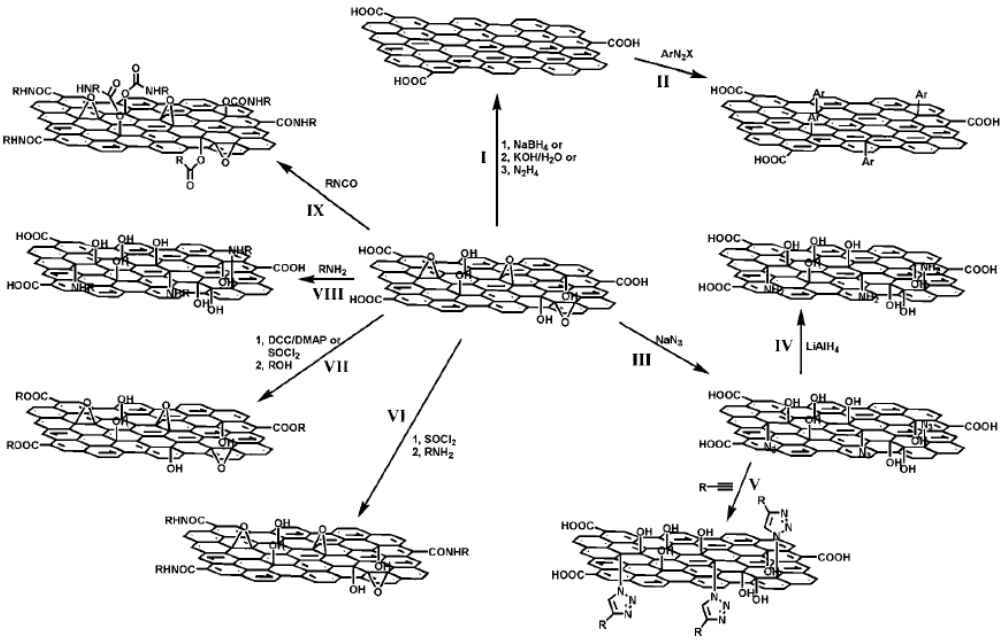

Figura I. 2.5. Esquema de la funcionalización covalente de grafeno y GO. I: Reducción de GO en grafeno a través de varias rutas (1, $NaBH_4$; 2, KOH/H_2O; 3, N_2H_4). II: Funcionalización superficial covalente de grafeno reducido vía reducción a través de reacciones con sales de diazonio (ArN_2X). III: Funcionalización de GO por reacción de GO con acida sódica. IV: Reducción de GO funcionalizado con acida mediante el empleo de $LiAlH_4$, obteniendo como resultado GO funcionalizado con grupos amino. V: funcionalización de acida–GO a través de reacciones de clic ($R–CHCH/CuSO_4$). VI: Modificación de GO con cadenas alquílicas largas (1, $SOCl_2$; RNH_2) a través de reacciones de acilación entre los gupos carboxílicos del GO y los alquilaminas (tras la activación de los grupos COOH con $SOCl_2$). VII: Esterificación de GO a través de DCC o de la reacción de acilación entre los grupos COOH del GO y los ROH de las alquilaminas. VIII: Reacción de apertura de anillos entre los grupos epoxido del GO y los grupos amino de moléculas orgánicas amino terminales (RNH_2). IX: Tratamiento del GO con isocianatos, que conduce a la derivatizacion de los gupos carboxílicos de los bordes e hidroxilicos de la superficie mediante la formación de amidas o ésteres de carbamato (RNCO). (Adaptado de la referencia[54])

La funcionalización no covalente del GO se basa en el establecimiento de interacciones de tipo débil, como son las fuerzas de Van der Waals, las interacciones π–π, y las interacciones electrostáticas, ente la nanoestructura y

[54] K.P. Loh, Q. Bao, P.K. Ang, J. Yang, J. Mater. Chem. 20 (2010) 2277–2289.

las moléculas. La hibridación sp^2 del GO favorece las interacciones π–π con otras moléculas aromáticas para formar materiales compuestos. La ventaja de este tipo de funcionalización es que no afecta a la conjugación de tipo π de la superficie del grafeno, mientras que la covalente puede dar lugar a la formación de defectos en la lámina de grafeno. Se han descrito numerosos conjugados formados a partir de poli(sodio 4-estirenosulfonato (PSS) , polianilina sulfonada, poli(3-hexiltiofeno) (P3HT), polielectrolito conjugado, porfirina y pireno[55], entre otros. Durante la reducción química de GO, las nanoláminas pueden estabilizarse a través de interacciones π–π con moléculas aromáticas.

A pesar de que el grafeno se conoce desde finales de la década de los 40[56] como estructura teórica, para el cálculo de diagramas de banda y para predecir propiedades electrónicas, el aprovechamiento de sus excelentes propiedades en casos prácticos se ha visto frenado por las dificultades en su obtención y procesamiento a gran escala.

[55] Q. Su, S. Pang, V. Alijani, C. Li, X. Feng, K. Mullen, Adv.Mater. 21 (2009) 3191–3195.
[56] P.R. Wallace, Physical Review 71(1947) 622–634.

I.4. MÉTODOS DE OBTENCIÓN DE GRAFENO

Las excelentes propiedades térmicas, mecánicas, estructurales y eléctricas que presenta el grafeno son de gran relevancia en la Nanociencia y Nanotecnología y dependen en gran medida de la forma en que la monocapa sea obtenida así como del número de capas que conformen el grafeno. En la bibliografía pueden encontrarse diversos métodos para la obtención de grafeno pero, sin embargo, todos ellos deben superar el reto de obtener dispersiones estables y homogéneas de láminas de grafeno individuales. Al igual que ocurre con otras nanoestructuras de carbono, como los nanotubos, el mayor desafío en la síntesis y procesado de grandes cantidades de nanoláminas es la agregación de éstas. Como ya se ha comentado con anterioridad, el grafeno es una estructura plana de un átomo de espesor, compuesta por átomos de carbono con hibridación sp^2 densamente empaquetados en una rejilla en forma de panal, con una gran área específica superficial. En cercanía a otras nanoláminas, el grafeno tiende a formar agregados a través del establecimiento de fuerzas de Van der Waals. Por lo tanto, la prevención del fenómeno de agregación es algo que las técnicas de obtención deben contemplar.

Entre las principales técnicas que se describen en la bibliografía, pueden destacarse dos categorías principales: las técnicas descendentes o *Top–Down* (distintos métodos de exfoliación) y las rutas ascendentes o *Bottom–Up* (deposición química de vapor, crecimiento epitaxial, arco de descarga, síntesis química, etc.). A continuación se resumen las principales técnicas que se han empleado en la producción de nanoláminas de grafeno, destacando sus principales ventajas e inconvenientes.

- *Exfoliación micromecánica.*

Desde 2004, cuando el grafeno fue aislado por primera vez por Geim y Novoselov, usando la exfoliación micromecánica de grafito usando cinta Scotck, éste se ha venido obteniendo aplicando el mismo principio mediante métodos más simplificados, de modo que en la actualidad se produce la exfoliación frotando directamente el grafito contra una superficie (generalmente Si/SiO2) como si se escribiera sobre la misma. Mediante este sencillo procedimiento resulta posible la obtención de láminas de grafeno monocapa en el rango de unos 10 μm y de una calidad tanto estructural como electrónica excelente. El problema radica en que, por ser un proceso totalmente manual, la obtención del material es considerablemente laboriosa y de un rendimiento extremadamente bajo. Además, las láminas han de ser cuidadosamente localizadas con la ayuda de un microscopio óptico entre una gran cantidad de pequeños copos de grafito que las enmascaran, resultando

un proceso tedioso que puede llevar varias horas para la identificación de unas pocas láminas de grafeno.

- *Exfoliación de grafito*

En el grafito, las láminas de grafeno se encuentran empaquetadas y separadas por una distancia de 3.41 A. Las fuerzas de van der Waals, que mantienen unida la estructura de grafito, son fuerzas débiles que permiten el deslizamiento de las láminas de forma perpendicular al eje c, pero no resultan suficientemente fuertes como para permitir la exfoliación en láminas individuales, de forma sencilla. Por lo tanto, superar el inconveniente que suponen estas fuerzas es el primer paso. Para ello se han ideado una serie de procedimientos basados en la exfoliación química y física del grafeno que permiten la obtención de cantidades considerables de láminas individuales de grafeno. La inmersión del grafito en un medio líquido reduce considerablemente la atracción generada por las fuerzas de van der Waals, por ello la mayoría de los procedimientos de exfoliación tienen lugar en disolución.

La exfoliación basada en métodos físicos y químicos mantiene la integridad de la lámina de grafeno pues se aprovecha de la existencia de este material como tal dentro de la estructura de grafito. De forma muy general, la exfoliación tiene lugar cuando se somete al grafito a un procedimiento de

vibración, asistido por ultrasonidos, por ejemplo, para romper la atracción entre las láminas, empleando sustancias químicas, con propiedades surfactantes, para conseguir la estabilización de las láminas de grafeno separadas e impedir que se vuelvan a unir. Pueden desarrollarse empleando determinados disolventes orgánicos como, N–metilpirrolidona[57] o tensioactivos, como dodecilsulfonato sódico (SDBS)[58] y colato de sodio (SC)[59] obteniéndose láminas de grafeno de gran calidad, aunque sus tamaños laterales se restringen a unos pocos cientos de nanómetros. Las moléculas de estas sustancias se disponen rodeando la lámina de grafeno y ayudan a estabilizarlo frente a la agregación a través de repulsiones de Coulumb entre moléculas de surfactante. La ventaja de este método radica en que se evitan los procesos previos de oxidación y reducción, lo cual redunda en un aumento en la calidad estructural de las láminas obtenidas pues ambos procesos generan inevitablemente defectos estructurales[60] que afectan a la organización electrónica del grafeno. Como contrapunto, la concentración de grafeno que se consigue es generalmente pequeña (aprox. 0.001 $mg{\cdot}mL^{-1}$), y las láminas obtenidas son monocapa en pequeña proporción (10 – 30 %), siendo el resto láminas de varias capas.

[57] Y. Hernandez, V. Nicolosi, M. Lotya, F.M. Blighe, Z. Sun, S. De et al., Nat. Nanotechnol. 3 (2008) 563–568.
[58] Lotya M, Hernandez Y, King PJ, Smith RJ, Nicolosi V, Karlsson LS, et al. J Am Chem Soc 131 (2009) 3611–3620.
[59] Green AA, Hersam MC., Nano Lett 9 (2009) 4031–4036.
[60] S. Stankovich, D.A. Dikin, R.D. Piner, K.A. Kohlhaas, A. Kleinhammes, Y. Jia, et al. Carbon 45 (2007)1558–1565.

Sacando partido de las propiedades físicas del grafito, que al ser calentado a altas temperaturas expande su tamaño considerablemente, puede favorecerse la intercalación de pequeñas moléculas entre las capas de grafito expandidas. La expansión puede alcanzarse también a bajas temperaturas aplicando una elevada presión de vacío. La unión no covalente de estas pequeñas moléculas sobre sus capas puede, además, reducir su aglomeración, haciendo que las láminas de grafito se mantengan intactas y alojen moléculas en su interior. La interacción entre estas moléculas y el grafito, a través de un mecanismo de transferencia de carga, provoca la separación de las láminas. En los procedimientos de este tipo se emplean altas temperaturas, necesarias para la expansión del grafito, y pequeñas moléculas como NaCl, hidrógeno y fluor[61].

En la Figura I.4.I puede apreciarse un esquema ilustrativo de este procedimiento.

[61] Li X, Zhang G, Bai X, Sun X, Wang X, Wang E, et al.. Nat Nanotechnol 3 (2008) 538–542.

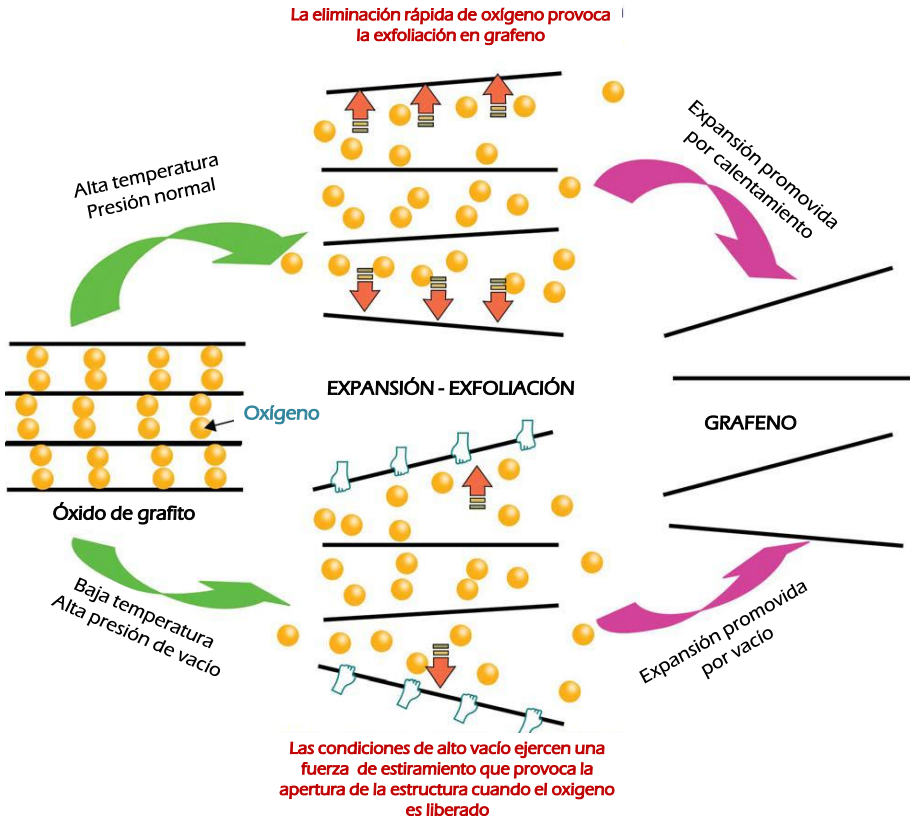

Figura I.4.1. Esquema del proceso de exfoliación por expansión de grafito. Adaptado de la referencia[62].

- *Deposición química en fase vapor (CVD).*

Esta técnica emplea normalmente metales de transición (níquel, rutenio, cobre) como superficies de crecimiento de nanoláminas de grafeno usando como precursores gases de hidrocarburos. El proceso se lleva a cabo a

[62] W. Lu, D. M. Tang, Y. B. He, C. H. You, Z. Q. Shi, X. C. Chen, et al., ACS Nano 3 (2009) 3730–3736.

una temperatura de 1000 ºC. Generalmente, se expone un sustrato metálico a hidrocarburos (metano), produciéndose una nucleación y crecimiento de una lámina de grafeno al descomponerse los hidrocarburos en la superficie metálica. Mediante este método se obtienen láminas monocapa de una gran calidad estructural, que pueden ser dopadas mediante la sustitución de átomos introduciendo diferentes gases durante el crecimiento. El hecho de necesitar altas temperaturas y bajas presiones lo convierte en un método muy costoso e instrumentalmente complejo.

Algunos grupos de investigación han incorporado ciertas modificaciones en este tipo de metodología, como por ejemplo, el empleo de hojas de cobre como superficie de crecimiento, con una mezcla de metano e hidrogeno como precursor, obteniendo un 95% de monocapas de grafeno[63]. La CVD a presión ambiental sobre películas de níquel policristalino tiene un bajo coste y proporciona grandes áreas de láminas simples y otras de varias capas[64]. El empleo de hexano como precursor líquido con láminas policristalinas de cobre es otra variante de esta técnica[65]. El uso de acetileno como gas precursor permite una disminución de la temperatura hasta 750 ºC[66]. También ha sido posible la obtención de de grafeno gracias el empleo de la deposición por plasma, que ofrece como ventajas menor tiempo de

[63] X. Li, W. Cai, J. An, S. Kim, J. Nah, D. Yang, R. Piner, et al., Science 324 (2009) 1312–1314.
[64] A. Reina, X. Jia, J. Ho, D. Nezich, H. Son, V. Bulovic, M. S. Dresselhaus J. Kong, Nano Lett. 9 (2009) 30–35.
[65] A. Srivastava, C. Galande, L. Ci, L. Song, C. Rai, D. Jariwala, K. F. Kelly, P. M. Ajayan, Chem.Mater. 22 (2010) 3457–3461.
[66] G. Nandamuri, S. Roumimov and R. Solanki, Nanotechnology 21 (2010) 145604.

deposición (menos de 5 minutos), y al igual que el caso anterior una reducción de la temperatura necesaria, pasando de los 1000ºC a los 650ºC. Las láminas de grafeno son depositadas verticalmente cuando se emplea este método a la dirección del campo eléctrico del plasma[67].

- *Crecimiento epitaxial*

El crecimiento epitaxial consiste en hacer crecer una capa uniforme de poco espesor sobre un sustrato semiconductor con una estructura cristalina similar. Los métodos que se han reportado para la obtención de grafeno, se fundamentan en la utilización de superficies eléctricamente aislantes, principalmente el carburo de silicio, SiC. En ellos tiene lugar la sublimación térmica del silicio a temperaturas entorno a 1200–1600 °C, a la vez que el carbono se reordena para formar una capa de grafeno. Se producen así láminas de una gran calidad estructural, aunque de nuevo la necesidad de trabajar en ultra alto vacio y la gran temperatura necesaria para producir la sublimación del silicio limitan enormemente su aplicación a gran escala. Sin embargo, recientes estudios realizados a presión atmosférica en Ar parecen indicar que es posible obtener láminas de una calidad estructural mejor incluso que la de las láminas obtenidas en vacío. En esta técnica también se han introducido algunas modificaciones como el empleo de sustratos como

[67] R. Vitchev, A. Malesevic, R.H. Petrov, R. Kemps ,M. Mertens, A. Vanhulsel, et al., Nanotechnolgy 21(2010) 095602.

4H-SiC pulido bajo condiciones de vacío[68], β-SiC cúbico[69], gránulos de SiC policristalino[70] .

- *Descarga de arco*

Para la obtención de grafeno, el arco de descarga tiene lugar conectando dos barras de grafito[71] o GO[72], actuando ambos como ánodo y cátodo, entre los que se aplica un voltaje de entre 100–150 A con el fin de evaporar el grafito o el GO, en atmósfera de H_2 y se sometiendo al sistema a cierta presión. También puede emplearse una atmosfera de NH_3, He, Ar, CO_2, una atmosfera mixta compuesta por H_2/He o simplemente el aire. Se ha demostrado que el empleo del sistema a altas presiones favorece la generación de grafeno, mientras que la aplicación de bajas presiones favorece la formación de otras nanoestructuras como son los nanocuernos y las nanoesferas[73]. Este método presenta las ventajas de que el grafeno sintetizado a partir de él muestra una buena cristalinidad, una alta estabilidad térmica, resistencia a la oxidación y presencia de pocos defectos estructurales. Como inconvenientes hay que mencionar el lento crecimiento de las

[68] S. Shivaraman, R.A. Barton, X. Yu, J. Alden, L. Herman et al., Nano Lett. 9 (2009) 3100–3105.
[69] V. Y. Aristov, G. Urbanik, K. Kummer, D. V. Vyalikh et al.,Nano Lett. 10 (2010) 992–995.
[70] D. Deng, X. Pan, H. Zhang, Q. Fu, D. Tan, X. Bao, Adv. Mater. 22 (2010) 2168–2171.
[71] K. S. Subrahmanyam, L. S. Panchakarla, A. Govindaraj, C. N. R. Rao, J. Phys. Chem. C 113 (2009) 4257–4259.
[72] Z.S. Wu, W. Ren, L. Gao, J. Zhao, Z. Chen, B. Liu, D. Tang, B. Yu, C. Jiang and H.M. Cheng, ACS Nano 3 (2009) 411–417.
[73] Z. Wang, N. Li, Z. Shi, Z. Gu, Nanotechnology 21 (2010) 175602.

nanoestructuras, y la generación de carbono amorfo y otras nanoestructuras de carbono.

- *Reducción de óxido de grafeno*

La reducción química del grafeno parece ser la ruta de obtención más prometedora puesto que permite la producción a gran escala y la obtención de grafeno funcionalizado a un coste asequible. Tradicionalmente ésta se ha realizado empleando varios agentes reductores entre los que se incluyen hidracina[74] y borohidrato de sodio[75]. La reducción con hidracina ha sido la más utilizada para la obtención de láminas similares al grafeno. Durante el proceso de reducción la dispersión de color marrón de GO se torna negra y las láminas reducidas se aglomeran y precipitan, debido a la eliminación de los átomos de oxígeno. La hidracina participa en la apertura de anillos hexagonales al reaccionar con los grupos epóxido[76]. El empleo de $NaBH_4$ como agente reductor da lugar a una reacción más lenta pero resulta más efectiva aun que la reducción con hidracina, resultando eliminados todos los grupos funcionales que contienen oxígeno[68]. Otras reducciones de tipo químico incluyen el empleo de hidroquinona[77], disoluciones fuertemente alcalinas[78] gases como el hidrógeno[79], pero no resultan tan efectivas como la

[74] C.G. Lee, S. Park, R.S. Ruoff, A. Dodabalapur., Appl Phys Lett. 95 (2009) 023304.
[75] H.J. Shin, K.K. Kim, A. Benayad, S.M. Yoon, H.K. Park, I.S. Jung, et al., Adv. Funct. Mater., 19 (2009) 1987–1992.
[76] L.I. Zalan, F. Fueloep., Curr. Org. Chem. 9 (2005) 657–669.
[77] S. Wang, P.J. Chia, L.L. Chua, L.H. Zhao, R.Q. Peng, et al., Adv Mater 20 (2008) 3440–3446.
[78] Fan, W. Peng, Y. Li, X. Li, S. Wang, G. Zhang, et al., Adv Mater 20 (2008) 4490–4493.

reducción con hidracina y borohidrato. Sin embargo, presenta los inconvenientes de que el GO, sintetizado normalmente a partir del método descrito por Hummers o alguna versión modificada de éste, requiere el uso de oxidantes fuertes y peligrosos como el acido sulfúrico y el permanganato potásico, sin mencionar la toxicidad e inestabilidad de la hidracina usada para la reducción. En los últimos años se han estudiado nuevas formas de reducir químicamente el GO que sean menos peligrosas y respetuosas con el medio ambiente. Recientemente ha sido posible obtener la reducción del GO mediante el empleo de o–carboximetilcelulosa[80] y a través de zumo de té verde y polifenol como agente reductor[81].

La reducción de GO también puede lograrse térmicamente. El tratamiento con calor ayuda a eliminar los grupos funcionales del GO, expulsándolos se superficie en forma de dióxido de carbono[82]. Para ello es necesario emplear temperaturas superiores a los 1000ºC y asumir la pérdida de, aproximadamente, un 30% de la masa, además de aceptar la aparición de vacantes y defectos estructurales que pueden afectar a las propiedades mecánicas y eléctricas del óxido de grafeno reducido (rGO). El tratamiento solvotermal puede resultar un método simple para la reducción de GO, en el

[79] Z.S. Wu, W. Ren, L. Gao, B. Liu, C. Jiang, H.M. Cheng., Carbon 47 (2009) 493–499.
[80] E. Araque, R. Villalonga, M. Gamella, P. Martínez-Ruíz,J. Reviejo, J.M. Pingarrón, J. Mater. Chem. B 1(2013) 2289–2296.
[81] S. Hongjie, L. Yi, Sichuan University, Patente 201010229528, julio 2010.
[82] M.J. McAllister, J.L. Li, D.H. Adamson, H.C. Schniepp, A.A. Abdala, et al., Chem Mater 19 (2007) 4396–4404.

que se obtienen dispersiones de rGO en disolventes orgánicos con una temperatura de 200ºC[83], bastante inferior a los 1000ºC que se describía unas líneas más arriba.

La reducción electroquímica es una herramienta efectiva para modificar los estados electrónicos variando el potencial externo para cambiar el nivel de energía de Fermi de la superficie del material. El tratamiento electroquímico supone un método muy rápido, simple, eficiente, de bajo coste y respetuoso con el medio ambiente. La técnica consiste en eliminar los grupos funcionales ricos en oxigeno de la superficie del óxido de grafeno mediante la aplicación un potencial eléctrico a una disolución que lo contiene. Conforme avanza la reducción, la disolución va cambiando de color amarillo a marrón muy oscuro. La electroreducción no afecta a la morfología del óxido grafeno, solo a los grupos funcionales, por lo que el sistema aromático queda intacto[84]. La exfoliación electrolítica de grafito en agentes dispersantes como las mezclas de agua y líquido iónico han resultado ser también una forma efectiva de preparar grafeno de alta calidad[85].

- *Otros métodos de síntesis*

La síntesis de grafeno a partir de hidrocarburos aromáticos policíclicos (PAHs) ha sido considerada como una posible ruta alternativa para su

[83] S. Dubin, S. Gilje, K. Wang, V.C. Tung, K. Cha, A.S. Hall, et al., ACS Nano 4 (2010) 3845–3852.
[84] M. Zhou, Y. Wang, Y. Zhai, J. Zhai, W. Ren, F. Wang, S. Dong, Chem.Eur. J.15 (2009) 6116–6120.
[85] H.L. Guo, X.F. Wang, Q.Y. Qian, F.B. Wang, X.H. Xia, ACS Nano 3 (2009) 2653–2659.

obtención. La utilización de PAHs supone varias ventajas como preservar la solubilidad a través de la adhesión de cadenas alifáticas en los bordes, mejorar la dispersabilidad y preservar la geometría plana, aportando versatilidad al proceso de síntesis. En la bibliografía pueden encontrarse ejemplos en los que pequeñas y estrechas GNRs han sido obtenidas a partir de la deposición térmica de diferentes precursores sobre una superficie de oro. Estos precursores son 1,4-diiodo-2,3,5,6-tetrafenilbenceno ensamblado con ácido bromofenilborícо[86] y 10,10-dibromo-9,9-biantril[87]. Los PAHs elegidos como precursores se someten, en primer lugar, a una etapa de eliminación de sustituyentes halogenados. Los monómeros actúan como bloques de construcción para originar GNRs. El proceso de ensamblaje está regulado por una primera etapa de activación, en la que especies biradicales se distribuyen a lo largo de la superficie mediante un proceso de difusión para formar cadenas poliméricas lineales unidas a través de enlaces C–C. En una segunda etapa de activación térmica tiene lugar la deshidrogenación de las moléculas ensambladas, dando lugar a un sistema aromático completo.

La descompresión o apertura de CNTs ha sido otra aproximación a la obtención de láminas de grafeno pero al igual que en el caso anterior, solamente ha sido posible obtener GNRs. Las técnicas empleadas para este fin

[86] X.Yang, X. Dou, A. Rouhanipour, L. Zhi, H.J. Rader, et al., J. Am. Chem. Soc. 130 (2008) 4216–4217.
[87] J. Cai, P. Ruffieux, R. Jaafar, M. Bieri, T. Braun, S. Blankenburg, et al., Nature, 466 (2010) 470–473.

fueron la litografía por haz de electrones[88] y la sonicación química[89] de SWCNTs, y grabado por plasma de argón de MWCNTs[90].

En la Figura I.4.2 se recogen las principales aplicaciones del grafeno en función del método a través del cual se obtenga y se resumen algunas de sus características más importantes.

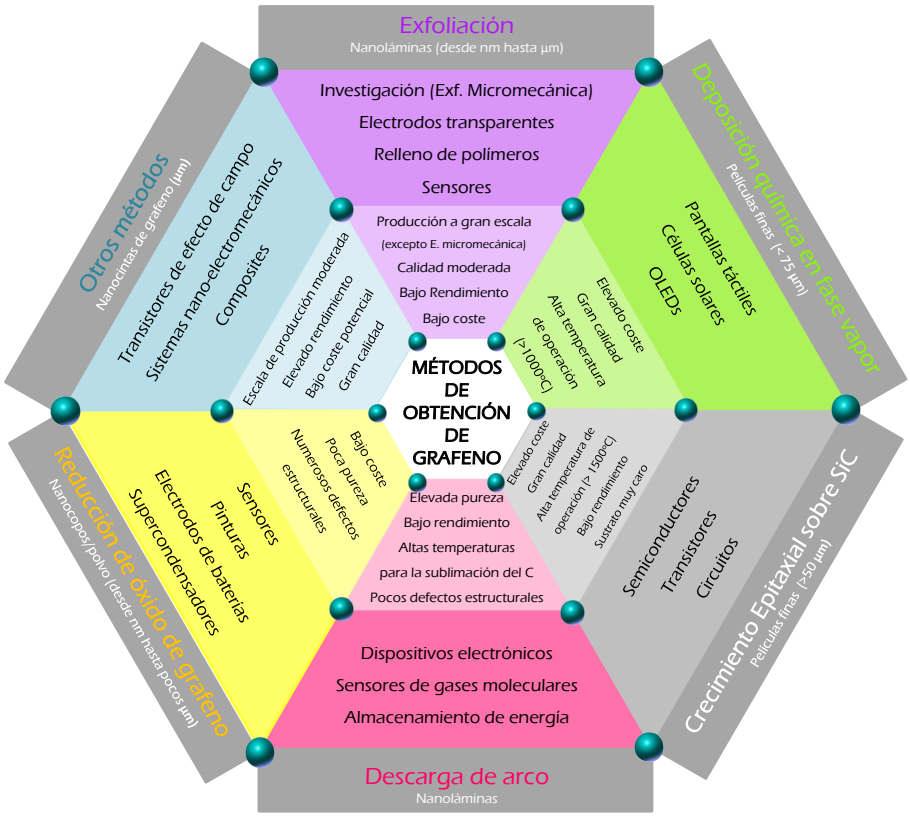

Figura I.4.2. Principales aplicaciones del grafeno según su método de obtención y características más importantes de cada método.

[88] M.Y. Han, B. Ozyilmaz, Y. Zhang, P. Kim, Phys. Rev. Lett. 98 (2007) 206805.
[89] J. Wu, H.A. Becerril, Z. Bao, Z. Liu, Y. Chen, P. Peumans, Appl. Phys. Lett. 92 (2008) 263302.
[90] L. Jiao, L. Zhang, X. Wang, G. Diankov, H. Dai, Nature 458 (2009) 877–880.

I.5. APLICACIONES ANALÍTICAS DEL GRAFENO Y SUS DERIVADOS

Las atractivas propiedades del grafeno y de los nanomateriales derivados de él (GO, rGO y GQDs) lo hacen un buen candidato para diversas aplicaciones electroquímicas como células de combustible, baterías y supersoncensadores, entre otras muchas.

Sus aplicaciones dentro del marco de la N&NA se centran principalmente en su empleo como material sorbente en procesos de extracción en fase sólida (SPE) y micro–extracción en fase solida (SPME), y en su aplicación a sistemas electroquímicos y ópticos para el desarrollo de sensores y biosensores.

Grafeno como material sorbente en extracciones.

El grafeno ha sido empleado como material sorbente en procesos de separación gracias a la gran capacidad de adsorción de distintos analitos debido su gran área superficial específica con carácter aromático, lo que le confiere una gran afinidad. Su morfología le confiere la capacidad de alcanzar un rápido equilibrio de absorción y elución del analito. Estas ventajas hacen

de él un material sorbente idóneo para la SPE y la SPME[91]. En este campo de aplicación el grafeno ha sido empleado en la extracción de diversos compuestos como contaminantes orgánicos[92] , medicamentos[93], metales[94], proteínas[95] y ácidos nucléicos[94]. Los resultados obtenidos empleando grafeno como material absorbente fueron, de forma general, mejores que los obtenidos mediante el empleo materiales sorbentes convencionales y otras nanopartículas de carbono.

Grafeno en electroanálisis.

En el campo del análisis electroquímico, el grafeno y los materiales de su familia han destacado notablemente debido a que poseen propiedades electroquímicas superiores a otros nanomateriales. El rGO ha sido el más empleado en este campo ya que muestra una alta conductividad eléctrica, flexibilidad y un transporte de las cargas sintonizable y eficiente. Puede usarse para detectar molecular que tienen un elevado potencial de oxidación o reducción[96]. Los defectos en la estructura de este nanomaterial y sus bordes le confieren una elevada velocidad de transferencia de electrones, de modo que cuanto más pequeñas son las láminas de rGO o grafeno, la detección

[91] Q. Liu, J. B. Shi, T. Wang, F. Guo, L. H. Liu, G. B. Jiang, J.Chromatogr. A 1257 (2012) 1–8.
[92] Q. Liu, J. Shi, J. Sun, T. Wang, L. Zeng, N. Zhu, G. Jiang, Anal.Chim. Acta, 708 (2011) 61–68.
[93] Y. B. Luo, Z. G. Shi, Q. A. Gao, Y. Q. Feng, J. Chromatogr. A 1218 (2011) 1353–1358.
[94] Y. Wang, S. Gao, X. Zang, J. Li, J. Ma, Anal. Chim. Acta 716 (2012) 112–118.
[95] Q. Liu, J. Shi, J. Sun, T. Wang, L. Zeng, G. Jiang, Angew. Chem. Int. Ed., 50 (2011) 5913–5917.
[96] M. Zhou, Y. Zhai, S. Dong, Anal. Chem. 81 (2009) 5603–5613.

electroquímica es más eficiente[97]. Estudios recientes han demostrado que esta velocidad de transferencia es mayor en rGO que en los electrodos de carbono vitrificado[98]. Los electrodos compuestos por rGO proporcionan una mayor área de reacción efectiva y capacidad de reacción gracias a la elevada relación superficie/volumen que presenta el óxido de grafeno reducido. Esta propiedad también le confiere la capacidad de ser un material apto para formar composites.

Los sensores electroquímicos basados en el grafeno, GO, y rGO han permitido la determinación de iones de metales pesados como, mercurio[99], cadmio y plomo[100], peróxido de hidrógeno[101] y biomoléculas como glucosa[102], catechol[103], ADN[104] y ATP[105], detectando incluso bacterias[106]. Entre las técnicas empleadas para su detección destacan la amperometría, la voltamperometría de pulso diferencial y la voltamperometría cíclica. Los límites de detección alcanzados con mediante el empleo de estas técnicas son del orden de los nanomoles y los micromoles por litro.

[97] A. Ambrosi, M. Pumera, Chem. Eur. J. 16 (2010) 10946–10949.
[98] X. L. Zuo, S. J. He, D. Li, C. Peng, Q. Huang, S. P. Song, C. H. Fan, Langmuir 26 (2010) 1936–1939.
[99] N. Zhou, J. H. Li, H. Chen, C. Y. Liao, L. X. Chen, Analyst 138 (2013) 1091–1097.
[100] J. Li, S. Guo, Y. Zhai and E. Wang, Anal. Chim. Acta 649 (2009) 196–201.
[101] J. W. Park, S. J. Park, O. S. Kwon, C. Lee, J. Jang, Anal. Chem. 86 (2014) 1822–1828.
[102] E. Araque, C.B. Arenas, M. Gamella, J. Reviejo, R. Villalonga, J.M. Pingarrón, J. Electroanalytical Chemistry 717-718 (2014) 96–102.
[103] E. Araque, R. Villalonga, M. Gamella, P. Martínez-Ruiz, A. Sánchez, V. García-Baonza, J.M. Pingarrón, Chem.Plus Chem. 79 (2014) 1334–1341.
[104] L. Wen, P. Wu, H. Zhang, C. X. Cai, Anal. Chem. 84 (2012) 7583–7590.
[105] B. J. Sanghavi, S. Sitaula, M. H. Griep, S. P. Karna, M. F. Ali, N.S. Swami, Anal. Chem. 85 (2013) 8158–8165.
[106] Y. Wan, Y. Wang, J. Wu, D. Zhang, Anal. Chem. 83 (2010) 648–653.

Grafeno en sensores ópticos.

Las propiedades ópticas del los materiales derivados del grafeno, y del grafeno en si mismo hacen de ellos nanomateriales muy interesantes para su aplicación en sensores ópticos para la detección de iones metálicos de plomo[107], ADN[108], proteínas[109] y pequeñas moléculas como dopamina[110]. Las técnicas ópticas más empleadas en el desarrollo de sensores ópticos basados en GO han sido la fluorescencia, la fotoluminiscencia y la transferencia de energía por resonancia de Föster (FRET), permitiendo la detección de estas sustancias a niveles tan bajos como nanogramos por litro.

En el caso de este tipo de sensores la mayoría de las aplicaciones que se han descrito se centran en el empleo de GO. La presencia de grupos funcionales en la superficie y bordes del GO hace que se confinen los electrones π dentro de los dominios de los carbonos con hibridación sp^2 dando lugar a una energía gap local que es inversamente proporcional al tamaño del dominio[111], que dan lugar a una brecha de energía local que escala inversamente con el tamaño del dominio. El óxido de grafeno puede mostrar fluorescencia desde el infrarrojo cercano hasta la región ultravioleta, sirviendo en ese caso como marcador en imágenes ópticas. Otras propiedades que hacen del GO una herramienta adecuada para el desarrollo de sensores

[107] X.H. Zhao, R.M. Kong, X.B. Zhang, H.M. Meng, W.N. Liu, et al., Ana.l Chem. 83 (2011) 5062–5066.
[108] X.L. Zhu, H.H. Zhang, C. Feng, Z.H. Ye, G.X. Li, RSC Adv. 4 (2014) 2421–2426.
[109] Y. Wang, L. Zhang, R. P. Liang, J. M. Bai, J. D. Qiu, Anal. Chem.85 (2013) 9148–9155.
[110] J.L. Chen, X.P. Yan, K. Meng, S.F. Wang, Anal. Chem. 83 (2011) 8787–8793.
[111] F. Long, A. Zhu, H.C. Shi, H.C. Wang, Anal. Chem. 86 (2014) 2862–2866.

ópticos son la elevada relación superficie/volumen, la habilidad para interaccionar con muchas moléculas a través de interacciones de tipo π–π, electroestáticas o hidrofóbicas.

Los puntos cuánticos de grafeno, como ya describimos en el apartado I.3 de esta introducción, son pequeñas láminas de grafeno con unas propiedades excepcionales que se han empleado extensamente en el campo de la Nanociencia y Nanotecnología Analíticas. Las aplicaciones esenciales de estos nanomateriales en este campo se centran en su empleo como sensores y biosensores de diverso tipo para la determinación de innumerables sustancias objeto de análisis.

En el Capítulo 1 de esta memoria se presenta un resumen detallado de las aplicaciones analíticas de los puntos cuánticos de grafeno más recientes. Además el capítulo enfoca la consideración de los GQDs como objeto de análisis (analito).

Capítulo 1

Graphene Quantum Dots in Analytical Science

Subbmited to TrAC–Trends in Analytical Chemistry

Submitted

Contents lists available at ScienceDirect

Trends in Analytical Chemistry

journal homepage: www.elsevier.com/locate/trac

Graphene Quantum Dots in Analytical Science

Sandra Benítez–Martínez and Miguel Valcárcel

Department of Analytical Chemistry, University of Córdoba, E-14071 Córdoba, Spain

Phone/Fax +34 957 218616; E-mail: qa1vacam@uco.es

Graphene quantum dots are small fluorescent nanoparticles that exhibit exceptional and unique properties, which make them attractive tools in several research areas. This review article provides an overview of their current position in the Analytical Chemistry field and resumes the analytical applications of GQDs. The review also covers the consideration of GQDs as target analyte, which is considered as one of the less explored facet of the Analytical Nanoscience and Nanotechnology. Herein an overview of the potential future directions of the analytical research field is also presented.

Keywords: graphene quantum dots, analytical science, analytical applications.

CONTENTS

1. INTRODUCTION

Graphene has attracted more and more attention on the scientific community since it was isolated as a single layer in 2004 by Novoselov and Geim using the "Scotch–tape method" from highly oriented pyrolytic graphite (HOPG) [1]. Graphene, with its truly two–dimentional (2D) planar structure, with a single atom thikness, consist of carbon atoms arranged in a honey–comb lattice with sp^2 hybridization. Between their unusual and exceptional properties it can be found a giant intrinsic mobility of the charge carriers, zero band–gap, high surface area and chemical stability. Graphene also exhibits superior mechanical, magnetic, optical and thermal properties [2]. The poor dispersion in solvents and the tendency to agglomerate are the main limitations of graphene. However, in the last years, the number of publications on this topic has been exponentially increased in many research areas, such as material science, physics, chemistry and engineering, but also in analytical chemistry (Figure 1).

Most recently, Graphene Quantum Dots (GQDs), a zero–dimensional photoluminescent (PL) carbon based nanomaterial, which consist on very small graphene sheets (typically between 3–20 nm) that exhibit exciton confinement and quantum size effect, has become an object of interest in the scientific community because of their exceptional properties. Due to graphene

is a zero–band gap nanomaterial it is not possible to observe their luminescence; however, it exhibits an infinite exciton Bohr radius and quantum confinement that could take place in finite sized graphenes [3]. The GQDs band gap is different to zero and can be tuned varying the size and the surface chemistry of GQDs [4]. These nanoparticles can be found as a single–, double– or multi–layer [5]. Quantum confinement and edge effect make them exhibit interesting properties such as fluorescent (FL) activity, robust chemical inertness, excellent photostability, high biocompatibility and low toxicity. It also should be highlighted their stable PL, resistance to photobleaching, tunable luminescence and great solubility in various solvents. Compared with colloidal inorganic semiconductors quantum dots (QDs), which have been attracted much attention in the last two decades owing to their electronic and optical properties [6], the use of GQDs is advantageous due to the high toxicity of QDs derived from the release of heavy metals from their core, namely cadmium, selenium, tellurium and zinc, buy also the toxicity of their coating.

On the contrary, GQDs are considered a kind of C-dots although some differences can be established in order to difference them. Carbon nanodots are considered quasi–spherical nanoparticles with diameters below 10nm which also exhibit PL properties. GQDs are defined as graphene nanosheets in single, double o few layers (less than 10) with lateral size below 100 nm which commonly presents functional groups (carboxylic, hydroxyl, carbonyl, epoxide)

at the edges which can act as reaction sites and produce changes in the PL emission due to the changing electron density [7] The quantum yield (QY) is an important factor to be considered when we talk about FL materials. GQDs show QY that ranged between 2% [8] and 46% [9] depending on the synthetic method and on the surface passivation [10], surface reduction [11] or further surface modification [12].

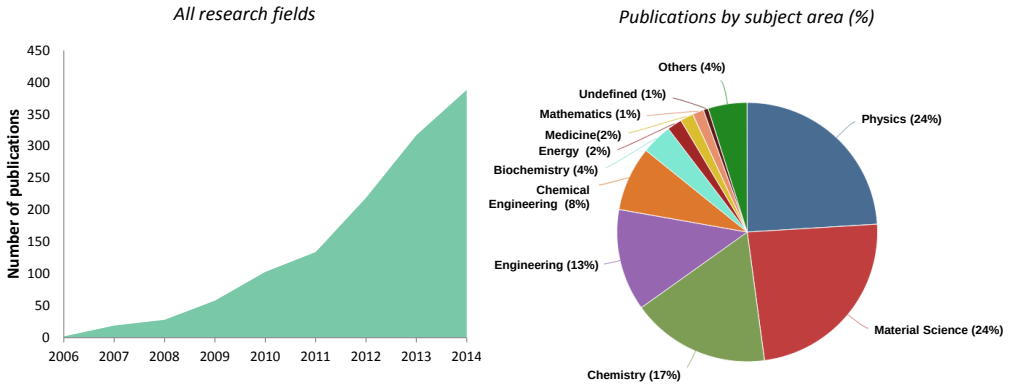

Figure 1. Exponential growth of the number of publications under the topic "GQDs" by year (left) and percentage of GQDs publications by application area (right).

2. SYNTHESIS

The synthetic methodologies of new nanomaterials are a crucial factor in Nanoscience and Nanotechnology since their exceptional properties can be tuned depending on synthesis, and subsequently, their shape, size, surface

characteristics and inner structure. Apart of that, in the presence of certain chemicals, the properties of such nanoparticles might be modified as well as distribution.

The strategies to synthesize nanomaterials can be traditionally classified in two main categories: the "top–down" and the "bottom–up" methods. A scheme of these both strategies is depicted in Figure 2.

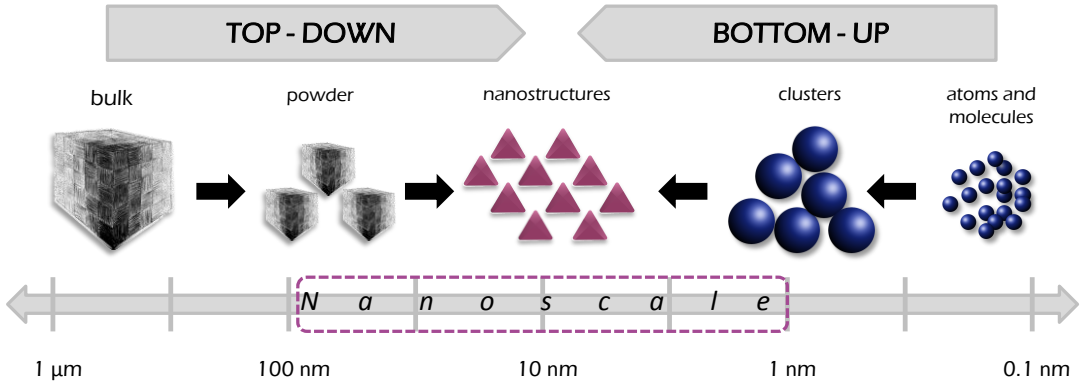

Figure 2. Scheme of the two approaches employed in the fabrication of nanomaterials:"top-down" and "bottom-up".

2.1. Top–down routes

In the top-down approaches, larger macroscopic materials (bulk materials) are restructured and externally controlled in order to reduce its size into a specific shape to obtain the desired nanomaterials. These new created

nanosized materials could exhibit very interesting and unique properties different from those showed by the raw materials. Generally, the top-down production of nanocomponents is expensive, slow, require of special equipment and critical synthesis conditions, with low production yield and may required toxic organic solvent and strong acids, making these approaches not suitable for large scale production [13, 10, 14]. In addition, such approaches introduce internal stress and imperfections in the crystallographic network that originate surface defects and structural damage, which may result in the modification of their superficial properties, owing to the high surface area per unit volume. However, these routes are the most commonly used in Nanoscience and Nanotechnology. The main precursors usually used in GQDs top–down synthesis are graphene oxide (GO) [15] coals [16] carbon fibbers [17], graphite (powder [18] and roads [19]), single–[20] and multi–walled carbon nanotubes [21] (SWCNTs and MWCNTs, respectively), carbon black [5], graphene [22] and, recently, metal–organic framework (MOF) derived porous carbon [23]. Amongst the top–down techniques the most widely used involve acidic treatment, hydrothermal and solvothermal synthesis, electrochemical preparation, laser ablation and exfoliation.

Synthetic chemical acidic procedures involve different acidic treatments for the cutting of bulk materials into GQDs. These treatments are based on the use of concentrated strong acids such as nitric acid [5, 24],

mixtures of nitric and sulphuric acids, in different proportions –(3:1) and (1:3) [15, 17]– but also some of them required ultrasonic radiation [20, 25] or nitric acid and amidative cutting treatment[18], all of them combined with temperatures up to 80ºC and solution stirring.

Hydrothermal routes for the GQDs production include those in which the carbon based raw materials are dissolved or dispersed in water and are put into a closed container (an autoclave, generally) and heated at temperatures above the water boiling point (180-200ºC) and high pressures for a time that range from 2 to 12 hours [19, 26–28]. Solvothermal synthesis of GQDs is characterized for the use of organic solvents, as dimethyl formamide (DMF) [29], and similar temperatures and times as hydrothermal routes. Figure 3 shows a schematic representation of the hydrothermal treatment of SWCNTs for the GQDs production.

Electrochemical preparation of GQDs could be achieved by applying an anodic potential of 1 V for 7, 11 and 15 h to a MWCNTs coated working electrode, in which the applied electric field initiates the fracture of the micromaterial [30]. The electrolysis of a graphite road with a current intensity in the range of 80–200mA cm^{-2} in a 0.1M NaOH solution [19] and the electrochemical reaction of a graphene oxide film working electrode into a

0.1M PBS solution by the application of a ± 3 V using cycling voltammetry [31] also allows the GQDs fabrication.

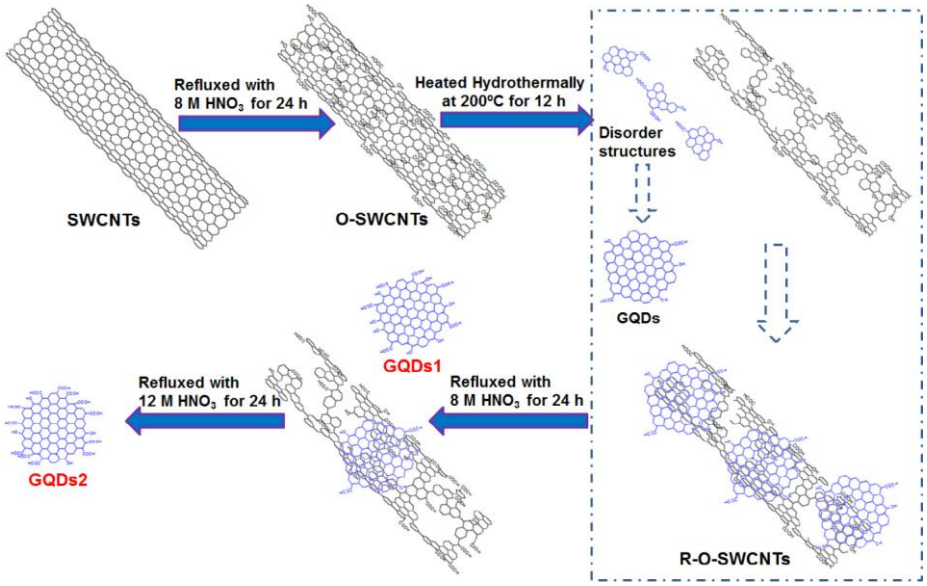

Figure 3. Diagram for the preparation of GQDs from the hydrothermal treatment of SWCNTs. Reproduced with permission of reference 20.

Recently, GQDs has been synthesized by laser ablation of HOPG in aqueous media using a fentosecond laser (800nm, 35s of pulse during 20 min) [32]. Graphite power has also been irradiated with a Nd:Yag laser in the presence of benzene (1064nm, 10 ns of pulse, for 30 min) in order to obtain GQDs [33].

Among the most used top–down method, it should be mentioned the ultrasonic assisted exfoliation of graphite nanofibbers [34], the electrochemically exfoliation of graphene [22], the organic solvent assisted exfoliation of graphite nanoparticles [35] and the exfoliation and disintegration of graphite flakes and MWCNTs by the intercalation of high reactive potassium between layers and walls, respectively [36]. The one–step ultrasonication–redox treatment of GO with $KMnO_4$ to obtain high quantum yield GQDs, in a short reaction time without the addition of any acid, has been recently published [37]

2.2. Bottom–up approaches

The bottom–up routes lead to the synthesis of nanomaterials from the assembly of basic building blocks with suitable properties, which can be grown from elemental precursors such as atoms, molecules, or nanoclusters, by controlling the interaction between them, resulting in an environmental–friendly production of GQDs large scale [38, 39]. These types of strategies have several advantages, such as introduction of fewer defects, achieved more homogeneous chemical composition, precise control over the morphology and the size distribution of the products. However, few publications about these promising approaches are found in the literature compared to those found for the top–down routes. For instance, ethylene gas was continuously injected into an argon plasma to generate a carbon atomic beam, which

being flowed through a carbon tube dispersed in a chamber, could generate size controllable GQDs [40]. Haloaromatic molecules, such as chlorobenzene and dichlorobenzene, have been also used as carbon sources for laser induced photochemical stitching [41]. The oxidation of polyphenylene dendritic precursors by solution chemistry led to the formation of GQDs [3]. Hydrothermal treatment combined with: (i) a previous carbonization of polycyclic aromatic hydrocarbons (PAHs) with strong acids (H_2SO_4) [42] and (ii) a microwave heating of glucose, sucrose or fructose water solutions [43] also allowed the GQDs creation. The pyrolysis over 200ºC of L–glutamic [44] and citric acid [45] (Figure 4) are two facile and quick bottom–up methods for the synthesis of these highly FL nanoparticles. As a combination of both routes, alginate has been pyrolyzed to form a graphitic carbon material which has been pulser laser ablated in order to form multilayer graphitic quantum dots [46].

In general, depending on the chosen synthetic route (top–down or bottom–up) and the synthetic conditions is possible to prepare GQDs with tunable blue, green, yellow or even red luminescence. It has been reported that the PL emission could be size–, excitation– and solvent– dependant commonly. Their diameter size can be ranged from 1.5 to 30nm and the quantum yield could be between 1.8 and 14%. The shape of their edges, zig–zag or armchair, also affects the GQDs properties and their PL.

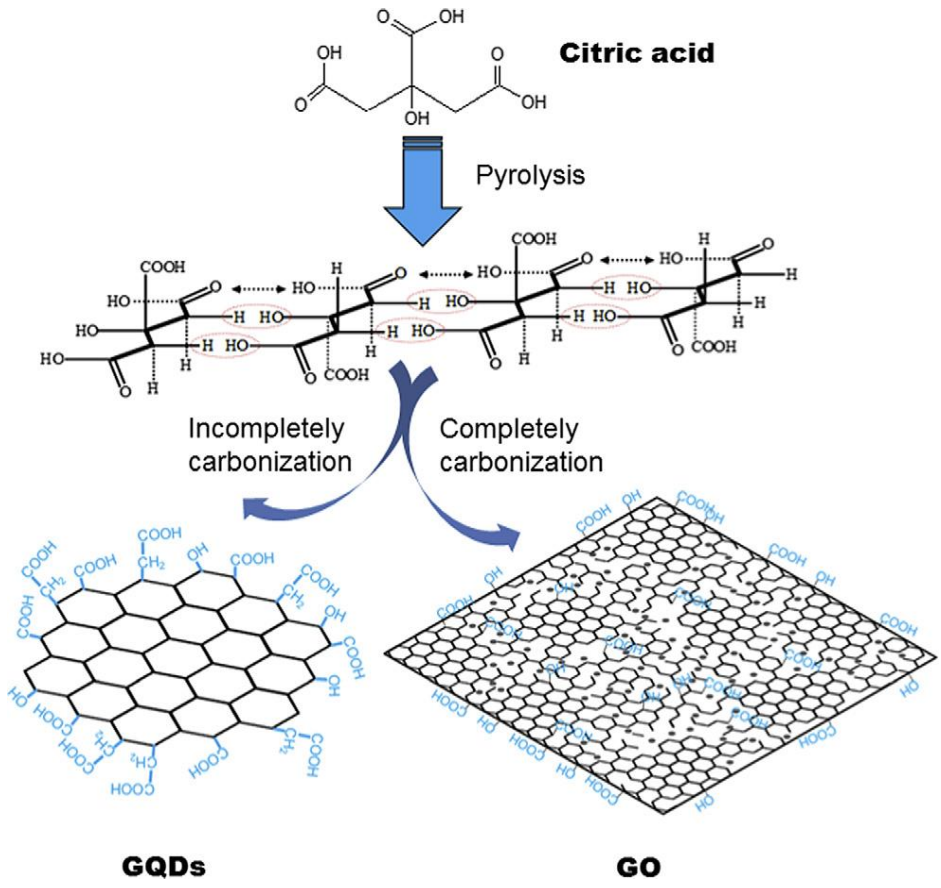

Figure 4. *Diagram for the synthesis of GQDs and GO. The black dots in the GO represent oxygen atoms. Reproduced with permission of reference 45.*

2.3. Doped and functionalized GQDs

The crystalline network of GQDs is composed of carbon atoms arrange in a honey comb lattice as graphene. The chemical structure of these nanoparticles is similar to that of graphene oxides (GO), having oxygenated

groups (hydroxyl, carboxyl, epoxy and carbonyl) at their edges [28]. Although GQDs can show strong FL, they often exhibit low QY and limited tunability. The introduction of heteroatoms (namely nitrogen [23, 47] and sulphur [48]) in the carbon chain allows the effectively tuning of their physical and chemical properties. Nitrogen has been widely used for doping carbon nanostructures owing to a comparable atomic size for bonding with carbon atoms. Sulphur, oxygen [49], boron [50] and fluoride [51] are other heteroatoms less used to obtain doped GQDs. Due to the quantum confinement and edge effects, heteroatoms could penetrate directly in the carbon lattice and modulate the electronic, optical and chemical properties creating more reactive sites.

Doped GQDs can be prepared as a consequence of both top–down and bottom–up routes. Among the top–down techniques the most used for getting N–doped GQDs (Figure 5) are hydrothermal [52–54] and solvothermal [55] synthesis from GO using different nitrogen sources such as ammonia [52, 53] ammonium hydroxide [54] or dimethylformamide (DMF) [55]. The cutting of preoxidized N–doped graphene could be another hydrothermal treatment to obtain N–GQDs [56]. Nitrogen doped GQDs have also been obtained from the streaming treatment of MOF–derived porous carbon in presence of HNO_3 [23].

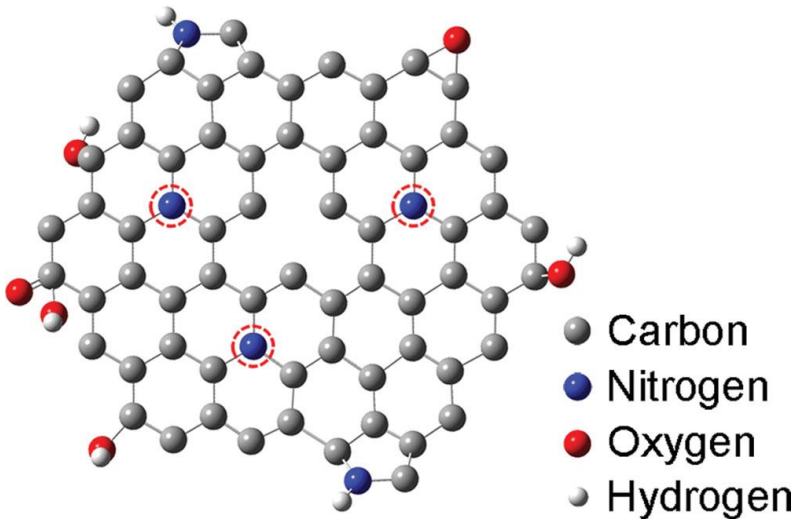

Figure 5. Schematic illustration of the structure of the N-GQDs. The red, dash circles highlight three substitutional N atoms. To demonstrate the possible defect structure of the N-GQDs, one C atom is removed from the center of the model. Reproduced with permission of reference 54.

Cyclic voltammogram on graphene can generates N–GQDs using tetrabutylammonium perchlorate (TBAP) in acetonitrile as electrolyte and nitrogen source [57]. The cutting of graphene, directly grown in a Cu substrate by CVD, using nitrogen plasma has also been described [47]. Figure 6 illustrates this process.

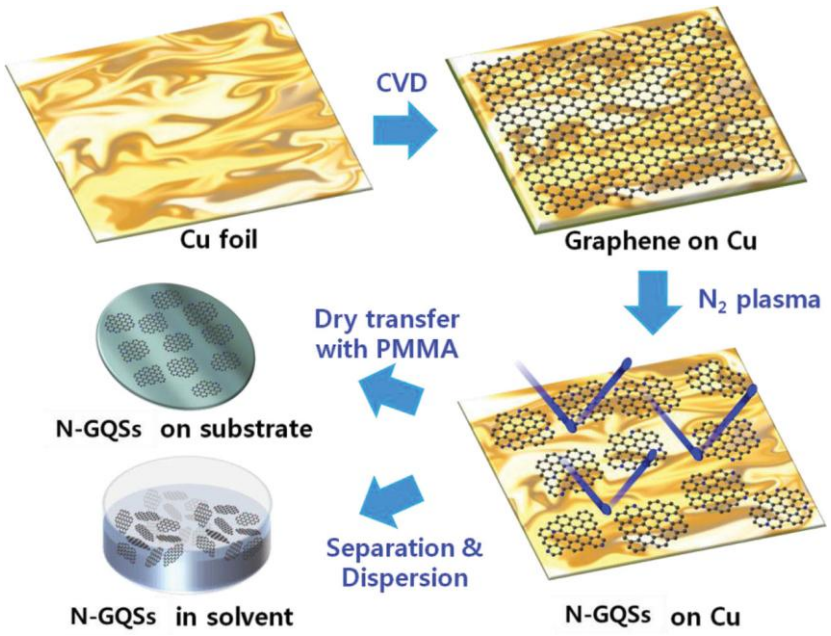

Figure 6. Schematic illustration of N–GQDs fabrication process by nitrogen plasma. Reproduced with permission of reference 47.

Among the bottom–up routes for the N–doping of these dots it is worthy to mention the hydrothermal carbonization of citric acid, as carbon source, in presence of ammonia [58], dicyandiamide [59, 90] and hydrazine [60]. N,S–codoped GQDs by hydrothermal [61, 62] and solvothermal [63] preparation, and O,N,F–GQDs [49] and graphene fluoroxide quantum dots [64] synthesis, have also been described in the literature.

Various chemical modification methods have been developed to modulate GQDs properties by introducing different functionalities. The amidation of the carboxylic groups at the edges has been extensively studied. For example, the surface modification with alkylamine increased the QY in 205% if compared with the non functionalized GQDs [67]. In fact, amino groups tuned the FL and enhanced the QY over 16.4%–40% [68–70]. After a hydrothermal treatment with ammonia solution, and aryl groups improved the GQDs QY for up to about six times [71]. The surface passivation of GQDs by polyethylene glycol (PEG) (trough the reaction of –OH from PEG with –COOH from GQDs) could only partially enhance their PL between 13%[65] and 15% [66], as well as PEG make them more soluble. Surface functionalization with small organic molecules such as alcohols, diamines, thiols, ionic liquid and glutathione (GSH) [72, 18, 20, 73] could also modulate the PL of GQDs. Recent studies on surface modification have shown that surface oxidation [74] or reduction [11, 75] can be used to alter the PL properties and improve the optical performance of GQDs. The post–synthesized hydrothermal treatment has also been proved to regulate the PL properties of GQDs obtained by different routes and bulk material by removing epoxy and hydroxyl groups from the GQDs surface (Figure 7) [76]. As a result of the combination of both doping and functionalization, N–doped and amino–functionalized GQDs (NA–GQDs) were obtained by a single–step thermolysis strategy by using

glycine as both carbon and nitrogen source [77]. Although all these alternative promising methods have been demonstrated to be effective approaches to enhance the GQDs luminescence, the enhanced PL mechanism remains unclear and needs to be explained in depth.

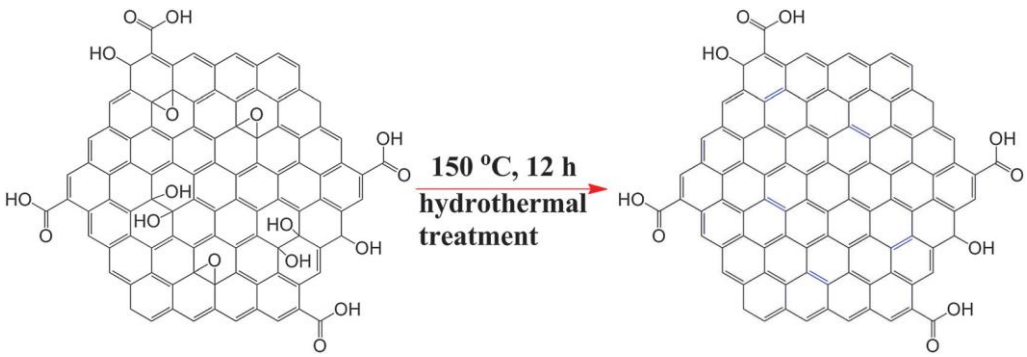

Figure 7. The scheme of hydrothermal treatment of GQDs. Reproduced with permission of reference 76.

3. ANALYTICAL APPLICATIONS OF GQDs

Since their emergence, GQDs has been widely used in several fields such as photovoltaics [79], organic light emitting diodes [44], fuel cells [80] and drug delivery [81]. In recent years, many applications have been developed in the Analytical Chemistry field owing to the ignited increased

research interest caused by the exceptional and unique properties of GQDs. In this area, GQDs have emerged as new potential tools in the design and tuning of PL sensors and biosensors (probes, electrochemical sensors and hybrid sensors), such as immunosensors and aptasensors. Other analytical areas such as Raman spectroscopy and capillary electrophoresis are far less explored.

3.1. Sensors and biosensors

On the basis of the exceptional properties of these nanoparticles, different types of sensors based on GQDs or doped and functionalized GQDs have been developed for the detection of metal ions, small organic molecules and biomaterials in order to improve sensibility, selectivity and nonspecificity of GQDs.

3.1.1. Photoluminescent–based sensors

GQDs–based FL sensors have been focused in the detection of ionic species, small organic molecules and biomaterials.

3.1.1.1.Probe sensors

Most studies involve the determination of Fe^{3+} [23, 24, 43, 49, 59, 61, 78], Cu^{2+} [69, 82, 83], Al^{3+} [84] and the hazardous Hg^{2+} [85, 86], Cr^{6+} [87] and Ni^{2+} [88]. The detection of Fe^{3+} has been the most studied up to now probably due to the important role played in biological systems for the role played in many regulatory processes. Recently, H. Xu et *al.* [24] reported a sensor based

on N–GQDs obtained from vapour cutting of MOF–derived porous carbon for the selective FL detection of Fe^{3+} in real water samples. The phenolic hydroxyl groups on N–GQDs coordinate the ferric ions providing the high selectivity of the proposed method. Such complex formation prootes the photo–induced charge transfer from N–GQDs to Fe^{3+}. This photo-induced charge transfer could cause a perturbation of the electronic states of the N-GQDs as well as non-radiative transitions, leading to a significant FL quenching. The limit of detection (LOD) achieved was 0.08 μM.

S. Li et *al.* [49] have synthesized sulphur–doped GQDs by one–step electrolysis of graphite and used them as an efficient FL probe for the selective detection of Fe^{3+} in human serum, with a LOD of 4.2 nM. The incorporation of S atoms in the carbonaceous skeleton tuned the electronic local density of GQDs promoting the coordination of the phenolic hydroxyl groups at the edges of S–GQDs and Fe^{3+}, being such a very specific interaction responsible of the PL quenching of S–GQDs. Figure 8 shows the performance of the Fe^{3+} sensing and the quenching mechanism of S–GQDs. L. Li et *al.* [78] have used NA–GQDs to develop a method for the determination of Fe^{3+}in tap water, through the attenuation of the FL emission. The LOD reached was 0.1 μM. N–doped and amino acid–functionalized GQDs were obtained by hydrothermal treatment of glycine as both carbon and nitrogen source. The role of nitrogen

atoms was mainly to act as chelating sites for the Fe^{3+}, being the FL of GQDs effectively quenched.

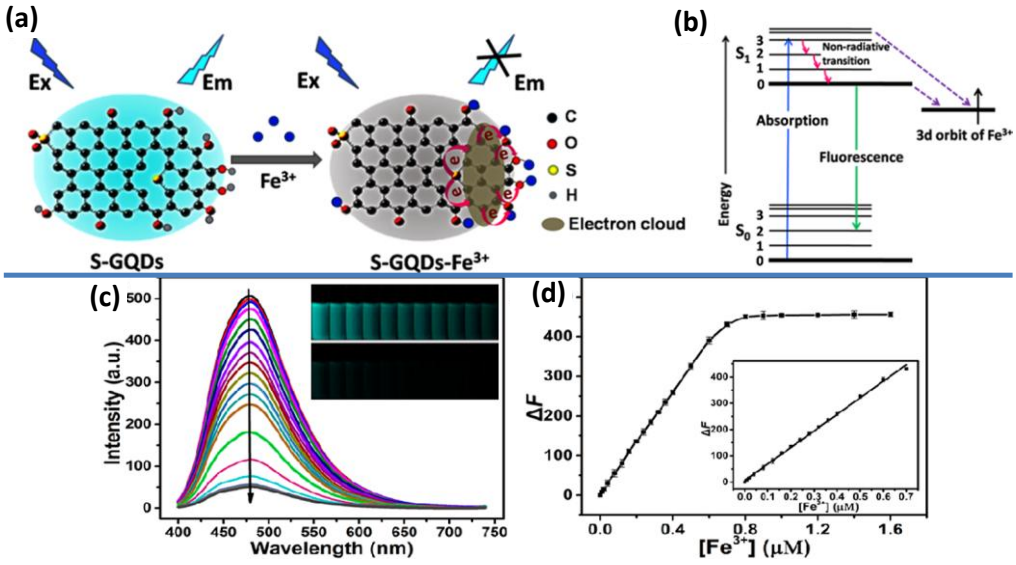

Figure 8. *(a) Fluorescence quenching mechanism of the S-GQDs in the presence of Fe^{3+} and (b) the Electron Transfer Process from S-GQDs to Fe^{3+}. (c) Fluorescence spectra of S-GQDs (5 μg/mL) with different concentration of Fe^{3+}. The inset in (c) shows photographs of S-GQD aqueous solutions with different concentration of Fe^{3+} under UV irradiation (365 nm). (d) The curve of the fluorescence quenching values ΔF vs Fe^{3+} concentration ranging from 0 to 1.60 μM. The inset in (d) is the linear calibration plot for Fe^{3+} detection. Reproduced with permission of reference 48.*

T. V. Tam et *al.* [59] reported the development of a green and inexpensive very sensitive and selective sensing platform for Fe^{3+}, by employing N–GQDs prepared from the carbonization of citric acid and their

post hydrothermal treatment in the presence of ammonia. Authors suggest that metal ions may form metal hydroxides by coordination with hydroxyl groups at the surface and edges of N–GQDs. The as–formed complexes would restrain the recombination excitons and facilitate the charge transfer, resulting in a FL quenching.

A. Ananthanarayanan et *al.* [23] took advantage of IL modified GQDs obtained from electrochemically treated 3D graphene assisted by ionic liquid to optically detect Fe^{3+}. The incorporation of $BMIMPF_6$ in the reaction media not only improved the exfoliation and dispersion of GQDs but also get stacked at the nanoparticle surface, increasing the affinity of ferric ions to GQDs through the imidazole rings. They proved that Fe^{3+} induced the aggregation of $BMIM^+$–GQDs since the ferric ions were acting as coordinating centre to bridge several functionalized GQDs. Consequently, the FL emission was quenched. Figure 8 shows a schematic illustration of the synthesis and mechanism detection described. The theoretical LOD of this approach was 7.22 μM.

A label free detection platform for the detection of Fe^{3+} in real water samples was reported by J. Ju et *al.* [61]. The authors used N–GQDs, synthesized through hydrothermal hydrazine treatment of GQDs, previously prepared by pyrolyzing citric acid, as FL probe. The estimated LOD was 90nM.

The chelation of ferric ions with N could bring them into close proximity, so the FL emission of N–GQDs decreased with increased the Fe^{3+} concentration. The detection could be achieved due to the nitrogen doping that could induce modulation of the chemical and electronic properties of GQDs and promote their complexation with ferric ions.

L. Zhou et *al.* [43] reported a sensitive and selective quenching effect of GQDs (created from the carbonization of PAH precursors, mainly pyrene) to Fe^{3+} with a LOD of 5 nM. The selectivity for ferric ions was also attributed to the specific coordination between phenolic hydroxyl groups, at the GQDs edges, and Fe^{3+}. The combination of GQDs and the Fe^{2+}/ Fe^{3+} redox couple was also exploited to serve as an efficient sensing platform for H_2O_2 detection. X. Wu et *al.* [45] also developed a label free GQDs–based colorimetric sensor for the detection of H_2O_2. GQDs were synthesized by the one–step pyrolysis of L–glutamic acid. Their system is based on the colour change of a containing peroxidise substrate ABTS (2,2'-azino-bis(3-ethylbenzothiazoline-6-sulphonic acid) GQDs solution, which change from yellow to green as consequence of the reduction of hydrogen peroxide (catalyzed by GQDs).

Copper ions play a critical role in biological and environmental areas since it is an essential trace element for plants, animals and humans. However, long term–exposure to high copper levels can cause gastrointestinal, liver and

kidney damage. For this reason, analytical GQDs–based methods have recently emerged. X. Liu et *al.* [82] described the easy absorption of Cu^{2+} ions on pristine GQDs prepared by the chemical oxidation of pitch graphite fibbers. Biothiol cysteine was added to the aqueous solution recovering the PL quenching caused by the complexation of GQDs and Cu^{2+}, owing to the ability of cysteine to capture metal ions, suppressing the charge transfer from GQDs to copper ions. This mechanism makes this system a turn–on method for the detection and quantification of Cu^{2+} in real water samples with a LOD of 0.33 μM.

F. Wang et *al.* [83] prepared GQDs via hydrothermal route using reoxidized graphene oxide in order to develop a FL sensing platform for highly efficient detection of Cu^{2+}, with a LOD of 0.226μM. The FL was effectively quenched through the complexation of Cu^{2+} and GQDs by a static mechanism. H. Sun el *al.* [69] used amino functionalized GQDs (af–GQDs) for the sensing of copper ions based on the higher binding affinity and faster chelating kinetics of Cu^{2+} with N and O widely presents on the af–GQDs, with a theoretical LOD of 6.9nM. The FL quenching, which was suggested to be caused for both static and dynamic mechanism, might was caused by the nonradiative electron/hole recombination annihilation through an effective electron transfer process.

Al^{3+} ions have negative effects in human health when they appear in drinking waters, have been found to. Z. Fan el *al.* [84] reported boron functionalized GQDs–based chemosensor for the detection of Al^{3+}. Green luminescent B–GQDs were electrochemically prepared from a graphite rod as anode and a Pt foil as cathode in a borax aqueous solution. The sensor exploits the FL intensity enhancement of B–GQDs after their interaction with aluminium ions (Figure 9). The LOD achieved was 3.64 μM, which was lower than that of the World Health Organization.

Among heavy metal ions, Hg^{2+}, Cr^{6+}, Ni^{2+} and Cd^{2+} are hazardous and pervasive pollutants with high toxicity and adverse impact on human health. Several methodologies have been developed in order to detect and quantify them in different media. B. Wang et *al.* [85] studied a GQDs–based sensing probe of Hg^{2+} in which the blue emitting FL dots were prepared by an ultrasonic route from graphene. The sensor was based on the gradually FL intensity decrease when increasing the Hg^{2+} concentration. The LOD achieved was of 10 μM. The FL quenching mechanism was attributed to both facilitate non–radiative electron/hole recombination annihilation through an effective electron transfer quenching, and the aggregated–induced quenching caused by the affinity of mercury ions towards carboxylated groups at the edge of GQDs.

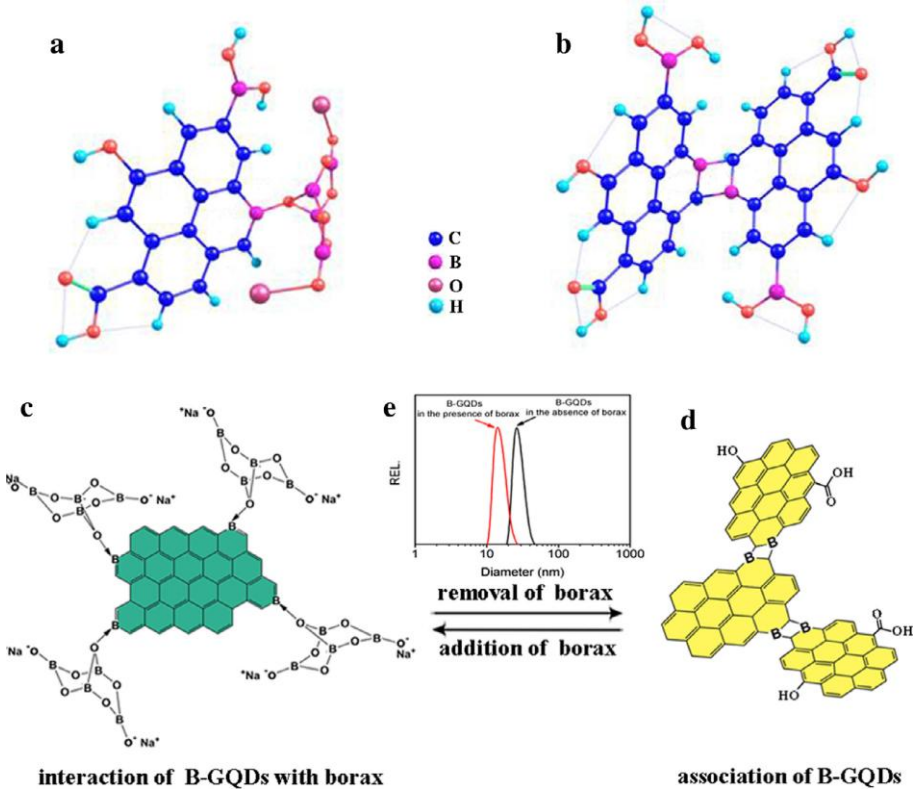

Figure 9. *The ground state structures of one luminescent unit of B-GQDs in the presence (a) and absence (b) of borax obtained by theoretical calculation with density function theory. (c) The size distribution of B-GQDs in the presence (left) and absence (right) of borax determined by DLS. The structure illustration of B-GQDs in the presence (d) and absence (e) of borax, respectively. Reproduced with permission of reference 83.*

Taken advantage of the same effect, H. Chakraborti et *al.* [86] developed a Hg^{2+}sensor in 100% aqueous solution with a LOD of 3.36 μM. GQDs, with carboxyl and hydroxyl functionalization at their edges, were obtained by tailoring the carbonization degree of citric acid and emitted blue PL. Functional groups could act as binding sites for Hg^{2+} and, in addition, their adsorption at GQDs surface could explain the FL quenching, being implied both static and dynamic mechanisms.

F. Cai et *al.* [87] determined Cr^{6+} using strong blue PL N–GQDs as FL probe in real waters samples with a LOD of 40 nM. The N–GQDs were obtained by one–pot hydrothermal treatment of citric acid and ammonia. The quenching–based sensing mechanism was attributed to reduction of Cr^{6+} to Cr^{3+}, which was probably promoted by –OH groups and nitrogen in the N–GQDs.

H. Huang et *al.* [88] reported a metal ion sensor based on a quenching–recovering strategy for the Ni^{2+} detection with a sensibility of 4.1 μM. GQGs, which emitted violet PL, were prepared by chemical oxidation of carbon fibbers. Photoinduced electron transfer from GQDs to metal ions (with partly filled d orbitals) could cause perturbation electronics effects on GQDs as well as non–radiative transitions, leading to the FL quenching of GQDs. The introduction of a competitive chelator for Ni^{2+}, such as dimethyldioxime (DMG)

as recovering agent, allowed achieving the selective detection of niquel ions. Mn^{2+}, Co^{2+}, Cu^{2+} can also be detected applying the same sensing strategy.

The monitoring of other anionic species in environmental matrices has also been an object of interest in the last years. T. Hallaj et *al.* [89] demonstrated that blue luminescent GQDs obtained by the direct pyrolysis of glucose could be used to detect ClO^- in presence of CTAB, giving rise a proportional chemiluminescent enhancement of GQDs, which was used as analytical signal. ClO^- was able to oxidize GQDs enhancing their chemiluminescence (CL). The LOD obtained was 30 μM and the sensing mechanism was attributed to a chemical reaction between GQDs and ClO^-. The system was applied to the determination of free chlorine in tap and pool waters. Y. Dong et *al.* [90] constructed another free chlorine sensor–based on surface passivated blue GQDs, synthesized by the pyrolysis of citric acid. In this case, the strong oxidative ClO^- was capable to destroy the self–passivated GQDs surface, leading to the FL quenching. The LOD of detection calculated was 50 μM.

A quantitative pH sensor for environmental and intracellular applications was developed by Z. L. Wu et *al.* [91] exploiting the FL properties of N–GQDs prepared by the hydrothermal treatment of dicyandiamide (DCD) and citric acid as nitrogen and carbon source, respectively. N–doped GQDs

(emitted at 452nm) were photostable and pH–sensitive between 1.81 and 8.96 giving a general pH sensor with a wide range of applications from real waters to intracellular contents.

J.–M. Bai et *al.* [92] proposed a rapid, sensitive, specific and pH dependent PL off–on GQDs–based sensor of phosphate ions. In this assay, GQDs FL is switched–off by the energy transfer after the addition of Eu^{3+}, due to the formation of a coordination complex with carboxylated groups that induce the GQDs aggregation. When phosphate is present, Eu^{3+} ions prefer their binding with oxygen donors of phosphate than with those of carboxylic groups at the GQDs edges, leading to the recovery of the FL of GQDs. The LOD was very low, 0.1 μM, and the method could be used in complex environmental samples.

J.–J. Liu et al. [93] also developed an "off–on" sensor based on glutathione functionalized GQDs (GQDs@GSH) as FL probes for ATP (adenosine triphosphate) and phosphate containing molecules, in general. Blue luminescent GQDs@GSH were prepared by the one–pot pyrolysis of citric acid and GSH. The sensor mechanism was based on the FL quenching of GQDs@GSH in the presence of Fe^{3+} due to GSH could acts as ligand for chelating ferric ions, establishing an effective electron transfer between GQDs@GSH and Fe^{3+}. Phosphate containing molecules acted as complexing

molecules for Fe^{3+}, since phosphate ions have a great affinity for iron ions through Fe–O–P bonds, leading to the FL recovery of the functionalized GQDs. The quenching effect was due to a dynamic mechanism. The estimated LOD was 22 μM for ATP, and it was applied in real samples assays in cell lysates and human blood serum.

In regards to small organic molecules and biomaterials, Y. Zhu et *al.* [38] used ultrasonication–reduction treatment of GO to prepare GQDs, which were used to detect alkaline phosphatise (ALP). Taken advantage of the coordination of GQDs with Cu^{2+} and pyrophosphate (PPi) affinity for Cu^{2+}, previously reported, the authors designed GQDs based sensor for the detection of ALP, in which the chelation of Cu^{2+} and PPi induced changes in the GQDs FL. For the general sensing procedure, ALP at different concentrations was incubated with PPi at 37 °C for 60 min in Tris-HCl. After incubation, Cu^{2+} was added into the reaction solution and incubated for 10 min. Ultimately, GQDs solution was added to the mixture containing ALP, PPi and Cu^{2+}, and incubated for 30 min at room temperature. After the addition of ALP, PPI was hydrolyzed to generate Pi disrupting the complexation between PPi and Cu^{2+}. The copper ions liberated reacts with GQDs through $–COO^{-}$ Cu^{2+}–OH and an energy transfer took place between Cu^{2+} and GQDs. Consequently, FL quenching of GQDs was observed and used as analytical signal for the determination of ALP. The LOD was found to be 17 pM. Based

on the fact that Cu^{2+} could quench the FL intensity of GQDs, the as-prepared GQDs can be directly used to detect Cu^{2+} with an incubation time of 30 min, achieving a LOD of detection of 13nM.

Q. Zhang et *al.* [94] designed a simple turn–on method for the PL sensing of amino acids based on the quenching caused by the formation of aggregates by the interaction of Eu^{3+} with GQDs as previously described in reference 90. The blue luminescent GQDs were obtained by oxidation with strong acids and showed both up–conversion and down–conversion PL properties. The PL could be recovered by the competition of amino acids with GQDs for Eu^{3+}, leading to the sensitive detection of glutamic acid (Glu) and aspartic acid (Asp). The LODs for Glu were of 0.19μM and 0.32 μM calculated by up– and down–conversion, respectively. The LODs achieved for Asp were of 0.18 μM and 0.32 μM also for both mechanisms. J. Ju et *al.* [59] presented a FL turn–on sensing system for the detection of GSH. Highly blue–luminescent N–GQDs were synthesized by the hydrothermal treatment of citric acid and dicyandiamide. The system is based on the PL quenching of N–GQDs by Hg^{2+} due to electrostatic interactions and electron energy transfer between both of them. Upon the addition of glutathione the PL of N–GQDs was recovered owing to a major affinity of mercury ions towards S atoms of GSH. The LOD of this label system was 87 nM. Also introducing Hg^{2+} in the sensing system,

L. Li et *al.* [95] developed a GQDs–based sensor for the detection of melamine. In this case, mercury ions coordinate with melamine and their complexation makes the blue FL of GQDs be quenched. Separately, neither mercury nor melamine produced significant changes in the GQDs emission. The LOD achieved by this turn–off sensing mechanism was 0.12 μM, which was comparable with other published methods. Z. Wu et *al.* [96] created a FL turn–on detection system based on GQDs for the detection of biothiols GSH, cys and homocysteine (Hcy). Hg^{2+} ions were used to quench the blue FL of GQDs prepared by citric acid pyrolysis, due to their complexation. When a specific biothiol molecule was added to the mixture GQDs–Hg^{2+}, it bounded to mercury ions through Hg–S bonding interactions between the thiol functional group and Hg^{2+}. Subsequently, the GQDs–Hg^{2+} complex was dissociated, the Hg^{2+} removed from GQDs surface and emission intensity of GQDs restored. The LOD achieved by this turn–on approach were 5, 2.5 and 5 nM for GSH, Cys and Hcy, respectively, being applied in real serum samples.

GQDs prepared by pyrolysis of citric acid served to Z. Li et *al.* [97] to develope a sensor for 2,4,6–trinitrophenol (TNP) in which such explosive substance was able to form a complex with GQDs through strong π–π stacking interactions. GQDs acts as donor and TNP as acceptor in a FL resonance energy transference (FRET). The presence of the nitro–group was demonstrated to be essential for the attenuation of the FL of GQDs as well as

the presence of both hydroxyl and nitro groups in the phenol structure. The LOD reached was 91nM. A few years before, L. Fan et *al.* [98] reported the ultrasensitive detection of 2,4,6–trinitrotoluene (TNT) in solution with the aid of multicolour GQDs prepared from the oxidation of GO strong acids. The proposed mechanism involved the energy transfer that was the same as the explained above for TNP, i. e. FRET when the TNT was bounded at the GQDs surface acting as an acceptor and suppressing the GQDs FL. TNT could clearly be detected from 2.2 μM (0.495 $mg{\cdot}L^{-1}$).

Y. Li et *al.* [99] found that dihydroxybenzene (DHB), in the form of o–DHB, p–DHB and m–DHB, could be oxidized to form a benzoquinone, in the presence of H_2O_2 and horse radish peroxidise (HRP), and effectively quench the blue FL of GQDs obtained from pyrolyzed citric acid. Benzoquinone as good electron acceptor could transport the electron from the conduction band to the valence one of the excited GQDs state, leading to a FL atenuation. Authors concluded than the nature of the quenching process involved static mechanism rather than dynamic one. The theoretical LODs for o–DHB, m–DHB and p–DHB were 20 nM, 80nM and 30nM, respectively. The method could be applied for DHB sensing in rain– and tap–water. By synthesizing the FL probes in the same way and applying the same oxidizing method, R. Sun et *al.* [100] achieved the sensitive detection of phenol in different water samples by resonance light scattering (RLS). Hydrogen peroxide combined with HRP

induced the oxidation of phenol to form quinone intermediates, which interact with GQDs through electrostatic interactions resulting in the formation of molecular aggregates that enhanced the RLS spectral band (310 nm). The LOD was 2.2 μM and the proposed method was successfully applied in waste and lake water samples.

L, Zhang, et *al.* [51] used B–GQDs, prepared by the hydrothermal cutting of boron–doped graphene, as PL probe for the selective label free glucose sensing. Their approach is based on the abnormal aggregation–induced PL enhancement caused by the creation of rigid structures of B–GQDs and glucose (Figure 10), probably originated through the reaction of the two *cis*–diol units in glucose with the two boronic acid groups on B–GQDs, which restricted the intramolecular rotations, being the PL intensity upgraded. The sensing system was able to detect concentrations of 0.03mM of glucose. Other boronic–GQDs sensor for the determitation of glucose [101] has been described. APBA–GQDs were obtained from the hydrothermal treatment of GO and their post functionalization with 3–aminobenzeneboronic acid in the presence of 1–ethyl–3–(3–dimethylaminopropyl) carbodiimide (EDC). The FL quencheing in the presence of glucose was due to the formation of a negative charged boronated complex when glucose molecules were binding APBA on GQDs. Coulomb repulsion between APBA and GQDs were observed; however, APBA–GQDs

were cross–linked by the covalent anchorage of glucose. Therefore, the efficient FL quenching could be caused by the surface states formed by stretching of the interface of APBA–GQDs, originated by the elastic tension introduced by both electrostatic repulsion and covalent cross–linking. The APBA–GQDs offers the detection of glucose in aqueous solution with a LOD of 5.0 μM or lower, which was demonstrated to be appropriate for real samples of rat brain microdialysate.

The detection of various monosaccharides, including glucose, in aqueous solution employing FL GQDs with a boronic acid–substituted bipyridinium salt (BBV) was also presented [102]. GQDs (negatively charged by polar surface carboxyl and hydroxyl groups) and BBV (cationic) interacted through a combination of affinity sensing and electrostatic interaction. BBV was able to quench the GQDs FL and acts as glucose receptor simultaneously. Electrostatic attraction between GQDs and BBV facilitate the excited–state electron transfer from the carbon nanoparticle to bipyridinium due to the formation of a ground state complex and thus leading to the reduction of the in the GQDs PL. When glucose was added to the system the boronic acid were converted to tetrahedral anionic glucoboronate esters, which neutralized the net charge of the cationic BBV reducing the quenching efficiency retorating the PL. The label–free sensing system was also sensible for

galactose and fructose and showed saccharide selectivity in th following order: fructose >> galactose > glucose.

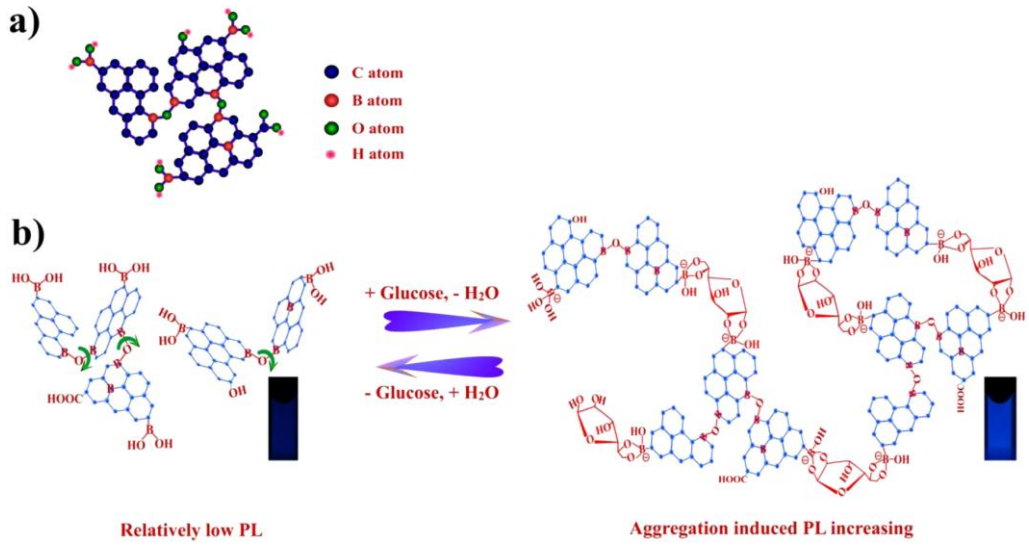

Figure 10. (a) Schematic Representation of the Boron-Doped Graphene Quantum Dots (BGQDs). (b) Proposed "Aggregation-Induced PL Increasing" Mechanism for the Glucose-Specific Sensing by BGQDs. Reproduced with permission of reference 50.

S. Benítez–Martínez et *al.* [103] developed a sensor for phenols presents in olive oil from GQDs obtained by the pyrolysis of citric acid. Phenols were extracted from olive oil, preconcentred, redisolved and finally mixed with GQDs to be quantified through their FL quenching. The quenching

mechanism was attributed to an energy transfer process from GQDs to phenols. The interaction between them could be explained through π–π staking and non–covalent interactions with the oxygen containing groups at the GQDs edges. Authors use gallic acid and oleuropein as standards, achieving LODs of 0.09 and 0.12 $mg{\cdot}L^{-1}$, respectively. The developed sensing system was proposed to detect the total phenol content in different olive oils. F. Yang et *al.* [28] proposed the potential application of GQDs, extracted from reduced GO by the ozonation pre–oxide method, as sensing platform for pyrocatechol. The FL of GQDs decreased when the concentration of pyrocatechol increased. The oxygen–containing groups in GQDs allow noncovalent interactions with pyrocatechol through electrostatic interaction, hydrogen bonding and π–π staking, leading to an energy transference that promotes the GQDs FL quenching.

The increasing use of nanoparticles in industrial application and their incorporation to commercial products such as cosmetics, foods, drugs and electronic devices, increase the human and environmental exposure to nanomaterials. Find effective analytical methods for the nanomaterial monitoring is an important issue which has to accomplish several requirements, such as be able to detect relevant concentrations (which fall in the nanogram per liter range), separating nanoparticles and avoiding the possible interferences present in the sample. There are several methods for this

purpose and recently some of them have been developed using GQDs as tools for the determination of such nanostructures. S. Benitez–Martinez et *al.* [104] proposed a GDQs–based sensor for the determination of GO in environmental samples, taken advantage of the GQDs FL was quenched in presence of GO. Graphene oxide was retained in a cellulose membrane from spiked river water samples and recovered by applying ultrasound radiation to the membrane. The attenuation of PL was attributed to an energy transfer between both types of carbon NPs; non–covalent interactions and π–π staking could act to maintain their proximity. The sensitivity of the developed method was 35 $\mu g{\cdot}L^{-1}$ GO.

Y. Liu et *al.* [105] studied the FL quenching between two unbounded structures, such as GQDs and gold nanoparticles (AuNPs), upon simple mixing. GQDs were prepared by the chemical treatment of XC–72 carbon black and AuNPs were synthesized by the reduction of $HAuCl_4$ by $NaBH_4$ with presence of tri–sodium citrate. After performing FL and UV–vis absorption studies, the authors proposed that both static and dynamic quenching mechanism coexisted in their system, which means that GQDs was quenched by citrate coated AuNPs in two possible ways: by forming the complex GQDs–AuNPs or by quenching at a distance without contact with GQDs, in such a way part of the GQDs were attached onto AuNPs surface with others remains monodispersed in water. GQDs and AuNPs were both negatively charged, the

first one through hydroxyl and carboxyl groups on their edges and the second one with citrate. A higher concentration of GQDs made AuNPs grow into larger structures due to the replacement of citrate ions by GQDs. A higher concentration of AuNPs made them self aggregate. Their results may help in the development of GQDs and AuNPs based sensors.

Most efforts in the development of the sensing applications outlined above have been guided in dope or functionalize GQDs to improve the methods selectivity and sensibility, being less studied the use of pristine GQDs.

3.1.1.2.Hybrid fluorescent sensors based on GQDs

In this section, the application of hybrid systems based on GQDs as sensing PL platforms is briefly described. GQDs are suitable to form composites with other nanoparticles (mainly carbon and metallic nanostructures) or even with biomaterials owing to the large number of reactive sites provided by their oxygen containing functional groups at the edges of the GQDs, or, in some isolated cases, on their surface.

Y. He el *al.* [106] used hemin–functionalized GQDs for the monitoring of blood glucose and also detection of H_2O_2. GQDs which were prepared by pyrolyzing citric acid were coupled to hemin by simply absorption on GQDs surface, through electrostatic and π–π stacking interactions, thanks to the

anionic charge of GQDs in aqueous solution are anionic and positively charges of hemin. The formation of hemin–GQDs nanocomposites reduce the GQDs FL about 9%, effects adscribed to changes in the surface state of GQDs due to the self assembling. This system was very sensitive to hydrogen peroxide; in fact, the addition of H_2O_2 to this platform leads to a significant FL attenuation of the hemin–GQDs signal, which could be attributed to the destruction of the surface passivation by the free radicals generated from hemin–media reaction. The LOD reached by this biosensor was 0.1μM. The coupling of the proposing biosensor with glucose oxidase made possible the extension of the sensing system for glucose detection with a LOD of 0.1μM. Real serum samples were used for the successfully detection of glucose in biological samples. Z. Li et *al.* [107] developed a method for the analysis of hydroquinone at trace levels involving a GQDs–enzyme hybrid system. GQDs, also obtained from the pyrolysis of citric acid, were diluted and mixed under vigorous stirring with a solution of the enzyme catalyzed mixture (hydroquinone–HRP–H_2O_2), incubated for 8 min. In the presence of a peroxidise and H_2O_2 hydroquinone could be catalyzed to produce 1,4–benzoquinona. When hydroquinone–HRP– H_2O_2 was added to the GQDs solution the FL was significantly quenched. There was reasonable evidence that suggest how the benzoquinone quenched the GQDs FL by affecting their surface states through electron transfer. The LOD of the proposed system was

0.084 μM. Y. Wang et *al.* [108] used GQDs as PL probes for the protein kinase sensing based on the selective aggregation of phosphorylated peptide–GQDs conjugates triggered by Zr^{4+} ions coordination. GQDs were prepared from graphene sheets by a hydrothermal treatment. For the preparation of covalently peptide–GQDs conjugates, EDC (N–(3–Dimethylaminopropyl)–N–Ethylcarbodiimide Hydrochloride), GQDs, NHS (N-hydroxysuccinimide) and peptide were mixed and shaken. For the detection procedure peptide–GQDs solution, Tris buffer, CK2 (casein kinase II) and ATP were added, diluted with ultrapure water and incubated in order to perform the phosphorylation reaction. Finally Zr^{4+} was added to induce aggregation of the phosphorilated peptide–GQDs through coordination with carboxylic groups on the GQDs surface. The PL of peptide–GQDs after tritation of Zr^{4+} ions did not change, which was ascribed to a covalent bond formation. The addition of CK2 in the presence of ATP catalyzed the peptide–GQDs phosphorylation. The titration of Zr^{4+} ions into the phosphorylated peptide-GQDs solution results in PL quenching, which can be attributed to the energy-transfer or electrontransfer processes as a result of the GQDs aggregation. The coordinate covalent interaction between Zr^{4+} ions and the phosphate groups on the peptide–GQDs surfaces should account for the formation of GQDs aggregates. The PL intensity decreases as the concentration of CK2 increases, being used as signal for the analytical performance. The LOD was as low as $0.03 U \cdot mL^{-1}$. The system

was applied for screening kinase inhibitors in biological systems. X. Ran et *al.* [109] demonstrated that GQDs decorated with silver nanoparticles (AgNPs) could be used in the label–free detection of Ag^+ and biothiols (GSH, Cys and Hcy). GQDs were prepared by microwave–assisted acidic cleavage of GO. Ag ions were electrostatically attached on the GQDs surface and their FL was quenched due to the formation of AgNPs/GQDs hybrids. The addition of Ag^+ to the hybrid solution made FL intensity decrease by a charge transfer process, and the addition of Cys resulted in further FL decrease since Cys was bonded to GQDs with AgNPs. The LOD of Ag^+ was found to be3.5 nM. Taken advance of the AgNPs decorated sensing platform the selective detection of GSH, Cys and Hcy (as examples of important biothiols in biological processes and diagnosis of disease) was performed since thiols formed Ag–S bonds on the surface of silver nanoparticles. FL of the AuNPs/GQDs hybrid system was attenuated in the presence of each one of the three bothiols. The LODs achieved were 6.2, 4.5 and 4.1 nM for Cys, Hcy and GSH respectively. The hybrid system was also studied as probe to detect thiol in human plasma. Y. Zhou et *al.* [110] synthesized a FL sensor based on GQDs for the determination of paranitrophenol (4-NP) in water samples, where molecularly imprinted polymer (MIP) was hybridized with GQDs. Silica–coated GQDs were fabricated by a simply hydrothermal method. The composite was developed by anchoring the MIP layer on the silica- coated GQDs using 3-

aminopropyltriethoxysilane as functional monomer and tetraethoxysilane as crosslinker. MIP–coated GQDs exhibited FL emission after their conjugation. MIP contributed to the method selectivity for 4-NP. When 4–NP was put in contact with MIP–coated GQDs, $-NH_2$ groups at the surface of MIP–coated GQDs acted as the binding sites to combine 4–NP through hydrogen bond interactions, being the FL of the hybrid system greatly quenched due to a resonance energy transfer from GQDs to 4–NP. The FL intensity decreased notably with the increasing of 4–NP concentrations. The LOD was 9.0 $ng{\cdot}mL^{-1}$, and the sensing system was applied to de detection of 4–NP in river water samples.

Biosensing of trypsin was possible by employing the method developed by X. Li et al. [111] in which GQDs are self–assembled by induction of cytochrome c (Cyt c). The latter is an electro transfer cationic protein which was able from complexes with anionic GQDs. When GQDs and Cyt c were coupled the FL emission of GQDs was greatly quenched due to the adsorption of GQDs on Cyt c, which also promoted the aggregation of GQDs by electrostatic attraction. However, upon the addition of trypsin the GQDs experimented a significant FL enhancement due to the hydrolysis of trypsin that could break Cyt c into fragments and destroy their FL quenching effect. In addition, Fe^{3+} present in Cyt c could also be reduced to Fe^{2+}, leading to the FL recovery. Finally trypsin cleaved peptide bonds of Cyt c into lysine and arginine

residues, both of which caused the chemical reduction of GQDs to r–GQDs, inducing an increase of FL intensity. The LOD for this biosensor was estimated to be 33 $ng{\cdot}mL^{-1}$.

3.1.2. Electrochemical sensors

3.1.2.1. Modified electrode

GQDs have been proved to be an efficient tool in the development of FL sensor and biosensor due to their stable luminescence and unique optical properties. However, in the electrochemical sensor field there has been little attention to GQDs despite they have been recognized as exceptional electron transporters and acceptors. Most examples found in the bibliography were focused on the modification of a different nature electrode.

M.Raushani et *al.* [112] developed an electrochemical sensor based on GQDs for the detection of persulfate ($S_2O_8^{2-}$). For this purpose, GQDs (synthesized from the acid citric pyrolysis) were coated on glassy carbon (GC) electrode surface by the drop casting method. The GC/GQDs electrode was activated and also coated with riboflavin. The modified electrode, GC/GQDs/RF showed direct electron transfer and excellent electrocatalytic activity to persulfate. Citric voltamperometry (CV) and chronoamperometry (CA) were used to study the electrochemical behavior of this sensor. GQDs served as support of riboflavin, which was mediator to shuttle electron

between $S_2O_8^{2-}$ and the working electrode and facilitated electrochemical regeneration following electron exchange with $S_2O_8^{2-}$. The sensitivity and the LOD of the sensor toward $S_2O_8^{2-}$ were found to be 0.8786 $\mu A \cdot \mu M^{-1}$ and 0.1 μM, respectively, using cyclic voltamperometry. The amperometric detection revealed lower LOD (0.02 μM) and a sensitivity of 4.7 $nA \cdot \mu M^{-1}$. The reusability of the GC/GQDs/RF modified electrode was examined and results indicated that after 100 repetitive cycles no detectable changes were observed at the peak height. GQDs modified Gold electrode was previously used by Y. Zhang et *al.* [113] to also detect H_2O_2. GQDs prepared by photo-Fenton reaction, were assembled on a gold electrode using cysteamine as cross–linker. Cysteamine molecules were chemically bonded to the electrode surface and the carbodiimide esters in the GQDs edges reacted with amine groups of cysteamine, forming amide bonds. CV and CA measurements were carried out and CV was selected to perform the catalytic response of GQDs/Au electrode to H_2O_2. Successive addition of H_2O_2 increased the cathode current. The LOD was 0.7 μM and the GQDs/Au electrode could be reused for more than 20 uses maintaining 90% of current response.

H. Razami et *al.* [114] reported a carbon ceramic electrode (CCE) modified with GQDs, as substrate for GOx, for the electrochemical sensing of glucose. GQDs solution, from hydrothermal treatment of GO, was casted on the CCE surface and dried at room temperature to obtain a homogeneous

GQDs|CCE, which was activated potentiostatically and a GOx solution was casted on the GQDs|CCE surface to finally obtain a GOx–GQDs|CCE. CV studies revealed that GOx catalized the reduction of oxygen. After glucose addition the reduction peak current decreased due to the reduction of oxygen on the electrode surface caused by enzyme–catalyzed reaction between the oxidized form of GOx and glucose. The current decrease was proportional to the added glucose concentration. The theoretical LOD was 1.73 μM and de sensitivity was 0.085 $\mu A{\cdot}\mu M^{-1}$. The modified electrode could be reused for 200 cycles and the peak currents remained almost 95% of the initial response.

3.1.2.2. Electrochemiluminescent sensors

Electrochemical sensors, in the form of probe sensor, were also described in the literature mainly for the metallic ions detection. Y. Chen et *al.* [115] designed an electrochemiluminescent (ECL) sensor to detect hexavalent chromium in environmental water samples. The sensing system is based on the excellent ECL of GQDs in the presence of $S_2O_8^-$. The correactant system GQDs/ $S_2O_8^-$ produces a strong cathodic signal, which was sensitively quenched by Cr (VI). Both GQDs and $S_2O_8^-$ were reduced to produce negatively charged GQDs and $SO_4^{\bullet -}$ radicals respectively. The electron transfer between them originated an excited–state GQD, which produced ECL signal when coming back to the ground estate. ECL signal can be quenched through static and dynamic mechanisms, like PL. Authors assumed a dynamic

mechanism for the ECL quenching since GQDs was deactivated upon contact with Cr (VI) leading to the ECL decrease of the correactant system. The LOD was detected to be about 20nM.The system was successfully applied to river water samples. L.–L. Li et *al.* [116] developed a Cd^{2+} ECL sensor based on greenish–yellow GQDs prepared by the graphene oxide (GO) cleavage under acidic conditions with the assistance of microwave radiation. Before Chen et *al.*, these authors investigated the ECL behaviours of GQDs using $S_2O_8^-$ as correactant proposing the ECL mechanism described above in reference 111, in which strongly oxidizing $SO_4^{\bullet -}$ radicals and $GQDs^{\bullet -}$ radicals were produced by electrochemical reduction of $S_2O_8^{2-}$ and GQDs, respectively. The Cd^{2+} sensing system was based on the coordination of metal ions with N and carboxyl and hydroxyl groups and the consequent GQDs aggregation, leading to the decrease of the ECL of GQDs. With the addition of Cys, as effective masking agent, the quenched ECL induced by other metal ions was recovered, except for Cd^{2+}, which FL still remained atenuated. The LODs achieved were comparable to other colorimetric methods and florescence sensors, being of 13nM.

3.1.2.3.Hybrid electrochemical sensors

M. Mazloum-Ardakani et *al.* [117] applied a modified glassy carbon electrode (GCE) to simultaneous detection of GSH, uric acid (UA) and tryptophan (Trp). In order to modify the GC electrode, it was immersed in a

GQDs solution for 12 h at room temperature. The GQDs/GC electrode was cycled in pH=7 PBS for 15 cycles in order to reduce oxygen contained groups in GQDs to form ERGQDs/GCE. This later was immersed in a $HClAu_4$ solution and AuNPs were electrochemically deposited on ERGQDs/GCE to obtain Au/ERGQDs/GCE electrode, which was immersed in a 4–(((4–mercaptophenyl)imino)methyl) benzene–1,2–diol (MIB) aqueous solution, to improve their catalytic activity, and the MIB/Au/ERGQDs/GCE was obtained. The presence of ERGQDs and AuNPs on the electrode caused an increase of their active surface. MIB has the ability of redox GSH, being oxidized at the MIB/Au/ERGQDs/GCE electrode surface. Cyclic voltamperometry (CV) and Chronoamerometry (CA) were used to study the GSH electrocatalytic activity. The high charge detaching efficiency of ERGQDs and Au nanoparticles promoted the electron transfer from the electrode surface to GSH and the self-assembled monolayer of MIB improved the LODs. The oxidation processes of GSH, UA and Trp at MIB/Au/ERGQDs/GCE were proved to be independent and the simultaneous determination of the three analytes was possible. Differential pulse voltamperometry (DVP) showed that increasing concentrations of GSH, UA and Trp increased the peaks current linearly. The selectivity of the modified electrode for GSH in presence of UA and Trp was 0.4722 and 0.0361 $\mu A{\cdot}\mu M^{-1}$ and the LOD were found to be 9nM, 5,5 μM and 6.5 μM for GSH, UA and Trp, respectively.

A. Muthurasu et *al.* [118] reported an electrochemical biosensor for H_2O_2 detection by employing HRP functionalized GQDs. The dots were prepared from the chemical treatment of GO and green PL spherical particles, which possessed oxygen rich functional groups, such as –OH and –COOH, were obtained. Owing to the presence of these active sites HRP anchorage on GQDs was possible using a peptide coupling reaction to form an amide linkage. HRP–GQDs were immobilized onto a GC electrode by drop–casting followed by dipping in chitosan solution (which acted as binder to prevent leaching of HRP enzyme). The studies for the hydrogen peroxide detection were carried out by monitoring the enzyme activity towards H_2O_2 reduction in aqueous phosphate buffer solution using CV and CA techniques. The enzyme modified electrode displayed a redox peak corresponding to Fe(III)/Fe(II) redox reaction of heme groups present within the enzyme. Upon addition of H_2O_2, a significant enhancement in the reduction current was observed. A systematic increase in H_2O_2 concentration results in systematic increase of the reduction current. CA was used to accomplish the analytical performance of the sensing system. Current was plotted versus concentration and two linear regions appeared for H_2O_2. Sensitivity and LOD were calculated from both regions. For the lowest concentration region, the sensitivity and the limit of detection were found to be 0.905 $\mu A \cdot \mu M^{-1}$ and 530.85 nM, respectively, and for the highest

concentration region the sensitivity was 7.057 $\mu A \cdot \mu M^{-1}$ and the detection limit, 2.16 μM.

J. Hou et *al.* [119] performed the electrochemical detection of malachite green (MG) using a GQDs–AuNPs modified GCE. GQDs solution, prepared by chemical oxidation of graphene sheets, was dropped on the GCE surface. The GQDs/GCE was immersed in a $HAuCl_4$ solution and the obtained AuNPs were electrodeposited on GDQs/GCE after the electrochemical reduction of chloroauric acid by applying a negative potential. Multilayer GQDs/Au was constructed by alternative doping of GQDs and electrodeposition of AuNPs. CV analysis demonstrated that the modified electrode showed an acceptable catalytic activity. The current signal was stronger in the case of four layers than for one layer. CA measurements showed redox reaction of MG, probably due to the mutual transformation of MG and poly(malachite green). DVP measurements demonstrated that the oxidation peak current was maximal at a four films. The oxidation peak current was used as analytical signal and it was proportional to the concentration of MG. The LOD was estimated to be 0.1 μM. Determination of MG in muscle of salmon real samples were successfully performed.

3.2. Inmunosensing and aptasensing

3.2.1. Immunosensors

Immunologic sensors are based on the recognition of the coupling between an antigen and an antibody, which form an antigen–antibody complex. Both, antigen or antibody, can be immobilized on the sensor surface and originate a change in the recorder signal when they form a complex with the corresponding antibody or antigen. Highly sensitive immunosensors can be formed using enzymatic reactions in which enzyme-labeled antigens are fixed. Immunosensors have great potential in clinical analysis owing to the specificity of the immunological reactions. They can be classified in: competitive or no competitive, homogeneous or heterogeneous. Generally, no competitive immunoassay gives more sensibility and more specificity. They can be classified in electrochemical, optical, piezoelectric, thermometric and magnetic immunosensors as a function of the transducer property [120].

L. Li et *al.* [121] reported a paper–based ECL immunodevice composed by nanoporous gold–chitosan hybrids and GQDs functionalized Au@Pt composites for the detection of carcinoembryonic antigen (CEA). Green GQDs, prepared from the solvothermal treatment of GO, were immobilized on amino–functionalized Au@Pt (with core–shell structure), monoclonal signal antibodies ($McAb_2$) were attached and GOx added to form labeled

$McAb_2$/GQDs/Au@Pt bioconjugates. Monoclonal capture antibodies ($McAb_1$) were immobilized onto a 3D origami ECL inmunodevice to prepare the working zone. For the ECL assay procedure, the ECL inmunodevice was firstly incubated with the sample solution and then also incubated with GOx/$McAb_2$/GQDs/Au@Pt bioconjutaded. The amplified ECL signal were achieved by efficient catalysis of the GOx towards the oxidation of glucose to in situ generated H_2O_2 When the inmunodevice was incubated with different concentrations of CEA an increase of ECL signal was observed. The loaded GQDs on Au@Pt produced an amplified ECL signal and further improved the sensitivity. By using this sandwich–type assay, the LOD was 0.6 $pg{\cdot}mL^{-1}$ and it could be effectively applied to real serum samples.

H. Yang et *al.* [122] presented a GQDs coated porous PtPd nanochains (pPtPd) labeled ECL immunosensor based on gold–silver nanocomposite–functionalized graphene for the detection of tumor marker in serum samples. To this end, AgNPs were attached on a PVP–coated graphene sheet and post surface decorated with AuNPs to form a GN–Ag–Au hybrid nanomaterial, which was deposited on a GCE electrode surface. Then, the modified GCE was dropped with the primary antibodies. Separately, GQDs and pPtPd were conjugated (pPtPd@GQDs) through $-NH_3^+$ groups present at the porous nanochains and COO^- groups in GQDs. Next, it was incubated with the secondary antibodies (Ab_2) to obtain the pPtPd@GQDs/Ab_2. Thus, the ECL

immunosensor was incubated with the sample (CA199) at different concentrations and, finally, with the prepared pPtPd@GQDs/Ab_2, obtaining a sandwich–type structure. The anodic ECL of the assay was measured in the presence of tripropylamine (TAP) as correactant. The ECL intensity of the immunosensor increased with the increasing concentration of CA199. The LOD was 0.96 $mU{\cdot}mL^{-1}$.

X. Wang et *al.* [123] studied the detection of avian leukosis virus subgroup J (ALVs–J) by a GQDs apoferritin–encapsulated Cu nanoparticles (CuNPs) double –assisted signal amplification electrochemical immunosensor. A bare GQDs–modified GCE electrode was incubated with Ab_1 followed by incubation with different concentrations of ALVs–J. Thereafter, the previously prepared Fe_3O_4@GQDs/Ab_2–Cu-apoferritin/BSA bioconjugates were dropped into the electrode surface and incubated. After the sandwich type assembly, Cu was released from the apoferritin cavity and then detected by DVP. The LOD achieved was 115$TCID_{50}{\cdot}mL^{-1}$. GQDs were used for both conjugation of ALVs–J Ab_1 and immobilization of ALVs–J Ab_2.

I. Al–Ogaidi et *al.* [124] developed an optical immunoassay for the detection of ovarian biomarker CA–125 based on the chemiluminescence resonance energy transfer (CRET) to GQDs, which were immobilized on an amino–modified glass chip through electrostatic attractions. Figure 11 shows

the schematic assembly of the immunoassay and the detection principle. Capture antibodies (cAb) were covalently linked to the GQDs via amide conjugation. When the CA-125 antigen was absent in the immunoassay the blue chemioluminescence (CL) occurred due to the horseradish peroxidase (HRP) enzyme catalyzes the production of the reactive oxygen species (ROS) from H_2O_2, which oxidizes luminol to the singlet dianion, generating the excited electrons that emitted after their jump from the excited state to the ground state. In the absence of the CA-125 antigen, When the CA-125 antigen was present in the immunoassay, the antibody–antigen complex was generated (GQDs–cAb + CA-125). This complex is exposed to Ab–HRP to form a sandwich structure, (GQDs–cAb +CA-125 + Ab–HRP). HRP was in close proximity to the GQDs. The dianion catalyzed by the HRP enzyme was close to the GQDs, which enables the resonance energy transfer from the dianion to the GQDs, quenching the chemiluminescence, which was inversely proportional to the CA-125 concentration. The theoretical LOD was calculated to be 0.05 $U{\cdot}mL^{-1}$. Assays of real samples containing 50% of human blood plasma and 50% PBS buffer were performed achieving a estimated LOD of 0.08 $U{\cdot}mL^{-1}$.

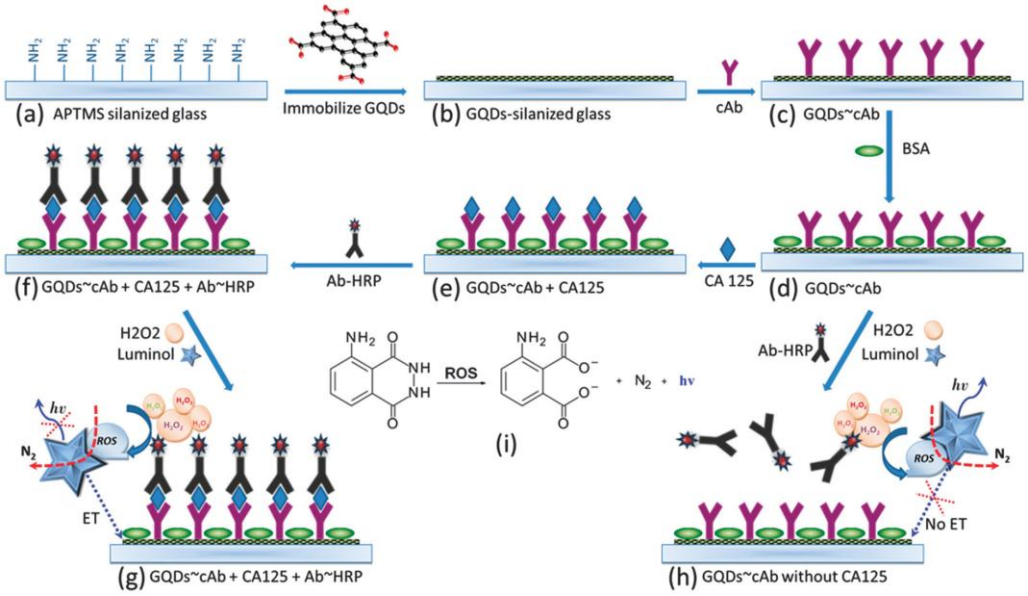

Figure 11. Scheme on the assembly of the immunoassay and the detection principle. Reproduced with permission of reference 123.

H. Zhao et *al.* [125] provided a fluoroimmunoassay based on the interaction of graphene and GQDs for the sensitive detection of human immunoglobulin G (IgG). In this immunosensing strategy graphene acts as an acceptor and mouse anti–human IgG (mIgG, antibody)–conjugated GQDs as donors. When graphene was added to mIgG–GQDs solution, both the π–π stacking interaction between graphene and GQDs and the nonspecific binding interaction of mIgG with the graphene surface could lead to a

luminescence resonance energy transfer (LRET) which facilitated the luminescence quenching of GQDs. The addition of human IgG, probably binded the mIgG by the specific antibody–antigen interaction, restored the luminescence of GQDs due to an increment of the distance between mIgG–GQDs and G surface. The LOD of this turn–on fluoroimmunoassay was established in 10 $ng{\cdot}mL^{-1}$.

1.1.1. Aptasensors

Aptasensor can be considered a sensing platform modified with oligonucleotides, selected in vitro by a combinatorial method, to exhibit a high affinity and specificity to a particular ligand. The presence of ligand induces a conformational change that allows an oligonucleotide molecular recognition event. The variety of potential ligands (from ions to whole cells) makes them very attractive not only as therapeutic agents and to control expression of genes but as molecular design for receptors sensing phases. As molecular receptors have the advantage that they may be subject to extreme conditions and undergo denaturation cycles without losing its affinity for the ligand. Aptasensor based analysis is continuously evolving with various detection schemes ranging from label-free methods such as surface plasmon resonance (SPR) and quartz crystal microbalance (QCM) measurements to label dependant methods such as electrochemistry, FL, chemiluminescence, field effect transistors, etc. However, currently electrochemical and optical

aptasensors constitute the two predominant types under development. Aptasensors have more potential than antibodies and they could be applied to biomarker detection, cancer diagnosis, detection of pathogens, and small molecules for food safety and environmental pollution [126].

In this context, Z. Sheng Qian et *al.* [127] reported the simultaneous detection of DNA and thrombin based on GQDs and GO, regulated by an "off–on" process. GQDs were synthesized from a microwave–assisted chemical oxidation route. In order to improve their quantum yield and sensitivity, 1,2–ethylendiamine–functionalizated GQDs (eGQDs) and reduced GQDs (rGQDs) were prepared and two different color GQDs solutios with different maximum emission were obtained, respectively. eGQD was condensed with the DNA probe (ssDNA–eGQDs) and rGQDs and thrombin aptamer were adopted to prepare thrombin probe (TA–rGQDs). Separate detection of DNA and thrombin, as well as simultaneous detection were possible to carry out. For the single detection, ssDNA–eGQDs or TA–rGQDs were mixed with GO, being absorbed on the GO surface through electrostatic attraction and π–π stacking interaction, where either the assembly ssDNA–eGQDs/GO or TA–rGQDs/GO was formed. The formation of the corresponding assembly leaded to the effective FL quenching of the probe through electron transfer between GQDs and GO. With the addition of target DNA or thrombin, the desorption of the probe from the GO occurs due to the rupture of the non–covalent interaction

between GQDs and GO after target DNA hybridized with the ssDNA–eGQDs/GO to produce a double strained DNA–GQDs through specific base paring, and thrombin form a complex with their probe because the aptamer specifically binds to thrombin exosite I by TT loops through a mix of hydrophobic and polar interactions. The liberation of both probes from the GO surface leaded to the apparent FL recovery. For the simultaneous detection of DNA and thrombin both probes were assembled to GO at the same time, and thus the dual nanosensor could synchronously respond of the presence of both DNA and thrombin due to the FL recovery induced by the release of their corresponding complex from GO. Single detection of DNA and thrombin shoed a LOD of 0.3 nM and 0.6 nM, respectively. The LODs applying simultaneous detection were established to be 6.7 and 7.9 nM for DNA and thrombin, respectively.

Other selective and sensitive FL sensing platform for DNA single detection, based on FRET between GQDs and GO, was previously established by these authors [128]. For the methodology development, GQDs (obtained from chemical oxidation of graphite powder) were reduced (rGQDs) with sodium borohydride and used to form a single–stranded (ss) labelled DNA probe; the detection mechanism was the same as described avobe for single detection of DNA, in which the ssDNA–rGQDs probe was absorbed on GO surface through π–π stacking interactions and electrostatic attractions, leading

to the subsequent FL quenching. The addition of target DNA (tDNA) led to the formation of dsDNA–rGQDs which were detached and liberated from GO, resulting in the FL recovery by the rupture of the π–π stacking interactions and electrostatic attractions of ssDNA–rGQDs. The LOD of the proposed "on–off–on" method was estimated to be 75pM. Other work, similar to this sensing approach [129], was also reported for DNA detection in a complex sensing system based on GQDs and oxidized MWCNTs (o–MWCNTs). The sensing mechanism was similar to that described in references 126 and 127 for single DNA detection, with the difference that o–MWCNTs were used as substrate for the GQDs probe FL quenching instead of GO.

A GQDs–based platform for the detection of DNA was described by J. Zhao et *al.* [130], whose developed a GQDs modified pyrolytic graphite (PG) electrode coupled to specific sequences ssDNA molecules as probe. PG electrode was dripped with a GQDs solution and dried at room temperature in order to obtain an uniform film on its surface. Then, The GQDs modified electrode was immersed in a Tris–HCl buffer containing ssDNA. For electrochemical measurements (carried out by DPV), the target should be firstly added to the solution containing ssDNA and incubated for 1 h before the immobilization and a Tris–HCl pH=6 buffer containing $[Fe(CN)_6]^{3-/4-}$ should be used as electrolyte. By adding the complementary ssDNA to the probe the formation of a double helix structure by self–assembly was possible and the

peak current of $[Fe(CN)_6]^{3-/4-}$ increased with the addition of complementary ssDNA, indicating that the formation of double stranded DNA disrupted the immobilization of the probe onto the modified electrode surface and higher electrochemical response could be observed. The LOD for target complementary ssDNA was 100nM. The probe ssDNA used in this study was also a thrombin aptamer, so, based on the same principle as described above for DNA, the electrochemical signal increased with the thrombin concentration. The detectable concentration of thrombin was 100nM. Results confirmed the important role of GQDs in this sensor system because PG electrode could not distinguish the conformational changes in the ssDNA probe.

W. Liu et *al.* [131] proposed an electrochemical DNA sensor by using a modified GCE and peroxidase–like magnetic $ZnFe_2O_4$/GQDs nanohybrid as a mimic enzymatic label (Figure 12). For the electrode modification, graphene sheets were deposited on GCE surface, followed by the casting of Pd nanowires on the electrode. The modified electrode was immersed on a ssDNA solution and treated with 6–mercapto–1–hexanol (MCH) to obtain a well–aligned DNA monolayer. Then, the modified electrode was firstly hybridized with target DNA (tDNA) and, secondly, with the $ZnFe_2O_4$/GQDs–ssDNA. The $ZnFe_2O_4$/GQDs nanohybrid in the sensing system showed superior peroxidase–like catalytic performance than HRP, maybe due to

synergistic effect of individual, not a simple addition of the activities of $ZnFe_2O_4$ and GQDs. The formed nanohybrid made the electron transfer from GQDs to $ZnFe_2O_4$ more effective. In addition, the small size, more intact aromatic structure and rich periphery carboxylic groups and un paired unpaired electrons on GQDs edge was also attribute to enhance the nanohybrid catalytic activity. DPV measurements were carried out at different tDNA concentrations. The reduction peak current increased gradually with the increase of the tDNA. The average reduction peak currents of the DNA biosensor were linearly proportional to the logarithm of the tDNA concentration. The LOD was $6.2x10^{-17}$ M.

J. Lu et *al.* [132] describe an aptasensor for the detection of ATP based on the ECL of blue GQDs. A solution containing ssDNA1 was dropped on a Au electrode surface, and treated with MCH to obtain a well–aligned DNA stand. The prepared electrode was immersed in a solution which contains hybrid nanostructures composed by SiO_2 nanospheres, GQDs and ssDNA2 (SiO_2/GQDs/ssDNA2) and different concentrations of ATP. In the presence of ATP, owing to the formation of a stable complex between the ssDNA1 and SiO_2/GQDs modified ssDNA2, SiO_2/GQDs ware caused to be immobilized onto the electrode surface, which resulting in ECL signal. However, in the absence of ATP, there was lower interaction between the two fragments, which results in a weak ECL signal from the electrode. The LOD of the method was

$1.5x10^{-12}$ M. The anodic ECL was possible to be observed by using H_2O_2 as correactant.

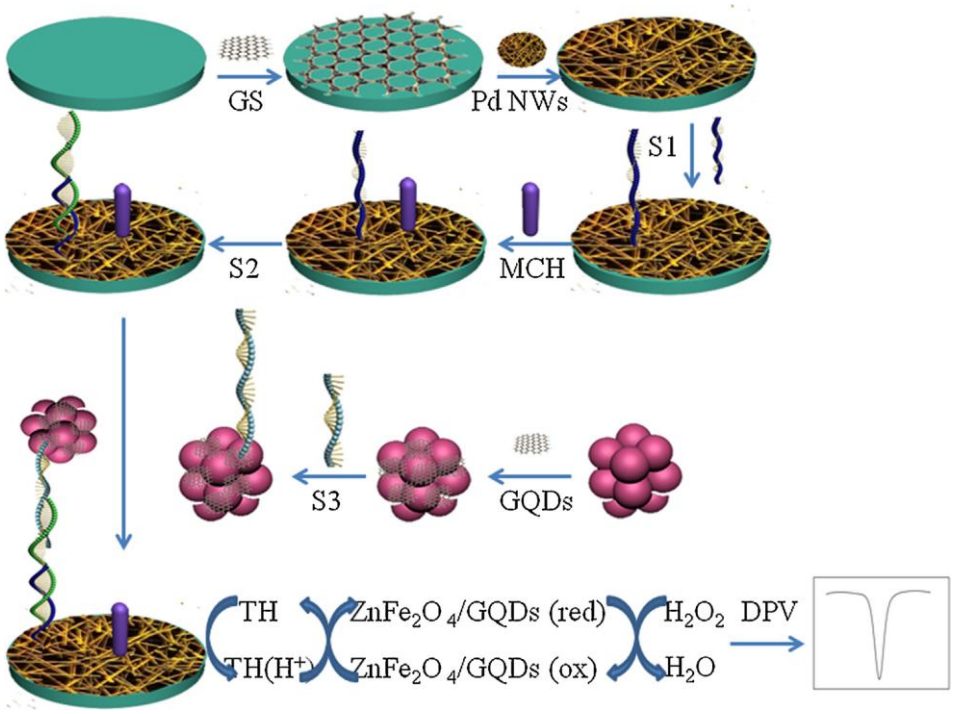

Figure 12. *Schematic illustration of ZnFe2O4/GQDs as a mimicking trace label for electrochemical detection of DNA. Reproduced with permission of reference 130.*

3.3. Other analytical applications

On the basis of exploit the unique properties of GQDs, derived from their nanometer size, various approaches have emerged as new opportunities to develop novel analytical methods and improve those well-established. In

this section, a few chromatographic and spectrometry recents applications are summarized.

G. Wang et *al.* [133]described a screening method for the detection and identification of radical scavenging natural antioxidants based on a free radical reaction combined with liquid chromatography with tandem mass spectrometry. Amine–functionalized GQDs were used for loading free radicals in the complex system. The detection was performed with and without a preliminary exposure of the samples to specific free radicals on the functionalized graphene quantum dots, which facilitated the charge transfer between free radicals and antioxidants, and could form a conductive interface facilitating the interfacial electron-transfer kinetics of the screening system with low electrontransfer resistance . The difference in chromatographic peak areas was used to identify potential antioxidants. The method provided simultaneously evaluation of the antioxidant power of a component versus a free radical, and their identification in a complex vegetal matrix. The antioxidants were identified using tandem mass spectrometry and comparison with standards. Fourteen compounds were found to possess potential antioxidant activity, and their free radical scavenging capacities were investigated. 4,5,6,7-Tetrahydroxyflavone showed the strongest capability for scavenging free radicals.

H. Cheng et *al*. [134]reported GQDs assembled nanotubes (GQD–NT) for surface enhance Raman spectroscopy. GQDs were obtained from the electrochemical oxidation of graphene. Under the application of a potential for several hours the GQDs were spontaneously deposited onto the nanochanels of an Au foil supported anodic aluminum oxide membrane to form nanotubes arrays. In the assembly, GQDs lost their O–related groups and the GQDs–NTs become insoluble in aqueous medium. The abundant hydrogen atoms terminated on the GQDs surface within nanotubes could play an important role in promoting efficient charge transfer and enables the SERS effect. The potential of GQDs–NTs as substrate in SERS applications was tested with Rhodamine 6G (R6G), a highly Raman active molecule. R6G molecules were absorbed on GQDs–NT by simply soaking. Their vibrational frequencies were similar to those on graphene and those on metal–based SERS substrate reported. An overall 40– to 74–fold enhancement was observed. The LOD of R6G was measured to be around 10^{-9} M. On the basis of these results, the capability of GQDs–NT for 2,4–dinitrotoluene (2,4–DNT) were investigated and a 59–fold Raman enhancement was achieved in comparison of the Raman intensity for the NO_2 stretching mode with that on the Si reference. The SERS effect of GQDs was attributed to the chemical mechanism.

GQDs have also been employed as surfactant to produce Pickering emulsions and novel polymer particles. H. Yang et *al.* [135] obtained high luminescent GQDs by eliminating oxygen contained group from their surface. The reduction was achieved by a thermal treatment of the GQDs, prepared from the chemical oxidation of CX–72 carbon black. For the surfactant procurement, GQDs were reduced in different degrees and dissolved in oil/water emulsions. Only GQDs reduced for a longer time were able to form the surfactant and were applied to PS colloidal particles and PS–*b*–PB particles with great potential in bioimaging and environmental applications.

4. GRAPHENE QUANTUM DOTs AS ANALYTE.

The current Analytical Nanoscience and Nanotechnology is based on two key facets that can be defined, on one side, by considering the nanomaterials as tool for the creation of new analytical methods and improvement and innovation of the analytical processes, methods and techniques well established. On the other hand, nanoparticles and nanostructure materials can be considered as target–analyte. Their consideration as an object of analysis requires analytical methods capable to detect and quantify the nanomaterials in different samples, including

biological and environmental complex matrices. However, it can be noted that there is a few contribution about this matter.

In the case of considerer GQDs as target analyte in the Analytical Chemical field, only two references were found. N. Fuhuno et *al.* [136] investigated the size–dependent luminescence properties of GQDs by using liquid chromatography. The PL GQDs were fabricated by a chemical oxidation process of pitch–based carbon fibers and separated by size–exclusion high performance liquid chromatograpy (HPLC). The dominant features of the separated GQDs showed discrete changes in the relative intensities depending on the overall size of GQDs, mainly corresponding to the emission wavelength of ~600, ~520, ~440 and ~330 nm, indicating that PL variation occurs because of differences in density, shape and size of sp^2 fragments availables in the GQDs solution. The optical properties were controlled thanks to the size separation. The emission was attributed to quasi molecular PL from fragments composed of small aromatic rings structures with oxygen containing functional groups.

Recently, S. Benítez–Martínez et *al.* [137] have developed a new strategy for the preconcentration and determination of GQDs , obtained by the pyrolysis of citric acid, in environmental and tap waters. The methodology is based on the GQDs retention in an amine quaternary functionalized SPE

cartridge. GQDs were eluted with 0.25M NaOH prior their flourimetric analysis. The authors attributed the interaction of the negatively charged GQDs (through the oxygen containing groups at their edges) with the positively charged quaternary amine via ionic interactions. For the elution, a change in the charge of GQDs is induced in order to their release from the sorbent. The LOD achieved was 7.5 $\mu g \cdot L^{-1}$ with percentages of recoveries between 84.4–99.3%

5. CONCLUSIONS AND FUTURE PERSPECTIVES

Graphene quantum dots have become a powerful tool in analytical Nanoscience and Nanotechnology owing to the abundantly available methods for their production. At the same time, they exhibit several properties that make them an interesting nanomaterial for analytical applications. Much effort has been directed to investigate their fundamental physical and chemical properties and the origin of their FL emission. However, the luminescent and electronic mechanisms are not fully understood yet. Current synthesis methods do not allow large-scale production due to the specificity of the necessary instruments to develop them, the dependence of several variables in synthetic routes, the low yields achieved and the variability in dimensions, sizes and qualities of the obtained nanomaterials. Generally,

GQDs presents low quantum yield which can be enhanced by doping with heteroatoms or by functionalization of their surface; although in these processed only a low modification is usually achieved.

In despite of all disadvantages GQDs have demonstrated their capability to be applied in the analytical field, specifically in the development of FL and electrochemical sensors and biosensors.

It can be expected that GQDs will be used in other analytical applications. Due to their increasingly widespread use in other applications, such as optoelectronic, electronic devices, energy storage and drug delivery, they could be released to the environment and be accumulated. They have been defined as low "in vitro" cytotoxic but their accumulation and interaction with other engineered nanoparticles in the environment could have serious consequences for human and animal health. For this reason, future efforts should be focused in the consideration of GQDs as a target analyte. This consideration will also contribute to the understanding of some mechanisms that still remain unclear.

6. REFERENCES

[1] K.S. Novoselov, A.K. Geim, S.V. Morozov, D. Jiang, Y. Zhang, S.V. Dubonos, I. V. Grigorgieva, A.A. Firsov, Electric Field Effect in Atomically Thin Carbon Films, Science, 306 (2004) 666–669.

[2] A.K. Geim, Graphene: Status and Prospects, Science, 324 (2009) 1530–1534.

[3] X. Yan, X. Cui, L.S. Li, Synthesis of Large, Stable Colloidal Graphene Quantum Dots with Tunable Size, J. Am. Chem. Soc., 132 (2010) 5944–5945.

[4] S. Kim, S.W. Hwang, M.K. Kim, D.Y. Shin, D.H. Shin, C.O. Kim, S.B. Yang, J. H. Park, E. Hwang, S.H. Choi, G. Ko, S. Sim, C. Sone, H.J. Choi, S. Bae, B.H. Hong, Anomalous Behaviors of Visible Luminescence from Graphene Quantum Dots: Interplay between Size and Shape, ACS Nano, 6 (2012) 8203–8208.

[5] Y. Dong, C. Chen, X. Zheng, L. Gao, Z. Cui, H. Yang, C. Guo, Y. Chi, C.M. Li, One-step and high yield simultaneous reparation of single– and multi–layer graphene quantum dots from CX–72 carbon black, J. Mater. Chem., 22 (2012) 8764–8766.

[6] C. Frigerio, D.S.M. Ribeiro, S.S.M. Rodrigues, V.L.R.G. Abreu, J.A.C. Barbosa, J.A.V. Prior, K.L. Marques, J.L.M. Santos, Application of quantum

dots as analytical tools in automated chemical analysis: A review, Anal. Chim. Acta, 735 (2012) 9–22.

[7] S.H. Jin, D.H. Kim, G.H. Jun, S.H. Hong, S. Jeon, Tuning the Photoluminescence of Graphene Quantum Dots through the Charge Transfer Effect of Functional Groups, ACS nano, 7 (2012) 1239–1245.

[8] M.L. Mueller, X. Yan, J.A. McGuire, L. Li, Triplet States and Electronic Relaxation in Photoexcited Graphene Quantum Dots, Nano Lett., 10(7) (2010) 2679–2682.

[9] H. Tetsuka, R. Asahi, A. Nagoya, K. Okamoto, I. Tajima, R. Ohta , A. Okamoto, Optically Tunable Amino-Functionalized Graphene Quantum Dots, Advanc. Mater., 24 (2012) 5333–5338.

[10] J. Shen, Y. Zhu, X. Yang, J. Zong, J. Zhang and C. Li, One-pot hydrothermal synthesis of graphene quantum dots surface-passivated by polyethylene glycol and their photoelectric conversion under near-infrared light, New J. Chem., 36 (2012) 97–101.

[11] Y. Feng, J. Zhao, X. Yan, F. Tang, Q. Xue, Enhancement in the fluorescence of graphene quantum dots by hydrazine hydrate reduction, Carbon, 66 (2014) 334 –339.

[12] P. Luo, Z. Ji, C. Li, G. Shi, Aryl-modified graphene quantum dots with enhanced photoluminescence and improved pH tolerance, Nanoscale, 5 (2013) 7361–7367.

[13] L.A. Ponomarenko, F. Schedin, M.I. Katsnelson, R. Yang, E.W. Hill, K.S. Novoselov, A.K. Geim, Chaotic dirac billiard in graphene quantum dots, Science, 320 (2008) 356–358.

[14] J.H. Shen, Y.H. Zhu, C. Chen, X.L. Yang, C.Z. Li, Facile preparation and upcon-version luminescence of graphene quantum dots, Chem. Commun., 47 (2011) 2580–2582.

[15] Y. Zhang, H. Gao, J. Niu, B. Liu, Facile synthesis and photoluminescence of graphene oxide quantum dots and their reduction products, New J. Chem., 38 (2014) 4970-4974.

[16] R. Ye, C. Xiang, J. Lin, Z. Peng, K. Huang, Z. Yan, N. P. Cook, E. L. Samuel, C.C. Hwang, G. Ruan, Coal as an abundant source of graphene quantum dots,

[17] Nat. Commun., 4 (2013) 1–6.

[18] J. Peng, W. Gao, B. Kumar Gupta, Z. Liu, R. Romero-Aburto, L. Ge, L. Song, L.B. Alemany, X. Zhan, G. Gao, S.A. Vithayathil, B.A. Kaipparettu, A.A. Marti, T. Hayashi, J.Zhu, P.M. Ajayan, Graphene Quantum Dots Derived from Carbon Fibers, Nano Lett., 12 (2012) 844−849.

[19] W. Kwon, Y. Kim, C. Lee, M. Lee, H.C. Choi, T. Lee, S. Rhee, Electroluminescence from Graphene Quantum Dots Prepared by Amidative Cutting of Tattered Graphite, Nano Lett., 14 (2014) 1306–1311.

[20] M. Zhang, L. Bai, W. Shang, W. Xie, H. Ma, Y. Fu, D. Fang, H. Sun, L. Fan, M. Han, C. Liub, S. Yang, Facile synthesis of water-soluble, highly fluorescent graphene quantum dots as a robust biological label for stem cells, J. Mater. Chem., 22 (2012) 7461–4767.

[21] Y. Dong, H. Pang, S. Ren, C. Chen, Y. Chi, T. Yu, Etching single-wall carbon nanotubes into green and yellow single-layer graphene quantum dots, Carbon, 64 (2013) 245-251.

[22] L. Minati, S. Torrengo, D. Maniglio, C. Migliaresi, G. Speranza, Luminescent graphene quantum dots from oxidized multi-walled carbon nanotubes, Mater. Chem. Phys., 137 (2012) 12–16.

[23] A. Ananthanarayanan, X. Wang, P. Routh , B. Sana , S. Lim , D. Kim , K. Lim , J. Li , P. Chen, Facile synthesis of graphene quantum dots from 3D graphene and their application for Fe^{3+} sensing. Adv. Funct. Mater., 24 (2014) 3021–3026.

[24] H. Xu, S. Zhou, L. Xiao, H. Wang, S. Li, Q. Yuan, Fabrication of a nitrogen-doped graphene quantum dot from MOF-derived porous carbon and its application for highly selective fluorescence detection of Fe^{3+}, J. Mater. Chem. C, 3 (2015) 291-297.

[25] Yongqiang Dong, Jianpeng Lin, Yingmei Chen, Fengfu Fu, Yuwu Chi*and Guonan Chen, Graphene quantum dots, graphene oxide, carbon quantum dots and graphite nanocrystals in coals

Nanoscale, 2014, 6, 7410–7415.

[26] D. Pan, L. Guo, J. Zhang, C. Xi, Q. Xue, H. Huang, J. Li, Z. Zhang, W. Yu, Z. Chen, Z. Lib, M. Wu, Cutting sp^2 clusters in graphene sheets into colloidal graphene quantum dots with strong green fluorescence, J. Mater. Chem., 22 (2012) 3314–3318.

[27] X. Zhu, X. Xiao, X. Zuo, Y. Liang, J. Nan, Hydrothermal Preparation of Photoluminescent Graphene Quantum Dots Characterized Excitation-Independent Emission and its Application as a Bioimaging Reagen, Part. Part. Syst. Charact., 31 (2014) 801–809.

[28] S. Zhu, J. Zhang, X. Liu, B. Li, X. Wang, S. Tang, Q. Meng, Y. Li, C. Shi, R. Hu, B. Yang, Graphene quantum dots with controllable surface oxidation, tunable fluorescence and up-conversion emission, R. Soc. Chem. Adv., 2 (2012) 2717–2720.

[29] F. Yang, M. Zhao, B. Zheng, D. Xiao, L. Wu, Y. Guo, Influence of pH on the fluorescence properties of graphene quantum dots using ozonation pre-oxide hydrothermal synthesis, J. Mater. Chem., 22 (2012) 25471–25479.

[30] S. Zhu, J. Zhang, C. Qiao, S. Tang, Y. Li, W. Yuan, B. Li, L. Tian, F. Liu, R. Hu, H. Gao, H. Wei, H. Zhang, H. Sunb, B. Yang, Strongly green-photoluminescent graphene quantum dots for bioimaging applications, Chem. Commun., 47 (2011) 6858–6860.

[31] D.B. Shinde, V.K. Pillai, Electrochemical preparation of luminescent graphene quantum dots from multiwalled carbon nanotubes. Chem. Eur. J., 18 (2012) 12522-12528.

[32] Y. Li, Y. Hu, Y. Zhao, G. Shi , L. Deng , Y. Hou , and L. Qu, An electrochemical avenue to green–luminescent graphene quantum dos as potential electron–acceptors for photovoltaics, Adv. Mater., 23 (2011) 776–780.

[33] P. Russo, A. Hu, G. Compagnini, W. Duleydand, N.Y. Zhou, Femtosecond laser ablation of highly oriented pyrolytic graphite: a green route frot large–sacle production of porous graphene and graphene quantum dots, Nanoscale, 6 (2014) 2381-2389.

[34] K. Habiba, V.I. Makarov, J. Avalos, M.J.F. Guinel, B.R. Weiner, G. Morell, Luminescent graphene quantum dots fabricated by pulsed laser synthesis, Carbon, 64 (2013) 341–350.

[35] Y. Shih, G. Tseng, C. Hsieh, Y. Li, A. Sakoda, Graphene quantum dots derived from platelet graphite nanofibers by liquid–phase exfoliation, Acta Mater., 78 (2014) 314–319.

[36] F. Liu, M. Jang, H.D. Ha, J. Kim, Y. Cho, T.S. Seo, Facile Synthestic Method for pristine graphene quantum dots and graphene oxide quantum dots: origin of blue and green luminescence, Adv. Mater., 25 (2013) 3657–3662.

[37] L. Lin, S. Zhang, Creating hidh yield water soluble luminescent graphene quantum dots via exfoliating and disintegrating carbon nanotubes and graphite flakes. Chem. Commun., 48 (2012) 10177–10179.

[38] Y. Zhu, G. Wang, H. Jiang, L. Chen, X. Zhang, One-step ultrasonic synthesis of graphene quantum dots with high quantum yield and its application in sensing of alkaline phosphatase, Chem. Commun., 51 (2015) 948-951.

[39] X. Yan, X. Cui, Large, solution-processable graphene quantum dots as light absorbers for photovoltaics, Nano Lett., 10 (2010) 1869–1973.

[40] R. Liu, D. Wu, X. Feng, K. Mullen, Bottom–up fabrication of photolumines-cent graphene quantum dots with uniform morphology, J. Am. Chem. Soc., 133 (2011) 15221–15223.

[41] J. Kim, J.S. Suh, Size-Controllable and Low-Cost Fabrication of Graphene Quantum Dots Using Thermal Plasma Jet, ACS Nano, 8(5) (2014) 4190–4196.

[42] R. Gokhale, P. Singh, Blue Luminescent Graphene Quantum Dots by Photochemical Stitching of Small Aromatic Molecules: Fluorescent Nanoprobes in Cellular Imaging, Part. Part. Syst. Charact., 31 (2014) 433–438.

[43] L. Zhou, J. Geng, B. Liu, Graphene Quantum Dots from Polycyclic Aromatic Hydrocarbon for Bioimaging and Sensing of Fe^{3+} and Hydrogen Peroxide, Part. Part. Syst. Charact., 30 (2013) 1086–1092.

[44] L. Tang, R. Ji, X. Cao, J. Lin, H. Jiang, X. Li, K.S. Teng, C.M. Luk, S. Zeng, J. Hao, S.P. Lau, Deep Ultraviolet Photoluminescence of Water-Soluble Self-Passivated Graphene Quantum Dots, *ACS Nano*, 6(6) (2012) 5102–5110.

[45] X. Wu, F. Tian, W. Wang, J. Chen, M. Wu, J.X. Zhao, Fabrication of highly fluorescent graphene quantum dots using L–glutamic acid for in vitro/in vivo imaging and sensing, J. Mater. Chem. C, 1 (2013) 4676-4684.

[46] Y. Dong, J. Shao, C. Chen, H. Li, R. Wang, Y. Chi, X. Lin, G. Chen, Blue luminescent graphene quantum dots and graphene oxide prepared by tuning the carbonization degree of citric acid, Carbon, 50 (2012) 4738–4743.

[47] P. Atienzar, A. Primo, C. Lavorato, R. Molinari, H. García, Preparation of Graphene Quantum Dots from Pyrolyzed Alginate, Langmuir, 29 (2013) 6141−6146.

[48] J. Moon, J. An, U. Sim, S. Cho, J.H. Kang, C. Chung, J. Seo, J. Lee, K.T. Nam, B.H. Hong, One-Step Synthesis of N-doped Graphene Quantum Sheets from Monolayer Graphene by Nitrogen Plasma, Adv. Mater., 26 (2014) 3501–3505.

[49] S. Li, Y. Li, J. Cao, J. Zhu, L. Fan, X. Li, Sulfur-Doped Graphene Quantum Dots as a Novel Fluorescent Probe for Highly Selective and Sensitive Detection of Fe^{3+}, Anal. Chem., 86(20) (2014) 10201–10207.

[50] R. Yan, H. Wu, Q. Zheng, J. Wang, J. Huang, K. Ding, Q. Guoa J. Wang, Graphene quantum dots cut from graphene flakes: high electrocatalytic activity for oxygen reduction and low cytotoxicity, RSC Adv. 4 (2014) 23097–23105.

[51] L. Zhang, Z. Zhang, R. Liang, Y. Li, J. Qiu, Boron-Doped Graphene Quantum Dots for Selective Glucose Sensing Based on the "Abnormal" Aggregation-Induced Photoluminescence Enhancement, Anal. Chem., 86 (2014) 4423−4430.

[52] Q. Feng, Q. Cao, M. Li, F. Liu, N. Tang, Y. Du, Synthesis and photoluminescence of fluorinated graphene quantum dots, Appl. Phys. Lett., 102 (2013) 013111-013114.

[53] X. Zhu, X. Zuo, R. Hu, X. Xiao, Y. Liang, J. Nan, Hydrothermal synthesis of two photoluminescent nitrogen-doped graphene quantum dots emitted green and khaki luminescence Mater. Chem. Phys., 147 (2014) 963–967.

[54] C. Hu, Y. Liu, Y. Yang, J. Cui, Z. Huang, Y. Wang, L. Yang, H. Wang, Y. Xiaob, J. Rong, One-step preparation of nitrogen-doped graphene quantum dots from oxidized debris of graphene oxide, J. Mater. Chem. B, 1 (2013) 39–42.

[55] Y. Dai, H. Long, X. Wang, Y. Wang, Q. Gu, W. Jiang, Y. Wang, C. Li, T.H. Zeng, Y. Sun, J. Zeng, Versatile Graphene Quantum Dots with Tunable Nitrogen Doping, Part. Part. Syst. Charact., 31 (2014) 597–604.

[56] Q. Liu, B. Guo , Z. Rao , B. Zhang, J.R. Gong , Strong Two-Photon-Induced Fluorescence from Photostable, Biocompatible Nitrogen-Doped Graphene Quantum Dots for Cellular and Deep-Tissue Imaging, Nano Lett., 13(6) (2013) 2436–2441.

[57] M. Li, W. Wu, W. Ren, H. Cheng, N. Tang, W. Zhong, Y. Du, Synthesis and upconversion luminescence of N-doped graphene quantum Dots, Appl. Phys. Lett., 101 (2012) 103107.

[58] Y. Li, Y. Zhao, H. Cheng, Y. Hu, G. Shi, L. Dai, L. Qu, Nitrogen-Doped Graphene Quantum Dots with Oxygen-Rich Functional Groups J. Am. Chem.Soc. 134 (2012) 15−18.

[59] Tran Van Tam, Nguyen Bao Trung, Hye Ryeon Kim, Jin Suk Chung, Won Mook Choi, One-pot synthesis of N-doped graphene quantum dots as a fluorescent sensing platform for Fe^{3+} ions detection, Sens. Actuators B, 202 (2014) 568–573.

[60] J. Ju, R. Zhang, S. He, W. Chen, Nitrogen-doped graphene quantum dots-based fluorescent probe for the sensitive turn-on detection of glutathione and its cellular imaging, RSC Adv., 4 (2014) 52583-52589.

[61] J. Ju, W. Chen, Synthesis of highly fluorescent nitrogen-doped graphene quantum dots for sensitive, label-free detection of Fe (III) in aqueous media, Biosens. Bioelectron., 58 (2014) 219–225.

[62] B. Zhang, H. Gao, X. Li, Synthesis and optical properties of nitrogen and sulfur co-doped graphene quantum dots, New J. Chem., 38 (2014) 4615-4621

[63] H. Li, H. He, Z. Ye, Preparation of Doped Graphene Quantum Dots with Bright and Excitation-Independent Blue Fluorescence, Adv. Mat. Res., 950 (2014) 44-47.

[64] Z. Luo, D. Yang, G. Qi, J. Shang, H. Yang, Y. Wang, L.Yuwen, T. Yu, W. Huang, L. Wang, Microwave-assisted solvothermal preparation of nitrogen and sulfur co-doped reduced graphene oxide and graphene quantum dots hybrids for highly efficient oxygen reduction, J. Mater. Chem. A, 2 (2014) 20605-20611.

[65] P. Gong, Z. Yang, W. Hong, Z. Wang, K. Hou, J. Wang, S. Yang, To lose is to gain: Effective synthesis of water-soluble graphene fluoroxide quantum dots by sacrificing certain fluorine atoms from exfoliated fluorinated graphene, Carbon, 83 (2015) 152–161.

[66] Z. Wang, J. Xia, C. Zhou, B. Via, Y. Xia, F. Zhang, Y. Li, L. Xia, J. Tang, Synthesis of strongly green-photoluminescent graphene quantum dots for drug carrier, Colloids S. B, 112 (2013) 192–196.

[67] J. Shen, Y. Zhu, X. Yang, J. Zong, J. Zhang, C. Li, One-pot hydrothermal synthesis of graphene quantum dots surface-passivated by polyethylene glycol and their photoelectric conversion under near-infrared light, New J. Chem., 36 (2012) 97–101.

[68] S. Zhu, J. Zhang, S. Tang, C. Qiao, L. Wang, H. Wang, X. Liu, B. Li, Y. Li, W. Yu, X. Wang, H. Sun, B. Yang, Surface Chemistry Routes to Modulate the Photoluminescence of Graphene Quantum Dots: From Fluorescence Mechanism to Up-Conversion Bioimaging Applications. Adv. Funct. Mater., 22 (2012) 4732–4740.

[69] H. Sun, N. Gao, L. Wu, J. Ren, W. Wei, X. Qu, Highly Photoluminescent Amino-Functionalized Graphene Quantum Dots Used for Sensing Copper Ions, Chem. Eur. J., 19 (2013) 13362–13368.

[70] G.S. Kumar, R. Roy, D. Sen, U.K. Ghorai, R. Thapa, N. Mazumder, S. Sahab K.K. Chattopadhyay, Amino-functionalized graphene quantum dots: origin of tunable heterogeneous photoluminescence, Nanoscale, 6 (2014) 3384–3391.

[71] H. Tetsuka, R. Asahi, A. Nagoya, K. Okamoto, I. Tajima, R. Ohta, A. Okamoto, Optically Tunable Amino-Functionalized Graphene Quantum Dots. Adv. Mater., 24 (2012) 5333–5338.

[72] P. Luo, Z. Ji, C. Li, G. Shi, Aryl-modified graphene quantum dots with enhanced photoluminescence and improved pH tolerance, Nanoscale, 5 (2013) 7361–7367.

[73] Z. Qian, J. Ma, X. Shan, L. Shao, J. Zhou, J. Chen, H. Feng, Surface functionalization of graphene quantum dots with small organic molecules from photoluminescence modulation to bioimaging applications: an experimental and theoretical investigation R. Soc. Chem. Adv., 3 (2013) 14571–14579.

[74] J. Liu, X. Zhang, Z. Cong, Z. Chen, H. Yang G. Chen, Glutathione-functionalized graphene quantum dots as selective fluorescent probes for phosphate-containing metabolites, Nanoscale, 5 (2013) 1810–1815.

[75] T. Han, X. Zhou, X. Wu, Enhancing the Fluorescence of Graphene Quantum Dots with a Oxidation Way, Adv. Mat. Res., 887-888 (2014) 156-160.

[76] H. Sun, L. Wu, N. Gao, J. Ren, X. Qu, Improvement of Photoluminescence of Graphene Quantum Dots with a Biocompatible Photochemical Reduction Pathway and Its Bioimaging Application, ACS Appl. Mater. Interfaces, 5 (2013) 1174−1179.

[77] P. Luo, Y. Qiu, X. Guanab L. Jiang, Regulation of photoluminescence properties of graphene quantum dots via hydrothermal treatment, Phys. Chem. Chem. Phys., 16 (2014) 19011–19016.

[78] L. Li, L. Li, C. Wang, K. Liu, R. Zhu, H. Qiang, Y. Lin, Synthesis of nitrogen-doped and amino acid-functionalized graphene quantum dots from glycine, and their application to the fluorometric determination of ferric ion. DOI: 10.1007/s00604-014-1383-6.

[79] I.P. Hamilton, B. Li, X. Yan, L. Li, Alignment of colloidal graphene quantum dots on polar surfaces, Nano Lett., 11 (2011) 1524-1529.

[80] Y. Li, Y. Zhao, H. Cheng, Y. Hu, G. Shi, L. Dai, L. Qu, Nitrogen-Doped Graphene Quantum Dots with Oxygen-Rich Functional Groups, J. Am. Chem. Soc., 134 (2012) 15-18.

[81] X. Wang, X. Sun, J. Lao, H. He, T. Cheng, M. Wang, S. Wang, F. Huang, Multifunctional graphene quantum dots for simultaneous targeted cellular imaging and drug delivery, Colloids Surf. B, 122 (2014) 638–644.

[82] X. Liu, W. Gao, X. Zhou, Y. Ma, Pristine graphene quantum dots for detection of copper ions, J. Mater. Res., 29 (2014) 1401-1407.

[83] F. Wang, Z. Gu, W. Lei, W. Wang, X. Xia, Q. Hao, Graphene quantum dots as a fluorescent sensing platform for highly efficient detection of copper (II) ions, Sensors Actuat. B, 190 (2014) 516– 522.

[84] Z. Fan, Y. Li, X. Li, L. Fan, S. Zhou, D. Fang, S. Yang, Surrounding media sensitive photoluminescence of boron-doped graphene quantum dots for highly fluorescent dyed crystals, chemical sensing and bioimaging, Carbon, 70 (2014) 149–156.

[85] B. Wanga, S. Zhuo, L. Chen, Y. Zhang, Fluorescent graphene quantum dot nanoprobes for the sensitive and selective detection of mercury ions, Spectrochim. Acta Mol. Biomol. Spectros., 131 (2014) 384–387.

[86] H. Chakraborti, S. Sinha, S. Ghosh, S.K. Pal, Fluorescent graphene quantum dot nanoprobes for the sensitive and selective detection of mercury ions, Mater. Lett., 97 (2013) 78–80.

[87] F. Cai, X. Liu, S. Liu, H. Liu, Y. Huang, A simple one-pot synthesis of highly fluorescent nitrogen-doped graphene quantum dots for the detection of Cr(VI) in aqueous media, RSC Adv., 4 (2014) 52016–52022.

[88] H. Huang, L. Liao, X. Xu, M. Zou, F. Liu, N. Li, The electron-transfer based interaction between transition metal ions and photoluminescent graphene quantum dots (GQDs): A platform for metal ion sensing, Talanta, 117(2013) 152–157.

[89] T. Hallaj, M. Amjadi, J.L. Manzoori, R. Shokri, Chemiluminescence reaction of glucose-derived graphene quantum dots with hypochlorite, and its application to the determination of free chlorine, Microchim. Acta, DOI 10.1007/s00604-014-1389-0

[90] Y. Dong, G. Li, N. Zhou, R. Wang, Y. Chi, G. Chen, Graphene quantum dot as a green and facile sensor for free chlorine in drinking water, Anal. Chem., 84 (2012) 8378–8382.

[91] Z.L. Wu, M.X. Gao, T.T. Wang, X.Y. Wan, L.L Zheng, C.Z. Huang, A general quantitative pH sensor developed with dicyandiamide N-doped high quantum yield graphene quantum dots, Nanoscale, 6 (2014) 3868–3874.

[92] J. Bai, L. Zhang, R. Liang, J. Qiu, Graphene Quantum Dots Combined with Europium Ions as Photoluminescent Probes for Phosphate Sensing, Chem. Eur. J., 19 (2013) 3822 – 3826.

[93] J. Liu, X. Zhang, Z. Cong, Z. Chen, H. Yang and G. Chen, Glutathione-functionalized graphene quantum dots as selective fluorescent probes for phosphate-containing metabolites, Nanoscale, 5 (2013) 1810–1815.

[94] Q. Zhang, C. Song, T. Zhao, H. Fu, H. Wang, Y. Wang, D. Kong, Photoluminescent sensing for acidic amino acids based on the disruption of graphene quantum dots/europium ions aggregates, Biosens. Bioelectron., 65 (2015) 204–210.

[95] L. Li, G. Wu, T. Hong, Z. Yin, D. Sun, E.S. Abdel-Halim, J. Zhu, Graphene Quantum Dots as Fluorescence Probes for Turn-off Sensing of Melamine in the Presence of Hg^{2+}, ACS Appl. Mater. Interfaces, 6 (2014) 2858−2864.

[96] Z. Wu, W. Li, J. Chen, C. Yu, A graphene quantum dot-based method for the highly sensitive and selective fluorescence turn on detection of biothiols, Talanta, 119 (2014) 538–543.

[97] Z. Li, Y. Wangb, Y. Ni, S. Kokot, A sensor based on blue luminescent graphene quantum dots for analysis of a common explosive substance and an industrial intermediate, 2,4,6-trinitrophenol, Spectrochim. Acta Mol. Biomol. Spectros., 137 (2015) 1213–1221.

[98] L. Fan, Y. Hua, X. Wang, L. Zhang, F. Li, D. Han, Z. Li, Q. Zhang, Z. Wanga, L. Niu, Fluorescence resonance energy transfer quenching at the surface of graphene quantum dots for ultrasensitive detection of TNT, Talanta, 101 (2012) 192–197.

[99] Y. Li, H. Huang, Y. Ma, J. Tong, Highly sensitive fluorescent detection of dihydroxybenzene based ongraphene quantum dots, Sensors Actuat. B, 205 (2014) 227–233.

[100] R. Sun, Y. Wang, Y. Ni, S. Kokot, Graphene quantum dots and the resonance light scattering technique for trace analysis of phenol in different water samples, Talanta, 125 (2014) 341–346.

[101] Z. Qu, X. Zhou, L. Gu, R. Lan, D. Sun, D. Yu, G. Shi, Boronic Acid Functionalized Graphene Quantum Dots as Fluorescent Probe for Selective and Sensitive Glucose Determination in Microdialysate, Chem. Commun., 49 (2013) 9830-9832.

[102] Y. Li, L. Zhang, J. Huang, R. Liang, J. Qiu, Fluorescent graphene quantum dots with a boronic acid appended bipyridinium salt to sense

monosaccharides in aqueous solution, Chem. Commun., 49 (2013) 5180–5182.

[103] S.Benítez-Martínez, M. Valcárcel, Graphene quantum dots as sensor for phenols in olive oil, Sensors Actuat. B, 197 (2014) 350–357.

[104] S. Benítez-Martínez, A.I. López-Lorente, M. Valcárcel, Graphene quantum dots sensor for the determination of graphene oxide in environmental water samples, Anal. Chem., 86 (2014) 12279-12284.

[105] Y. Liu, W.Q. Loh, A. Ananthanarayanan, C. Yang, P. Chen, C. Xu, Fluorescence quenching between unbounded graphene quantum dots and gold nanoparticles upon simple mixing, RSC Adv., 4 (2014) 35673–35677.

[106] Y. He, X. Wang, J. Sun, S. Jiao, H. Chen, F. Gao, L. Wang, Fluorescent blood glucose monitor by hemin-functionalized graphene quantum dots based sensing system, Anal Chim Acta., 810 (2014)71-78.

[107] Z. Li, R. Sun, Y. Ni S. Kokot, A novel fluorescent probe involving a graphene quantum dot–enzyme hybrid system for the analysis of hydroquinone in the presence of toxic resorcinol and catechol, Anal. Methods, 6 (2014) 7420–7425.

[108] Y. Wang, L. Zhang, R. Liang, J. Bai, J. Qiu, Using Graphene Quantum Dots as Photoluminescent Probes for Protein Kinase Sensing, Anal. Chem., 85 (2013) 9148–9155

[109] X. Ran, H. Sun, F. Pu, J. Ren, X. Qu, Ag Nanoparticle-decorated graphene quantum dots for label-free, rapid and sensitive detection of Ag^{+} and biothiols, Chem. Commun., 49 (2013) 1079–1081.

[110] Y. Zhou, Z. Qu, Y. Zeng, T. Zhou, G. Shi, A novel composite of graphene quantum dots and molecularly imprinted polymer for fluorescent detection of paranitrophenol, Biosens. Bioelectron., 52 (2014) 317–323.

[111] X. Li, S. Zhu, B. Xu, K. Ma, J. Zhang, B. Yang, W. Tian, Self-assembled graphene quantum dots induced by cytochrome c: a novel biosensor for trypsin with remarkable fluorescence enhancement, Nanoscale, 5 (2013) 7776-7779.

[112] M. Roushani, Z. Abdi, Novel electrochemical sensor based on graphene quantumdots/riboflavin nanocomposite for the detection of persulfate, Sensors Actuat. B, 201 (2014) 503–510.

[113] Y. Zhang, C. Wu, X. Zhou, X. Wu, Y. Yang, H. Wu, S. Guo, J. Zhang, Graphene quantum dots/gold electrode and its application in living cell H_2O_2 detection. Nanoscale, 5 (2013) 1816–1819.

[114] H. Razmi, R. Mohammad-Rezaei, Graphene quantum dots as a new substrate for immobilization and direct electrochemistry of glucose oxidase: Application to sensitive glucose determination, Biosens. Bioelectron., 41 (2013) 498–504.

[115] Y. Chen, Y. Dong, H. Wu, C. Chen, Y. Chi, G. Chen, Electrochemiluminescence sensor for hexavalent chromium based on the graphene quantum dots/peroxodisulfate system. Electrochim. Acta, 151 (2015) 552–557.

[116] L. Li, J. Ji, R. Fei, C. Wang, Q. Lu, J. Zhang, L. Jiang, J. Zhu, A Facile Microwave Avenue to Electrochemiluminescent Two-Color Graphene Quantum Dots, Adv. Funct. Mater., 22 (2012) 2971–2979.

[117] M. Mazloum-Ardakani, R. Aghaei, M. Abdollahi-Alibeik, A. Moaddeli, Fabrication of modified glassy carbon electrode using graphene quantum dot, gold nanoparticles and 4-(((4-mercaptophenyl)imino)methyl) benzene-1,2-diol by self-assembly method and investigation of their electrocatalytic activities, J. Electroanal. Chem., 738 (2015) 113–122.

[118] A. Muthurasu, V. Ganesh, Horseradish Peroxidase Enzyme Immobilized Graphene Quantum Dots as Electrochemical Biosensors, Appl Biochem Biotechnol., 174 (2014) 945-959.

[119] J. Hou, F. Bei, M. Wang, S. Ai, Electrochemical determination of malachite green at graphene quantum dots–gold nanoparticles multilayers–modified glassy carbon electrode, J. Appl. Electrochem., 43 (2013) 689–696.

[120] D. Wild, E. Kodak. The immunoassay handbook, Elservier Ltd., 2013.

[121] L. Li, W. Li, C. Ma, H. Yang, S. Ge, J. Yu, Paper-based electrochemiluminescence immunodevice for carcinoembryonic antigen using nanoporous gold-chitosan hybrids and graphene quantum dots functionalized Au@Pt, Sensors Actuat. B, 202 (2014) 314-322.

[122] H. Yang, W. Liu, C. Ma, Y. Zhang, X. Wang, J. Yu, X. Song, Gold-silver nanocomposite-functionalized graphene based electrochemiluminescence immunosensor using graphene quantum dots coated porous PtPd nanochains as labels, Electrochim. Acta, 123 (2014) 470-476.

[123] X. Wang, L. Chen, X. Su, S. Ai, Electrochemical immunosensor with graphene quantum dots and apoferritin-encapsulated Cu nanoparticles double-assisted signal amplification for detection of avian leukosis virus subgroup J, Biosens. Bioelectron., 47 (2013) 171-177.

[124] I. Al-Ogaidi, H. Gou, Z.P. Aguilar, S. Guo, A.K. Melconian, A.K.A. Al-kazaz, F. Meng, N. Wu, Detection of the ovarian cancer biomarker CA-125 using chemiluminescence resonance energy transfer to graphene quantum dots, Chem. Commun., 50 (2014), 1344-1346.

[125] H. Zhao, Y. Chang, M. Liu, S. Gao, H. Yu, X. Quan, A universal immunosensing strategy based on regulation of the interaction between graphene and graphene quantum dots, Chem. Commun., 49 (2013) 234-236.

[126] A. Sett, S. Das, P. Sharma, U. Bora, Aptasensors in Health, Environment and FoodSafety Monitoring, Open Journal of Applied Biosensor, 1 (2012) 9-19.

[127] Z.S. Qian, X.Y. Shan, L.J. Chai, J.R. Chen, H. Feng, Dual–colored graphene quantum dotslabeled nanoprobes/graphene oxide: functional carbon materials for respective and simultaneous detection of DNA and thrombin, Nanotechnology, 25 (2014) 415-501.

[128] Z. S. Qian, X. Y. Shan, L. J. Chai, J. J. Ma, J. R. Chen, H. Feng, A universal fluorescence sensing strategy based on biocompatible graphene quantum dots and graphene oxide for the detection of DNA. Nanoscale, 6 (2014) 5671–5474.

[129] Z.S. Qian, X.Y. Shan, L.J. Chai, J.J. Ma, J.R. Chen, H. Feng, DNA nanosensor based on biocompatible graphene quantum dots and carbon nanotubes, Biosens. Bioelectron., 60 (2014) 64–70.

[130] J. Zhao, G. Chen, L. Zhu, G. Li, Graphene quantum dots-based platform for the fabrication of electrochemical biosensors, Electrochem. Commun., 13 (2011) 31–33.

[131] W. Liu, H. Yang, C. Ma, Y.Ding, S. Ge, J. Yu, M. Yan, Graphene–palladium nanowires based electrochemical sensor using ZnFe2O4–graphene quantum dots as an effective peroxidase mimic, Anal. Chim. Acta, 852 (2014) 181–188.

[132] J. Lu, M. Yan, L. Ge, S. Ge, S. Wang, J. Yan, J. Yu, Electrochemiluminescence of blue-luminescent graphene quantum dots and its application in ultrasensitive aptasensor for adenosine triphosphate detection, Biosens. Bioelectron., 47 (2013) 271-277.

[133] G. Wang, X. Niu, G. Shi, X. Chen, R. Yao, F. Chen, Functionalized graphene quantum dots loaded with free radicals combined with liquid chromatography and tandem mass spectrometry to screen radical scavenging natural antioxidants from Licorice and Scutellariae, J. Sep. Sci., 37 (2014) 3641-3648.

[134] P

[135] S. Benítez–Martínez, M. Valcárcel, Fluorescent determination of graphene quantum dots in water samples. Subbmited to Analytical Chimica Acta.

BLOQUE II

Herramientas Analíticas

En el desarrollo experimental de la presente Tesis Doctoral se han empleado diferentes herramientas analíticas, que se describen brevemente en este Bloque. Éstas incluyen a los nanomateriales, analitos, reactivos y muestras empleados. La descripción de los métodos utilizados para la síntesis de nanopartículas también ha sido incluida, encontrando al final de este bloque, la descripción de los instrumentos, aparatos y otros materiales utilizados y los métodos de tratamiento de muestra, dispersión, extracción y preconcentración empleados.

II.1. NANOMATERIALES

Los nanomateriales empleados durante el desarrollo experimental de esta Tesis Doctoral son los que se detallan a continuación:

1.1. Nanopartículas de carbono

1.1.1. Grafeno

Se han empleado nanoláminas de grafeno dispersas en colato de sodio. Las dispersiones fueron suministradas por NanoIntegris (Stokie, IL, USA) con una pureza en peso>98%. La tabla II.1 muestra la distribución de láminas proporcionada por el distribuidor.

Tabla II. 1. Distribución de láminas de los dos tipos de grafeno adquiridos.

	Grafeno tipo 1 "Research Grade"	Grafeno tipo 2 "Industrial Grade"
1 lámina	27%	6%
2 láminas	48%	23%
3 láminas	20%	27%
4+ láminas	5%	44%

También se ha empleado grafeno en polvo que fue proporcionado por Avanzare Tecnológica SL (Logroño, España). Este grafeno se caracterizó por poseer entre 1 y 6 láminas.

1.1.2. Nanotubos de carbono.

Los nanotubos de carbono de pared simple (SWNTs) fueron proporcionados por Shenzhen Nanotech Port Co. Ltd (NTP), China, con una pureza superior al 90%, y un área superficial específica de 500-700 m^2g^{-1}.

1.1.3. Óxido de grafeno y puntos cuánticos de grafeno

El óxido de grafeno (GO) y los puntos cuánticos de grafeno (GQDs) fueron obtenidos en el laboratorio. Ambos procedimientos de obtención se detallan en el apartado II.3 de este bloque, junto al procedimiento para la introducción de grupos funcionales en los nanotubos de carbono.

1.2. Nanopartículas de oro

Se han empleado nanopartículas de oro con citrato, cuya síntesis se detalla en el apartado II.3 de este bloque.

1.3. Nanopartículas de óxido de titanio

Las nanoparticulas de dióxido de titanio (IV) con un diámetro <150 nm fueron obtenidas de Sigama–Aldrich.

II.2. ANALITOS, REACTIVOS Y MUESTRAS

Durante el desarrollo de la Tesis Doctoral se han utilizado los siguientes reactivos:

- Reactivos para la síntesis de nanopartículas: ácido tetracloroaúrico ($HAuCl^4$), citrato sódico dihidrato 99.5%, ácido cítrico 99%, y glicina 98%, de Sigma-Aldrich. L-cisteina 99.5%, de Fluka.
- Tensioactivos: Colato de sodio, de Sigma–Aldrich.
- Sales: Acetato de amonio, carbonato sódico, de Sigma–Aldrich.
- Ácidos:, Ácido sulfúrico, de Sigma–Andrich. Ácido nítrico y ácido clorhídrico, de Panreac

- Bases: hidróxido sódico, hidróxido potásico de Sigma-Aldrich.
- Disolventes: n–hexano y acetona (Sigma-Aldrich), *N,N*–dimetilformamida (Panreac), metanol y acetonitrilo (Carlo Erba Reagents) y agua ultrapura (obtenida a través de un sistema MilliQ de Millipore).
- Analitos: Los antiinflamatorios no esteroideos (ibuprofeno, ketoprofeno, fenbufeno, flurbiprofeno, naproxeno), el violeta de cristal, el metronidazol, el ácido gálico y la oleuropeina, de Sigma–Aldrich. En la tabla II.1 se muestra la estructura de todos ellos.
- Otros reactivos: Folin&ciocalteu(2N) de Sigma–Aldrich.

Todos los estándares, reactivos y disolventes empleados a lo largo de la investigación fueron de pureza analítica o superior.

Tabla II.1. *Estructuras químicas de los analitos empleados.*

FAMILIA DE COMPUESTOS	ANALITO	ESTRUCTURA QUÍMICA
Aintiinflamatorios no esteroideos (arilpropiónicos)	Ibuprofeno	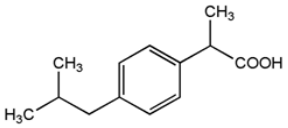
	Ketoprofeno	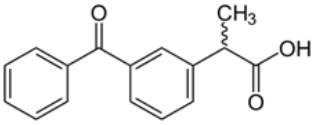
	Fenbufeno	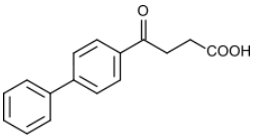
	Flurbiprofeno	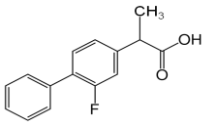
	Naproxeno	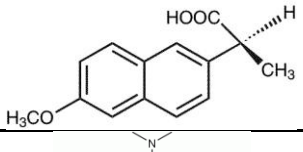
Rosanilinas	Violeta de cristal	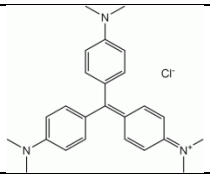
Nitroimidazoles	Metronidazol	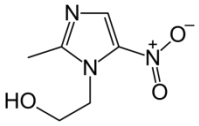
Polifenoles	Ácido Gáilco	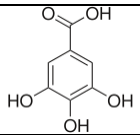
	Oleuorpeina	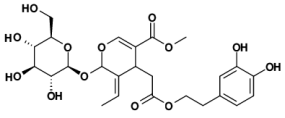

2.1. Muestras

Para llevar a cabo el estudio de la utilidad analítica de los distintos métodos de determinación de nanopartículas desarrollados para su aplicación en muestras medioambientales, se seleccionaron muestras de agua de río y muestras de manantial.

Las muestras de agua de río fueron recolectadas y almacenadas en frascos de vidrio ámbar sin dejar espacio de cabeza a 4ºC. Las muestras de manantial fueron tratadas del mismo modo y fueron tomadas en las inmediaciones de la localidad de Montilla (Córdoba, España). Las muestras se recogieron de varios afluentes del Rio Guadalquivir a su paso por Córdoba (España).

Las muestras de aceite de oliva fueron suministradas por Sovena España–Consumer Goods (Sevilla, España) y almacenadas en oscuridad a temperatura ambiente en el envase original.

Las muestras de crema solar fueron adquiridas en un comercio local y almacenadas en el laboratorio a temperatura ambiente en su envase original.

II.3. SÍNTESIS Y FUNCIONALIZACIÓN DE NANOPARTÍCULAS

3.1. Síntesis de nanopartículas de oro con citrato

Las nanopartículas de oro se sintetizaron de manera análoga al método propuesto por Turkevich et al.[1] con algunas modificaciones. En primer lugar se limpió el material de vidrio necesario para la síntesis con agua regia (mezcla 1:3 de HNO3:HCl), se lavó con agua ultrapura y se secó con una corriente de aire. Las disoluciones de HAuCl 4 y citrato sódico fueron preparadas en agua ultrapura y filtradas antes de su empleo. Se preparon 50 mL de una disolución de HAuCl4 0.01% que se calentó con agitación magnética. Cuando la disolución empezó a hervir se añadieron añadieron 0.254 mL de una disolución de citrato sódico al 1%. Se dejó reaccionar durante 15 minutos y a continuación se añadieron 5mL de HAuCl4 0.01% caliente seguidos de 0.254 mL de citrato sódico al 1%. Se dejó reaccionar nuevamente durante otros 15 minutos y una vez transcurrido este tiempo, se apagó el calentador de la placa manteniendo la agitación mientras la disolucíon alcanzó la temperatura ambiente. La disolución fue almacenada en un frasco de color topacio a 4ºC.

[1] J. Turkevich, P.C. Stevenson, J. Hillier, J. Discuss. Faraday Soc. 11 (1951) 55-75

3.2. Síntesis de puntos cuánticos de grafeno (GQDs)

Los puntos cuánticos de grafeno, o GQDs, fueron obtenidos siguiendo el procedimiento descrito por Dong et al. [2] con algunas modificaciones. Para ello, 2 g de ácido cítrico se pesaron en un vial de vidrio de 10 mL de capacidad. Dicho vial se introdujo en un termoreactor que se mantuvo a 200ºC durante 30 minutos, hasta que ácido cítrico cambió de polvo blanco a una especie se sirope de color entre anaranjado y marrón. El resultante sirope fue añadido a 100mL una disolución de NaOH de 10 $mg{\cdot}mL^{-1}$ que estaba siendo agitada vigorosamente. Una vez finalizado el trasvase, la disolución resultante se mantuvo durante 10 minutos más bajo agitación. Finalmente la disolución se ajustó al pH requerido y se almacenó a 4ºC en un frasco topacio.

3.3. Obtención de óxido de grafeno (GO)

Con el fin de introducir grupos funcionales ricos en oxigeno en la estructura de grafeno, se añadieron 100 mg de grafeno, con 1–6 capas, en forma de polvo a un matraz de vidrio de fondo redondo de 100 mL y se mezcló con 20 mL de una mezcla de H_2SO_4/HNO_3 en proporción 3:1. La mezcla se calentó y se mantuvo en reflujo durante 1 hora. Seguidamente, se centrifugaron las fracciones diluidas de la mezcla a 1000 rpm durante 20 minutos y se realizaron lavados con agua ultrapura hasta que el sobrenadante

[2] Y. Dong, J. Shao, C. Chen, H. Li, R. Wang, Y. Chi, X. Lin, G. Chen, Carbon 50 (2012) 4738–4743.

dejó de tener pH ácido. Finalmente, el GO fue obtenido y se secó a 60ºC en una estufa. Después de la oxidación química, la superficie del GO está cargada negativamente gracias a la presencia de los gropos funcionales y resulta ser muy soluble y estable en disolución acuosa.

3.4. Funcionalización de nanotubos de carbono (SWNTs)

De forma análoga al procedimiento anterior, se oxidaron nanotubos de carbono monocapa (SWCNTs), con la diferencia de que se centrifugó a 10000 rpm durante 10. Los SWCNTs están cargados negativamente y presentan los extremos abiertos, lo que los hace solubles en agua.

Ambos métodos de funcionalización están basados en el procedimiento descrito por Xue y Cui[3], con algunas modificaciones.

3.5. Funcionalización de puntos cuánticos de grafeno

Los GQDs fueron funcionalizados con glicina y L–cisteína separadamente y de forma análoga adaptando la síntesis al procedimiento descrito por Tam et al.[4] para otros compuestos nitrogenados.

Para la funcionalización con glicina, 2 g de ácido cítrico (como fuente de carbono) y 0.62 g de glicina se disolvieron en 5mL de agua en un vial de 10

[3] W. Xue, T. Cui, Nanotechnology, 18 (2007) 145709/1-145709/7
[4] Tam, T.V.; Trung, N.B.; Kim, H.R.; Chung, J.S.; Choi, W.M. *Sens. Actuators B* **2014**, *202*, 568–573.

mL que se introdujo en un termoreactor para ser calentado a 200ºC durante 3h. La disolución marrón oscura obtenida, con aspecto de sirope, fue diluida en 100 mL de NaOH 0.25M que se agitó vigorosamente durante el trasvase y 20 minutos después para alcanzar la estabilidad de la reacción. El material funcionalizado se almacenó a 4ºC en un frasco topacio.

Para la funcionalización de GQDs con L-cisteina se siguó el mismo procedimiento que para los funcionalizados con glicina. De este modo, 2g de ácido cítrico y 0.5 g de L-cisteina se disolvieron en 5 mL de agua, se calentaron a 200ºC en un termoreactor durante 3 horas y se diluyeron en 100 mL de de NaOH 0.25M, almacenándose finalmente en un frasco topacio a 4ºC.

3.6. Sintesis de óxido de grafeno fluorescente

El óxido de grafeno fluorescente fue obtenido siguiendo el procedimeinto descrito por Dong. et al.[2] mediante la pirolisis del ácido cítrico con ligeras modificaciones. Para ello, 2 g de ácido cítrico se pesaron en un vial de vidrio de 10 mL de capacidad. Dicho vial se introdujo en un termoreactor que se mantuvo a 200ºC durante 2 horas, hasta que ácido cítrico cambió de polvo blanco a una especie se sirope de color negro. El resultante sirope fue añadido a 50mL de una disolución de NaOH de 10 $mg{\cdot}mL^{-1}$ que estaba siendo agitada vigorosamente. Una vez finalizado el trasvase, la disolución resultante

se mantuvo durante 10 minutos más bajo agitación. Finalmente la disolución se ajustó al pH requerido y se almacenó a 4ºC en un frasco topacio.

II.4. INSTRUMENTACIÓN Y OTROS MATERIALES

En el desarrollo experimental de la presente Tesis Doctoral se ha hecho uso de diferentes equipos instrumentales, los cuales se describen a continuación.

4.1. Electroforesis capilar

La separación de antiinflamatorios no esteroideos, empleando una fase pseudoestacionaria de nanoláminas de grafeno, por electroforesis capilar se realizó utilizando un equipo Agilent CE ChemStation (Santa Clara, CA, USA) equipado con un detector UV-Vis de diodos en fila (DAD). Los capilares de sílice fundida utilizados fueron de 75 μm de diámetro interno. El equipo dispone del software HP ChemStation para el control del instrumento y la recogida y tratamiento de datos.

4.2. Espectrómetro Raman portátil

Para la caracterización del sustrato híbrido creado a partir de multicapas de grafeno y nanoparticulas de oro, así como para su empleo como sustrato en SERS se ha trabajado con espectrómetro Raman portátil de B&W

TEK Inc., conocido como inno-Ram con un láser de785 nm y una potencia de láser máxima en el puerto de excitación de 350 mW y 285 mW en la sonda. Los objetos fueron observados a través de un objetivo Nikon (50x/0.80). La señal Raman fue adquirida por medio un detector de carga acoplada (CCD) enfriado a –20ºC. Para tratar los datos se utilizó el softwareBWSpec 3.27 y Excel Enterprise 2007.

4.3. Espectroscopia de fluorescencia molecular.

La medida de la emission de la fluorescencia (FL) se llevó a cabo empleando un espectroflorímetro PTI QuantaMaster™ de la compañía Photon Technology International (Barcelona, España) equipado con una lámpara xenón de 75 Wde arco corto y un sistema de detección 814 PTM. Para la adquisión de los datos y control del equipo se empleó el software Felix 32.

4.4. Espectrofotometría UV-Vis

Para llevar a cabo las medidas UV-Vis se emplearon dos equipos diferentes: (i) se utilizó lámpara de halógeno como fuente de excitación acoplada al monocromador y detector fotónico de un espectrofluorímetro PTI QuantaMasterTM como detector (Photon technology International) controlado por el software FeliX32.(ii) Se empleó un espectrofotómetro Lambda 35 ES UV/Vis de la compañía Perkin Elmer (Madrid, Spain) equipado

con dos fuentes de excitación (una lámpara de deuterio y otra lámpara de tungsteno–halógeno) y detector de fotodiodo.

4.5. Espectroscopia infrarroja

Las medidas de infrarrojo se llevaron a cabo usando un espectrómetro FT- Bruker tensor 27FT–MIR equipado con un microscopio Hyperion 2000, usando pastillas de KBr.

4.6. Microscopía electrónica (TEM y SEM)

Para la caracterización de las nanopartículas se utilizaron los siguientes equiposde microscopía electrónica:

Microscopía de barrido electrónico: microscopio electrónico de barrido (SEM) JEOL JSM 6300 con una capacidad de aumento de entre 70x y 300.000x y una resolución de 3~4 nm (a 30 Kv). Servicio central de apoyo a la investigación (SCAI) de la Universidad de Córdoba.

Microscopía de transmisión electrónica: Microscopio Electrónico de Transmisión de alta resolución JEOL JEM 2010 con una resolución punto a punto de 0.194 nm, equipado con sistema de microanálisis de rayos X por dispersión de energía. SCAI, Universidad de Córdoba.

Microscopio electrónico de transmisión de alta resolución TECNAI F30 a 300 kV dotado de cañón de emisión de campo, modo STEM y detectores HAADF y EDX en el ICMS. Instituto de Materiales, CSIC, Sevilla.

Aparatos y Materiales

Durante el desarrollo del trabajo experimental realizado en esta Tesis Doctoral, se emplearon los siguientes **aparatos**:

- Bomba peristáltica Gilson Miniplus-3 (Middleton, Estados Unidos).
- Ultracentrífuga controlada por microprocesador (Centronic BL-II, J.P. Selecta, Barcelona, España).
- Baño de ultrasonidos 50 W, 60 Hz (J.P. Selecta, Barcelona, España).
- Sonda ultrasonidos VibracellTM 75041(750 W, 20 KHz, Bioblock Scientific, Illkirch, Francia), equipada con una sonda de 3 mm.
- Agitador Vortex (Heidolph, Mérida, España).
- Agitador magnético (Velp Científica, Milán, Italia).
- Placa calefactora con agitación magnética Agimatic-N (J.P. Selecta, Barcelona, España)
- Termoreactor 350 W, 50 Hz, 1,5 A (J.P. Selects, Barcelona, España)

- Horno cromatográfico HP 5890 (Agilent Technologies, Palo Alto, CA, USA).
- pH-metro (Crison, modelo micropH 2000).
- Balanza analítica Cobos AI-220CB (Cobos, Barcelona, España).
- Balanza analítica de precisión OHAUS Explorer (OHAUS, Nänikon, Suiza).
- Equipo de agua Milli-Q (Millipore, Bedford, MA, EEUU).

Asimismo se ha empleado el siguiente **material**:

- Jeringas de plático de 1 y 10 mL (Albus, España),
- Filtros de jeringa de nylon de tamaño de poro 0.20μm y 0.45 μm (Análisis Vínicos, España)
- Papel de filtro
- Membranas de acetato de celulosa de tamaño de poro de 0.20 μm (Sartorius Stedim Biotech, Alemania).
- Cristales ópticos de CaF_2 de 20mm de diámetro y 1mm de espesor (CristalTechno, Moscow, Russia)
- Pipetas pasteur de vidrio (Albus, España)
- Tubos de centrifuga de polipropileno

- Tubos de FIA
- Rejillas Formvar Carbon Film (Electron Microscopy Sciences, EEUU)
- Microjeringas Hamilton de 1 y 10μL (Análisis Vínicos, España).
- Micropipetas automáticas (Análisis Vínicos, España).
- Micro Cubeta de cuarzo de Hellma con un paso óptico de 10 mm.
- Cubetas de polipropileno
- Material de vidrio de laboratorio, clase A.
- Envases de vidrio para el correcto almacenamiento de los estándares, muestras y otras disoluciones.

II.5. MÉTODOS DE TRATAMIENTO DE MUESTRA, DISPERSIÓN, EXTRACCIÓN Y PRECONCENTRACIÓN

5.1. Extracción líquido-líquido convencional

En este caso se llevó a cabo una extracción líquido–líquido convencional adaptada de la bibliografia[5,6]. Para ello, se empléo n–hexano para diluir las muestras con base oleosa que se combinaron con de un mezcla

[5] F. M. Pirisi, P. Cabras, C. F. Cao, M. Migliorini, M. Muggelli, Journal of Agricultural and Food Chemistry 48 (2000) 1191–1196.
[6] C. Contado, A. Pagnoni, Anal. Chem. 80 (2008) 7594–7608.

metanol/agua en un tubo de centrifuga. . La mezcla se agitó en un vortex durante unos minutos ,y se centrifugó posteriormente varias fases claramente diferenciadas. Entonces, la fase metanólica se separó de las otras fases y se repitió el procedimiento de extracción dos veces más, añadiendo solamente el correspondiente volumen de la mezcla metanol/agua. Una vez completada la extracción, se combinaron los extractos y se sometieron a una etapa de limpieza que se realizó con n–hexano. La etapa de limpieza del extracto se repitó varias veces. Para ello, el extracto metanólico se mezclo con el hexano, se agitó y se centrifugó para favorecer la separación de las fases. La fase que contenía el hexano fue desechada. Y los analitos quedaron contenidos en la fase metanólica.

5.2. Extracción y preconcentración de puntos cuánticos de grafeno

Para la extracción de GQDs se seleccionó el procedimiento de extracción en fase sólida se eligiendo cartuchos comerciales SAX (Intercambio aniónico fuerte, Biotage, Hengoed, United Kingdom), de 50mg/1mL. Para el procedimiento de extracción, se lavó la columna con 1 mL de agua ultrapura, seguido de 1 mL de acetato amónico 0.1M y 1mL del mismo tampón a una concentración de 15 Mm. A continuación se pasó la muestra a un ritmo constante de 1mL por minuto. Para conseguir el flujo constante se automatizó la etapa de carga de la muestra mediante el empleo de una bomba peristáltica. Tras la carga de la muestra el sorbente fue secado pasando aire a

través de la columna. La elución se llevó a cabo empleando 0.5 mL de una una disolución de NaOH 0.25 M a una velocidad constante de 0.1 mL por minuto, consiguiendo al mismo tiempo la preconcentración de las nanoestructuras.

5.3. Preconcentración de GO en membranas de celulosa.

Se han preconcentrado láminas de GO en muestras acuosas mediante el uso de una membrana de celulosa de 0.20 μm. Para ello se microfiltraron 5 mL de muestra acuosa usando un sistema de filtración Millipore con ayuda de una bomba peristáltica para mantener un flujo constante. Posteriormente se pasó 1 mL de una disolución de NaOH a pH 13 para eliminar posibles interferencias, y, finalmente, se pasa 1 mL de agua ultrapura.

5.4. Preconcentración de analitos mediante evaporación con nitrógeno

Se han preconcentrado polifenoles y nanoparticulas de titanio, tras su extracción de determinadas matrices, mediante el empleo de una corriente de nitrógeno que produjo el borboteo constante de las disoluciónes mientras estas de mantenían a una temperatura constante de 35ºC, en el caso de los polifenoles, y 70ºC , en el caso de las nanopartículas de titanio, para favorecer su evaporación, con ayuda de un termoreactor.

5.5. Dispersión de nanotubos de carbono y óxido de grafeno

Los nanotubos de carbono y el grafeno son insolubles en agua y tienen una gran tendencia a la agregación. En la presente Tesis Doctoral se

han seguido aumentar su carácter hidrofílico mediante la introducción de grupos funcionales como se ha explicado anteriormente. Para facilitar la dispersión se sometieron las disoluciones de SWCNTs y GO a un tratamiento de ultrasonidos empleando una punta sónica.

BLOQUE III

El grafeno y sus derivados en la Nanociencia y Nanotecnología Analíticas

III.1 Electroforesis Capilar

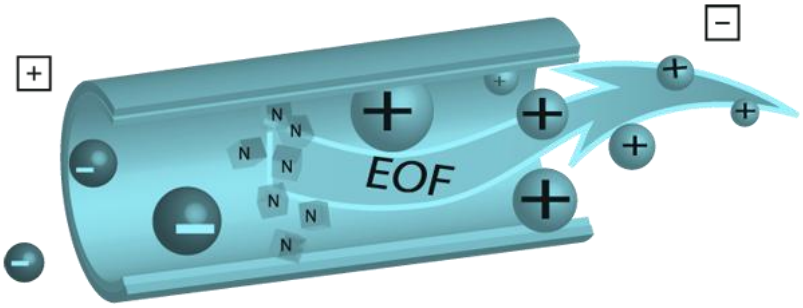

Desde su aparición, las nanopartículas han sido ampliamente utilizadas en el ámbito analítico como herramienta para la mejora del proceso analítico a través del desarrollo de nuevos métodos que permitan sacar mayor provecho de las técnicas disponibles, o bien, implementar métodos bien establecidos consiguiendo ventajas en cuanto a sensibilidad y precisión obtenidos.

La electroforesis capilar (CE) es una técnica bien implantada en los laboratorios de rutina que permite una elevada velocidad de separación de los analitos al emplear altos voltajes y capilares relativamente cortos con una alta eficacia y unos volúmenes de muestra muy pequeños que reducen considerablemente el consumo de disolventes y reactivos.

En lo que a CE se refiere, el grafeno ha sido incorporado como material composite en el desarrollo de nuevos electrodos para la determinación de constituyentes varias moléculas[1,2], así como fase estacionaria[3].

Los antiinflamatorios no esteroideos (AINEs) han sido objeto de numerosos estudios para su determinación mediante el empleo de técnicas cromatografías (HPLC[4], GC–MS)[5] .

El capítulo 2 de esta tesis doctoral describe el empleo de nanoláminas de grafeno estabilizadas en tensioactivo como fase pseudoestacionaria para la mejora de la separación electroforética de AINEs.

[1] X. Wang, J. Li, W. Qu, G. Chen, Journal of Chromatography A, 1218 (2011) 5542–5548.
[2] B. Chen, L. Zhang, G. Chen, Electrophoresis, 32(2011) 870–876
[3] R.P. Liang, C.M.Liu, X.Y. Meng, J.W. Wang, J.D. Qiu, Journal of Chromatography A, 1266 (2012) 95– 102.
[4] Z. Es'haghi, E.Esmaeili-Shahri, Journal of Chromatography B, 973,(2014) 142-151.
[5] H. Zhang, P. Zhang, Y. Ji, J. Tian, Z. Du, Chemical Engineering Journal, 262 (2015) 11081115.

Capítulo 2

Graphene Nanoparticles as Pseudostationary Phase for the Electrokinetic separation of nonsteroidal anti-inflammatory drugs

Electrophoresis 34 (2013) 2561–2567

Electrophoresis 2013, *34*, 2561–2567

Sandra Benítez-Martínez
Bartolomé M. Simonet
Miguel Valcárcel

Department of Analytical Chemistry, University of Córdoba, Campus of Rabanales, Córdoba, Spain

Research Article

Graphene nanoparticles as pseudostationary phase for the electrokinetic separation of nonsteroidal anti-inflammatory drugs

The exceptional properties of graphene were exploited here to facilitate capillary electrokinetic separations. Two types of commercially available graphene consisting of nanoparticles containing 1–3 and 4–6 graphene sheets, respectively, were compared for this purpose. Both proved effective in separating the arylpropyl derivatives of non-steroidal anti-inflammatory drugs (NSAIDs). The highest resolution and shortest migration times were obtained with graphene containing high amount of single and double graphene nanosheets. Graphene affords higher resolution than other types of nanoparticles; stable suspensions can be easily prepared and used as background electrolyte (BGE) without the need for adds an additional surfactant. This results in a high reproducibility in migration times and stability in background noise. The limits of detection (LOD) and quantitation (LOQ) obtained by using graphene nanoparticles as pseudo-stationary phases spanned the range 0.29–1.18 $mg{\cdot}L^{-1}$ and 0.95–3.95 $mg{\cdot}L^{-1}$, respectively, and the relative standard deviation (RDS) was less than 4.7 % in all instances.

Keywords: Capillary electrophoresis, graphene, non-steroidal anti-inflammatory drugs, pseudo-stationary phase.

1. INTRODUCTION

Analytical Nanoscience and Nanotechnology have two complementary connotations dependent on the particular role played by nanomaterials, which can act as object–analytes (the targets of analysis of the nanoworld) or as tools for improving analytical processes. Nanoparticles have so far largely been used to improve sample preparation [1], particularly with functionalized and non-functionalized carbon nanoparticles such as fullerenes, carbon nanotubes (CNTs) and carbon nanohorns, which are the most widely employed as sorbents in solid-phase (micro)extraction (SPE, SPME) and dispersive microextraction, among other techniques. In recent years, graphene (G) and graphene oxide (GO) have attracted considerable interest by virtue of their exceptional properties in relation to other carbon nanoparticles.

Graphene, which was first synthesized by Geim and Novoselov [2] in 2004, has a planar structure consisting of nanosheets formed by carbon atoms with sp^2 hybridization in a honeycomb lattice with properties in between those of a metallic conductor and a semiconductor material. Worth special note are their high Young's modulus (about 1100 GPa), charge mobility ($2 \cdot 10^5$ $cm^2 \cdot V^{-1} \cdot s^{-1}$), surface area (*ca.* 2630 $m^2 \cdot g^{-1}$), chemical stability and hydrophobicity —hence their strong tendency to form nanosheet aggregates, which is the origin of some of the unique properties of graphene.

G and GO have been used in Analytical Science ever since they became commercially available. The earliest natural application of both types of carbon nanoparticles was the preparation of electrodes for sensing and biosensing [3]. However, their unique sorbent properties have been exploited to improve sample preparation in SPE, SPME and MALDI–TOF–MS, among other techniques [4].

The combined use of G or GO and capillary electrophoresis (CE) has enabled various applications according to the particular role played by the nanomaterial. For example, GO has been used as the target analyte for CE fractionation and analysis with a view to monitoring its production by exfoliation of graphite oxide [5] or by chemical oxidation of flake graphite and ultrasonication [6].

Also, G and GO can be used as tools for improving the CE separation and determination of a variety of analytes. Our group has critically reviewed the role of carbon nanoparticles —G and GO excluded— in this context [7]. G and GO can be used in various ways in the capillary electrophoretic process. Thus, they can be used as components of the inner stationary phase to improve separations (e.g. by immobilizing GO nanosheets onto the capillary wall with silane as coupling agent [8, 9] or using β-cyclodextrin functionalized GO–magnetic nanocomposites as a tunable stationary phase in chip-based

open-tubular capillary electrochromatography (EKC) [10]). Also, G and GO can be used as sorbents in new electrochemical devices for sample introduction in CE [11]. In addition, G and GO have been used as electrode nanocomponents for electrochemical detection in CE —their commonest application to date [12–17].

To the authors' knowledge, G and GO have never previously been used as pseudo-stationary phases in CE, even though other carbon nanoparticles such as carbon nanotubes (both single-walled and multi-walled), fullerenes and nanocones have been extensively used for this purpose [7]. In general, G and GO are used as surfactant-coated nanoparticles or in functionalized form (as soluble oxidized nanoparticles). The main aim of this work was to demonstrate the compatibility and usefulness of graphene nanosheets dispersed in the electrophoretic carrier as pseudo-stationary phases for CE in order to develop an additional separation mechanism for improving analyte separation. Five non-steroidal anti-inflammatory drugs were used as model analytes for this purpose.

2. MATERIALS AND METHODS

2.1. Reagents and standards

The NSAIDs used as model analytes (ibuprofen, ketoprofen, fenbufen, flurbiprofen and naproxen) were purchased from Sigma–Aldrich (Madrid,

Spain). A mixture of the five and individual stock standard solutions were prepared at a 1 $g{\cdot}L^{-1}$ concentration in methanol and stored at 4 °C. Working-strength solutions of the NSAIDs were prepared on a daily basis by dilution of the stock solutions in ultrapure water obtained from a water purifying apparatus (Millipore, Madrid, Spain).

Sodium hydroxide, HPLC-grade methanol, ammonium acetate and sodium cholate were purchased from Sigma–Aldrich (Madrid, Spain), and hydrochloric acid was obtained from Panreac Chemical, SAU (Barcelona, Spain). Two types of graphene nanoparticles with a different distribution were purchased from NanoIntegris (Stokie, IL, USA), namely:

- PureSheets (Research Grade), Batch# G-10-964R, henceforth designated G1.
- PureSheets (Industrial Grade), Batch# G-10-126I , henceforth designated G2.

Platelet layer distribution was provided by the commercial firm. The characterization of graphene flakes was carried out by using atomic force microscopy (AFM) and Raman spectroscopy. The production and characterization method was developed by Green *et al.* [18]"

All reagents were stored according to the manufacturers' instructions.

Table 1 shows the platelet layer distribution of the two types of graphene nanoparticles.

Table 1. Influence of the graphene nanosheet concentration in the pseudo-stationary phase.

TYPE 1 GRAPHENE		TYPE 2 GRAPHENE	
Graphene concentration = 1.25 $mg{\cdot}L^{-1}$		Graphene concentration = 1.875 $mg{\cdot}L^{-1}$	
Single layers (27%)	0.337 $mg{\cdot}L^{-1}$	Single layers (6%)	0.1125 $mg{\cdot}L^{-1}$
Double layers (48%)	0.6 $mg{\cdot}L^{-1}$	Double layers (23%)	0.431 $mg{\cdot}L^{-1}$
Triple layers (20%)	0.25 $mg{\cdot}L^{-1}$	Triple layers (27%)	0.506 $mg{\cdot}L^{-1}$
4+ layers (5%)	0.062 $mg{\cdot}L^{-1}$	4+ layers (44%)	0.825 $mg{\cdot}L^{-1}$

2.2. Instrumentation

Electrokinetic separation was performed on an Agilent CE ChemStation (Agilent, Santa Clara, CA, USA) equipped with a deuterium lamp, a UV–Vis detector and a diode-array detector (DAD). The CE system was controlled and data acquired by using the HP ChemStation software.

2.3. Instrumental operating conditions

The uncoated fused-silica capillary column used (75 μm I.D., 370 μm O.D.) was purchased from Beckman Coulter (Fullerton, CA, USA). The column was initially conditioned by passing 1 M HCl (5 min), 0.1 M NaOH (10 min) and ultrapure water (5 min). The capillary was conditioned with 0.1 M sodium

hydroxide (5 min), ultrapure water (5 min) and BGE (5 min) prior to first use each day; with 0.1 M NaOH (3 min), ultrapure water (3 min) and running buffer (3 min) between runs; and with ultrapure water for 10 min at the end of each day. These treatments were all performed at 1000 mbar and in the stated sequence in each case.

An aqueous solution containing 50 mM ammonium acetate at pH 4.0 was used as BGE. The capillary (effective length, 40 cm; total length, 48 cm) was maintained at 25 ºC throughout and the samples were kept at room temperature on the autosampler. Samples were injected in the hydrodynamic mode for 10 s, followed by 2 s of running buffer, both at 50 mbar. Electrophoretic separation was carried out in the positive polarity mode, using a constant applied voltage of 15 kV. The current was around 88 μA in all runs. When a graphene-modified BGE was used, the current was set at 90–107 μA depending on the graphene type and whether sonication was applied. The highest current values were those for G1. Although current was high these values are reasonable taken into account that the system limit is established in 300 μA. Moreover the presence of surfactant increases the ionic strength, also increasing current values. The developed method is based in aqueous solutions and there are not organic solvents, so bubbles formation, which could disrupt the separation process, is not given nor Joule effect observed.

Spectra were recorded at 210 nm. The analytes were identified by using solutions spiked with the individual compounds.

2.4. Preparation of the modified BGE

The modified running buffer used as pseudo-stationary phase (PSP) was prepared by adding G1 and G2 nanosheets at a 1.25 and 1.875 $mg{\cdot}L^{-1}$ concentration, respectively, to 0.8 mL of 50 mM ammonium acetate at pH 4.0. The mixtures were sonicated for 3 minutes with a Vibracell™ 75041 ultrasonic probe (750W, 20 KHz, Bioblock Scientific, Illkirch, France) equipped with a 3 mm probe set at 20% amplitude in an ON/OFF cycle of 20 s each. The graphene PSP was replaced after 15 analyses, all of which were highly precise.

3. RESULTS AND DISCUSSION

The use of commercial graphene solutions dispenses with the need for the additional surfactant required to stabilize other types of nanoparticles such as CNTs, fullerenes and nanocones.

The compatibility of graphene nanoparticles with the analytical system is a critical consideration when the graphene is used as a pseudo-stationary phase. The potencial of graphene as PSP was studied for fenbufen, ibuprofen, ketoprofen, naproxen and flurbiprofen. Due to their structure based on

aromatic rings, NSAIDs could interact with graphene (which posses an aromatic system delocalized on their surface) through π–π interactions.

In this work, compatibility was maximized by determining the optimum amount of graphene, pH of the BGE and method of dispersion of the graphene nanosheets, in addition to examining the effect of sodium cholate present in commercial graphene solutions.

3.1. Electrophoretic conditions

The NSAIDs studied exhibited very similar migration times when analysed jointly in a mixture in 50 mM ammonium acetate buffer. Peaks overlapped throughout the pH range examined (4.0–8.0), but especially in the basic region. This led us to modify the BGE with variable amounts of the two types of graphene nanoparticles at the optimum pH.

3.2. Influence of the pH of the background electrolyte

Using the optimum pH for the running buffer is crucial in capillary electrophoresis since whether the analytes are ionized will depend on such a pH. The pH range studied for the 50 mM ammonium acetate buffer was between pH 4.0 and pH 8.0. The former value was found to ensure optimal electrophoretic separation of the NSAIDs —peak resolution was worse at basic pH than at acid pH. Therefore, pH 4.0 was used in all subsequent analyses.

3.3. Isolation of graphene nanosheets from sodium cholate

Commercial graphene nanosheets dispersed in 2% sodium cholate (SC) were isolated from the surfactant to obtain separate nanosheets. To this end, 30 μL of the commercial solution were rinsed with 300 μL of toluene and 300 μL of water. The mixture was manually agitated for 1 min and left to stand for 15 min to separate the phases. Water phase was discarded and toluene phase was appropriately evaporated. The procedure was repeated twice. 0.8mL of 50 mM ammonium acetate buffer pH 4.0 were added to the isolated graphene sheets and introduced in the system to carry out the separation of NSAIDs. The isolated graphene sheets thus obtained were unstable in the electrophoretic system and precipitated on incorporation into the BGE. This required examining the effect of adding the commercial graphene solutions —containing SC— to the BGE and that of SC on analyte separation.

3.4 Nanosheet dispersion in the modified BGE

Graphene commercial nanosheets and the BGE were mixed in three different ways. First, graphene nanosheet-modified BGE was manually shaken for 1 min and used directly to separate the NSAIDs. Second, modified running buffer was sonicated in an ultrasonic bath (Bransonic 3510, 100 W, 42 kHz ± 5%, Danbury, CT, USA) for 15 min. Third, graphene was dispersed in the buffer solution with the aid of an ultrasonic probe for 3 min, using 20-s ON/OFF. The manually shaken graphene nanosheets formed no homogeneous solution

and started to precipitate in the vial that contains de modified buffer after a few minutes. All graphene nanosheets did not precipitate at the same time, remaining in suspension some of them. The sonicated nanosheets formed a not stable whitish solution that also starts to precipitate in the vial after several minutes. By contrast, the nanosheets dispersed with an ultrasonic probe formed a homogeneous solution that remained stable for more than a week. However the modified running buffer was prepared daily. In the last case, the BGE changed from transparent to grey- coloured. Although the ultrasonic radiation exposure time was low when ultrasonic probe was used, the dispersion using this method was more effective because the applied power was higher than that applied with ultrasonic bath. Moreover the ultrasonic radiation is applied directly on the sample and this makes more effective the nanosheet dispersion. Based on the foregoing, the modified BGE was prepared by using an ultrasonic probe.

3.5 Influence of the graphene concentration in the BGE

The ammonium acetate running buffer (50 mM, pH 4.0) was modified with variable amounts of the two types of graphene. G1 contained a high proportion of single and double nanosheets, whereas G2 contained an increased proportion of nanosheets of 3, 4 and even more than 4 layers.

The G1 and G2 concentrations added to the running buffer were 0.3125, 0.625, 1.25, 1.875 and 2.5 mg·L^{-1}. The best results in terms of resolution and sensitivity were obtained with 1.25 mg·L^{-1} of G1 and 1.875 mg·L^{-1} of G2. Analyses were performed in the presence and absence —manual shaking— of ultrasound. Figures 1 and 2 show the migration times of the analytes at different graphene concentrations in the BGE, with and without sonication.

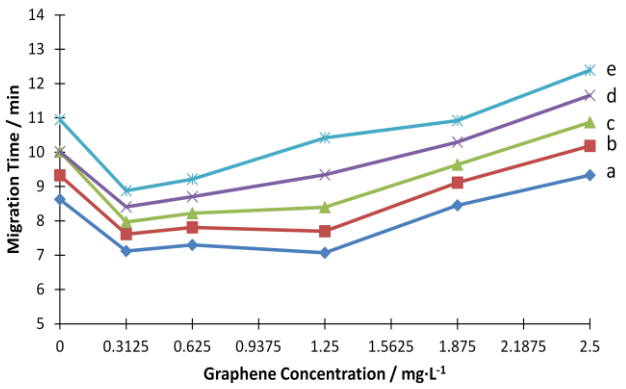

Figure 1. Effect of sonication on the type 1 graphene pseudo-stationary phase. a fenbufen, b ibuprofen, c ketoprofen, d naproxen, e flurbiprofen.

The actual nanosheet concentrations at these optimum values are shown in Table 1. As can be seen, the concentration of single and double layers in G1 was higher than that in G2, even though the amount of G1 added to the BGE was smaller than that of G2.

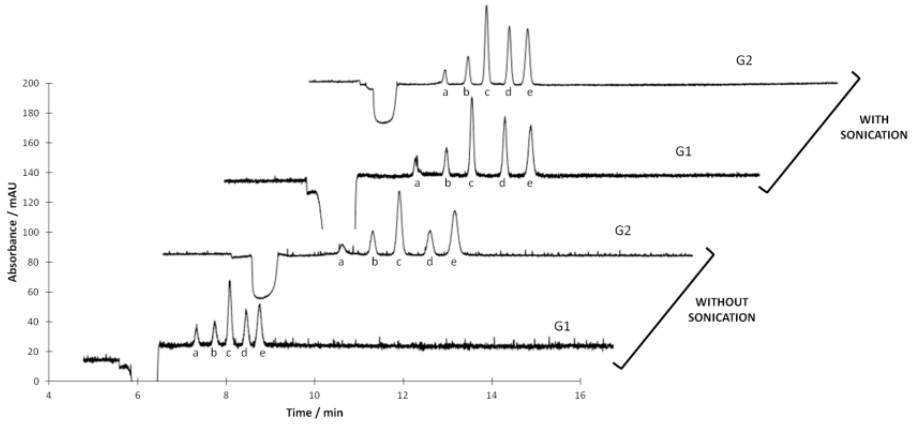

Figure 2. Typical electropherogram for the graphene pseudo-stationary phases. The two types of graphene are compared in the presence and absence of sonication. G1 type 1 graphene, G2 type 2 graphene. a fenbufen, b ibuprofen, c ketoprofen, d naproxen, e flurbiprofen. BGE_{G1} 0.8 mL of 50 mM $AcNH_4$ pH 4.0 + 1.25 $mg{\cdot}L^{-1}$ G1; BGE_{G2} 0.8 mL of 50 mM $AcNH_4$ pH 4.0 + 1.845 $mg{\cdot}L^{-1}$ G2. Values of plate number and resolution have been calculated for the electropherograms showed in this figure. As an illustration, values of G1 with sonication are indicated below. Plate number for a 14157, b 126865, c 129537, d 175640, e 101629. Resolution for a-b 5.8, b-c 5.7, c-d, 6.4, d-e 4.38.

Therefore, the improved peak resolution obtained was due to the presence of single and double layers rather than to aggregated nanoparticles. In addition, sonicating the graphene-modified buffer resulted in improved peak resolution, migration time, sensitivity and background noise through decreased nanoparticle aggregation —and an increased presence of monolayers and bilayers in solution. The electropherograms of Fig. 2 illustrate the effect of sonication on peak resolution, migration time, sensitivity and background

noise for the target NSAIDs. As can be seen, the modified BGE led to essentially similar or even shorter migration times than the unmodified BGE.

Graphene concentrations well above their optimal levels increased migration times; also, the ensuing aggregates might have clogged the capillary column. A single capillary column sufficed to perform all tests and never during their conduct was the column clogged by graphene aggregates.

3.6 Influence of sodium cholate

As noted earlier, both types of graphene nanoparticles were stabilized with a 2% w/v concentration of the anionic surfactant sodium cholate (SC). Although this amount did not exceed its critical micelle concentration (CMC), we investigated whether the improved separation of NSAIDs was due to the graphene nanosheets rather than to its presence. To this end, the running buffer was modified with variable concentrations of SC equivalent to those present in the graphene solution added to the BGE. The specific concentrations of SC added to the running buffer were 0.54, 1.08 and 1.63 mM, and respectively equivalent to the SC concentrations present in the 0.625, 1.25 and 1.875 $mg{\cdot}L^{-1}$ solutions of graphene added to the BGE. Tests were performed at pH 4.0, 5.0, 6.0 and 7.0. None of the previous concentrations resulted in effective resolution of peaks. Therefore, adding SC to the modified BG did not ensure separation of the NSAIDs; also, the presence of SC caused

no change in electrophoretic mobility in the analytes. Figure 3 compares the results obtained with the sonicated graphene pseudo-stationary phase and an SC-modified BGE.

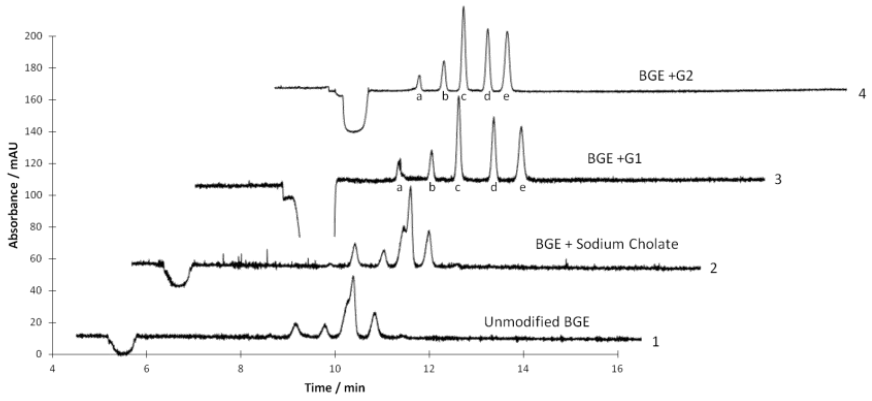

Figure 3. Typical electropherograms for unmodified BGE and SC- and graphene-modified pseudo-stationary phases. The figure compares the use of a graphene (G1 or G2)-modified BGE under optimum conditions with an unmodified and a surfactant (SC)-modified BGE. (1) Unmodified BGE. (2) SC-modified BGE. (3) Sonicated type 1 graphene PSP. (4) Sonicated type 2 graphene PSP. a fenbufen, b ibuprofen, c ketoprofen, d naproxen, e flurbiprofen. BGE_1 0.8 mL of 50 mM $AcNH_4$ pH 4.0, BGE_2 0.8 mL of $AcNH_4$ 50 mM pH 4.0 + 1.63 mM SC; BGE_3 0.8 mL of 50 mM $AcNH_4$ pH 4.0 + 1.25 $mg{\cdot}L^{-1}$ G1, BGE_4 0.8 mL of 50 mM $AcNH_4$ pH 4.0 + 1.875 $mg{\cdot}L^{-1}$ G2.

3.7 Analytical figures of merit

The performance of graphene as a PSP was assessed in terms of sensitivity, limit of detection (LOD), limit of quantitation (LOQ) and precision (% RDS). Ibuprofen, ketoprofen, fenbufen, flurbiprofen and naproxen were used as model analytes for this purpose. Analytical features were calculated by

using unmodified buffer and buffers modified with 1.25 $mg{\cdot}L^{-1}$ of G1 and one of 1.875 $mg{\cdot}L^{-1}$ of G2, with and without sonication. With unmodified buffers, the NSAIDs were injected individually rather than in mixture in order to avoid peak overlap. Five calibration graphs were constructed by plotting absorbances versus NSAID concentrations in the unmodified buffer and four others were used with the graphene-modified BGE. The linear range was from 5 to 25 $mg{\cdot}L^{-1}$. The results are summarized in Table 2.

The reproducibility of the proposed method was assessed in terms of peak area and migration time from five independent measurements of 10 and 20 $mg{\cdot}L^{-1}$ solutions. The RSD values thus obtained were 0.34–6.02 % for peak area and 0.31–6.20% for migration time.

As can be seen from Table 3, using sonication to disperse the graphene nanosheets significantly improved LODs and LOQs, as well as correlation. Thus, LODs ranged from 0.29 to 2.37 $mg{\cdot}L^{-1}$ and LOQs from 0.95 to 7.91 $mg{\cdot}L^{-1}$. Also, the calibration graphs exhibited good correlation for the five analytes, with coefficients exceeding 0.9905 in all cases. Finally, NSAIDs were separated with a resolution of 3.7–6.4 and the plate number was between 1588–2665 for the sonicated G2 and 14157–175640 for the sonicated G1.

Table 2. *Analytical figures of merit of the determination of NSAIDs under different experimental conditions.*

	LOD ($mg{\cdot}L^{-1}$)	LOQ ($mg{\cdot}L^{-1}$)	$S_{y/x}$	Slope ± S_s	Intercept ± S_i	R^2
50 mM $AcNH_4$ pH 4.0						
Fenbufen	2.13	7.09	4.79	4.89 ± 0.23	6.21 ± 3.47	0.9912
Ibuprofen	0.95	3.19	4.80	11.59 ± 0.23	-1.59 ± 3.70	0.9980
Ketoprofen	1.46	4.86	20.90	33.78 ± 1.01	-7.15 ± 16.43	0.9982
Naproxen	1.87	6.26	30.46	35.73 ± 1.47	-18.05 ± 22.28	0.9950
Flurbiprofen	1.40	4.66	12.47	20.57 ± 0.60	12.13 ± 9.60	0.9974
50 mM $AcNH_4$ pH 40 + 1.25 $mg{\cdot}L^{-1}$ G1 without sonication						
Fenbufen	0.96	3.23	1.59	3.59 ± 0.08	1.52 ± 1.16	0.9983
Ibuprofen	0.47	1.56	1.34	6.26 ± 0.07	-0.01 ± 0.98	0.9996
Ketoprofen	0.76	2.55	6.66	21.09 ± 0.42	-5.25 ± 5.54	0.9992
Naproxen	0.75	2.52	6.75	19.63 ± 0.32	7.63 ± 4.94	0.9991
Flurbiprofen	0.97	3.25	8.59	20.47 ± 0.54	9.7 ± 6.65	0.9978
$AcNH_4$ 50 mM pH 4.0 + 1.25 $mg{\cdot}L^{-1}$ G1 with sonication						
Fenbufen	0.74	2.49	2.32	6.74 ± 0.11	-2.25 ± 1.68	0.9989
Ibuprofen	0.45	1.50	1.55	7.97 ± 0.10	0.38 ± 1.20	0.9996
Ketoprofen	0.62	2.08	7.00	24.63 ± 0.33	6.42 ± 5.12	0.9994
Naproxen	0.45	1.51	2.40	12.75 ± 0.15	-1.93 ± 1.93	0.9997
Flurbiprofen	0.29	0.95	1.88	15.20 ± 1.27	-0.82 ± 1.45	0.9998
AcNH4 50 mM pH 4.0 + 1.875 $mg{\cdot}L^{-1}$ G2 without sonication						
Fenbufen	1.18	3.95	2.27	4.16 ± 0.10	1.86 ± 1.65	0.9972
Ibuprofen	0.50	1.68	2.07	9.50 ± 0.10	-1.18 ± 1.60	0.9996
Ketoprofen	0.62	2.06	7.88	27.80 ± 0.40	-6.58 ± 5.72	0.9993
Naproxen	0.81	2.72	5.83	16.48 ± 0.28	2.24 ± 4.49	0.9991
Flurbiprofen	0.44	1.46	5.17	25.54 ± 0.24	-6.53 ± 3.74	0.9996
$AcNH_4$ 50 mM pH 4.0 + 1.875 $mg{\cdot}L^{-1}$ G2 with sonication						
Fenbufen	1.06	3.53	2.00	4.13 ± 0.09	2.35 ± 1.46	0.9983
Ibuprofen	0.47	1.56	1.55	7.68 ± 0.09	1.02 ± 1.20	0.9995
Ketoprofen	0.35	1.19	4.59	21.73 ± 0.21	5.27 ± 3.32	0.9996
Naproxen	0.79	2.63	3.99	12.96 ± 0.20	-3.31 ± 3.41	0.9992
Flurbiprofen	0.40	1.33	3.41	19.84 ± 0.21	2.1 ± 2.64	0.9996

a) Calibration graphs were obtained at five different concentration levels. The calibration range was 5–25 $mg{\cdot}L^{-1}$.
b) LOD was calculated as $3{\cdot}S_i$/slope.
c) LQD was calculated as $10{\cdot}S_i$/slope.
d) "Sy/x" is defined as Standard Error of the Estimate (SEE).
e) "Slope ±Ss" is defined as Slope ± error in the slope.
f) "Intercept ± Si" is defined as Intercept ± error in the intercept.

Table 3. Precision of the proposed method under different experimental conditions.

	AREA (% RSD)		MIGRATION TIME (% RSD)	
	10 $mg{\cdot}L^{-1}$	20 $mg{\cdot}L^{-1}$	10 $mg{\cdot}L^{-1}$	20 $mg{\cdot}L^{-1}$
50 mM $AcNH_4$ pH 4.0				
Fenbufen	1.36	3.27	4.10	2.63
Ibuprofen	0.77	2.04	1.11	0.91
Ketoprofen	2.91	4.64	1.52	1.46
Naproxen	4.29	2.18	4.70	2.34
Flurbiprofen	1.67	2.35	1.33	1.38
50 mM $AcNH_4$ pH 4.0 + 1.25 $mg{\cdot}L^{-1}$ G1 without sonication				
Fenbufen	2.25	3.35	2.31	1.19
Ibuprofen	1.08	2.05	2.19	0.77
Ketoprofen	1.94	1.58	2.79	0.91
Naproxen	2.32	3.39	2.34	0.95
Flurbiprofen	3.55	2.22	2.23	0.98
50 mM $AcNH_4$ pH 4.0 + 1.25 $mg{\cdot}L^{-1}$ G1 with sonication				
Fenbufen	2.90	1.97	1.13	0.83
Ibuprofen	2.46	1.82	1.01	0.29
Ketoprofen	0.34	1.91	1.06	0.24
Naproxen	2.62	1.90	1.25	0.28
Flurbiprofen	1.60	1.87	1.09	0.31
50 mM $AcNH_4$ pH 4.0 + 1.875 $mg{\cdot}L^{-1}$ G2 without sonication				
Fenbufen	2.62	3.81	2.00	3.00
Ibuprofen	3.29	3.55	2.22	3.41
Ketoprofen	3.19	4.24	2.49	4.44
Naproxen	4.75	4.40	2.61	4.05
Flurbiprofen	3.52	3.25	2.83	3.49
50 mM $AcNH_4$ pH 4.0 + 1.875 $mg{\cdot}L^{-1}$ G2 with sonication				
Fenbufen	2.31	3.63	1.95	1.2
Ibuprofen	1.88	1.86	1.41	1.18
Ketoprofen	1.98	3.82	1.47	1.31
Naproxen	2.38	1.96	1.64	1.40
Flurbiprofen	2.76	0.75	1.49	1.39

a) The repeatability of peak areas and migration times, measured as %RSD, was calculated at 10 and 20 $mg{\cdot}L^{-1}$.
b) The relative standard deviation of peak areas was calculated from 5 measurements.
c) The relative standard deviation of migration times was calculated from 5 measurements.

4. CONCLUDING REMARKS

Graphene was for the first time used as a pseudo-stationary phase (PSP) in this work to compare in terms of sensitivity and resolution the electrophoretic behaviour of NSAIDs as analytes in a BGE containing two different types of graphene nanosheets in the presence and absence of sonication. An unmodified BGE was also used for comparison. Graphene was found to have a favourable effect on the determination, even if the BGE contained sodium cholate. Therefore, using graphene nanosheets as a pseudo-stationary phase improves the CE separation of NSAIDs with an important enhancement of resolution. Type 1 graphene afforded better separation than type 2 graphene, even if used in smaller amounts. Applying ultrasonic energy to prepare the BGE was found to improve sensitivity, resolution and background noise, especially with type 2 graphene because it increased the proportion of single nanosheets. The results obtained with sonicated solutions of the two types were very similar. Therefore, the use of sonicated G2 as a pseudo-stationary phase is recommended over G1 because it is less expensive.

All graphene dimensions fall on the nanoscale; by contrast, CNTs are nanometric in diameter only and tend to easily clog capillaries, which can be avoided by using a graphene-based pseudo-stationary phase.

Acknowledgements

The authors wish to thank Junta de Andalucía for financial support (Project FQM 4801). S. Benítez-Martínez is also grateful to Junta de Andalucía for the award of a Research Training Fellowship.

The authors have declared no conflict of interest.

5. REFERENCES

[1] Lucena, R., Simonet, B. M., Cárdenas, S., Valcárcel, M. *J. Chromatogr. A*, 2011, *1218,* 620–637.

[2] Novoselov, K. S., Geim, A.K., Morozov, S.V., Jiang, D.,Zhang, Y., Dubonos, S. V., Grigorieva, I. V., (...), Firsov, A. A. *Science,* 2004, *306*, 666–669.

[3] Pumera, M., Ambrosi, A., Bonanni, A., Chng, E. L. K., Poh, H. L. *Trends Anal. Chem.*, 2010, *29*, 954–965.

[4] Liu, Q., Shi, J., Jiang, G., *Trends Anal. Chem.*, 2012, *37*, 1–11.

[5] Müller, M.B., Quirino, J.P., Nesterenko, P.N., Haddad, P.R., Gambhir, S., Li, D., Wallace, G. G. *J.Chromatogr. A.*, 2010, *1217*, 7593–7597.

[6] Zhao, J., Chen, G., Zhang, W., Li, P., Wang, L., Yue, Q., Wang, H., Dong, R., Yan, X., Liu, *J. Anal. Chem.,* 2011, *83*, 9100–9106.

[7] Moliner–Martínez, Y., Cárdenas, S., Simonet, B.M., Valcárcel, M. *Electrophoresis*, 2009*, 30*, 169 -175.

[8] Qu, Q., Gu, C., Hu, X. *Anal. Chem.*, 2012, *84*, 8880–8890.

[9] Ye, N., Li, J., Xie, Y., Liu, C. *Electrophoresis*. Article in press. DOI: 10.1002/elps.201200516.

[10] Liang, R. P., Liu, C. M., Meng, X. Y., Wang, J. W., Qiu, J. D. *J. Chromatogr. A*, 2012, *1266*, 95–102.

[11] Palatzky, P., Zöpfl, A., Hirsch, T., Matysik, F.M. *Electroanalysis*, 2013, *1*, 117–122.

[12] Liu, Y., Wang, X., Chen, D., Chen, G. *Electrophoresis,* 2011, *32*, 1906–1912.

[13] Sheng, S., Zhang, L., Chen, G. *Electrochem. Commun.*, 2012, *24*, 13–16.

[14] Wang, X., Li, J., Qu, W., Chen, G. *J. Chromatogr. A*, 2011, *1218*, 5542–5548.

[15] Chen, B., Zhang, L., Chen, G. *Electrophoresis*, 2011, *32*, 870–876.

[16] Sheng, S., Liu, S., Zhang, L., Chen, G. *J. Sep. Sci.* Article in Press. DOI: 10.1002/jssc.201200856

[17] Chen, Q., Zhang, L., Chen, G. *Anal. Chem.*, 2012, *84*, 171–178.

[18] Green, A. A., Hersam, M. C. *Nano Letters*, 2009, 9, 4031– 4036.

III.2 Espectroscopia Raman

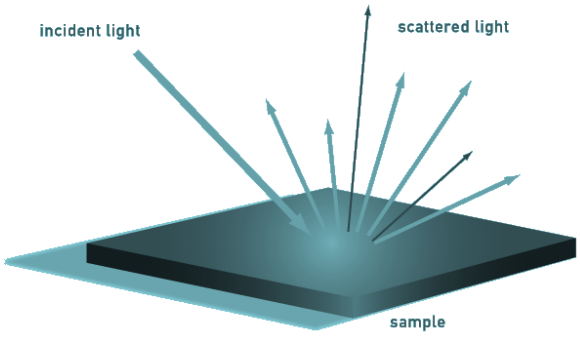

Las excepcionales propiedades del grafeno han sido ampliamente estudiadas empleando técnicas como la espectroscopia Raman, sirviendo además este modo de espectroscopia para describir la capacidad que presenta el grafeno para amplificar la señal Raman de algunas sustancias de interés.

La espectroscopia Raman por amplificación de superficies, más conocida por sus siglas en inglés, SERS, se favorece normalmente del efecto de sustratos modificados con nanopartículas de oro y plata, gracias al establecimiento de mecanismos de tipo electromagnético y químico.

En este capítulo se presenta un sustrato híbrido, resultado de la combinación de multicapas de grafeno y nanopartículas de oro para la determinación de antibióticos como el metronidazol.

Capítulo 3

Multilayer Graphene–Gold Nanoparticles hybrid substrate for the SERS determination of metronidazole

Microchemical Journal, DOI: 10.1016/j.microc.2015.01.006

DOI: 10.1016/j.microc.2015.01.006

Multilayer Graphene–Gold Nanoparticles hybrid substrate for the SERS determination of metronidazole

Sandra Benítez–Martínez, Ángela Inmaculada López-Lorente, Miguel Valcárcel*

Department of Analytical Chemistry, University of Córdoba, E-14071 Córdoba, Spain Phone/Fax +34 957 218616; E-mail: qa1vacam@uco.es

In this paper, a simple, quick and reproducible SERS substrate combining the properties of multilayer graphene (≈ 4 layers) and gold nanoparticles has been developed. The Raman signal of metronidazole is enhanced at a factor of 124 when deposited on the hybrid substrate enabling its determination at low concentrations. The five most relevant added values of

the paper as regards other similar proposed procedures are: i) better sensibility, ii) good reproducibility , iii) rapidity, iv) reusability and v) instrumental simplicity. The procedure presented is capable of detecting and quantifying small quantities of metronidazole without implying any preconcentration step, just using an affordable and portable Raman spectrometer. LOD and LOQ achieved with this hybrid substrate were 1.1 and 3.68 $mg{\cdot}L^{-1}$ of the analyte. The use of graphene provides high reproducibility to the SERS active hybrid substrate. The RSD was 7.76% within a substrate and 10.92 % between substrates. The developed SERS active hybrid substrate can be reused without loss in sensitivity.

Keywords: graphene, gold nanoparticles, SERS, hybrid substrate, metronidazole.

GRAPHICAL ABSTRACT

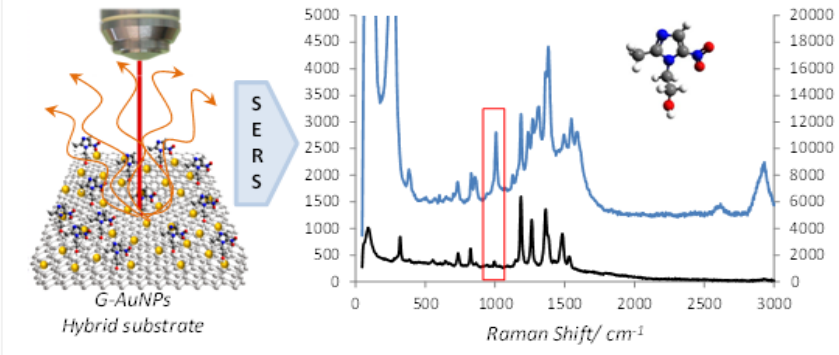

1. INTRODUCTION

Surface–enhanced Raman spectroscopy (SERS) has acquired great importance in the last years in a wide range of research fields such as surface science, electrochemistry, biology, material science, art, forensics and analytical chemistry. SERS provides structural information of the sample [1] and combines molecular fingerprint specificity with single–molecule sensitivity. For this reason, it can be regarded as an attractive tool for sensing molecules in trace amounts [2]. However, SERS technique has not been established as a routine analytical technique due to the low reproducibility of the SERS signal [1]. Traditionally SERS studies have been limited to gold, silver and copper nanoparticles [3-7].

In the last years, graphene, a one atom thick sheet with sp^2 hybridized carbon atoms arranged in a two–dimensional honeycomb lattice, has attracted considerable interest in all research fields due to its exceptional properties, namely high thermal conductivity, high charge carrier mobility, large specific surface area, chemical stability, excellent mechanical properties and a strong hydrophobic nature [8]. Recently, graphene and graphene–family nanomaterials (single layer graphene, bi–layer graphene, multilayer graphene, graphene oxide (GO) and reduced graphene oxide

(rGO)) have been used by several authors as substrate for SERS [9-11] but the enhancement it provided is limited.

Several works have described the synthesis of graphene–gold nanohybrids by different methods [12-15]. The hybridization of graphene with metal nanoparticles (copper [16], silver [17] and gold [12, 18]) provides an improvement in the optical and electrical properties of this nanomaterial [14] leading to an enhancement in the Raman spectra of molecules deposited on these hybrid substrates [19-23]. Gold nanostructures are usually deposited and grown on graphene surface, although in some cases they are placed between layers. The possible interactions between graphene and gold nanostructures can took place through i) covalent bindings, in which graphene, gold nanostructure or both of them are functionalized ii) non–covalent attachments, in the form of π–π interactions and iii)van der Waals forces, which may occur when graphene surface is not modified [12, 19]. The decoration of graphene with gold nanoparticles has been used for studying the enhanced Raman spectrum of graphene [9, 24-28]. It has been also employed for biosensing cancer and cancer stem cells [29], multiplex DNA detection [30] or as Hg^{2+} sensor [31].

Metronidazole (MNZ) is an antibiotic and antiparasitic drug from the nitromidazole family, used in the treatment of infections caused by bacteria

and protozoa in humans and animals. Its use has been banned by the European Commission and the US food and drug administration (FDA) in food-producing animals due to their suspected genotoxic, carcinogenic, and mutagenic properties [32].

This article describes a quantitative method for the determination of metronidazole [2–2–methyl–5–nitroimidazol–1–yl)ethanol] by using a simple and quick graphene-AuNPs (G-AuNPs) hybrid substrate active in SERS, without any functionalization. Herein we demonstrate the interaction of gold nanoparticles with multilayer graphene, enhancing the Raman spectra of the carbon nanomaterial. Moreover, we have taken advantage of the synergistic effect of the combination of metallic NPs and graphene over the Raman signal of metronidazole, enabling their determination and quantification. The developed method boasts great reproducibility and high sensitivity, improving the reported limits of detection for this analyte in SERS [32].

2. EXPERIMENTAL SECTION

2.1 Materials and reagents

All reagents were of analytical grade or better. Graphene, used as SERS substrate, was purchased from NanoIntegris (Skokie, Illinois) as multilayer

(PureSheets QUATTRO™) solution (0.05 mg·mL^{-1}) dispersed in an aqueous 2% w/v sodium cholate solution. CaF_2 optical crystal, with dimensions of 20 mm of diameter and 1mm in width, used as support to graphene nanosheets, was acquired from CristalTechno (Moscow, Russia). Methanol (HPLC grade), supplied by Panreac (USA), and Milli–Q ultrapure water (Millipore Corp., Madrid, Spain) were employed to remove the surfactant of the graphene solution. $HAuCl_4$ (Sigma Aldrich, Madrid, Spain) and sodium citrate dehydrate 99.5% (Sigma Aldrich, Madrid Spain) were used to synthesize AuNPs. Nitric acid 69% and hydrochloric acid 37% (Panreac, USA) were used to wash the glassware materials prior the synthesis of the nanoparticles.

Crystal violet (CV) and metronidazole [2–(2–methyl–5–nitroimidazol–1–yl)ethanol] were purchased from Sigma–Aldrich (Madrid, Spain). The stock solution of CV and metronidazole were prepared in methanol at a concentration of 1 g·L^{-1} and stored at 4 ºC. Working solutions were prepared at room temperature by dilution of the stock solutions in methanol.

2.2 Equipment

Raman measurements were performed with a portable Raman spectrometer system provided by B&W TEK Inc., known as inno–Ram, at room temperature, with a wavelength of 785 nm and a maximum laser output power at system's excitation port of 350 mW and 285 mW in the probe. The

output laser power in the probe set to about 11 mW, although graphene surface could endure 100 % of laser power without any damage. During the measurements, the laser beam was focused to the sample through a 50x/0.80 Nikon objective. Raman signals were acquired by a CCD array detector cooled to –20ºC. Spectra were recorder with one second integration time. Spectral data were collected and treated by the BWSpect 3.27 software. Dimensions of surface observed with this objective were 156.5 x 117.2 μm and the diameter of the laser beam was 8 μm, approximately.

Scanning Electron Microscopy (SEM) images were recorded by use of a JEOL JSM 6300 operating at an accelerating voltage of 5 KV (S.C.A.I., Córdoba).

2.3 Synthesis of gold nanoparticles

AuNPs were synthesized following the citrate reduction method proposed by Turkevich *et al.* [33] with modifications similar to [34]. Firstly, all glass material used in the synthesis was cleaned with a 1:3 mixture of nitric acid and hydrochloric acid, rinsed twice with ultrapure water and dried in air. 0.01% $HAuCl_4$ and 1% sodium citrate solutions were prepared in ultrapure water and filtered through a 0.45 μm nylon membrane prior to use. 25 mL of 0.01% $HAuCl_4$ were heated to boiling while being magnetically stirred. When the boiling point was reached, 0.127 mL of 1% sodium citrate solution were

added and stirred for 15 min. After this time, 0.5 by 0.5 mL of a total of 2.5 mL of 0.01% $HAuCl_4$ were added followed by 0.127 mL of 1% sodium citrate leaving boiling and stirring for other 15 min. After the synthesis, the colloidal suspension was kept stirring until room temperature was reached and then stored in an amber bottle at 4ºC.

2.4 SERS measurements

The SERS-active hybrid substrate was prepared following this procedure: 10 drops of a 0.05 $mg{\cdot}mL^{-1}$ commercial graphene solution were deposited drop–wise on a CaF_2 plate, previously cleaned with piranha water (1:4 H_2O_2: H_2SO_4). This plate was continuously heated at 50ºC until the end of the deposition. Each drop contained 10 μL of the commercial graphene solution. Between drops the deposited graphene was cleaned twice, firstly with 50 μL of methanol in order to remove the surfactant from the graphene surface and then with 50 μL of ultrapure water to remove methanol traces. At the end of the deposition, 0.005 mg of graphene were placed on the plate with a diameter of 0.64±0.04 cm. In a second step, the synthesized AuNPs were deposited drop – wise (10 μL each drop) on the graphene surface to reach a total of 300 μL of the AuNPs solution. The CaF_2 plate was continuously heated at 50 ºC to facilitate solvent evaporation.

Once the graphene–gold nanoparticles SERS substrate was prepared, 1 μL of the analyte (crystal violet or metronidazole) solution was added to the substrate. The analyte was always added in the centre of the SERS substrate with a Hamilton syringe while it scattered over the entire substrate surface.

The deposited analyte was analyzed using SERS detection by means of a portable Raman spectrometer with a 785 nm diode laser. For each analyte concentration three different substrates were prepared. SERS measurements were acquired from 10 randomly selected places within the plate, resulting in a total of thirty SERS signals. The laser power was set to 11 mW. A 1-second acquisition was employed for measurements. The intensity of CV band around 1171 cm^{-1} and metronidazole band at 1186 cm^{-1} were selected as analytical signal and subsequently used in order to quantify the samples.

3. RESULTS AND DISCUSSION

3.1 Characterization of synthesized gold nanoparticles

Synthesized gold nanoparticles have been characterized by ultraviolet-visible spectroscopy and high resolution transmission electron microscopy (HTEM) in order to determine their size and shape (Figure 1). HTEM studies allowed the calculation of the nominal colloid size which was 39 ± 6 nm.

AuNPs appear homogeneous in shape and size and of polygonal yet nearly spherical shape being well dispersed in solution. Their average diameter and concentration were also calculated by UV-vis spectroscopy according to the procedure described by Haiss et al. [35], resulting in an approximated diameter of 32±6 nm, value which is in the range provided by microscopic studies, with a concentration of $2.27 \cdot 10^{-10}$ M.

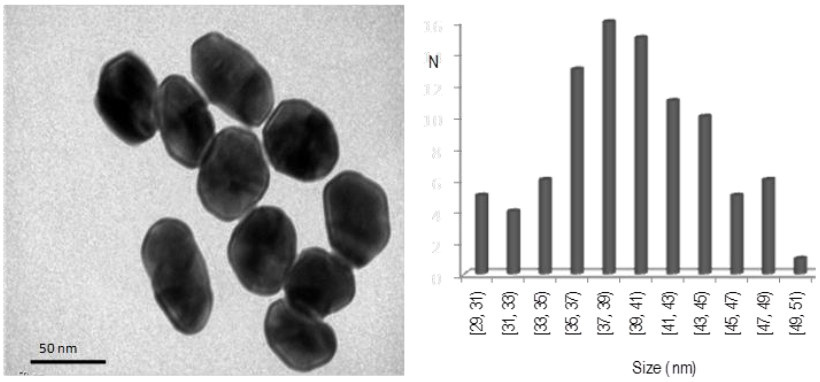

Figure 1. (Left) HTEM image of AuNPs obtained through citrate reduction. (Right) Size distribution of AuNPs calculated from their HTEM images.

3.2 Optimization of the preparation of the SERS substrate and measurements

In order to obtain the best conditions for the formation of the SERS substrate several variables were optimized. CV, a minimally fluorescent dye, which is very active in SERS due to its high symmetry, was selected as model

analyte for these studies enabling the direct evaluation of the enhancement factors. 1 µL of a 10^{-4} M CV solution was used to record the evolution of the Raman intensity signal at 1171 cm^{-1}. CaF_2 plates were selected for the deposition of the SERS substrate, reducing the fluorescence in the Raman spectra, thus enabling more sensitive detection of the analytes.

Three different procedures for the preparation of the hybrid substrate were tested. Firstly, AuNPs were deposited drop–wise on the previously deposited graphene surface. The second attempt consisted on introducing the CaF_2 plate with the deposited graphene in the synthesis procedure so that AuNPs were directly grown on graphene surface. And finally, in the third option, 0.5mL of graphene commercial solution was added at the beginning of the AuNPs synthesis and then, such hybrid nanomaterial, was deposited on the plate.

The first approach led to a high density distribution of homogeneous-sized gold nanoparticles (Figure 2 D). The large amount of hotspot present on the substrate yields to a high enhancement of the signal of the analyte as compared with Raman measurements without the substrate. The second procedure resulted in a distribution of gold nanoparticles over the graphene surface with two different size distributions calculated from SEM images (Figure 2 A and C): one around 32±6 nm –corresponding to AuNPs formed in

the bulk of the solution-, and bigger ones around 0.53±0.09 μm, as a consequence of the nucleation process on the graphene surface. Enhancement of the Raman signal of CV was observed with this configuration, although in less extension than that observed with the previous one.

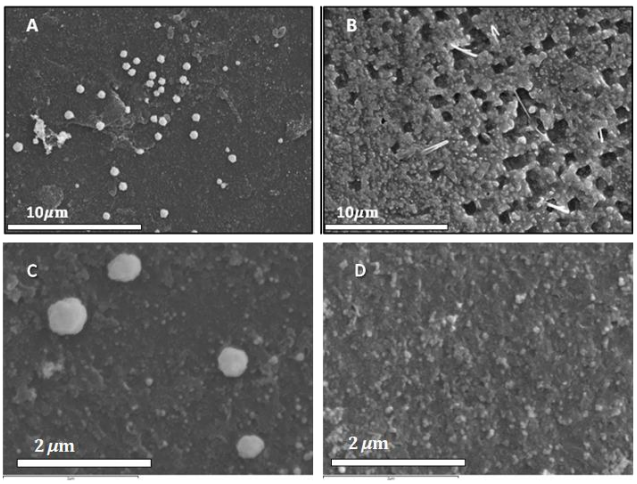

Figure 2. Scanning Electron Microscopy images of the hybrid substrates obtained with the three synthetic approaches assayed. (A) Deposited Graphene is introduced on the AuNPs synthesis procedure, (B) 0.5 mL of graphene solution were introduced on the AuNPs synthesis, (C) Higher magnification SEM image of the higher-sized AuNPs obtained when AuNPs were grown on the deposited graphene surface, and (D) SERS substrate obtained with the two-step drop-wise deposition of graphene and gold nanoparticles. This method of preparation of the substrate was selected for further experiments.

The last route for the formation of the substrate, in which graphene sheets are introduced in the precursor $HAuCl_4$ solution that leads to the

formation of AuNPs, resulted in a purple solution of hybrid graphene-AuNPs, meaning bigger nanoparticles as a consequence of the presence of free graphene during the nucleation step. The substrate, once deposited on the CaF_2 plate, showed an irregular porous structure (Figure 2 B) with no significant enhancement effect over the analyte. Thus, the first approach was selected for further experiments.

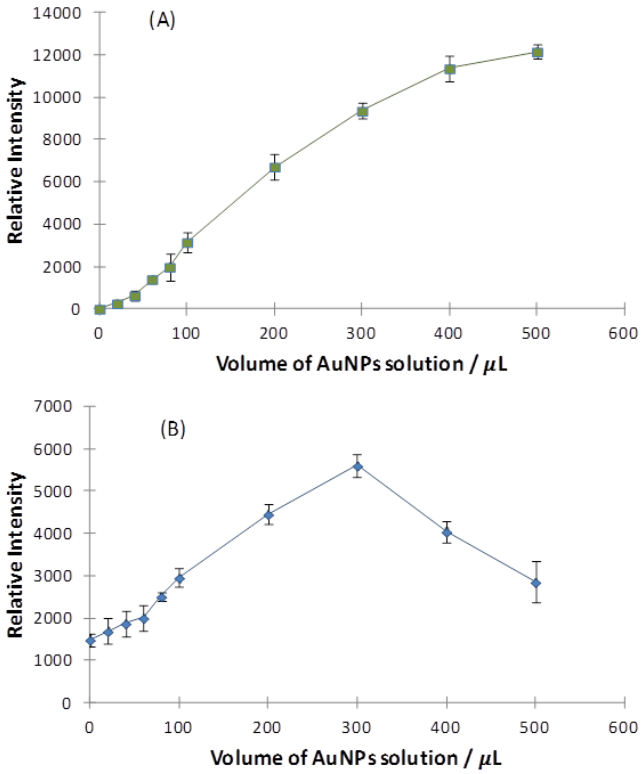

Figure 3. *Raman intensity of CV (A) and graphene (B) when increasing the AuNPs volume on the graphene surface. 300 μL of AuNPs was selected as the optimal volume. Changes in 1186 cm^{-1} band were studied in CV and G–band in graphene.*

The selected procedure involves the two-step drop-wise deposition of graphene and, subsequently, gold nanoparticles. Thus, the amount of AuNPs deposited over the graphene substrate was optimized. Volumes from 20 to 500 µL of the prepared AuNPs solution were added to the deposited graphene. Measurements at each volume were performed in triplicate. Figure 3 shows the Raman intensity of the analyte at increasing volumes of AuNPs.

Both the response of the analyte –CV- and graphene were investigated. The signal of CV increased as higher amounts of AuNPs were deposited. A high concentration of AuNPs, however, produces a decrease in the Raman signal of graphene due to the thickness of the gold layer. 300 µL of AuNPs were selected as the optimum volume in order to explode the synergy between graphene and gold nanoparticles, since the increase observed above 300 µL may be produced only to AuNPs effect.

Moreover, the deposition sequence of graphene, AuNPs and analyte was evaluated. Two different configurations were investigated. In the first one, graphene was deposited on the heated plate prior AuNPs and, finally, the analyte. In a second approach the analyte is placed on the previously deposited graphene surface while AuNPs are added on the top of the analyte. The fist approach led to the best results being, thus, selected for further experiments.

Finally, the instrumental variables for SERS measurement have been also optimized. Firstly, the influence of laser power in the spectra was studied, finding that the optimum laser power was 11 mW with a laser wavelength of 785 nm. Moreover, spectra were recorded with an acquisition time ranging from 0.5 to 20 s. The best conditions in terms of sensitivity of the spectrum and duration of the acquisition were 1 second.

3.3 Study of the reusability of SERS–active hybrid substrate

The reusability of the SERS–active hybrid substrate was evaluated. Methanol was added 0.5 by 0.5 mL (a total of 5.0 mL) in order to remove the CV from the G–AuNPs surface. Additionally, 5.0 mL of ultrapure water were subsequently passed in the same way. By proceeding in this way, very low amounts of CV were detected. In order to achieve complete removal of the CV from the substrate, the same procedure was repeated increasing the total volume of each solvent to 10 mL. Using this latter approach, the analyte, $1x10^{-4}$M CV, was not detectable while AuNPs remained in the surface. By using this cleaning procedure, gold nanoparticles were dramatically washed out of the graphene surface after four cleaning stages, so the substrate can be reused for 4 cycles. Figure 4 shows the evolution of SERS signal when the G-AuNPs hybrid substrate was cleaned and reused.

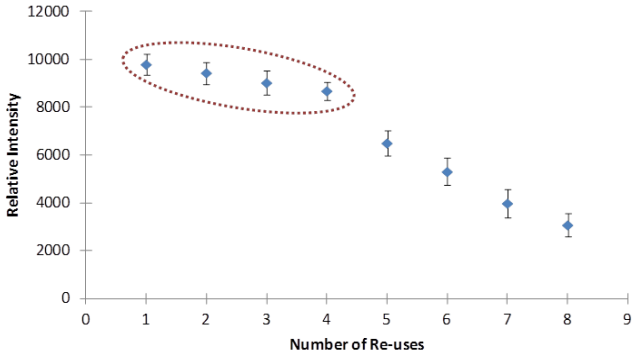

Figure 4. Study of the reusability of the SERS active hybrid substrate as regards intensity of 1171 cm^{-1} band of CV. The substrate could be re-used for 4 times with high sensitivity.

3.4 SERS spectrum of graphene

The SERS effect of gold nanoparticles over the graphene Raman spectrum has been investigated. When graphene is in contact with metallic nanoparticles two effects might contribute to the enhancement of their Raman signal. Firstly, the collective oscillation of electrons in metallic nanoparticles leads to the so-called plasmon resonance, which can resonate with the energy of the excitation laser, exhibiting, thus, high local optical fields (electromagnetic field enhancement). In addition, the electronic interaction between graphene and metal nanostructures can result in an increased Raman signal ("chemical" enhancement).

The most prominent features in the Raman spectrum of graphene are the so-called G band appearing around 1582 cm^{-1} (graphite) and the G′ band at about 2700 cm^{-1} using laser excitation at 2.41 eV. In the case of a disordered sample or at the edge of a graphene sample, we can also see the so-called disorder-induced D-band, at about half of the frequency of the G′ band (around 1350 cm^{-1} using laser excitation at 2.41 eV) [36]. The D peak is due to the breathing modes of six-atom rings and requires a defect for its activation. The 2D peak is the second order of the D peak. This is a single peak in single-layer graphene, whereas it splits in four in bilayer graphene, reflecting the evolution of the band structure [37].

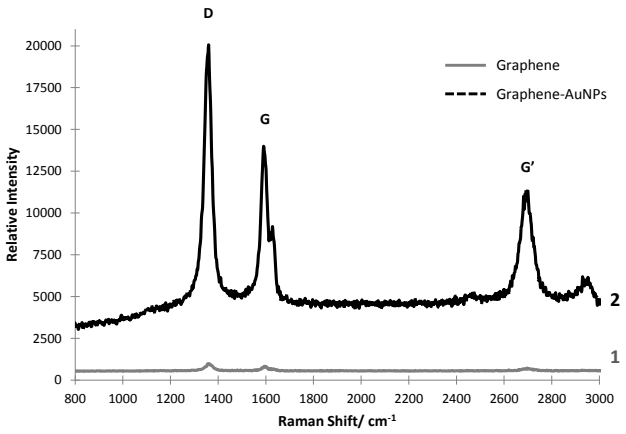

Figure 5. Raman (A) and SERS (B) spectra of graphene. A 21-fold enhancement of the Raman signal is achieved when gold nanoparticles are deposited over the graphene substrate.

Figure 5 shows the SERS spectra of graphene obtained when gold nanoparticles are deposited on their surface compared with the Raman spectra of graphene on a CaF_2 plate without metallic NPs. An increase in the D, G and G' bands of graphene can be observed. A 21-fold enhancement of the Raman signal was achieved by comparing the intensity of the D and G bands, using the same laser power and Raman measurement conditions for the two spectra. As can be seen in Figure 5, D band of graphene appears at 1307 cm^{-1}, G band at 1597 cm^{-1} and G' band at 2607 cm^{-1}.

3.5 Raman enhancement of the SERS spectra of crystal violet and metronidazole.

In order to establish the SERS enhancement factor of the gold nanoparticles coated graphene hybrid substrate, the Raman signal of 1 µL of 4 gL^{-1} solution of CV deposited onto a bare CaF_2 plate was measured and compared with the signal obtained when placing 1 µL of 0.408 gL^{-1} solution of CV onto the AuNPs-graphene hybrid substrate. Figure 6a shows both spectra.

The enhancement factor of the hybrid substrate can be calculated by using the following equation [38]:

$$EF = (I_{SERS}/I_{Raman})\cdot(N_{Raman}/N_{SERS})$$

where the intensity I is the height of the CV band at 1171 cm^{-1} and N represents the total number of analyte molecules deposited in the substrate. An enhancement factor of 4415 was determined.

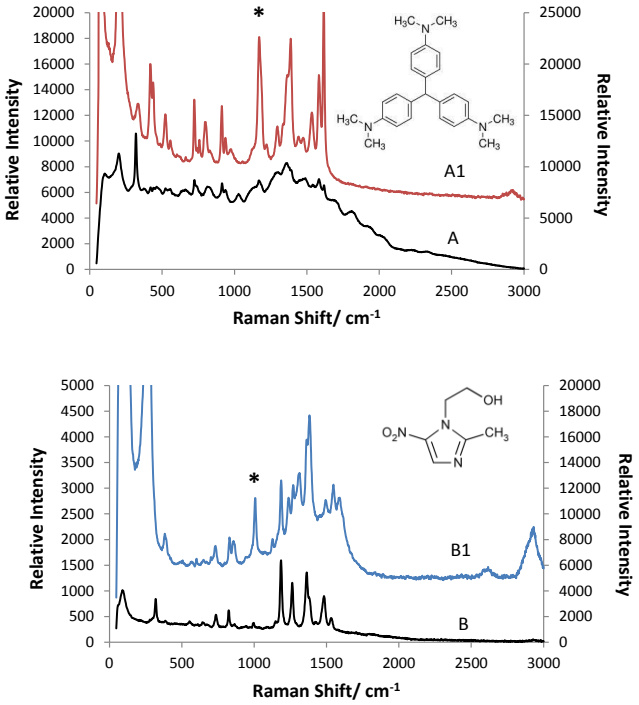

Figure 6. Raman and SERS Spectra of CV (A, A1) and Metronidazole (B, B1) on CaF_2 plate and G–AuNPs hybrid substrate, respectively. A) Raman signal of 4 $g{\cdot}L^{-1}$ CV. A1) SERS response of 408 $mg{\cdot}L^{-1}$ CV. B) Raman signal of 1 $g{\cdot}L^{-1}$ metronidazole. B1) SERS response of 30 m $g{\cdot}L^{-1}$. Right axis correspond to SERS spectra of both analytes. Left axis correspond to the Raman signal. The * indicates the band which has been employed for quantification in each analyte, bands at 1171 cm^{-1} and 1186 cm^{-1} for CV and metronidazol, respectively.

The suitability of the AuNPs-graphene hybrid substrate for the sensitive determination of metronidazole was also investigated. Similarly to that described for CV, the SERS enhancement factor for metronidazole was established by measuring the Raman signal of 1 µL of 1 gL^{-1} solution of metronidazole deposited onto a bare CaF_2 plate and comparing it with the signal obtained when placing 1 µL of 0.03 gL^{-1} solution of metronidazole onto the G-AuNPs hybrid substrate. The height of the band of metronidazole at 1186 cm^{-1} was employed for comparison. In such conditions an enhancement of 124-fold was obtained.

3.7. Comparison of the Raman enhancement on AuNPs, graphene and AuNPs-graphene hybrid substrate

The enhancement observed in the Raman spectrum of metronidazole when deposited on the AuNPs-graphene hybrid substrate was compared with that observed on a substrate composed by AuNPs or graphene individually. Measurements were performed at the same conditions of laser power, integration time, AuNPs/graphene and sample volumes. Firstly, AuNPs were immobilized on a CaF_2 plate drop by drop (10 μL each one) at the same conditions as previously described when added to the graphene surface. 1 μL of 30 $mg{\cdot}L^{-1}$ metronidazole was added on AuNPs surface and dried at 50ºC. SERS spectra of metronidazole were obtained with an enrichment factor of 38.

Measurements on graphene substrate were also carried out. For this purpose, graphene was deposited as described in section 2.3. 1 µL of a 30 $mg{\cdot}L^{-1}$ metronidazole solution were added and dried on the graphene surface. In spite of the fact that some authors have described SERS activity using only graphene as substrate [1,10], no SERS effect was found under such experimental conditions. The absence of SERS effects could be attributed to the use of multilayer graphene. As reported in literature [9], the Raman enhancement is dependent on the layer number, observing that the Raman enhancement efficiency drops from monolayer to thicker graphene (Figure 7).

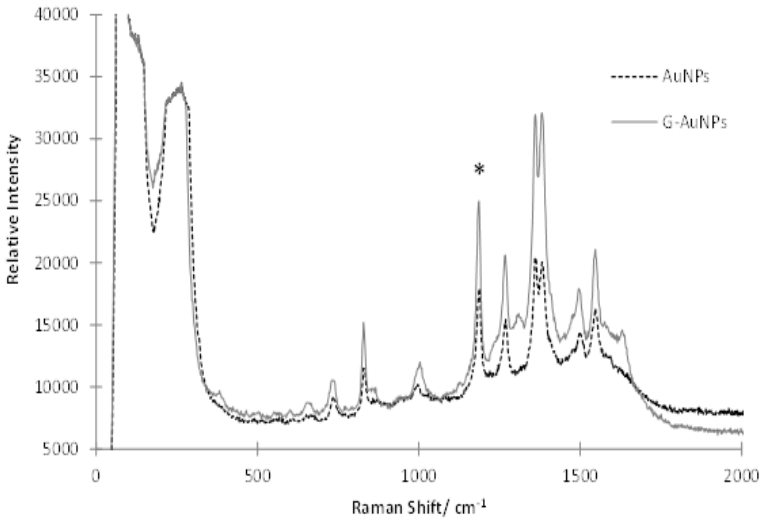

Figure 7. SERS spectra of metronidazole (1 µL of a 30 mg·L-1 solution) on the SERS substrate composed by AuNPs (dotted line), and the hybrid graphene-AuNPs substrate (continuous line). The * shows the band of metronidazole at 1186 cm^{-1} employed to calculate the enhancement.

As can be seen in Table 1, comparing the three types of substrates, the SERS effect achieved by using our SERS active hybrid substrate was 3.3 times fold higher than by using only AuNPs. The reproducibility of measurements on the different substrates was also evaluated. Studies were performed within a substrate and between substrates and it was expressed as % Relative Standard Deviation (% RDS). 20 randomly measurements were performed for each substrate. Three different substrates were prepared and measured to evaluate the reproducibility between them (three substrates for AuNPs substrate and three for AuNPs-graphene hybrid substrate).Our SERS hybrid substrate showed better reproducibility 7.7% versus 15.6 % obtained when only AuNPs were present, thus, overcoming one of the main limitations of SERS for quantitative analysis. Table 1 shows the reproducibility values obtained with the different substrates.

Table 1. Relative standard deviation (RSD) and enhancement factor (EF) obtained for metronidazole with the different substrates tested: graphene, AuNPs and hybrid AuNPs-graphene substrate.

Type of substrate	%RSD of a substrate (n=20)	% RSD between substrates (n=3, x 20 measurements each one)	Enhancement Factor (EF)
Graphene	Not SERS effect found	Not SERS effect found	0
AuNPs	15.6	18.2	38
G–AuNPs	7.7	11.9	124

3.8 Application to the determination of metronidazole

The analytical performance of the proposed method was studied in order to evaluate its usefulness for quantitative analysis. The SERS–active hybrid substrate was evaluated in terms of sensitivity –limits of detection (LOD) and quantification (LOQ)– and precision. Metronidazole was used as model analyte for characterization of the method. Analytical features were calculated by deposition of the optimal volume of AuNPs on the graphene surface, while metronidazole volume was 1 µL for all tested concentrations. A calibration graph was constructed by plotting the Raman intensity of the selected peak versus metronidazole concentration (Figure 8). Each concentration level was analyzed in triplicates (measuring each sample at ten randomly selected locations within the substrate). Error bars depicts the standard deviation of the mean value. The intensity of the band at 1186 cm^{-1} of metronidazole was adopted as analytical signal. The linear interval was found between 5–50 $mg{\cdot}L^{-1}$ with a R^2= 0.9989. The detection and quantification limits, calculated as three and ten times the signal of S_a between the scope, were 1.1 and 3.68 $mg{\cdot}L^{-1}$, respectively.

In order to study the reproducibility of the proposed substrate, twenty independent measurements at a 30 $mg{\cdot}L^{-1}$ concentration were carried out. The RSD thus obtained was 7.76 %. Additionally, the reproducibility was evaluated between samples (n=3), the RSD obtained being 10.92 %. It should be

emphasized that the precision of this substrate is high, which can be attributed to the use of graphene as substrate for AuNPs.

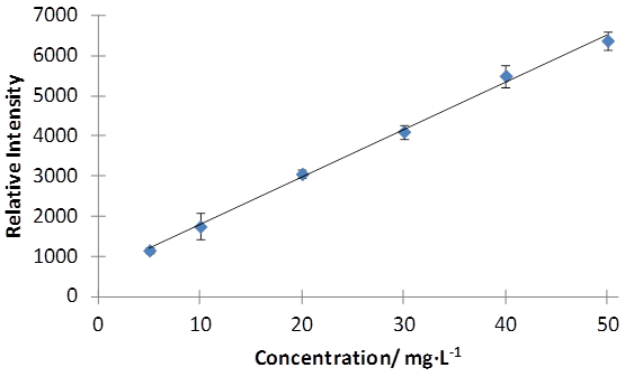

Figure 8. *Calibration graph of metronidazole obtained at seven different concentration levels on G–AuNPs hybrid substrate. The calibration range was found between 5–50 mg·L^{-1}.*

Results are summarized in Table 2. As can be seen, the LOD and LOQ achieved with the SERS – active substrate developed here were relatively low. In this work, a 785 nm laser has been employed to carry out SERS measurements, whose wavelength is not resonant with the gold nanoparticles plasmon, thus the chemical mechanism is expected to be the only contribution to the enhancement obtained. The achieved results demonstrate the high SERS performance of the AuNPs-graphene substrate. In fact, the results obtained herein with the AuNPs-graphene substrate improve that reported by

Han et al. [32] for the SERS determination of metronidazole using a SERS substrate composed by a silver nanorods array, which was 10 $mg{\cdot}L^{-1}$.

Table 2. Analytical features of the method for the determination of metronidazole

Calibration equation	S=(123±1)[MNZ]+(534±45)
R^2	0.9989
LOD	1.10 $mg{\cdot}L^{-1}$
LOQ	3.68 $mg{\cdot}L^{-1}$
RSD[a] (%) (intra-substrate)	7.76%
RSD[b] (%) (inter-substrates)	10.92%

[MNZ]: Concentration of metronidazole in mgL^{-1}.
[a]Relative standard deviation, determined from 20 measurements at a 30 mgL^{-1} concentration of metronidazole within the same substrate.
[b]Relative standard deviation, determined from the average value of 20 measurements at a 30 mgL^{-1} concentration of metronidazole in three different substrates.

4. CONCLUSIONS

In this paper, a simple and quick procedure for the formation of an AuNPs-graphene hybrid substrate is described. Such substrate demonstrated a SERS enhancement of crystal violet and metronidazole of 4415- and 124-fold, respectively, as compared with normal Raman spectra of the analytes. The performance of this hybrid substrate has been compared with substrates composed by these nanomaterials individually. The improvement achieved with G–AuNPs is 3.3–fold greater than that obtained using only AuNPs as SERS substrate, while no enhancement was observed when using multilayer

graphene. The use of graphene in this SERS active hybrid substrate provides a stable and very reproducible substrate which can be reused for 4 cycles and several months after their preparation with high sensitivity.

Moreover, the combination of multilayer graphene and gold nanoparticles used as SERS–active hybrid substrate was found to be a useful and reproducible method for the determination of metronidazole. The procedure presented is capable of detecting and quantifying small quantities of metronidazole without implying any preconcentration step, just using an affordable and portable Raman spectrometer. The detection limit achieved was fairly low, about 1.1 $mg{\cdot}L^{-1}$, improving the limits reported in literature for the SERS determination of this analyte. It should be remarked that improved reproducibility is obtained with the G-AuNPs hybrid substrate as compared with only AuNPs, thus, overcoming one of the main limitations of SERS for their use in quantitative analysis.

ACKNOWLEDGEMENTS

The authors would like to express their gratitude to the Junta de Andalucía for the financial support (Proyect FQM 4801). S. Benítez–Martínez also wishes to thank the Junta de Andalucía for the award of a Research Training Fellowship. The authors are grateful to Professor Dr. Bernhard Lendl for his comments.

The authors have declared no conflict of interest.

5, REFERENCES

[1] K. Hering, D. Cialla, K. Ackermann, T. Dörfer, R. Möller, H. Schneidewinds, R. Mattheis, W. Fritzche, P. Rösch and J. Popp, SERS: a versatile tool in chemical and biochemical diagnostics, Anal. Bioanal. Chem. 390 (2008) 113–124.

[2] D. Cialla, A. März, R. Böhme, F. Theil. K. Weber, M. Schmitt, J. Popp, Surface-enhanced Raman spectroscopy (SERS): progress and trends, Anal. Bioanal. Chem. 403 (2012) 27–54.

[3] P. Pienpinijtham, X.X. Han, S. Ekgasit, Y. Ozaki, An ionic surfactant-mediated Langmuir–Blodgett method to construct gold nanoparticle films for surface-enhanced Raman scattering, Phys. Chem. Chem. Phys. 14 (2012) 10132–10139.

[4] S. Keskin, M. Culha, Label-free detection of proteins from dried-suspended droplets using surface enhanced Raman scattering, Analyst 137 (2012) 2651–2657.

[5] A. Virga, P. Rivdo, E. Descrovi, A.Chioleiro, G. Digregorio, F.Frascella, M. Soster, F. Bussolino, S. Marchio, F. Geobaldo, F. Giorgis, SERS active Ag nanoparticles in mesoporous silicon: detection of organic molecules and peptide–antibody assays, J. Raman Spectrosc. 43 (2012) 730–736.

[6] X. Qin, W. Lu, Y. Luo, G. Chang, A. M. Asiri, A. O. Al–Youbi, X. Sun, Ag Nanoparticles Decorated 2,4,6-Tris (2-pyridyl)-1,3,5-triazine Nanobelts:

Synthesis and Their Application as Sensitive SERS Substrate, Curr. Nanosci.8 (2012) 393–397.

[7] Q. Shao, R. Que, M. Shao, L. Cheng, S.T. Lee, Copper Nanoparticles Grafted on a Silicon Wafer and Their Excellent Surface-Enhanced Raman Scattering, Adv. Funct. Mater. 22 (2012) 2067–2070.

[8] K. S. Novoselov, A. K. Geim, S.V. Morozov, D. Jiang, Y. Zhang, S. V. Dubonos, I. V. Grigorieva, A. A Firsov, Electric Field Effect in Atomically Thin Carbon Films, Science 306 (2004) 666–669.

[9] C. Qiu, H. Zhou, H. Yang, M. Chen, Y. Guo, L. Sun, Investigation of n-Layer Graphenes as Substrates for Raman Enhancement of Crystal Violet, J. Phys. Chem. C. 115 (2011) 10019–10025.

[10] W. Xu, N. Mao, J. Zhang, Graphene: A Platform for Surface-Enhanced Raman Spectroscopy, Small 9 (2013) 1206-1224.

[11] Y. Ouyang, A simple method for achieving surface-enhanced Raman scattering of single-layer and few-layer graphene, J. Mol. Struct. 1040 (2013) 213–215.

[12] Y. K Kim, H. K. Na, Y.W. Lee, H. Jang, S.W. Han, The direct growth of gold rods on graphene thin films, Chem. Commun. 46 (2010) 3185–3187.

[13] K. Jasuja, V. Berry, Implantation and Growth of Dendritic Gold Nanostructures on Graphene Derivatives: Electrical Property Tailoring and Raman Enhancement, ACS Nano 3 (2009) 2358–2366.

[14] G. Goncalves, P. A. A. P. Marques, C. M. Granadeiro, H. I. S. Nogueira, M. K. Singh, J. Grácio, Surface Modification of Graphene Nanosheets with Gold Nanoparticles: The Role of Oxygen Moieties at Graphene Surface on Gold Nucleation and Growth, Chem. Mater. 21 (2009) 4796–4802.

[15] Z. G. Le, Z. Liu, Y. Qian, C. Wang, A facile and efficient approach to decoration of graphene nanosheets with gold nanoparticles, Appl. Surf. Sci. 258 (2012) 5348–5353.

[16] K. L Zhang, Fabrication of copper nanoparticles/graphene oxide composites for surface-enhanced Raman scattering, Appl. Surf. Sci. 258 (2012) 7327–7329.

[17] H. Zhao, H. Fu. T. Zhao, L. Wang, T. Tan, Fabrication of small-sized silver NPs/graphene sheets for high-quality surface-enhanced Raman scattering, J. Colloid Interface Sci. 375 (2012) 30–34.

[18] A. N. Sidorov, G. W. Slawinsk, A. H. Jayatissa, F. P. Zamborini, G. U. Sumanasekera, A surface-enhanced Raman spectroscopy study of thin graphene sheets functionalized with gold and silver nanostructures by seed-mediated growth, Carbon 50 (2012) 699–705.

[19] J. Huang, L. Zhang, B. Chen, N. Ji, F. Chen, Y. Zhang, Z. Zhang, Nanocomposites of size-controlled gold nanoparticles and graphene oxide: Formation and applications in SERS and catalysis, Nanoscale 2 (2010) 2733–2738.

[20] T .Tite, C. Donnet, A. S. Loir, S. Reynaud, J. Y. Michalon, F. Vocason, F. Garrelie, Graphene-based textured surface by pulsed laser deposition as a robust platform for surface enhanced Raman scattering applications, Appl. Phys. Lett. 104 (2014) 041912.

[21] M. Illuit, C. Leordean, V. Canpean, C. M. Teodorescu, S. Astilean, A new green, ascorbic acid-assisted method for versatile synthesis of Au–graphene hybrids as efficient surface-enhanced Raman scattering platforms, J. Mater. Chem. C 1 (2013) 4094–4104.

[22] Y. Wang, Z. Ni, H. Hu, Y. Hao, C. P. Wong, T. Yu, J. T. L. Thong, Z. X. Shen, Gold on graphene as a substrate for surface enhanced Raman scattering study, Appl. Phys. Lett. 97 (2010) 163111.

[23] W. Wang, D. He, J. Duan, S. Wang, H. Peng, H. Wu, M. Fu, Y, Wang, X. Zhang, Simple synthesis method of reduced graphene oxide/gold nanoparticle and its application in surface-enhanced Raman scattering, Chem. Phys. Lett. 582 (2013) 119–122.

[24] N. Kim, M. K. Oh, S. Park, S. K. Kim, B. H. Hong, Effect of Gold Substrates on the Raman Spectra of Graphene, Bull. Korean Chem. Soc. 31 (2010) 999–1003.

[25] J. Lee, S. Shi, B. Kim, H. S. Shin, Surface-Enhanced Raman Scattering of Single-and Few-Layer Graphene by the Deposition of Gold Nanoparticles, Chem. A Eur. J. 17 (2011) 2381–2387.

[26] C. Qiu, H. Zhoou, B. Cao, L. Sun, T. Yu, Raman spectroscopy of morphology-controlled deposition of Au on graphene, Carbon 59 (2013) 487–494.

[27] X. Fu, F. Bei, X. Wang, S. O'Brian, J. R. Lombardi, Excitation profile of surface-enhanced Raman scattering in graphene–metal nanoparticle based derivatives, Nanoscale 2 (2010) 1461–1466.

[28] P. Wang, D. Zhang, L. Zhang, Y. Fang, The SERS study of graphene deposited by gold nanoparticles with 785 nm excitation, Chem. Phys. Lett. 556 (2013) 146–150.

[29] M. Manikandam, H. N. Abdelhamid, A. Talib, H. F. Wu, Facile synthesis of gold nanohexagons on graphene templates in Raman spectroscopy for biosensing cancer and cancer stem cells, Biosens. Bioelectron. 55 (2014) 180–186.

[30] S. He, K.K. Liu, S. Su, J. Yan, X. Mao, D. Wang, Y. He, L.J. Li, S. Song, C. Fan, Graphene-Based High-Efficiency Surface-Enhanced Raman Scattering-Active Platform for Sensitive and Multiplex DNA Detection, Anal. Chem. 84 (2012) 4622–4627.

[31] X. Ding, L. T. Kong, J. Wang, F. Fang, D. Li, J. Liu, Highly Sensitive SERS Detection of Hg2+ Ions in Aqueous Media Using Gold Nanoparticles/Graphene Heterojunctions, ACS Appl. Mater. Interfaces. 5 (2013) 7072–7078.

[32] C. Han, J. Chen, X. Wu, Y. W. Huang, Y. Zhao, Detection of metronidazole and ronidazole from environmental Samples by surface enhanced Raman spectroscopy, Talanta 128 (2014) 293–298.

[33] J. Turkevich, P.C. Stevenson, J. Hillier, A study of the nucleation and growth processes in the synthesis of colloidal gold, Discuss. Faraday Soc. 11 (1951) 55–75.

[34] A. I. López–Lorente, B. M. Simonet, M. Valcárcel, Rapid analysis of gold nanoparticles in liver and river water samples, Analyst 137 (2012) 3528–3534.

[35] W. Haiss, N. T. K. Thanh, J. Aveyard, D. G. Fernig, Determination of size and concentration of gold nanoparticles from UV-vis spectra, Anal. Chem. 79 (2007) 4215–4221.

[36] L. M. Malard, M. A. Pimenta, G. Dresselhaus, M. S. Gresselhaus, Raman spectroscopy in graphene, Physics Reports 473 (2009) 51–87.

[37] F. Schedin, E. Lidorikis, A. Lombardo, V. G. Kravets, A. K. Geim, A.N. Grigorenko, K. S. Novoselov, A. C. Ferrari, Surface-enhanced Raman spectroscopy of graphene, ACS Nano 4 (2010) 5617–5626.

[38] W.W. Yu, I.M. White, A simple filter-based approach to surface enhanced Raman spectroscopy for trace chemical detection, Analyst 137 (2012) 1168–1173.

III.3 Espectroscopia de Fluorescencia

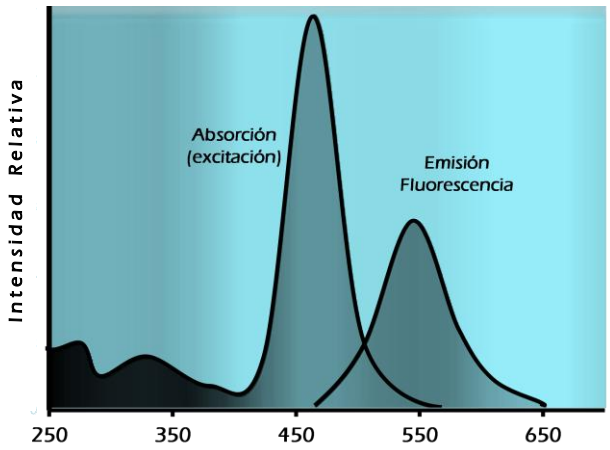

III.3 .1. Extracción *líquido–líquido*

Etapa previa de tratamiento de muestra

Los puntos cuánticos de grafeno (GQDs) han sido empleados en innumerables aplicaciones analíticas como herramienta para la mejora de sistemas sensores y biosensores fundamentalmente, sacando partido de sus propiedades fotoluminiscentes, o bien aprovechando otras propiedades como las electroquímicas.

En cuanto a la determinación del contenido total de fenoles presentes en el aceite de oliva, no existe hasta el día de hoy una metodología oficial. Sin embargo, un procedimiento muy empleado para este fin es el método colorimétrico Follin & Ciocalteu[6]. La técnica presenta la desventaja de necesitar largos periodos de incubación de los extractos fenólicos con el reactivo que lleva su mismo nombre, además de ser sensible a los cambios de temperatura.

En el capítulo 4 se describe un método alternativo, miniaturizado, rápido y sencillo, para la determinación del índice de fenoles totales en aceite de oliva basada en el empleo GQDs como sensor nanométrico.

[6] A. L. Waterhouse, Determination of total phenolics. John Wiley & Sons, 2001.

Capítulo 4

Graphene Quantum Dots as Sensor for Phenols in Olive Oil

Sensors and Actuators B 197 (2014) 350–357

Sensors and Actuators B 197 (2014) 350–357

Contents lists available at ScienceDirect

Sensors and Actuators B: Chemical

journal homepage: www.elsevier.com/locate/snb

Graphene quantum dots as sensors for phenols in olive oil

Sandra Benítez-Martínez, Miguel Valcárcel

Department of Analytical Chemistry, University of Córdoba, Campus of Rabanales, 14071, Córdoba, Spain

A new method for the determination of the phenol fraction of olive oil is reported. An optical nanosensor based on graphene quantum dots, obtained by pyrolysis of citric acid, was specifically developed for this purpose. The ensuing fluorescence sensing method, which is simple, and highly sensitive and reproducible, was used here to determine gallic acid and oleuropein as model analytes commonly found in olive oils, as well as the phenolic concentration of olive oil real samples. The detection limits were lower than 0.12 $mg{\cdot}L^{-1}$ and the precision, expressed as relative standard deviation, lower than 1.7%.

Keywords: graphene quantum dots, sensor, total phenols, fluorescence quenching, liquid–liquid extraction, olive oil.

Abbreviations: GQDs, graphene quantum dots; EVOO, extra virgin olive oil; VOO, virgin olive oil; LOO, "lampante" olive oil; ROO, refined olive oil; FL, fluorescence.

1. INTRODUCTION

Graphene, a one-atom thick layer consisting of carbon atoms arranged in a honeycomb lattice with sp^2 hybridization, has attracted much attention among the scientific community in recent years by virtue of its exceptional electronic, mechanical and thermal properties [1]. Graphene is a zero-band gap nanomaterial with an infinite excitation Bohr radius —a result of the linear energy dispersion relationship of its charge carriers [2]—; this conceals its luminescence. Graphene quantum dots (GQDs), which are emerging luminescent carbon-based nanomaterials, have lately aroused increasing interest in their optical and electronic properties. GQDs are graphene sheets with lateral size smaller than 100 nm in single, double and multiple layers [3], and diameters spanning the range 3–20 nm mainly. These materials possess special properties including low toxicity, high biocompatibility, high fluorescent activity, robust chemical inertness and excellent photostability [4] by effect of quantum confinement and edge (armchair or zigzag) effect. These properties confer GQDs a variety of potential uses in photovoltaic devices, bioimaging instruments, sensors and biosensors, among others [5].

So far, GQDs have been produced by using top–down or bottom–up methods. The former include electron beam lithography [6], chemical vapor deposition (CVD) [7], chemical oxidation [8, 9], hydrothermal [10, 11] and solvothermal treatments [12], sonication [13], hydrazine hydrate reduction

[14], electrochemical preparation [15] and exfoliation, and disintegration. Most top–down methods use carbon black [3], graphene oxide (GO) [4, 5, 10, 13, 14] or carbon nanotubes (either single-wall [16] or multiwall [17]) as raw material. The bottom–up methods involve solution chemistry [18]; carbonization of organic precursors such as glucose [19], citric acid [20] or HBC (hexa-peri-hexabenzocoronene) [21]; or fragmentation of C_{60} [22]. The top–down methods have the advantage that they afford large-scale production, are simple to operate and use readily available raw materials; however, they require special equipment and typically provide low yields. By contrast, the bottom–up methods involve complex synthetic procedures and use special precursors.

Like other carbon-based materials, GQDs exhibit largely size-dependent photoluminescence (PL), which has been ascribed mainly to quantum confinement, composition, structure and shape. GDQ photoluminescence typically ranges from blue to green or, less commonly, yellow to red, with smaller GQDs having longer PL emission wavelengths than larger ones. Photoluminescence in most —but not all— GQDs is excitation wavelength-dependent; also, their PL wavelength is not pH-dependent, but its emission intensity is. Interestingly, the influence of pH varies with the synthetic method used; thus, some GQDs prepared under alkaline conditions exhibit strong PL,whereas others obtained under acid or neutral conditions exhibit maximal

PL emission [23]. The presence of oxygen-containing (carbonyl, epoxy, hydroxyl and carboxyl) functional groups at the edge of GQDs makes them very readily soluble in water and in most polar organic solvents [8]. The quantum yield (QY) of the GQDs varies with the particular synthetic method and the chemistry of their surface; thus, QY typically ranges from 2% to 22.9 % for GQDs with an unpassivated surface and can easily exceed 46 % for surface-passivated GQDs [6].

Graphene quantum dots have scarcely been used in analytical chemistry. The few, recent exceptions involve the determinations of glucose [24], free chlorine in drinking water [25], Cd^{2+} [26], TNT [27], Fe^{3+}[28], pyrocatechol [29], immunoglobulin G [30] and specific DNA sequences [31].

This paper reports a new application of GQDs: their use in a sensor for phenolic compounds from olive oil. The antioxidant potential of olive oil is known to be due to its containing phenols. In recent years, antioxidant properties have aroused considerable interest on account of their benefits on human health (e.g. protection against coronary heart diseases and tumors) and their impact on olive oil stability and shelf life [32].

2. METRIALS AND METHODS

2.1. Reagents and standards

All chemical reagents were analytical-grade and used without additional purification. The reagents citric acid (≥ 99.0 %), gallic acid (≥ 98.0 %), oleuropein (≥ 98.0 %), sodium carbonate (≥ 99.5%) and folin&ciocalteu(2N), and the solvents acetone and *n*–hexane, both in HPLC-grade, were all purchased from Sigma–Aldrich (Madrid, Spain). Sodium hydroxide and *N,N*–dimethylformamide were obtained from Panreac Chemical, SAU (Barcelona, Spain). HPLC-grade methanol (≥ 99.9 %) and acetonitrile (≥ 99.9 %) were purchased from Carlo Erba Reagents (Barcelona, Spain) and VWR Chemicals (Barcelona, Spain), respectively. The olive oil samples used in the optimization tests were supplied by Sovena España–Consumer Goods (Seville, Spain).

2.2. Instrumentation

Fourier transform mid infrared (FT-MIR) spectra were obtained on a Bruker Tensor 27FT–MIR spectrophotometer equipped with a Hyperion 2000 microscope, using KBr pellets. High-resolution transmission electron microscopy (HRTEM) images were obtained on a JEOL JEM 2010 electron microscope available at the Research Support Service (SCAI) of the University of Córdoba. The instrument had a point-to-point resolution of 0.194 nm and was operated at a medium acceleration voltage of 200 kV.

Fluorescence emission spectra were recorded on a PTI QuantaMaster™ spectrofluorometer from Photon Technology International (Barcelona, Spain) equipped with a 75 W xenon short arc lamp and an 814 PTM detection system. The software FeliX32 was used for data acquisition and instrument control. The excitation and emission slits were both 3.8 nm wide. All measurements were made at room temperature, using micro quartz cuvettes of 10 mm lightpath. UV–Vis absorption spectra were obtained on a Lambda 35 ES UV/Vis spectrophotometer from Perkin Elmer (Madrid, Spain) equipped with two radiation sources (deuterium and tungsten–halogen lamps) and photodiode detectors; measurements were made in polypropylene cuvettes at room temperature.

2.3.Synthesis of GQDs

Dots were obtained by pyrolysis of citric acid, using a slightly modified version of the procedure by Dong et *al* [20]. To this end, an amount of 2 g of citric acid was placed in a vial and heated at 200 ºC on a thermoblock from JP Selecta (Barcelona, Spain) until the citric acid changed from a white dust to a dark orange liquid, which took about 30 min. The resulting liquid was added dropwise to 100 mL of a 10 $mg{\cdot}mL^{-1}$ NaOH solution under vigorous stirring. The GQD aqueous solution thus obtained was adjusted to pH 10 with nitric acid and stored at 4 ºC in an amber bottle.

2.4.Sample treatment

Refined olive oil (ROO), used as a blank in the recovery and sensitivity tests described below, was spiked with gallic acid to a final concentration in the range 0–6 $mg{\cdot}L^{-1}$. A stock standard solution containing 1 $g{\cdot}L^{-1}$ gallic acid in methanol was prepared and stored at 4 °C. Working-strength solutions were obtained by dilution of the stock in methanol. Aliquots of 0.1 $g{\cdot}L^{-1}$ gallic acid methanolic solution (0–120 µL) were added to a polypropylene (PP) centrifuge tube and dried at 35 °C under a nitrogen stream. Then, an amount of 2 g of ROO was placed in the tube and agitated on an MS 3 Basic vortex mixer from IKA (Staufen, Germany) at 2000 rpm for 5 min prior to liquid–liquid extraction as described below.

2.4.1. LLE extraction of phenolic compounds from olive oil

For liquid–liquid extraction, 1 mL of *n*–hexane and 2 mL of (60/40 v/v) methanol/water mixture were added to 2 g of olive oil according to Pirisi et *al* [33]. The mixture was stirred in a vortex at 2500 rpm for 2 min and centrifuged at 4000 rpm for 10 min. Then, the methanol layer was separated and the extraction repeated twice. Once extraction was completed, the extracts were combined and cleaned up by (*a*) low-temperature fat precipitation at –20° C overnight or (*b*) washing with *n*-hexane (3×2 mL). The combined methanol extracts and the n–hexane used to clean up in the latter procedure were mixed in a vortex at 3000 rpm for 30 s and centrifuged at 4000 rpm for 10

min. Then, the *n*-hexane was discarded and the methanolic solution evaporated to dryness under a nitrogen stream at 35 °C. The ensuing residue was recovered with 200 µL of methanol (theoretical concentration factor, 10×). The low-temperature fat precipitation procedure provided poor results because fats were incompletely removed from the extracts. This led us to select cleanup with *n*-hexane.

In a typical run, 200 µL of GQD solution at pH 10 (final concentration, 1.125 $mg{\cdot}mL^{-1}$) was passed through a 0.22 µm mesh nylon syringe filter and mixed with the methanolic extract (200 µL) obtained from the liquid–liquid extraction of olive oil in a fluorescence quartz microcuvette for measurement at an excitation wavelength of 380 nm.

Real samples of four different olive oil grades [viz., extra virgin olive oil (EVOO), virgin olive oil (VOO), lampante olive oil (LOO) and refined olive oil (ROO)] were analyzed by using the proposed sensing method and compared for total phenol index.

2.5.Total phenol (TP) content

The total phenol contents of the olive oils extracts was determined colorimetrically at 765 nm, using Folin–Ciocalteu (FC) reagent according to Waterhouse [34], in order to compare our sensing system with a reference

method. The spectrophotometric analysis was repeated 3 times with each type of extract. The results were expressed as gallic acid equivalents (GAE,in $mg{\cdot}L^{-1}$).

We used the microscale protocol for Follin–Ciocalteu Colorimetric method as adapted for small sample volumes in order to reduce costs and waste production. The reaction was performed directly in the measuring cuvette. For total phenol determination, 20 µL of sample, 1.58 mL of ultrapure water and 100 µL of FC reagent were placed in a 10 mm, 2 mL plastic cuvette, mixed thoroughly by pipetting and incubated for 6 min. Then, 300 µL of sodium carbonate solution was added and the mixture incubated at room temperature for 2 h. The sample absorbance was measured at 765 nm. The absorbance of the blank was subtracted from all readings and a calibration curve constructed from the standard (gallic acid at concentrations from 0 to 500 $mg{\cdot}L^{-1}$). The curve was used to determine the corresponding gallic acid concentration in the real samples. All samples and standards were analyzed in triplicate.

3. RESULTS AND DISCUSSION

The GQDs used in this work were flat circular nanosheets of average diameter 3.6 ± 0.9 nm which were characterized by HRTEM. FT-MIR spectra

revealed the presence of carboxyl and hydroxyl groups. Figure 1 shows an HRTEM image and FT-MIR spectrum for the studied GQDs.

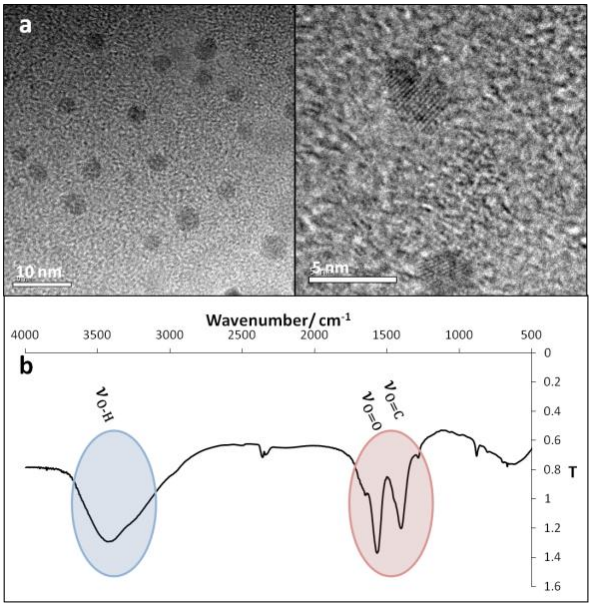

Figure 1. HR-TEM images (a) and FT-MIR spectra (b) of the GQDs.

Our dots emitted blue light (474 nm) upon excitation at 365–420 nm — the maximum emission occurred at 379 nm excitation, so 380 nm was used in all measurements. As can be seen from Figure 2, the GQD emission wavelength was excitation wavelength-independent, but the fluorescence intensity was not. The GQD concentration after synthesis was 2.25 $mg{\cdot}mL^{-1}$

and the GQD quantum yield at working conditions was 4.5 % by using quinine sulfate as standard.

GQDs are surface–passivated in the synthesis procedure [20] and the oxygen-containing functional groups, which confers them good water solubility and stability, namely carboxyl and hydroxyl groups, are only present at the edge of the dot. The interaction of gallic acid and oleuropein with GQDs can be explain through the aromatic network at the GQDs surface and the phenol aromatic character, by π–π stacking [27, 29].

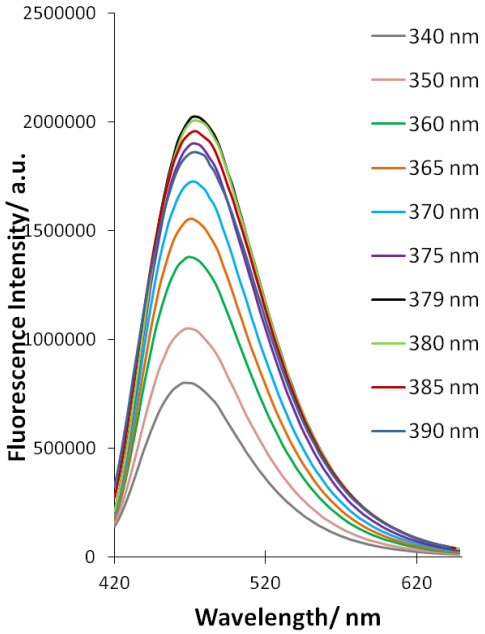

Figure 2. Variation of the excitation wavelength of the GQDs. FL emission peaked at an excitation wavelength of 379 nm. The emission wavelength (474 nm) was excitation

wavelength-independent and the FL intensity increased or decreased depending on the particular excitation wavelength.

However it cannot be dismissed that the analyte binding may also occurs by non–covalent interactions (hydrogen bond) between phenols with the functional groups presents at the edge of GQDs. So both processes could act together. The phenol-GQDs complex formation results in the quenching of the GQDs fluorescence trough a charge transfer mechanism in which GQDs act as donor. The emission band has a green shift when phenols from real samples are added, indicating a common charge transfer fluorescence quenching. In addition, higher quenching was observed when the polarity of the solvent tested increased, confirming a charge transfer quenching mechanism [35].

A temperature study was made in order to interpret the quenching mechanism. The effect of the temperature in the quenching of GQDs was investigated from 20 to 40ºC. For this, the mixture of GQDs solution and 50 $mg{\cdot}L^{-1}$ gallic acid, in the 1:1 ratio optimized, was heated at different temperatures. Temperature was controlled by a digital thermometer probe. The mixture was measured when the solution reached 20 (room temperature), 25, 30 and 40ºC into the sample compartment. 50 $mg{\cdot}L^{-1}$ oleuropein was also tested at the same conditions. The experiments were repeated in triplicate. As a result, significant changes in the quenching of GQDs by both solution standards were not observed at the tested temperatures; the RSD (n=3) of the

FL quenching between temperatures been 2.1% and 3.6% for gallic acid and oleuropein, respectively. So, it can be concluded that the temperature does not affect the sensitivity of the sensor system. It should be mentioned that the fluorescence levels of the GQDs blanks and the mixtures of GQDs-standards decreased linearly with the temperature increment but the quenching remains constant.

3.1.Influence of the pH of the GQDs aqueous solution

One important variable in the procedure used to develop the proposed sensing system was the pH of the GQD solution, which was found to affect the fluorescence of our sensor and its interactions with gallic acid —the specific phenol used as model analyte. The pH of the GQD solution immediately after preparation was over pH 13 and FL (fluorescence) emission very high as a result; however, FL emission peaked at pH 7 (see Fig. 3a). FL decreased markedly with increasing pH in alkaline media; also, it was pH-dependent, but no so markedly, in acid media.

pH also influenced the interaction between GQDs and phenols (specifically, gallic acid, used as model analyte). Although FL peaked at pH 7, nanoparticles interacted very scarcely with the analyte —and little fluorescence quenching was observed— at neutral pH. The influence of GQDs solution pH on FL quenching was examined over the range 6–13. Based on the results, the

quenching effect of gallic acid on the GQDs FL intensity was stronger in alkaline media than in acid media. A 50 $mg{\cdot}L^{-1}$ gallic acid concentration was used to assess the GQDs response. Quenching was maximal when the GQDs solution was initially at pH 10 (see Figure 3b), which was thus selected for our sensing system. Notice that the final pH of the mixture of GQDs and standard is slightly more alkaline due to the addition of methanol.

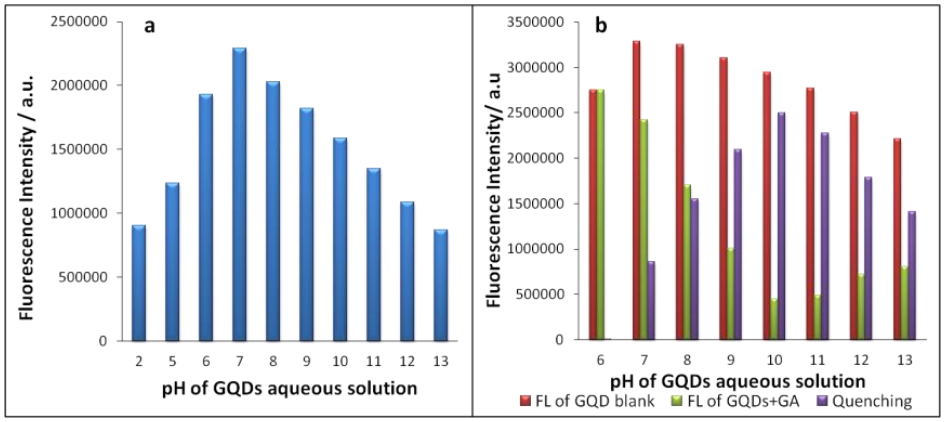

Figure 3. (a) Variation of FL with pH. Fluorescence emission peaked at pH 7. However, quenching, at a gallic acid concentration of 50 $mg{\cdot}L^{-1}$, peaked at pH 10(b).

3.2.Influence of the solvent

The response of the GQD sensor to gallic acid dissolved in various polar solvents was also examined in order to optimize the sensing system. To this

end, 1 $g{\cdot}L^{-1}$ gallic acid solutions in acetone (ACT), acetonitrile (ACN), *N,N*–dimethylformamide (DMF), methanol (MeOH) and ultrapure water were prepared and stored at 4 °C. These stock standards were used to obtain 40 $mg{\cdot}L^{-1}$ solutions by appropriate dilution. For measurement, a 200 µL volume of GQD aqueous solution was placed in a micro fluorescence cuvette and supplied with 200 µL of a 40 $mg{\cdot}L^{-1}$ gallic acid solution in each of the previous solvents; this was followed by thorough mixing by pipetting (final concentration of gallic acid, 20 $mg{\cdot}L^{-1}$) and immediate measurement at 380 nm. Identical volumes of GQDs and the solvents were also mixed for use as blanks. Dilution with all polar solvents used (final concentration of GQDs, 1.125 $mg{\cdot}mL^{-1}$) increased the fluorescence of GQDs (1.44 times with ACT, 1.34 with ACN, 1.63 with DMF, 1.42 with MeOH and 1.07 with ultrapure water). Also, the solvents shifted the maximum fluorescence emission to a shorter wavelength: by 12 nm ACT and MeOH, 6 nm ACN, 10 nm DMF and 3 nm ultrapure water. The reaction of GQDs with gallic acid quenched the fluorescence by 42.3% with ACT as solvent, 38.8% with ACN, 41% with DMF, 38.4 % with MeOH and 21.3% with ultrapure water. This trend was examined in triplicate over time. Replicated measurements made after 30 and 60 min exposed a different effect from the solvents. Thus the fluorescence of gallic acid in ACT continued to be quenched after 30 min —the signal decreased by 47% and then leveled off for up to 60 min. Quenching in ACN decreased (i.e.,

FL increased) from 38.8 to 32.6% after 30 min and remained virtually constant after 60 min. The DMF solutions exhibited decreased FL quenching at 30 min (from 41% to 31%) and 60 min (29.1%). On the other hand, quenching in the MeOH solution remained constant throughout. Mixing gallic acid aqueous solution with GQDs led to very slow interactions; as a result, FL quenching occurred from the very beginning. Quenching increased from 21.3 to 30.3% within 30 min and then rose to 35% after 60 min. Based on the sensor response to gallic acid in each solvent, we chose to use MeOH to redissolve the phenolic fraction after extraction on the grounds of the increased stability over time and efficient FL quenching obtained.

Figure 4 summarizes the results of the solvent tests. Fig. 4a illustrates FL quenching in the different solvents and Fig. 4b the temporal variation of the response of GQDs to gallic acid.

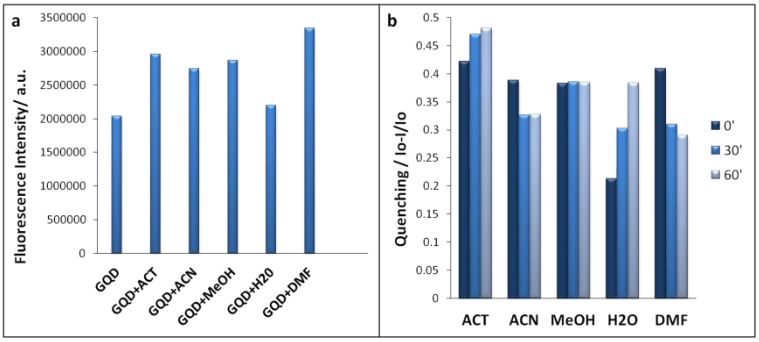

Figure 4. Influence of the solvent used to prepare the GQDs. (a) FL intensity of GQDs in each solvent (the maximum intensity was obtained with DMF). (b) Response of GQDs to gallic acid over time (methanol provided the most stable response).

3.3. Influence of the GQD/sample ratio on the fluorescence quenching response

The influence of the GQD/sample ratio on fluorescence quenching was examined by using sensors prepared in variable ratios; this was accomplished by using variable volumes of GQD solution (100, 200 or 300 μL) and methanolic gallic acid solution (300, 200 or 100 μL) to obtain a constant final volume of 400 μL. The final concentration of GQDs after dilution by effect of mixing with the sample was 1.12 $mg{\cdot}mL^{-1}$ with a 1:1 GQD/sample ratio (200 μL GQD + 200 μL sample), 0.56 $mg{\cdot}mL^{-1}$ with a 1:3 ratio (100 μL GQD + 300 μL sample) and 1.69 $mg{\cdot}mL^{-1}$ with a 3:1 ratio (300 μL GQD + 100 μL sample). A different sample (gallic acid) concentration was used in each case (viz., 200, 133 and 400 $mg{\cdot}L^{-1}$ gallic acid for the 1:1, 1:3 and 3:1 ratio, respectively) in order to obtain the same concentration after dilution with GQD solution and facilitate comparison of the sensitivity of GQDs (final concentration of the gallic acid solution, 100 $mg{\cdot}L^{-1}$). GQDs and methanol where mixed at the same ratios as the samples and used as blanks in parallel. The results obtained at each GQD/sample ratio are shown in Fig. 5. The original fluorescence of the GQDs increased with increasing methanol dilution in all cases and peaked at a GQD/sample ratio of 1:1 (see Fig. 5a). Fluorescence quenching by effect of the interaction between GDQs and gallic acid was examined. Quenching was measured as $(I_0 - I)/I_0$, where I_0 is the fluorescence of the blank (methanol

diluted GQDs) and *I* that in the presence of 100 mg·L^{-1} gallic acid in methanol. Quenching was maximal at a 1:1 GQD/sample ratio (Fig. 5b), which was thus selected to prepare the sensor.

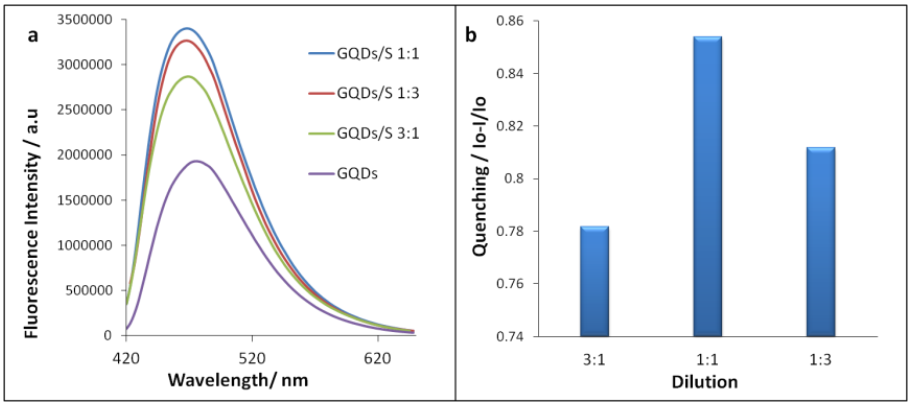

Figure 5. (a) Influence of the GQD/sample ratio. FL increased with increasing dilution in methanol at any ratio (a). (b) The best results in terms of FL quenching were obtained with a 1:1 GQD/sample ratio.

Additional dilutions (1:1, 1:5 and 1:10) were made in order to probe the sensor response at lower GQDs concentrations, with a final concentration of gallic acid of 50 mg·L^{-1}. When the fluorescent nanoparticles concentration decreases, quenching also decreases, but they are still sensitive to the standard. Under this conditions, when the GQDs is used in 1:1 ratio approximately 60 % of the fluorescence signal was quenched. The 1:5 ratio produced 30% of FL quenching and the 1:10 ratio, 9%. The system could still working but probably low sensitivity could be achieved. So, it can be

concluded that the sensor system proposed works with high sensitivity due to the high nanoparticles concentration.

3.4.Analytical features

The fluorescence response of the GQDs as sensing elements to increasing concentrations of gallic acid was measured. The response of the GQD phenol sensor was assessed in terms of sensitivity [limits of detection (LOD) and quantitation (LOQ)] and precision under the above-described optimum operating conditions. The FL intensity of the GQDs proved highly sensitive to gallic acid and decreased with increasing concentration of the phenol. The analytical features of the sensor were determined from its fluorescence response to increasing concentrations of the acid. A calibration curve was constructed by plotting the relative FL response $(I_0 - I)/I_0$ as a function of the gallic acid concentration. Quenching was linearly related to the phenol concentration over the range 5–40 $mg{\cdot}L^{-1}$. The equation for the calibration curve was

$$(I_0 - I)/I_0 = 0.0119 + 0.0116C \quad (R^2 = 0.996) \quad (1)$$

The proposed GQD sensor for gallic acid provided an LOD of 1.08 $mg{\cdot}L^{-1}$ and an LOQ of 3.6 $mg{\cdot}L^{-1}$. The theoretical limit of detection was calculated as $3S_a/b$, S_a being the standard error of the intercept and b the slope of de calibration curve (n = 3). Similarly, the limit of quantitation was

calculated as $10S_a/b$. The precision, expressed as relative standard deviation (RSD) in terms of repeatability ($n = 5$), at a concentration level of 20 mg·L^{-1} was 1.25 %.

We studied another analyte (oleuropein) to demonstrate that our sensor was also sensitive to phenols with a complex structure. The procedure was identical with that described above for gallic acid. Thus, a calibration curve was constructed by plotting the relative FL response, $(I_0 - I)/I_0$, at variable oleuropein concentrations. The curve was linear over the concentration range 2–30 mg·L^{-1} and its equation

$$(I_0 - I)/I_0 = -0.0029 + 0.0067C \quad (R^2 = 0.9982) \qquad (2)$$

The LOD and LOQ for oleuropein were 0.56 and 1.86 mg·L^{-1}, respectively, and the precision, as RSD, at a concentration level of 10 mg·L^{-1}, 0.98 % ($n = 5$).

Fig. 6a shows the calibration curves with error bars of gallic acid and oleuorpein.

The repeatability of the GQD synthetic procedure was also evaluated. For this purpose, the procedure was performed five times under identical conditions and FL for each GQD solution thus obtained measured at excitation

wavelength of 380 nm after adjustment to pH 10. The RSD between replicates thus obtained was 8.7% (n = 5).

3.4.1. Application of the proposed sensing system

The applicability of the proposed sensing method was evaluated on four different types of real olive oil samples (viz., EVOO, VOO, LOO and ROO). A calibration graph was constructed from gallic acid spiked ROO samples that was linear over the range 0.3–3 mg·L^{-1} and conformed to the following equation:

$$(I_0 - I)/I_0 = 0.0024 + 0.085C \quad (R^2 = 0.9912) \quad (3)$$

The sensor was also evaluated in terms of sensitivity (LOD and LOQ) and precision. To this end, spiked and real samples were subjected to the process described in Section 2.4 (liquid–liquid extraction and preconcentration of phenols). The preconcentration step was necessary to obtain an acceptable LOD.

A calibration curve was constructed by plotting the relative FL response, $(I_0 - I)/I_0$, at variable gallic acid concentrations added to ROO. The LOD and LOQ thus obtained with the proposed extraction–preconcentration–sensing method were 0.09 and 0.3 mg·L^{-1}, respectively. Within-day precision (n = 5), expressed as %RSD, was 0.96%, and between-day precision (n = 5) 1.3%.

Refined olive oil was also spiked with oleuropein and the procedure repeated for this analyte in order to assess the sensor response to a complex phenol. A calibration graph was also constructed from oleuropein spiked ROO samples that was linear over the concentration range 0.4–3 $mg{\cdot}L^{-1}$ and conformed to the following equation:

$$(I_0 - I)/I_0 = -0.003 + 0.056C \quad (R^2 = 0.9901) \quad (4)$$

The calibration curve for oleuropein was constructed by plotting the relative FL response $(I_0 - I)/I_0$ as a function of the concentration of this phenol added to ROO.

The LOD and LOQ thus obtained was 0.12 and 0.39 $mg{\cdot}L^{-1}$, respectively. Within-day precision (n = 5), expressed as %RSD, was 0.98%, and between-day precision (n = 5) 1.7%. Fig. 6b shows the calibration curves with error bars of gallic acid and oleuorpein spiked ROO.

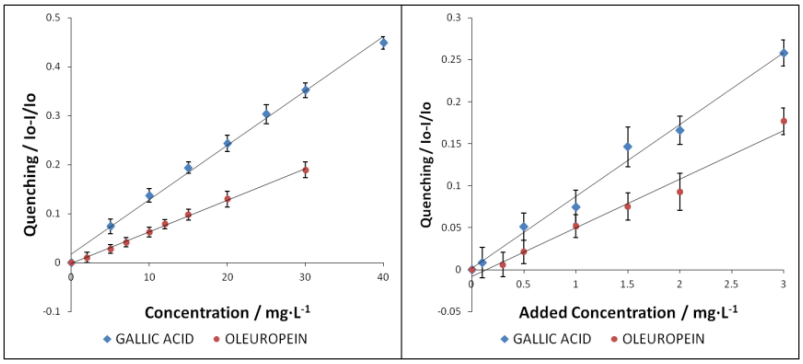

Figure 6. Calibration graphs of the gallic acid and oleuropein standard solutions (a) and calibration graphs of the spiked ROO samples (b)

The recoveries of the two analytes (Table 1) were calculated from the following equation:

$$\% \text{ recovery} = [(C_{found} - C_{sample})/C_{added}] \times 100 \quad (5)$$

Both were better than 71%.

The relative FL intensity of each real sample as measured with the sensor was interpolated in calibration curve for gallic acid spiked ROO in order to calculate its phenolic concentration in gallic acid equivalents (GAE), which is the typically reported value. At $t = 0$, the phenol concentrations sensed in the real samples were lower than those obtained with the Folin–Ciocalteu colorimetric method; however, if the sensor was allowed enough time to provide a response, the results were very similar (see Table 2, which summarizes the results obtained with the FC assay and the proposed sensing method). This suggests that the reaction of GQDs with phenols in the phenolic fraction of oil is more intricate and slower than that with gallic acid owing to the presence of structurally complex phenols and polyphenols. We recommend a minimum measurement time of 30 min when real samples are analyzed since 97% of the phenol content was found to react within that length of time (see Fig. 7).

Table 1. Efficiency of the extraction–preconcentration procedure for refined olive oil spiked with different concentrations of gallic acid and oleuropein. Recoveries were calculated from three analyses at each added concentration.

Spiked analyte	Sample	Amount added ($mg{\cdot}L^{-1}$)	Amount after preconcentration ($mg{\cdot}L^{-1}$)	$(I_0 - I)/I_0$	Amount found ($mg{\cdot}L^{-1}$)	Recovery (%)
Gallic acid	ROO	0.5	5	0.05131	4.41	88.2
	ROO	1	10	0.08346	7.09	71.0
	ROO	1.5	15	0.14625	12.59	83.9
	ROO	2	20	0.19186	16.52	82.6
Oleuropein	ROO	0.5	5	0.02711	4.04	81.0
	ROO	1	10	0.04932	7.36	73.6
	ROO	1.5	15	0.07929	11.84	78.9
	ROO	2	20	0.10793	16.11	80.5

Table 2. Concentrations of total phenols found in real samples, expressed in GAE.

Sample	Total phenol concentration (GAE, $mg{\cdot}L^{-1}$)	
	GQD sensing method	Folin–Ciocalteu method
Extra virgin olive oil	115.6	130.7
Virgin olive oil	103.8	116.6
Lampante olive oil	70.9	74.2
Refined olive oil	0.001	0.009

A shift in maximum emission to a higher wavelength was observed with real samples: from 470 nm for GQD/MeOH (1:1) to 480 nm for GQD/EVOO and GQD/VOO. The emission wavelength for GQD/LOO shifted to 474 nm, whereas that for GQD/ROO remained at 470 nm. We can

therefore conclude that high phenol content in oil shifts the maximum emission wavelength of GQDs.

Since the sensor response to the standards was similar each time that the calibration curve was repeated (n=3) and ambient factor such as temperature do not affect the sensitivity of the sensor, it is not necessary to make a new calibration curve before measurements of different batch of olive oil samples. However, despite the fact that the synthesis yield GQDs with high reproducibility, a new calibration would be recommendable when a new batch of GQDs is synthesized in order to assure the accuracy of the method. Calibration curves present in this work were constructed by using the same batch of GQD solution.

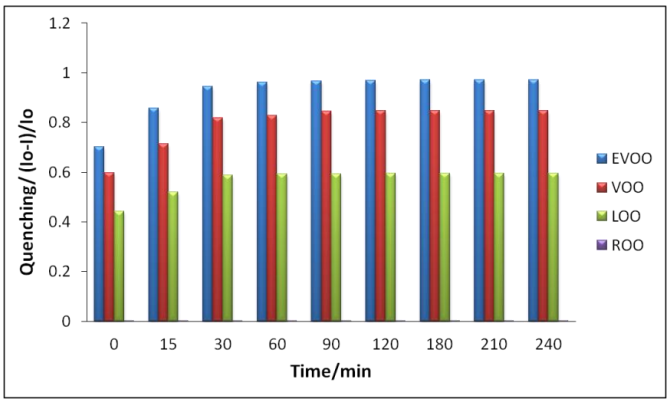

Figure 7. Response of GQDs to real samples over time. A proportion of 97% of total phenols in all samples reacted with the GQD sensor within the first 30 min. By exception, the refined olive oil (ROO) samples, which contained no phenols, gave flat signals.

4. CONCLUSIONS

A GQDs based optical nanosensor for determining the phenol fraction of olive oil was developed. Phenols react with GQDs via π–π stacking and non–covalent interactions and quench their FL intensity as a result. The proposed sensing method is very simple, sensitive and reproducible. Its limit of detection, 90 $\mu g \cdot L^{-1}$, is very low and similar to those of official methods. The sensor provides a fast response (less than 1 min to standards of gallic acid and oleuropein, and 30 min to the phenol fraction of olive oil) and is therefore much more expeditious than colorimetric methods. The results obtained in this work testify to the potential of the proposed sensing system for determining phenols in olive oil samples.

Acknowledgements

The authors wish to thank Junta de Andalucía for financial support (Project FQM 4801). S. Benítez-Martínez is also grateful to Junta de Andalucía for the award of a Research Training Fellowship.

The authors have declared no conflict of interest.

5. REFERENCES

[1] H. Brody, Graphene, Nature 483 (2012) S29.

[2] X. Yan, X. Cui, L. Li, Synthesis of large, stable colloidal graphene quantum dots with tunable size, Journal of the American Chemical Society 132 (2010) 5944–5945.

[3] Y. Dong, C. Chen, X. Zheng, L. Gao, Z. Cui, H. Yang, C. Guo, Y. Chi, C. M. Li, One-step and high yield simultaneous reparation of single– and multi–layer graphene quantum dots from CX–72 carbon black, Journal of Materials Chemistry 22 (2012) 8764–8766.

[4] J. Shen, Y. Zhu, X. Yang, J. Zong, J. Zhang, C. Li, One-pot hydrothermal synthesis of graphene quantum dots surface-pasivated by polyethylene glycol and their photoelectric conversion under near–infrared light, New Journal of Chemistry 36 (2012) 97–101.

[5] S. Zhuo, M. Shao, S. T. Lee, Upconversion and downconversion fluorescent graphene quantum dots: ultrasonic preparation and photocatalysis, ACSNano 6 (2012) 1059–1064.

[6] L. A. Ponomarenko, F. Schedin, M. I. Katsnelson, R. Yang, E. W. Hill, K. S. Novoselov, A. K. Geim, Chaotic dirac billard in graphene quantum dots, Science 320 (2008) 356–358.

[7] L. Fan, M. Zhu, X. Lee, R. Zhang, K. Whang, J. Wei, M. Zhong, D. Wu, H. Zhu, Direct synthesis of graphene quantum dots by chemical vapor

deposition, Particle & Particle Systems Characterizations 30 (2013) 764–769.

[8] J. Peng, W. Gao, B.K. Gupta, Z. Liu, R. Romero–Aburto, L. Ge, L. Song, L. B. Alemany, X. Zhan, G. Gao, S. A. Vithayathil, B. A. Kaipparettu, A. A. Marti, T. Hayashi, J. J. Zhou, P. M. Ajayan, Graphene quantum dots derived from carbon fibers, Nano Letters 12 (2012) 844–849.

[9] M. Xie, Y. Su, X. Lu, Y. Zhang, Z. Yang, Y. Zhang, Blue and green photoluminescence graphene quantum dots synthesized from carbon fibers, Material Letters 93 (2013)161–164.

[10] D. Pan, L. Guo, J. Zhang, C. Xi, Q. Xue, H. Huang, J. Li, Z. Zhang, W. Yu, Z. Chen, Z. Li, M. Wu, Cutting sp^2 clusters in graphene sheets into colloidal graphene quantum dots with strong green fluorescence, Journal of Materials Chemistry, 22 (2012) 3314–3318.

[11] D. Pan, J. Zhang, Z. Li, M. Wu, Hydrothermal route for cutting graphene sheets into blue–luminiscent graphene quantum dots. Advanced Materials 22 (2010) 734–738.

[12] S. Zhu, J. Zhang, C. Qiao, S. Tang, Y. Li, W. Yuan, B. Li, L. Tian, F. Lui, R. Hu, H. Gao, H. Wei, H. Zhang, H. Sun, B. Yang, Strongly green-photoluminescent graphene quantum dots for bioimaging applications, Chemical Communications 47 (2011) 6858–6860.

[13] S. Zhu, J. Zhang, X. Liu, B. Li, X. Wang, S. Tang, Q. Meng, Y. Li, C. Shi, R. Hu, B. Yang, Graphene quantum dots with controllable surface oxidation, tunable fluorescence and up-conversion emission, RSC Advances 2 (2012) 2717–2720.

[14] J. Shen, Y. Zhu, C. Chen, X. Yang, C. Li, Facile preparation and upconversion luminescence of graphene quantum dots, Chemical Communications 47 (2011) 2580–2582.

[15] D. B. Shinde, V. K. Pillai, Elecrochemical preparation of luminescent graphene quantum dots from multiwalled carbon nanotubes. Chemistry A European Journal 18 (2012) 12522–12528.

[16] L. Lin, S. Zhang, Greating high yield water soluble luminescent graphene quantum dots via exfoliating and disintegrating carbon nanotubes and graphite flakes, Chemical Communications 48 (2012) 10177–10179.

[17] L. Minati, S. Torrengo, D, Maniglio, C. Migliaresi, G. Speranza, Luminiscent graphene quantum dots from oxidized multi-walled carbón nanotubes, Materials Chemistry and Physics 137 (2012) 12–16.

[18] L. Li, X. Yan, Colloidal graphene quantum dots, Journal of Physical Chemistry Letters 1 (2010) 2572–2576.

[19] L. Tang, R. Ji, X. Cao, J. Lin, H. Jiang, X. Li, K.S. Teng, C. M. Luk, S. Zeng, J. Hao, S. P. Lau, Deep ultraviolet photoluminescence of water–soluble self–passivated graphene quantum dots, ACSNano 6 (2012) 5102–5110.

[20] Y. Dong, J. Shao, C. Chen, H. Li, R. Wang, Y. Chi, X. Lin, G. Chen, Blue luminescent graphene quantum dots and graphene oxide prepared by tunning the carbonization degree of citric acid, Carbon 50 (2012) 4738–4743.

[21] R. Lui, D. Wu, X. Feng, K. Müllen, Bottom–up fabrication of photoluminescent graphene quantum dots with uniform morphology, Journal of the American Chemical Society 133 (2011) 15221–15223.

[22] J. Lu, P. S. E. Yeo, C. K. Gan, P. Wu, K. P. Loh, Transforming C_{60} molecules into graphene quantum dots, Nature Nanotechnology 6 (2011) 247–252.

[23] L. Li, G. Wu, G. Yang, J. Peng, J. Zhao, J. J. Zhu, Focussing on luminescent graphene quantum dots: current status and future perspectives, Nanoscale 5 (2013) 4015–4039.

[24] H. Razmi, R. Mohammad–Rezaei, Graphene quantum dots as a new substrate for inmobilization and direct electrochemistry of glucose oxidase: Applications to sensitive glucose determination, Biosensors and Bioelectronics 41 (2013) 498–504.

[25] Y. Dong, G. Li, N. Zhou, R. Wang, Y. Chi, G. Chen, Graphene quantum dot as a gren and facile sensor for free cholorine in drinking water, Analytical Chemistry 84 (2012) 8378–8382.

[26] L. L. Li, G. Gi, R. Fei, C. Z. Wang, Q. Lu, J. R. Zhang, L. P. Jiang, J. J. Zhu, A facile microwave avenue to electrochemiluminescent two–color graphene quantum dots, Advanced Functional Materials 22 (2012) 2971–2979.

[27] L. Fan, Y. Hu, X. Wang, L. Zhang, F. Li, D. Ham, Z. Li, Q. Zhang, Z. Wang, L. Niu, Fluorescence resonance energy transfer quenching at the surface of graphene quantum dots for ultrasensitive detection of TNT, Talanta 101 (2012) 192–197.

[28] D. Wang, L. Wang, X. Dong, Z. Shi, J. Hin, Chemically tailoring graphene oxides into fluorescent nanosheets for Fe^{3+} ion detection, Carbon 50 (2012) 2147–2154.

[29] F. Yang, M. Zhao, B. Zheng, D. Xiao, L. Wu, Y. Guo, Influence of pH on the fluorescence properties of graphene quantum dots using ozonation pre-oxide hydrothermal synthesis, Journal of Materials Chemistry 22 (2012) 25471 – 25479.

[30] H. Zhao, Y. Chang, M. Lui, S. Gao, H. Yu, X. Quan, A universal immunosensing strategy based on regulation of the interaction between graphene and graphene quantum dots, Chemical Communications 49 (2013) 234–236.

[31] J. Zhao, G. Chen, L. Zhu, G. Li, Graphene quantum dots-based platform for the fabrication of electrochemical biosensors, Electrochemistry Communications 13 (2011) 31–33.

[32] A. Carrasco–Pancorbo, L. Cerretani, A. Bendini, A. Segura–Carretero, T. Gallina–Toschi, A. Fernandez–Gutierrez. Analytical determination of polyphenols in olive oils, Journal of Separation Science 28 (2005) 83–858.

[33]F. M. Pirisi, P. Cabras, C. F. Cao, M. Migliorini, M. Muggelli, Phenolic compounds in virgin olive oil. 2. Reappraisal of the extraction, HPLC separation, and quantification procedures, Journal of Agricultural and Food Chemistry 48 (2000) 1191–1196.

[34] A. L. Waterhouse, Determination of total phenolics. In R. E. Wrolstad, T. E. Acree, E. A. Decker, M. H. Penner, D. S. Reid, S. J. Shwartz, C. F. Shoemaker, D. Smith, P. Sporns (Eds.) 1st ed. Hoboken, New Jersey, USA; John Wiley & Sons, 2001, 463–470.

[35]A. Cayuela, M.L. Soriano, M. Valcárcel. Strong luminescence of Carbon Dots induced by acetone passivation: Efficient sensor for a rapid analysis of two different pollutants, Analytica Chimica Acta 804 (2013), 246–251.

Biographies

S. Benítez–Martínez obtained the Environmental Sciences degree in 2007 at the University of Córdoba. In order to expand her scientific knowledge she attended a scientific Post degree Master in Advanced Fine Chemistry carrying out a Master Project focused in using graphene nanosheets as pseudostationary phase in electrokinetic chromatography. Nowadays she has

an official research grant from the "Junta de Andalucía" for the development of her PhD Thesis focused on graphene nanoparticles as tool for the improvement of analytical process.

M. Valcárcel is full professor of analytical chemistry at the University of Córdoba since 1976. He is the author and co-author of 800 scientific articles (with a Hirsh factor of 41), 7 monographs, 8 textbooks and 16 chapters of books. He was the coordinator of 25 research Spanish scientific projects and 14 of international nature, as well as 12 contracts with private firms and promoter of a spin-off devoted to nanotechnology. Prof. Valcárcel has been the cosupervisor of 68 doctoral thesis and an invited lecturer in 70 international meetings. He is the recipient of relevant scientific national (e.g. Award in Chemistry in Spain, 2006) and international (e.g. Robert Boyle Medal of RSC, 2004) prizes as well as Doctor Honoris Causa by the University of Valencia (Spain, 2010).

Capítulo 5

Glycine–functionalized Graphene Quantum Dots based fluorescence sensor for the direct determination of TiO_2 nanoparticles

Submitted to Analytical Chemistry

analytical chemistry

Article Submitted

Glycine-functionalized graphene quantum dots based fluorescence sensor for the direct determination of TiO_2 nanoparticles

Sandra Benítez-Martínez, Ángela Inmaculada López-Lorente, Miguel Valcárcel*

Department of Analytical Chemistry, University of Córdoba, E-14071 Córdoba, Spain Phone/Fax +34 957 218616; E-mail: qa1meobj@uco.es

The paper proposes a simple procedure for the determination of titanium oxide (TiO_2) nanoparticles (NPs) from sunscreens using glycine-functionalized graphene quantum dots (gly-GQDs). The method is based in the liquid-liquid extraction of the TiO_2 nanoparticles present in the sunscreen and the subsequent fluorescence analysis of the extracts by the quenching effect produced on the gly-GQDs solution due to interaction of the aminoacid with the extracted TiO_2 nanoparticles owing to electrostatic interaction or to hydrogen bonding. The limit of detection was 1.4 $\mu g \cdot g^{-1}$. The precision, for a 5 $\mu g \cdot g^{-1}$ concentration of TiO_2 NPs is 6.95%. The optimized procedure has been

successively applied to the determination of TiO_2 nanoparticles content in sunscreens of different sun protector factors.

Keywords: graphene quantum dots, glycine, titanium oxide nanoparticles, fluorescence, quenching, sunscreens.

GRAPHICAL ABSTRACT

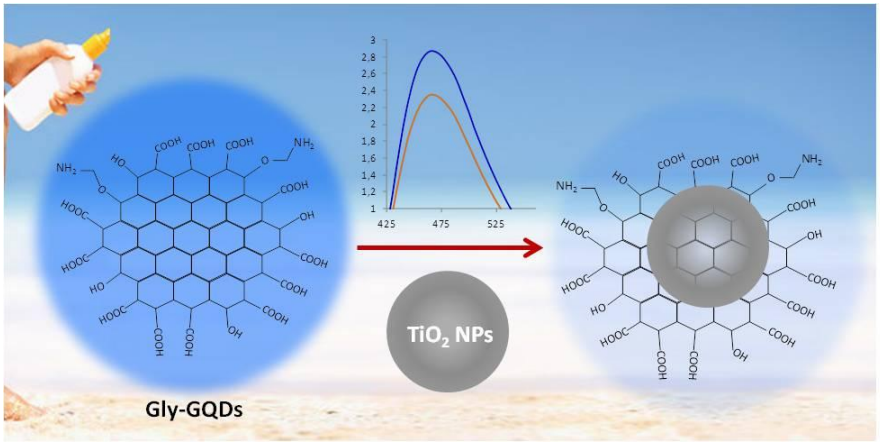

1. INTRODUCTION

Engineered nanomaterials (ENMs) are increasingly employed in personal care products (PCPs). Among them, titanium dioxide nanoparticles (TiO_2 NPs) are widely used since they are highly stable, nonreactive with other materials, thermally stable and non-flammable having a low cost[1]. They are usually employed in products such as toothpastes and sunscreens, as well as food additives, such as in candies, sweets, and chewing gums [2]. The potential for exposure and the consequences to human health from ENMs in PCPs are not well quantified [3], neither their possible release and accumulation in environmental compartments. It has been estimated that in the US zinc oxide (ZnO) and TiO_2 represent 94 % of ENMs released into the environment from the use of PCPs [4].

In sunscreens the high refractive index of TiO_2 added in nano-particulate form protects the skin from UV radiation of the sunlight [5]. The radiation reflection and scattering efficiencies depend on its concentration and particle size [6]. Recently there is a controversy about the possible adverse affects of these NPs. While a study reported the lack of skin carcinogenicity of TiO_2 NPs in a medium-term mouse skin bioassay [7], recent studies, however, have shown that they are not completely harmless to the human body [8,9].

The determination of the content of TiO_2 in sunscreen samples has been attempted with different techniques, such as volumetry [10], atomic absorption spectrometry [11], inductively coupled plasma optical emission spectrometry (ICP-OES) [12], and X-ray fluorescence spectrometry [13]. For particle size characterization, different field-flow fractionation (FFF) techniques [14] have been reported for TiO_2 particles in commercial sunscreen products, for example sedimentation-FFF [15] or flow-FFF [1,5] coupled with both inductively coupled plasma mass spectrometry (ICP-MS) or inductively coupled plasma-atomic emission spectrometer (ICP-AES). Recently, ICP spectrometry has been employed for the determination of titanium from TiO_2 NPs in tissues [16] and TiO_2 NPs in nitric acid and river water [17].

Graphene quantum dots (GQDs) are zero–dimensional luminescent carbon-based nanomaterials that consist on very small graphene sheets with lateral size less than 100nm in single, double or multiple layers. They show exciton confinement, quantum size effect and diameters ranging from 3 to 20 nm, approximately [18]. The GQDs bandgap is different from zero and can be tuned varying the size and the surface chemistry of GQDs [19]. They show excellent properties such as their high fluorescence activity, low toxicity, high biocompatibility, excellent photostability and robust chemical inertness [20], which has driven their use in several fields, among them the development of sensors [21, 22] and biosensors [23].

In this paper, glycine functionalized GQDs have been synthesized and employed for the simple and rapid quantification of TiO_2 NPs in sunscreen samples, due to their widespread presence in their formulae and the complexity of the matrix. The adhesion of the metallic nanoparticles with the gly-GQDs –possibly due to electrostatic interaction or to hydrogen bonding- leads to a decrease in the fluorescence intensity –quenching- of gly-GQDs, which has been used as analytical signal for the quantification of the presence of TiO_2 NPs after extraction from the sunscreen lotion. As far as we are concerned, this is the first approach to the fluorimetric determination of TiO_2 nanoparticles from sunscreen samples based on the use of graphene-derived nanomaterials.

2. METHODS

2.1. Materials and reagents.

All chemical reagents were analytical-grade and were used without additional purification. Citric acid (≥99.0%) and glycine (98%) were purchased from Sigma–Aldrich (Madrid, Spain). L-cysteine (99.5%) was purchased from Fluka (Buchs, Switzerland). Titanium (IV) oxide (99%), mixture of rutile and anatasa nanoparticles with < 150 nm particle size (DLS) was also provided by Sigma-Aldrich. HPLC-grade methanol (≥99.9%) was acquired from Carlo Erba Reagents (Barcelona, Spain). Sunscreens of different brands were used for the

fortification of the sample (Solcare, SPF 15) and those whose composition includes TiO_2 NPs were also analyzed (Garnier, SPF 20 and SPF 30).

2.2. Equipment

Fluorescence emission spectra were recorded on a PTI Quanta Master™ spectrofluorometer from Photon Technology International (Barcelona, Spain) equipped with a 75 W xenon short arc lamp and an 814 PTM detection system. The software FeliX32was used for data acquisition and instrument control. The excitation and emission slits were both 2.3 nm wide. Measurements were made at room temperature, using a micro quartz cuvette of 10 mm light path.

A Vibracell™ 75041 ultrasonic probe (750 W, 20 KHz, Bioblock Scientific, Illkirch, France) equipped with a 3 mm probe was employed for treatment of the sample with the water and methanol solvent extracts in the different steps of the TiO_2 NPs extraction procedure.

High-resolution transmission electron microscopy (HRTEM) images of gly-GQDs were obtained on a TECNAI F30 electron microscope available at the Institute of Materials (CSIC) in Seville (Spain). The instrument was operated at a medium acceleration voltage of 300 kV. A drop of diluted nanoparticles suspension was drop-cast on a copper TEM grid with a hollow carbon forward.

Fourier transform mid infrared (FT-MIR) spectra were obtained on a Bruker Tensor 27FT-MIR spectrophotometer equipped with a Hyperion 2000 microscope, using KBr pellets.

Transmission electron microscopy (TEM) images of TiO_2 nanoparticles were acquired with a JEOL JEM-1400 microscope. A drop of the nanoparticles suspension was drop-cast on a copper TEM grid with a Carbowax forward.

2.3. Synthesis of fluorescent nanomaterials

2.3.1. Graphene quantum dots (GQDs)

GQDs were obtained by pyrolysis of citric acid, similarly to that described in [21] using a slightly modified version of the procedure by Dong et al.[24]. To this end, an amount of 2 g of citric acid was placed in a vial and heated at 200◦C on a thermoblock from JP Selecta (Barcelona, Spain) until the citric acid changed from a white dust to a dark orange liquid, which took about 30 min. The resulting liquid was added dropwise to 100 mL of a 10 mg L^{-1} NaOH solution under vigorous stirring. The GQD aqueous solution thus obtained was stored at 4◦C in an amber bottle.

2.3.2. Glycine-functionalized graphene quantum dots (gly-GQDs)

The glycine functionalized GQDs were prepared by hydrothermal treatment of citric acid as carbon source in the presence of glycine, adapting the procedure described for other nitrogen compounds [25]. Citric acid

monohydrate (2 g) and glycine (0.62 g) were dissolved in 5 mL of water and the solution heated at 200◦C on a thermoblock from JP Selecta (Barcelona, Spain) for 3 h. The black syrup product was then diluted in 100 mL of a 0.25 mol·L^{-1} NaOH solution and stored at 4ºC in an amber bottle.

2.3.3. L-cysteine-functionalized graphene quantum dots (L-cys-GQDs)

The L-cysteine functionalized GQDs were prepared by mixing citric acid and L-cysteine and their thermal treatment similar to that described for gly-GQDs. Citric acid monohydrate (2 g) and L-cysteine (1 g) were dissolved in 5 mL of water and heated at 200◦C on a thermoblock from JP Selecta (Barcelona, Spain) for 3 h. The black syrup product was diluted in 100 mL of NaOH solution (0.25 mol·L^{-1}) and stored at 4ºC in an amber bottle.

2.3.4. Fluorescent graphene oxide (GO)

GO was obtained by pyrolysis of citric acid in a similar way than unfunctionalized GQD, according to the procedure by Dong et al. [24]. 2 g of citric acid was placed in a vial and heated at 200◦C on a thermoblock from JP Selecta (Barcelona, Spain) during 2 hours, which leads to the complete carbonization of the citric acid, which changed from a white dust to a dark orange liquid. The resulting liquid after 2 h was added dropwise to 100 mL of a 10 mg L^{-1} NaOH solution under vigorous stirring. The GO aqueous solution thus obtained was stored at 4◦C in an amber bottle.

2.4. TiO_2 NPs extraction and determination procedure from sunscreens

Extraction of the TiO_2 nanoparticles from the sunscreen lotion (SPF 15) was carried out according to following procedure modified from that described by Contado and Pagnoni [1]. 0.1 g of sunscreen cream were was accurately weighed into clean, dry centrifuge vials. The sunscreen lotion was first dispersed in 2 mL of water and the mixture was submitted to ultrasound treatment. Amplitude of the ultrasonic vibrations was set at 20% of maximum nominal power for 30 s (cycles of 5 s on and 5 s off). Afterwards, 2 mL of methanol are added to the vial and again tip sonicated in the same conditions than in the previous step in order to enable the mixture of the components of the solution. The third step comprises the addition of 2 mL of hexane. The suspension was vigorously shaken for 20 s and then centrifugated at 6000 rpm for 15 min for separation of the organic and aqueous phases. The aqueous extract containing the TiO_2 NPs was submitted to two further clean-up step with 1 mL of hexane for fat removal and subsequent centrifugation (6000 rpm, 15 min). The extract was evaporated to dryness at 70ºC under a N_2 stream and, finally, reconstituted in 200 µL of methanol. Figure 1 shows a scheme of the procedure followed.

The procedure was slightly modified for the extraction of TiO_2 NPs from sunscreens SPF 20 and 30, due to the higher density of the lotion. After

treatment with water and methanol similar to that previously described, 2 mL of hexane were added and centrifugated at 10000 rpm during 30 min. Then, samples were cleaned twice with 1 mL of hexane and centrifugated at 10000 rpm for 15 min. Finally, the extract was evaporated to dryness at 70ºC under a N_2 stream and reconstituted in 200 µL of methanol.

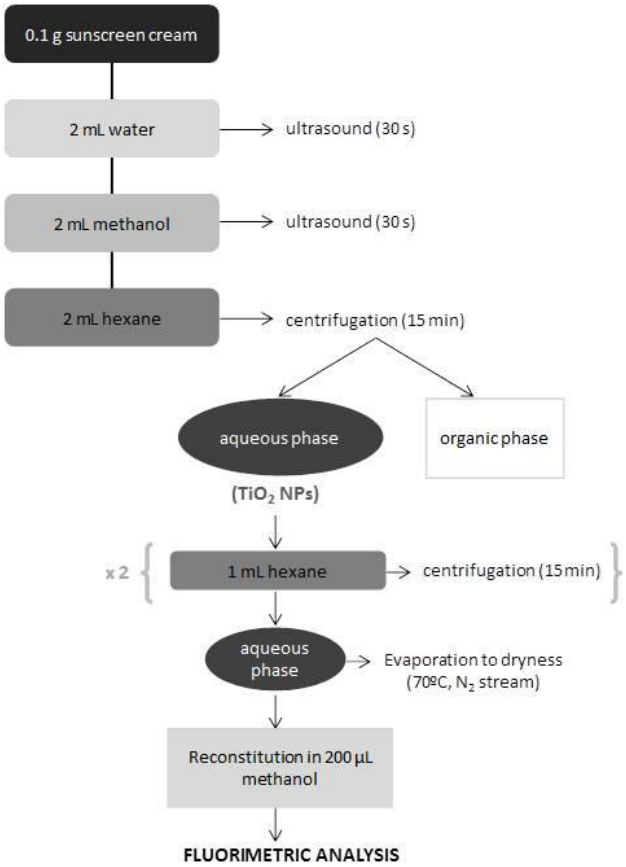

Figure 1. Scheme of the procedure for the extraction of TiO_2 NPs from sunscreen samples prior fluorimetric analysis

Fluorescence measurements were performed at an excitation wavelength of 385 nm recording the emission between 400 and 650 nm. Measurements were performed in a micro quartz cuvette of 10 mm light path. 100 µL of a 4-fold diluted gly-GQD solution were blended thoroughly with 200 µL of the methanolic extract in which TiO_2 NPs are reconstituted. Once mixed, fluorescence spectrum was acquired.

3. RESULTS AND DISCUSSION

3.1. Selection of the fluorescent nanomaterial

Different carbon based nanomaterials with fluorescent properties were studied as possible sensors for the determination of the TiO_2 nanoparticles content in sunscreens, namely unfunctionalized graphene quantum dots, glycine and L-cysteine functionalized graphene quantum dots and graphene oxide. Graphene quantum dots modified with aminoacids were selected due to the possible interaction among the aminoacid with the TiO_2, as previously described [26]. Different parts of an amino acid may interact with the surface of titanium oxide. Simple carbonic acids form two equivalent bonds between the carboxyl oxygen and Ti atoms, while the acid proton dissociates off and binds to an oxygen bridging [26]. The weak adhesion of aminoacids can be owing to electrostatic interaction or to hydrogen bonding [26].

The response of the luminescence of the nanomaterials towards the presence of TiO_2 nanoparticles in the solution was investigated. Significant quenching of the fluorescence of the nanomaterial was observed for those glycine functionalized GQDs, thus this nanomaterial was selected for the development of the sensor. The interaction of glycine with TiO_2 has been previously reported by Lausmaa et al.[27] who studied the adsorption of glycine from TiO_2 surfaces by thermal desorption spectroscopy, which involves the carboxylic group of the aminoacid. As described below, these gly-GQDs have been characterized, and the conditions for both the extraction of the TiO_2 nanoparticles from sunscreen and the subsequent fluorimetric measurements have been studied.

3.2. Characterization of gly-GQDs

Gly-GQDs were synthesized through a "bottom-up" procedure involving the pyrolysis of citric acid, which leads to flat circular nanosheets of average diameter 12 ± 2 nm as calculated from high resolution transmission electron microscopy (HRTEM) images (see Figure 2a). gly-GQDs were obtained at a concentration of 5807 mg L^{-1} Moreover, obtained gly-GQDs were characterized by FT-MIR showing the presence of carboxyl, hydroxyl and amino groups (Figure 2b). The bands observed at around 1600-1700 cm^{-1} correspond to the C=O stretching of carboxyl groups whereas the bands at around 1400 cm^{-1} can be attributed to the C-N stretching. Finally, the band

around 3400 cm^{-1} is assigned to the O-H and N-H stretching vibration of hydroxyl and amine groups.

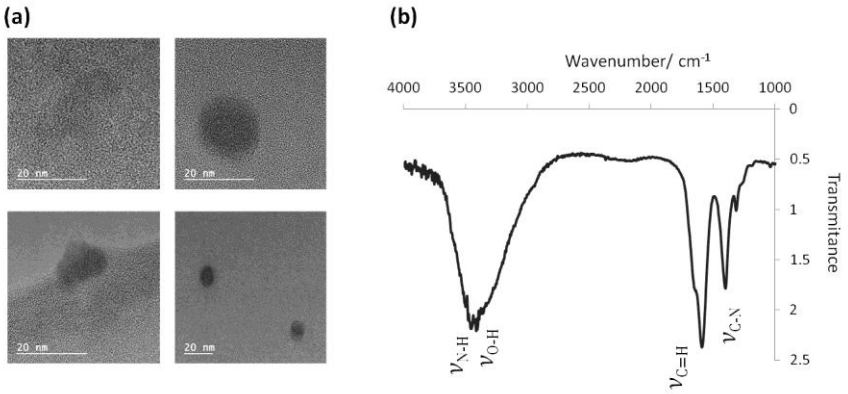

Figure 2. (a) HTEM images of the synthesized gly-GQDs, (b) FT-MIR spectra of gly-GQDs showing the presence of carboxyl, amino and hydroxyl groups.

The synthesized gly-GQDs showed blue emission at 460 nm. Their photoluminiscent quantum yield (Φ) was calculated using quinine sulfate as standard. Gly-GQDs showed better Φ behavior, calculated as 10.04%, as compared with unfunctionalized GQDs, which yielded to just 4.5%.

The reproducibility of the synthesis was evaluated. Five independent batches of gly-GQDs solutions were synthesized and their fluorescence measured after 10-fold dilution. Fluorescence values showed a relative

standard deviation of 3.52%, confirming, thus, the high reproducibility of the production of nanomaterials involved in the sensor.

3.3. Characterization of TiO_2 nanoparticles

The TiO_2 NPs involved as analytes in this study have been characterized by transmission electron microscopy and their average size has been calculated. Those nanoparticles appear homogeneous in shape and size and of polygonal yet nearly spherical shape. Of particular interest is also the fact that TiO_2 NPs are well dispersed with neither aggregates observed. The average diameter of the nanoparticles was determined to be 33 ± 5 nm. Figure 3 shows TEM images of the nanoparticles as well as the size distribution of the nanoparticles analyzed.

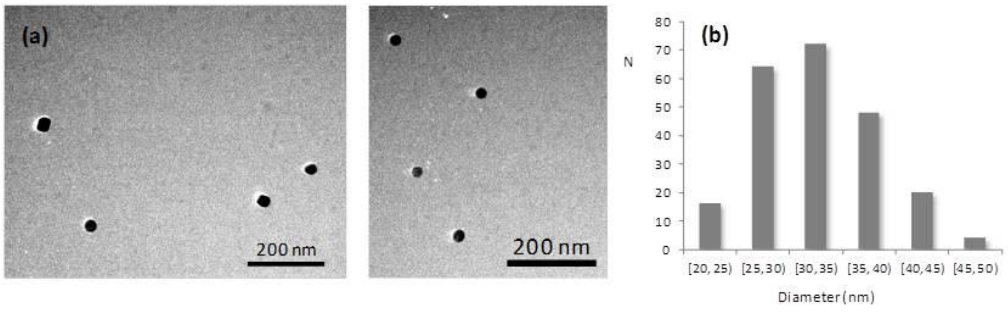

Figure 3. (a) TEM images of collected individual TiO_2 nanoparticles standards employed for the study. (b) Size distribution of the nanoparticles resulting in d_{ave}= 33 ± 5 nm.

3.4. Study of the TiO_2 NPs extraction conditions

TiO_2 nanoparticles were extracted from sunscreen samples following a procedure similar to that of Contado and Pagnoni [1] with some modifications, as shown in Figure 1. Both the ultrasound and centrifugation conditions and time were studied. 30 seconds of 20% amplitude of tip sonication in cycles of 5 seconds on and 5 second off were selected for treatment of the sunscreen sample with the aqueous, firstly, and, subsequently, methanol fractions. The centrifugation process was carried out at 6000 rpm during 15 min, which proved to be enough for a good phase separation.

Moreover, the final volume in which the extract is reconstituted was investigated. Different extracts in triplicate were reconstituted in different volumes, namely 100, 200 and 300 µL, and were subjected to fluorimetric detection. A volume of 200 µL was finally selected for further experiments.

3.5. Study of conditions for quenching measurements

Firstly, the influence of the pH of the gly-GQDs solution was investigated. Gly-GQDs showed different fluorescence values at different pH. The pH of the as-synthesized GQDs solution is basic. Moreover, the influence of pH over the quenching response of the sensor was also evaluated. The pH obtained directly from the synthesis was selected as the better conditions of sensibility for analyte detection were observed.

The solvent employed for the reconstitution of the extract and the subsequent interaction with the gly-GQDs also play a significant role in the performance of the sensor. Different solvents were investigated, namely water, methanol (MeOH), dimethylsulfoxide (DMSO), acetonitrile (ACN) and dimethylformamide (DMF). As can be seen in Figure 4a with water better response in terms of quenching signal were obtained. However, the reaction is slower in this medium and the signal need a long time to reach a stable value. A similar effect is observed in the case of acetonitrile, needing also a long time to obtain a stable measurement. When the TiO_2 NPs sample is reconstituted and mixed with the gly-GQDs in methanol medium the signal become stable in a short time. Thus, a compromise between sensibility and reaction time was acquired, finally selecting methanol as the medium for further measurements.

The concentration of the gly-GQD solution was also investigated. The response of the sensor when using different dilutions of the synthesized glycine functionalized GQDs was studied. Higher fluorescence value of the gly-GQDs solution was observed when the sample was diluted 4-fold. Moreover, the ratio of volume between the gly-GQD and sample solution containing the TiO_2 NPs was also investigated. Different volume ratio of gly-GQDs and TiO_2 NPs-extract were tested (1:1, 1:2, 2:3, 3:2 and 2:1), observing that at a 1:2 ration the higher values in terms of sensitivity were observed (Figure 4b),

finally selecting 100 µL of the gly-GQDs solution (4-fold diluted) and 200 µL of the extract in methanol as the final conditions for further measurements.

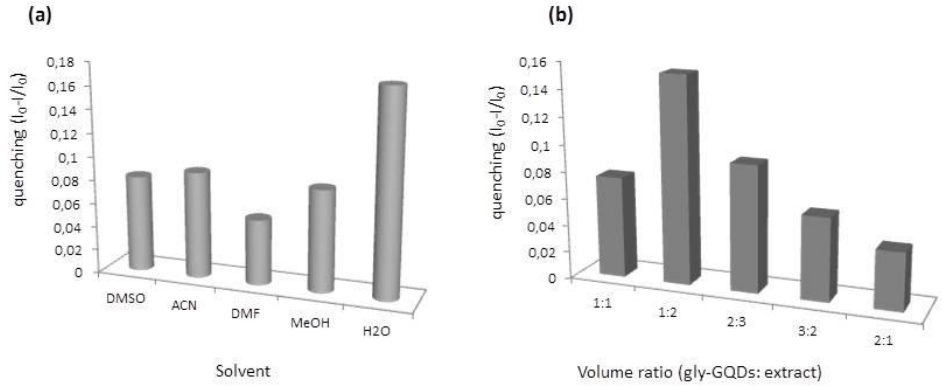

Figure 4. (a) Study of the response of the gly-GQDs sensor to the presence of 200 µg·g^{-1} of TiO_2 nanoparticles in different medium: dimethylformamide (DMSO), acetonitrile (ACN), dimethylformamide (DMF), methanol (MeOH) and water. (b) Influence of the volume ratio of gly-GQDs and sample extract in the quenching response of 200 µg·g^{-1} of TiO_2 nanoparticles.

3.6. Direct determination of aqueous solutions of TiO_2 nanoparticles

In order to demonstrate the interaction between gly-GQDs and TiO_2 nanoparticles, standard aqueous solutions of TiO_2 NPs at different concentrations were mixed with the fluorescent nanoparticles and the quenching effect produced on their luminescence was calculated. As can be seen in Figure 5, as much TiO_2 nanoparticles are in the standard less

fluorescence intensity from the sample is recorder, that is, major quenching effect is observed. Measurements were acquired with 2.3 nm wide of both excitation and emission slits. Standards with concentrations ranging from 1 to 30 mg·L^{-1} were measured. Each concentration level was analyzed in triplicate. Error bars depicts the standard deviation of the mean value. The response was linear in the range of concentrations tested (R^2 = 0.998) following the equation: y=0.0076x+0.036.

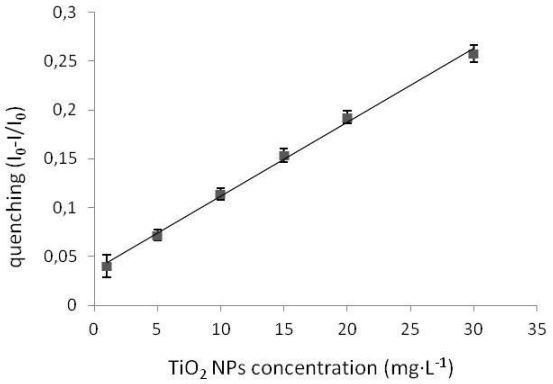

Figure 5. Representation of the quenching observed in the fluorescence of gly-GQDs with increasing concentrations of TiO_2 nanoparticles in standards aqueous solutions.

3.7. Analytical features for the determination of TiO_2 NPs from sunscreen matrices

The analytical performance of the proposed method was studied in order to evaluate its usefulness for quantitative analysis by using spiked

sunscreens samples. Sunscreens samples were spiked with different concentrations of TiO_2 nanoparticles and subjected to the extraction process. The fluorescence response of gly-GQD to increasing concentrations of TiO_2 NPs was assayed under the above described optimal conditions.

The analytical signal –relative fluorescence response $(I_0\text{-}I)/I_0$- was plotted against TiO_2 concentration for standard solutions. The quenching effect was linearly related to the TiO_2 NPs concentration over the range 0–30 $\mu g \cdot g^{-1}$. Each concentration level was analyzed in triplicate. Error bars depicts the standard deviation of the mean value. The response was linear in the range of concentrations tested ($R^2 = 0.998$).

Analytical features of the method are summarized in Table 1. The theoretical limits of detection (LOD) and quantification (LOQ) were calculated as $3S_a/b$ and $10S_a/b$, respectively, S_a being the standard error of the intercept and b the slope of de calibration curve (n = 3). Values found are 1.4 $\mu g \cdot g^{-1}$ and 4.67 $\mu g \cdot g^{-1}$ as LOQ. The precision of the measurements was evaluated at a concentration of 5 $\mu g \cdot g^{-1}$ obtaining a relative standard deviations (n = 5) of 6.95 %.

Table 1. Analytical features of the method for spiked sunscreens samples.

Calibration equation	$(I_0-I)/I_0 = (0.0072\pm0.0002)[TiO_2\ NPs]+(0.081\pm0.003)$
R^2	0.999
Lineal range	0-30 $\mu g \cdot g^{-1}$
LOD[a]	1.4 $\mu g \cdot g^{-1}$
RSD[b] (%)	6.95 %

[TiO_2 NPs]: Concentration of TiO_2 NPs in the sunscreen cream in $\mu g \cdot g^{-1}$.
[a]Limit of detection, determined as $(3S_a)/b$, for $y=bx+a$.
[b] Relative standard deviation, determined from the average value of n=5 at a concentration of 5 $\mu g \cdot g^{-1}$ GO.

In order to demonstrate the accuracy of the proposed method, a recovery test of the analysis of spiked sunscreen samples was also carried out following the developed procedure. For the recovery study, three fortification levels were assayed; the recoveries values are shown in Table 2. The obtained recoveries ranged from 84.6% to 105.9% depending on the concentration level. Each sample was analyzed in triplicate in order to evaluate the precision of the method. The coefficients of variation ranged from 4.6% to 9.0%.

Table 2. Recovery study of spiked sunscreen samples.

Sunscreen Sample	Added concentration of TiO_2 NPs ($\mu g \cdot g^{-1}$)	Found concentration of TiO_2 NPs[a] ($mg \cdot L^{-1}$)	Recovery (%)	RSD (%)
1	5	4.5±0.3	91.6-103.3	7.7
2	10	9.4±0.8	84.6-100.7	9.0
3	15	15.5±0.7	98.0-105.9	4.6

[a]Average of three independent spiked samples±CI ($p < 0.05$).

3.8. Application to the determination of the content of TiO_2 in sunscreens.

In order to evaluate the efficiency of the method for the determination of the content of TiO_2 NPs in sunscreen samples, two different sunscreens (SPF 20 and 30) with TiO_2 NPs in their formulation were selected and analyzed.

The density of these samples is higher than the sunscreen with SPF 15 employed for the analysis of spiked samples. The extraction procedure is similar to that employed with the other sunscreen with a slight modification, that is, the centrifugation was carried out at 10000 rpm during 30 min. The clean-up of the extract was performed with 1 mL of hexane and further centrifugation at 10000 rpm during 15 min.

Table 3 shows the concentration of TiO_2 NPs found in the two analyzed samples as well as the relative standard deviation (%RSD) obtained after 5 measurements of each type of sunscreen.

Table 3. Analysis of sunscreen samples containing TiO_2 NPs.

Sunscreen Sample	Concentration of TiO_2 NPs[a] ($\mu g \cdot g^{-1}$)	RSD (%)
SPF 20	112±3	2.68
SPF 30	109±4	3.70

[a]Average of five independent samples±CI ($p < 0.05$).

The values of content of TiO_2 in the sunscreen samples with the method proposed herein are in the same range than those reported by using flow field flow fractionation on-line with inductively coupled plasma mass spectrometry [5], which are in the range of 33.6-195.2 $mg{\cdot}Kg^{-1}$, depending on the sunscreen sample and solvent (water or 25% hexane) employed. Thus, this demonstrate that the developed procedure could be applied to the determination of TiO_2 nanoparticles in real samples, in spite of the complexity and high fatty content of the matrix subjected to analysis.

4. CONCLUSIONS

A simple and sensitive gly-GQD-based sensor has been developed for the determination of TiO_2 nanoparticles from sunscreen samples. The sunscreen lotion was submitted to an extraction procedure with water, methanol and hexane, and the extract finally reconstituted in methanol. The interaction of TiO_2 nanoparticles with gly-GQDs leads to a decrease –quenching- of the fluorescence of gly-GQDs, which was employed as analytical signal for their quantification.

The procedure has been applied for the determination of TiO_2 NPs in fortified SPF 15 sunscreen samples. The quenching response to increasing

concentrations of the metallic nanoparticles was linear. Moreover, the procedure was applied to the determination of the content of TiO_2 NPs in sunscreen samples (SPF 20 and 30) which already contain those nanoparticles in their composition. Both the extraction procedure and fluorimetric sensor proved their suitability for the quantification of the content of nanoparticulated TiO_2 in the tested sunscreens samples.

This work covers the two different facets of Analytical Nanoscience and Nanotechnology, this is, nanomaterials as analytical tools or objects (target of the analysis). Gly-GQDs have been employed as analytical tool owing to their exceptional fluorescence properties for the determination and quantification of TiO_2 NPs in sunscreen samples.

ACKNOWLEDGMENTS

The authors wish to thank Spain's Ministry of Economy and Competitivity for funding Project CTQ2011-23790 and Junta de Andalucía for Project FQM4801. S. Benítez-Martínez is also grateful to Junta de Andalucía for the award of a Research Training Fellowship.

The authors declare no competing financial interest.

5. REFERENCES

[1] Contado, C.; Pagnoni, A. *Anal. Chem.* **2008**, *80*, 7594–7608.

[2] Weir, A.; Westerhoff, P.; Fabricius, L.; Hristovski, K.; von Goetz, N. *Environ. Sci. Technol.* **2012**, *46*, 2242–2250.

[3] Nazarenko, Y.; Zhen, H.; Han, T.; Lioy, P.J.; Mainelis, G. *Environ. Heath Perpect.* **2012**, *120,* 885–892.

[4] Keller, A.A.; Vosti, W.; Wang, H.; Lazareva, A. *J. Nanopart. Res.* **2014**, *16*, 2489.

[5] Nischwitz, V.; Goenaga-Infante, H. *J. Anal. At. Spectrom.* **2012**, *27*, 1084-1092.

[6] Popov, A.P.; Lademann, J.; Priezzhev, A.V.; Myllylä, R. *J. Biomed. Opt.* **2005**, *10*, 1–9.

[7] Furukawa, F.; Doi, Y.; Suguro, M.; Morita, O.; Kuwahara, H.; Masunaga, T.; Hatekeyama, Y.; Mori, F. *Food Chem. Toxicol.* **2011**, *49*, 744–749.

[8] Freyre-Fonseca, V.; Delgado-Buenrostro, N.L.; Gutierrez-Cirlos, E.B.; Calderon-Torres, C.M.; Cabellos-Avelar, T.; Sanchez-Perez, Y.; Pinzon, E.; Torres, I.; Molina-Jijon, E.; Zazueta, C.; Pedraza-Chaverri, J.; Garcia-Cuellar, C.M.; Chirino, Y.I. *Toxicol. Lett.* **2011**, *202*, 111–119.

[9] Tsuji, J.S.; Maynard, A.D.; Howard, P.C.; James, J.T.; Lam, C.; Warheit, D.B.; Santamaria, A.B. *Toxicol. Sci.* **2006**, *89*, 42–50.

[10] Kim, Y.S.; Kim, B.M.; Park, S.C.; Jeong, H.J.; Chang, J.S. *J. Cosmet. Sci.* **2006**, *57*, 377–381.

[11] Mason, J.T. *J. Pharm. Sci.* **1980**, *69*, 101–102.

[12] Salvador, A.; Pascual-Martí, M.C.; Adell, J.R.; Requeni, A.; March, J.G.; *J. Pharm. Biomed. Anal.* **2000**, *22*, 301–306.

[13] Melquiades, F.L.; Ferreira, D.D.; Appoloni, C.R.; Lopes, F.; Lonni, A.G.; Oliveira, F.M.; Duarte, J.C. *Anal. Chim. Acta* **2008**, *613*, 135–143.

[14] Contado, C.; Pagnonia, A. *Anal. Methods* **2010**, *2*, 1112-1124.

[15] Samontha, A.; Shiowatana, J.; Siripinyanond, A. *Anal. Bioanal. Chem.* **2011**, *399*, 973–978.

[16] Krystek, P.; Tentschert, J.; Nia, Y.; Trouiller, B.; Noël, L.; Goetz, M.E.; Papin, A.; Luch, A.; Guérin, T.; de Jong, W.H. *Anal. Bioanal. Chem.* **2014**, *406*, 3853-3861.

[17] Geertsen, V.; Tabarant, M.; Spalla, O. *Anal. Chem.* **2014**, *86*, 3453–3460.

[18] Dong, Y.; Chen, C.; Zheng, X.; Gao, L.; Cui, Z.; Yang, H.; Guo, C.; Chi, Y.;. Li, C.M. *J. Mater. Chem.* **2012**, *22*, 8764–8766.

[19] Kim, S.; Hwang, S. W.; Kim, M. K.; Shin, D. Y.; Shin, D. H.; Kim, C. O.; Yang, S.B.; Park, J. H.; Hwang, E.; Choi, S. H.; Ko, G.; Sim, S.; Sone, C.; Choi, H.J.; Bae, S.; Hong, B. H. *ACS Nano* **2012**, *6*, 8203–8208.

[20] Shen, J.; Zhu, Y.; Yang, X.; Zong, J.; Zhang, J.; Li, C. *New J. Chem.* **2012**, *36*, 97–101.

[21] Benítez–Martínez, S.; Valcárcel, M. *Sens. Actuators B* **2014**, *197*, 350–357.

[22] Benítez-Martínez, S.; López-Lorente, A.I.; Valcárcel, M. *Anal. Chem.* **2014**, DOI: 10.1021/ac5035083.

[23] Li, X.; Zhu, S.; Xu, B.; Ma, K.; Zhang, K.; Yang, B.; Tian, W. *Nanoscale* **2013**, *5*, 7776–7779.

[24] Dong, Y.; Shao, J.; Chen, C.; Li, H.; Wang, R.; Chi, Y.; Lin, X.; Chen, G. *Carbon* **2012**, *50*, 4738–4743.

[25] Tam, T.V.; Trung, N.B.; Kim, H.R.; Chung, J.S.; Choi, W.M. *Sens. Actuators B* **2014**, *202*, 568–573.

[26] Langel, W.; Menken, L.; *Surf. Sci.* **2003**, *538*, 1–9.

[27] Lausmaa, J.; Löfgren, P.; Kasemo, B. *J. Biomed. Mater. Res.* **1999**, *44*, 227-242.

III.3 .2.Preconcentración en Membranas

Etapa previa de tratamiento de muestra

Los avances en la Nanotecnología y el uso cada vez más extendido de las nanopartículas en aplicaciones industriales y productos comerciales hacen que el riesgo de liberación de estos nanomateriales al medio ambiente sea cada vez más alto. Todo esto unido a la posibilidad de acumulación en el medio y a la consecuente repercusión en la salud humana y de los ecosistemas, hace necesario el desarrollo de metodologías para la detección y determinación de nanomateriales en matrices complejas.

Aprovechando las excepcionales propiedades ópticas de los GQDs, en el capítulo 6 se presenta un nuevo método para la determinación de GO en agua de río.

Capítulo 6

Graphene Quantum Dots Sensor for the Determinaniton of Graphene Oxide in Environmental Water Samples

Analytical Chemistry 86 (2014) 12279–12284

analytical chemistry

Article Anal. Chem. 2014, 86, 12279–12284

Graphene quantum dots sensor for the determination of graphene oxide in environmental water samples

Sandra Benítez-Martínez, Ángela Inmaculada López-Lorente, Miguel Valcárcel

Department of Analytical Chemistry, University of Córdoba, Campus of Rabanales, 14071, Córdoba, Spain

The paper proposes a simple and sensitive approach for the preconcentration and determination of graphene oxide (GO) in environmental samples by using fluorescent graphene quantum dots (GQDs). The method is based on the preconcentration of GO on a cellulose membrane and their subsequent elution prior fluorescence analysis of the quenching effect produced on the GQD solution due to the hydrophobic interactions between GO and GQDs. The limit of detection was 35 $\mu g \cdot L^{-1}$. The precision, for a 200 $\mu g \cdot L^{-1}$ concentration of GO is 5.16%. The optimized procedure has been successively applied to the determination of traces of GO in river water samples.

Keywords: *graphene quantum dots, graphene oxide, fluorescence, quenching.*

GRAPHICAL ABSTRACT

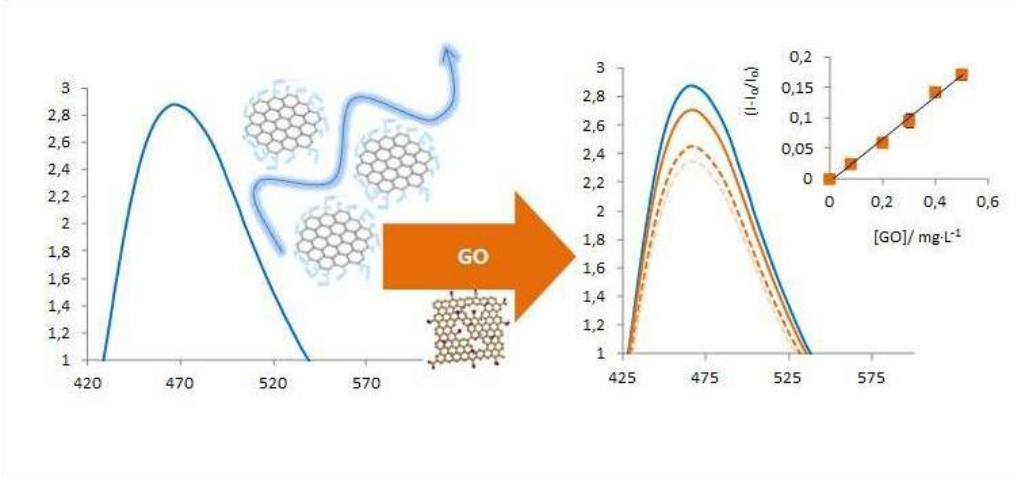

1. INTRODUCTION

The increasing use of nanomaterials in industrial applications as well as the commercialization of nanomaterial based products such as cosmetics, foods, drugs and electronic devices will increase the human and environmental exposure to such nanomaterials. Carbon nanoparticles such as fullerenes, carbon nanotubes and most recently, graphene -a two dimensional single sheet of carbon atoms arranged in an aromatic network with sp^2 hybridization- have attracted great interest in the last decades due to their exceptional properties[1]. The unusual and extraordinary mechanical, optical, thermal and electronic properties[2] of graphene have encouraged their use in several fields such a electronics, energy sector, catalysis, (bio)medicine and materials science, as well as in the analytical chemistry field [3, 4].

Due to the growing production (predicted to reach 573 tons in 2017)[5] and use of graphene and graphene-family nanomaterials it is necessary to evaluate their possible effects in the environment and, subsequently, on the ecosystem health, including humans. GO nanoparticles could reach the environment through atmospheric emissions and waste stream in production and research facilities. Nanoparticles in the environment would contaminate soil, surface and underground water and interact with organism[6]. However, nowadays there are still few analytical methodologies available for the

detection and quantification of engineered nanomaterials, although some approaches have been developed in the case of carbon nanotubes[7–9] or metallic nanoparticles[10, 11]. Recently, the stability and transport of GO has been investigated in both artificial ground– and surface waters[12].

Graphene oxide (GO) possesses an unique structure composed of sp^2 carbons surrounded by sp^3 carbons and oxygen containing functional groups[13] which confer it an excellent aqueous solubility -hence their potential presence as contaminant of environmental waters-, surface functionalizability and fluorescence quenching ability[14]. GO has been used as a sensor for the detection of DNA[15], proteins[16] and metal ions[17]; as sorbent for solid–phase extraction[18] and microextraction[19]. Recently it has been employed as adsorbent of heavy metals and organic compounds in the wastewater treatment[20] as well as novel carrier for drug delivery[21].

The toxicological effects of GO have been evaluated. It has been demonstrated that GO is able to penetrate through the plasma membrane, altering cell morphology, inducing membrane damage and oxidative stress in adenocarcinomic human cells[22]. Moreover, GO toxicity, genotoxicity and cytotoxicity have been reported in human[23] and animal cells[24], immune cells[25] and blood components[26]. In vivo studies in mice showed that GO can be accumulated in lungs, liver and spleen[27].

Graphene quantum dots (GQDs) are zero–dimensional luminescent carbon-based nanomaterials that consist on very small graphene sheets with lateral size less than 100 nm in single, double or multiple layers, which exhibit exciton confinement and quantum size effect. Their diameter ranges from 3 to 20 nm, approximately [28]. The GQDs band gap is different from zero and can be tuned varying the size and the surface chemistry of GQDs[29]. These small graphene sheets possess special and different properties from graphene; it should be noted their high fluorescence activity, low toxicity, high biocompatibility, excellent photostability and robust chemical inertness[30]. These properties made GQDs a useful tool in the development of photovoltaic devices[31], bioimaging[32], sensors[4] and biosensors[33].

In this paper, GQDs have been employed to develop a simple, fast and sensitive fluorescence-based sensor for the determination of GO in natural river water samples. The interaction of GO with GQDs through hydrophobic π-π interactions leads to a decrease in the fluorescence intensity –quenching- of GQDs, which has been used as analytical signal for the quantification of the presence of GO after preconcentration and subsequent elution on an acetate of cellulose membrane. As far as we are concerned, this is the first approach to the determination of graphene oxide from environmental waters.

2. EXPERIMENTAL SECTION

2.1. Materials and reagents

All chemical reagents were analytical-grade and were used without additional purification. Graphene (avangraphene-2, <2 nm and <6 sheets) was supplied by Avanzare Innovacion Tecnologica SL (Logroño, Spain). Citric acid (≥99.0%) was purchased from Sigma–Aldrich (Madrid, Spain). H_2SO_4, HNO_3 and sodium hydroxide were provided by Panreac (Barcelona, Spain). HPLC-grade methanol (≥99.9%) was acquired from Carlo Erba Reagents (Barcelona, Spain). Acetate of cellulose membranes of 0.2 μm pore size were supplied from Sartorius Stedim Biotech (Germany).

2.2. Equipment

Fluorescence emission spectra were recorded on a PTI Quanta Master™ spectrofluorometer from Photon Technology International (Barcelona, Spain) equipped with a 75 W xenon short arc lamp and an 814 PTM detection system. The software FeliX32was used for data acquisition and instrument control. The excitation and emission slits were both 3.8 nm wide. All measurements were made at room temperature, using micro quartz cuvettes of 10 mm light path.

A Vibracell™ 75041 ultrasonic probe (750 W, 20 KHz, Bioblock Scientific, Illkirch, France) equipped with a 3 mm probe was also employed to prepare the dispersions.

High-resolution transmission electron microscopy (HRTEM) images were obtained on a JEOL JEM 2010 electron microscope available at the Research Support Service (SCAI) of the University of Córdoba. The instrument has a point-to-point resolution of 0.194 nm and was operated at a medium acceleration voltage of 200 kV. Fourier transform mid infrared (FT-MIR) spectra were obtained on a Bruker Tensor 27FT-MIR spectrophotometer equipped with a Hyperion 2000 microscope, using KBr pellets.

2.3. Synthesis of graphene quantum dots

GQDs were obtained by pyrolysis of citric acid, similarly to that described in[4] using a slightly modified version of the procedure by Dong et al.[34]. To this end, an amount of 2 g of citric acid was placed in a vial and heated at 200◦C on a thermoblock from JP Selecta (Barcelona, Spain) until the citric acid changed from a white dust to a dark orange liquid, which took about 30 min. The resulting liquid was added dropwise to 100 mL of a 10 mg L^{-1} NaOH solution under vigorous stirring. The GQD aqueous solution thus obtained was adjusted to pH 7 with nitric acid and stored at 4◦C in an amber bottle.

2.4. Synthesis of Graphene Oxide

The analyte, graphene oxide (GO) was prepared by adding 100 mg of graphene to 20 mL of a 3:1 H_2SO_4/HNO_3 mixture into a glass flask similar to the procedure for oxidation of carbon nanotubes described in[7]. The mixture was refluxed for 1 hour, after that diluted fractions were centrifuged at 10000 rpm for 20 minutes and washed with water. The centrifugation process was repeated until the supernatant phase stopped having acidic pH. Finally, carboxylated derivates were dried at 60ºC in a heater. After acid treatment, graphene possess carboxylic (–COOH) groups on the sidewalls, being negatively charged, which make them highly water soluble.

2.5. Analyte preconcentration procedure

Graphene oxide (GO) solutions were preconcentrated on a cellulose membrane of 0.2 µm of pore size by the filtration of 5 mL of the solution with the aid of a Millipore filtration system and a peristaltic pump coupled to a flow system for the automatic dropwise filtration. Afterwards, 1 mL of a 0.25 $mol{\cdot}L^{-1}$ NaOH solution is passed through the membrane in order to remove the organic matter and, finally, 1 mL of ultrapure water. The cellulose membrane with the GO retained on it was introduced in a 1-mL vial and 200 µL of ultrapure water were added. The membrane submerged in the aqueous solution were treated with 40 seconds of ultrasonication using a Vibracell™ 75041 ultrasonic probe (750W, 20 KHz, Bioblock Scientific, Illkirch, France)

equipped with a 3 mm probe set at 20% of amplitude in order to recover the GO retained in the membrane and obtain a homogeneous dispersion of them. Pulses of energy of 2 s on and 10 s off were employed in order to avoid sample heating.

2.6. Fluorescence measurements

Fluorescence measurements were performed at an excitation wavelength of 379 nm recording the emission between 420 and 650 nm. Measurements were performed in a micro quartz cuvette of 10 mm light path. 200 µL of GQD solution at pH 7 were blended thoroughly with 200 µL of the aqueous solution containing the GO for 30 seconds. Once mixed, the solution was kept for 5 minutes prior the fluorescence spectrum was acquired.

3. RESULTS AND DISCUSSION

GQDs obtained with the synthesis procedure employed [34] are surface-passivated with oxygen-containing functional groups, namely carboxyl and hydroxyl groups, only present at the edge of the dot which confers them good water solubility and stability. The abundant hydrophilic edges as well as the hydrophobic plane in the GQDs[35] confer them the ability to interact with GO through π-π stacking interactions leading to a decrease of fluorescence –

quenching- which was employed as analytical signal to quantify the presence of GO in the aqueous samples. In order to achieve better detection limits, the aqueous samples were submitted to a preconcentration and clean-up step prior fluorescence quantification.

The hydrophobic interaction of graphene and graphene quantum dots has been previously described in literature[36] as well as with other aromatic compounds[37, 38], In addition to the hydrophobic interaction between the planar aromatic structures of graphene oxide and graphene quantum dots, since in this case we have two nanoparticles with functional groups on their edges, it cannot be dismissed that the analyte binding may also occurs by non-covalent interactions between those groups[4]. Thus, both processes could act together.

3.1. Characterization of GQDs

GQDs were synthesized through a "bottom-up" procedure involving the pyrolysis of citric acid, which leads to flat circular nanosheets of average diameter 3.6 ± 0.9 nm as calculated from high resolution transmission electron microscopy (HRTEM) images (see Figure 1a). GQDs were obtained at a concentration of 2.25 mg L^{-1}. Moreover, obtained GQDs were characterized by FT-MIR showing the presence of carboxyl and hydroxyl groups (Figure 1b). The bands observed at around 1730 cm^{-1} correspond to the carboxyl groups

whereas the bands at around 3400 cm^{-1} are attributed to the stretching vibration of hydroxyl groups.

The main feature of GQDs, which is the basis of the developed sensor, is their fluorescence properties. Synthesized GQDs showed blue emission at 474 nm upon excitation at its maximum of 379 nm (Figure 1c). They showed 4.5% of photoluminiscent quantum yield at working conditions calculated using quinine sulfate as standard.

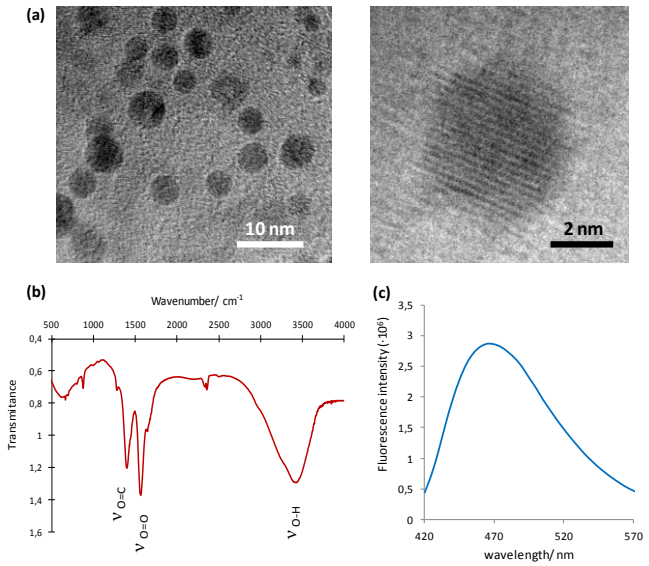

Figure 1. (a) HTEM images of the synthesized GQDs, (b) FT-MIR spectra of GQDs showing the presence of carboxyl and hydroxyl groups and (c) fluorescence spectrum of GQDs after synthesis once adjusted to pH 7.

3.2. Selection of conditions for the preconcentration of GO

Membranes of different nature were evaluated, namely acetate of cellulose, nylon, polyamide and PTFE for the preconcentration of GO. PTFE membranes were directly discharged since they have hydrophobic nature and water solution of GO did not pass through them. The compatibility of the membranes with different solvents for the re-extraction of the GO was studied. Nylon and polyamide membranes were compatible with all the solvents investigated, namely water, methanol, acetonitrile, dimethylformamide, acetone and ethyl acetate; while acetate of cellulose membranes resulted damaged with the majority of the solvents except water and methanol. Nevertheless, acetate of cellulose membranes provided the better results in terms of recoveries of GO after ultrasound treatment for their release of the membrane, and, in spite of their lower compatibility with solvents, these membranes were selected for further experiments. Acetate of cellulose membranes with different pore sizes were studied: 0.2 and 5 μm. Membranes with the smallest pore size were selected in order to assure complete retention of GO.

Moreover, both filtration and elution volumes were optimized, finally selecting 5 and 0.2 mL, respectively, which leads to a theoretical preconcentration of 25. Conditions of vacuum as well as flow rate of the peristaltic pump for the deposition of the GO on the membrane were also

optimized selecting 0.1 bar and 0.209 $mL \cdot min^{-1}$ respectively. In order to recover the GO retained on the membrane into 200 µL of solution, ultrasound energy was applied. Such conditions were also optimized. 40 seconds proved to be enough to recover the GO when using an ultrasonic probe of 3 mm (750W, 20 KHz) applying 20% of amplitude and pulses of 2 s on and 10 s off in order to prevent heating and subsequent evaporation of the sample.

3.3. Influence of pH on the fluorescence of GQDs

The pH of the GQD solution is an important variable in the procedure used to develop the proposed sensing system since it was found to affect the fluorescence of our sensor and its interactions with graphene oxide. The pH of the as-synthesized GQDs solution is basic around 13. The influence of pH of this solution on the sensor efficiency was investigated. The fluorescence of GQD solution at different pH values ranging from 2 to 14 was measured. GQDs showed the highest fluorescence values at pH 7 (see Figure 2a).

Moreover, the influence of pH over the quenching response of the sensor was also evaluated when the sample was eluted into two different solvents, namely water and a 98% (v/v) methanol solution. When the graphene oxide dissolved in water was mixed with the GQDs at pH 7 the highest quenching effect was observed, thus, pH 7 being selected as the conditions for further measurements (Figure 2b).

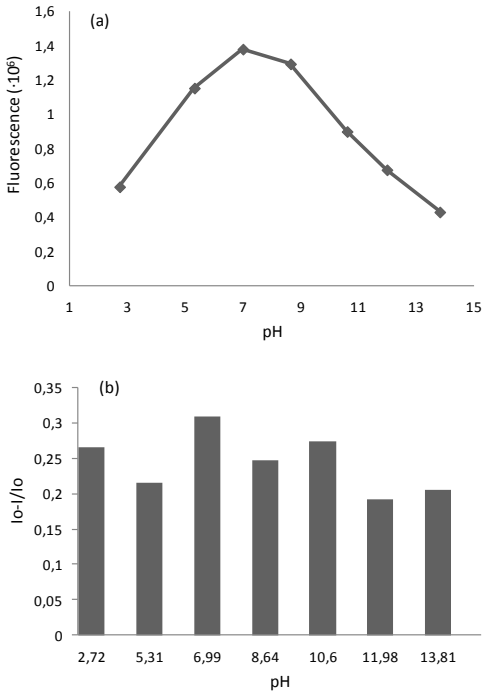

Figure 2. (a) Effect of pH on the fluorescence of GQDs, (b) influence of pH of the GQD solution on the quenching response of the sensor. pH 7 was selected for further experiments.

3.4. Influence of solvent on the fluorescence of GQDs

As mentioned above, both water and 98% (v/v) methanol solution were assayed for the elution of the graphene oxide previously retained on the cellulose membrane. Both solvents are compatible with the selected membranes –of cellulose nature-.

As can be seen in Figure 3, water showed better response in terms of quenching effect at every value of pH tested. Further experiments were, thus, performed using 200 µL of ultrapure water for recovering the graphene oxide from the membrane, and, finally, reacting with the GQD sensor.

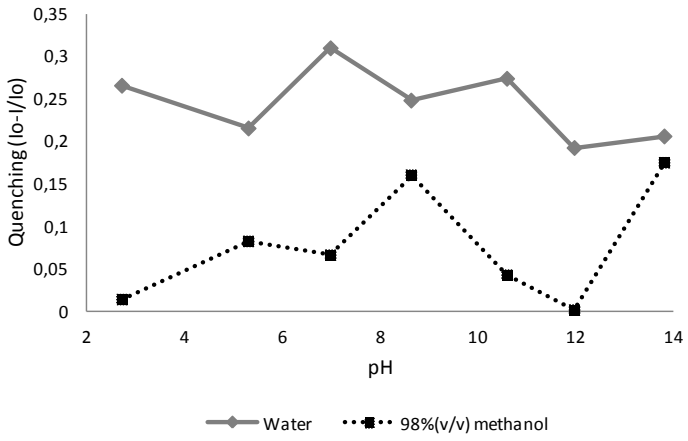

Figure 3. Influence of pH in the quenching response of the GQD sensor at two different solvents, namely water and 98% (v/v) methanol. Water was selected as the solvent for the elution of GO and further quantification by fluorimetric measurements.

3.5. Selection of the conditions for quenching measurements

The concentration of the GQD solutions as well as the reaction time was also investigated. The response of the sensor when using different dilutions of the synthesized GQD solution was tested. This was accomplished by using variable volumes of GQD solution (50, 66, 100 and 200 µL) at a fixed

volume of aqueous GO solution of 200 µL adjusting the volume of ultrapure water needed for a constant final volume of 400 µL. The differences in the quenching effect at the concentration assayed showed no high variations, thus, selecting the concentration obtained through the synthesis for further experiments.

The time needed for the interaction of GO with GQDs through hydrophobic π-π interactions was also studied. 5 min of rest showed to be enough to obtain a reproducible fluorescent signal which does not change over time.

3.6. Analytical features of the proposed method

The analytical performance of the proposed method was studied in order to evaluate its usefulness for quantitative analyses. The fluorescence response of GQD to increasing concentrations of GO was assayed under the above described optimal conditions. The analytical signal –relative fluorescence response $(I_0-I)/I_0$- was plotted against GO concentration for standard solutions.

Quenching was linearly related to the GO concentration over the range 0–500 µg L^{-1}. Each concentration level was analyzed in triplicate. Error bars depicts the standard deviation of the mean value (Figure 4). The response was linear in the range of concentrations tested (R^2 = 0.9940).

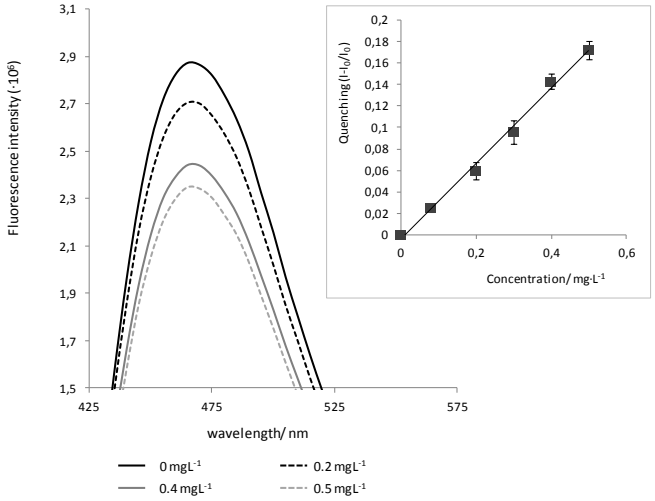

Figure 4. *Quenching of the fluorescence observed at increasing concentrations of GO. The inset depicts a calibration graph of GO standard solutions under the optimal operational conditions.*

The analytical features of the method developed are summarized in Table 1. The theoretical limits of detection (LOD) and quantification (LOQ) were calculated as $3S_a/b$ and $10S_a/b$, respectively, S_a being the standard error of the intercept and b the slope of de calibration curve (n = 3). The values found were a LOD of 35.008 $\mu g \cdot L^{-1}$ and 116.69 $\mu g \cdot L^{-1}$ as LOQ. The precision of the measurements was evaluated at a concentration of 200 $\mu g \cdot L^{-1}$ obtaining a relative standard deviations (n = 5) of 5.16 %.

Table 1. *Analytical features of the method.*

Calibration equation	$(I_0-I)/I_0 = (0.35\pm0.01)[GO]-(0.004\pm0.004)$
R^2	0.9940
Lineal range	0-500 $\mu g \cdot L^{-1}$
LOD[a]	35.008 $\mu g \cdot L^{-1}$
RSD[b] (%)	5.16%

[GO]: Concentration of GO in the aqueous media in $mg \cdot L^{-1}$.
[a]Limit of detection, determined as $(3S_a)/b$, for y=bx+a.
[b] Relative standard deviation, determined from the average value of five measurements of 5 mL 200 $\mu g \cdot L^{-1}$ GO.

3.7. Application to the determination of graphene oxide in river water samples

In order to validate the proposed method, water samples from Rabanales River were analyzed following the recommended procedure. Despite the fact that no graphene oxide was expected to be found on them, the recoveries obtained were above the anticipated for spiked samples. It was found to be caused by the interference of the organic matter present in the river water. In order to overcome it, after the filtration of the sample through the membrane 1 mL of a 0.25 $mol \cdot L^{-1}$ NaOH solution was passed through in order to eliminate the organic matter retained in the membrane. Later, 1 mL of ultrapure water is passed and the membrane is ready for subsequent elution and fluorimetric analysis. The recoveries obtained after this clean-up step are similar to those obtained in standards where no organic matter is present.

In order to demonstrate the accuracy of the proposed method, a recovery test of the analysis of spiked river water samples was also carried out following the modified procedure which includes the filtration of the basic solution to remove organic matter. For the recovery study, three fortification levels were assayed; the recoveries values are shown in Table 2. The obtained recoveries ranged from 83.7% to 108.2% depending on the concentration level. Each sample was analyzed in triplicate in order to evaluate the precision of the method. The coefficients of variation ranged from 7.4% to 8.9%.

Table 2. Recovery study of spiked river samples.

River Water Sample	Added concentration of GO ($mg{\cdot}L^{-1}$)	Found concentration of GO[a] ($mg{\cdot}L^{-1}$)	Recovery (%)	RSD (%)
1	0.2	0.19±0.02	83.7-100.4	8.9
2	0.3	0.30±0.02	93.6-107.7	7.4
3	0.4	0.39±0.03	94.5-108.2	7.6

[a]Average of three independent spiked samples±CI ($p < 0.05$).

Finally, a study was carried out in order to check if other carbon nanomaterials, such as carbon nanotubes, could interfere the measurements if present in the water sample. When oxidized single-walled carbon nanotubes (c-SWNTs) are present in water at the same level of concentration than GO, no significant decrease of fluorescence in the GQD solution was observed.

4. CONCLUSIONS

A simple and sensitive GQD-based sensor has been developed for the determination of graphene oxide. GO is retained in acetate of cellulose membranes for their preconcentration being subsequently recovered in a water solution by ultrasound irradiation. The interaction of graphene oxide with GQDs through hydrophobic π-π stacking of the GO with the aromatic network at the GQDs surface leads to a decrease –quenching- of the fluorescence of GQDs, which was employed as analytical signal for their quantification.

The procedure has been applied for the determination of GO in environmental river water samples. In such case a clean-up step was necessary in order to remove the interfering organic matter. The filtration of a sodium hydroxide solution which eliminated the retained organic matter overcame such interference, being possible to quantify the presence of GO obtaining good values of recoveries.

In this work the two facets of Analytical Nanoscience and Nanotechnology –nanomaterials as analytical tools or objects- have been covered. GQDs are used as analytical tools owing to their exceptional fluorescence properties for the determination and quantification of GO in environmental samples.

ACKNOWLEDGMENTS

The authors wish to thank Spain's Ministry of Innovation and Science for funding Project CTQ2011-23790 and Junta de Andalucía for Project FQM4801. S. Benítez-Martínez is also grateful to Junta de Andalucía for the award of a Research Training Fellowship.

The authors declare no competing financial interest.

5. REFERENCES

(1) Novoselov, K. S.; Geim, A. K.; Morozov, S. V.; Jiang, D.; Zhang, Y.; Dubonos, S. V.; Grigorieva, I. V.; Firsov, A. A. *Science,* **2004**, *306*, 666–669.

(2) Novoselov, K. S.; Fal'ko, V. I.; Colombo, L; Gellert, P. R.; Schwab M. G.; Kim, K. *Nature*, **2012**, *490*, 192–200.

(3) Benítez–Martinez, S.; Simonet, B.M.; Valcárcel. M. *Electrophoresis*, **2013**, *34*, 2561–2567.

(4) Benítez–Martínez, S.; Valcárcel, M. *Sens. Actuators, B*, **2014**, *197*, 350–357.

(5) Sivudu K. S. & Mahajan Y. Mass production of high quality graphene: An analysis of worldwide patents, http://www.nanowerk.com/spotlight/spotid=25744.php (2012)

(6) Klaine, S.K.; Alvarez, P.J.J.; Batley, G.E.; Fernandez, T.F.; Handy R.D.; Lyon, D.Y.; Mahendra, S.; McLaughlin, M.J.; Lead, J. R. *Environ. Toxicol. Chem.*, **2008**, *27*, 1825–1851.

(7) López-Lorente, A.I.; Simonet, B.M.; Valcárcel, M. *Talanta*, **2013**, *105*, 75–79.

(8) López-Lorente, A.I.; Simonet, B.M.; Valcárcel, M.; Mizaikoff, B. *Anal. Chim. Acta*, **2013**, *788*, 122–128.

(9) López-Lorente, A.I.; Polo-Luque, M.L.; Valcárcel, M. *Anal. Chem.*, **2013**, *85*, 10338–10343.

(10) Li, L.; Leopold, K.; *Anal. Chem.*, **2012**, 84, 4340-4349.

(11) López-Lorente, A.I.; Simonet, B.M.; Valcárcel, M. *Analyst*, **2012**, 137, 3528–3534.

(12) Lanphere, J.D.; Rogers, B.; Luth, C.; Bolster, C.H.; Walker, S.L.; *Environ. Eng. Sci.*, **2014**, *31*, 350–359.

(13) Loh, K. P.; Bao, Q.; Eda, G.; Chhowalla, M. *Nat. Chem.*, **2010**, *2*, 1015–1024.

(14) Chung, C; Kim, Y. K.; Shin, D; Ryoo, S.R.; Hong, B. H.; Min, D. H. *Acc. Chem. Res.,* **2013**, *46*, 2211–2224.

(15) Li, J.; Huang, Y; Wang, D; Song, B; Li, Z; Song, S; Wang, L; Jiang, L; Jiang, B; Zhao, X; Yang, J; Liu, R; He, D; Fan, C. *Chem Commun.*, **2013**, *49*, 3125–3127.

(16) Zhou, D.M.; Xi, Q.; Liang, M.F.; Chen, C.H.; Tang,L.J.; Jiang, J.H. *Biosens. Bioelectron.*, **2013**, *41*, 359–365.

(17) Li, M.; Ding, W.D.; Guo, S.W.; Wu, N.Q. *Biosens. Bioelectron.*, **2013**, *41*, 889–893.

(18) Liu, Q.; Shi, J.; Sun, J.; Wang, T.; Zeng, L.; Jiang,G. *Angew. Chem. Int. Ed.,* **2011**, *50*, 5913–5917.

(19) Xu, L.; Feng, J.; Li, J; Liu, X.; Jiang, S. *J. Sep. Sci.,* **2012**, *35*, 93–100.

(20) Kyzas, G.Z.; Deliyanni, E. A.; Matis, K. A. *J. Chem. Technol. Biotechnol.*, **2014**, *89*, 196–205.

(21) Sun, X; Liu, Z; Welsher, K; Robinson J. T.; Goodwin, A.; Zaric, S.; Dai, H. *Nano* Res., **2008**, *1*, 203–212.

(22) Chang, Y.; Yang, S.T.; Liu, J.H.; Dong, E.; Wang, Y.; Cao, A.; Liu, Y.; Wang, H. *Toxicol. Lett.*, **2011**, *200*, 201–210.

(23) Lammel, T.; Boisseaux, P.; Fernandez-Cruz, M.L.; Navas, J.M. *Part. Fibre Toxicol.*, **2013**, *10*, 27.

(24) Wang, A.; Pu, K.; Dong, B.; Liu, Y.; Zhang, L.; Zhang, Z.; Duan, W.; Zhu, Y. *J. Appl. Toxicol.*, **2013**, *33*, 1156–1164.

(25) Qu, G.; Liu, S:; Zhang, S.; Wang, L.; Wang, X.; Sun, B.; Yin, N.; Gao, X.; Xia, T.; Chen, J.J.; Jiang, G.B. *ACS Nano*, **2013**, *7*, 5732–5745.

(26) Liao, K.H.; Lin, Y.S.; Macosko, C.W.; Haynes, C.L. *ACS Appl. Mater. Interfaces*, **2011**, *3*, 2607–2615.

(27) Wang, K; Ruan, J; Song, H.; Zhang, J.; Wo, Y.; Guo, S.; Cui, D. *Nanoscale Res. Lett.,* **2011**, *6*, 8–15.

(28) Dong, Y.; Chen, C.; Zheng, X.; Gao, L.; Cui, Z.; Yang, H.; Guo, C.; Chi, Y.;. Li, C.M. *J. Mater. Chem.*, **2012**, *22*, 8764–8766.

(29) Kim, S.; Hwang, S. W.; Kim, M. K.; Shin, D. Y.; Shin, D. H.; Kim, C. O.; Yang, S.B.; Park, J. H.; Hwang, E.; Choi, S. H.; Ko, G.; Sim, S.; Sone, C.; Choi, H.J.; Bae, S.; Hong, B. H. *ACS Nano*, **2012**, *6*, 8203–8208.

(30) Shen, J.; Zhu, Y.; Yang, X.; Zong, J.; Zhang, J.; Li, C.; *New J. Chem.*, **2012**, 36, 97–101.

(31) Zhu, Z.; Ma, J.; Wang, Z.; Mu, C.; Fan, Z.; Du, L.; Bai, Y.; Fan, L.; Yan, H.; Phillips, D.L.;Yang S. *J. Am. Chem. Soc.*, **2014**, *136*, 3760−3763.

(32) Fan , Z.; Li , Y.; Li , X.; Fan, L.; Zhou, S.; Fang , D.; Yang, S. *Carbon*, **2014**, *70*, 149–156.

(33) Li, X.; Zhu, S.; Xu, B.; Ma, K.; Zhang, K.; Yang, B.; Tian, W. *Nanoscale*, **2013**, *5*, 7776–7779.

(34) Dong, Y.; Shao, J.; Chen, C.; Li, H.; Wang, R.; Chi, Y.; Lin, X.; Chen, G. *Carbon*, **2012**, *50*, 4738–4743.

(35) Lin, L.; Rong, M.; Luo, F.; Chen, D.; Wang, Y.; Chen, X. *Trends in Analytical Chemistry,* **2014**, *54*, 83–102.

(36) Zhao, H.M.; Chang, Y.Y.; Liu, M.; Gao, S.; Yu, H.T.; Quan, X. *Chem. Commun.* **2013**, *49*, 234–236.

(37) Yang, F.; Zhao, M.; Zheng, B.; Xiao, D.; Wu, L.; Guo, Y. *J. Mater. Chem.* **2012**, *22*, 25471–25479.

(38) Fan, L.; Hu, Y.; Wang, X.; Zhang, L.; Li, F.; Han, D.; Li, Z.; Zhang, Q.; Wang, Z.; Niu, L. *Talanta* **2012**, *101*, 192–197.

III.3.3. Extracción en fase sólida

Etapa previa de tratamiento de muestra

Desde su aparición, los puntos cuánticos de grafeno han sido definidos como nanopartículas fluorescentes con estructura de grafeno y dimensiones laterales pequeñas que presentan propiedades como la biocompatibilidad y la baja citotoxicidad. Sin embargo, estudios recientes han puesto de manifiesto que podrían acumularse en órganos como riñón, hígado y pulmones, entre otros. Este hecho, unido a la cada vez más creciente fabricación de nanopartículas hace necesario el desarrollo nuevos métodos para su determinación.

En el capítulo 7, y último de esta memoria, se presenta una estrategia para la detección y cuantificación de puntos cuánticos de grafeno en aguas naturales y agua de grifo a través de la extracción en fase sólida de los mismos.

Capítulo 7

Fluorescent Determination of Graphene Quantum Dots in Water Samples

Submitted to Analytica Chimica Acta

Submitted

Contents lists available at ScienceDirect

Analytica Chimica Acta

journal homepage: www.elsevier.com/locate/aca

Fluorescent determination of graphene quantum dots in water samples

Sandra Benítez–Martínez, Miguel Valcárcel

Department of Analytical Chemistry, University of Córdoba, E-14071 Córdoba, Spain
Phone/Fax +34 957 218616; E-mail: qa1meobj@uco.es

This work presents a simple, fast and sensitive method for the preconcentration and quantification of graphene quantum dots in aqueous samples. GQDs are considered an object of analysis (analyte) not an analytical tool which is the most frequent situation in Analytical Nanoscience and Nanotechnology. This approach is based on the preconcentration of graphene quantum dots on an anion exchange sorbent by solid phase extraction and their subsequent elution prior flourimetric analysis of the solution containing graphene quantum dots. Parameters of the extraction procedure such as sample volume, type of solvent, sample pH, sample flow rate and elution conditions were investigated in order to achieve extraction efficiency. The limits of detection and quantification were 7.5 $\mu g \cdot L^{-1}$ and

25 $\mu g \cdot L^{-1}$, respectively. The precisition for 200 $\mu g \cdot L^{-1}$, expressed as %RSD, was 2.8%. Recoveries percentages between 84.4–99.3% were obtained for two different concentration levels. Interferences from other nanoparticles were studied and no significant changes were observed at the concentration levels tested. Consequently, the optimized procedure has great potential to be applied to the determination of graphene quantum dots at trace levels in drinking and environmental waters.

Keywords: graphene quantum dots, solid phase extraction, fluorescence, water samples, interferences.

GRAPHICAL ABSTRACT

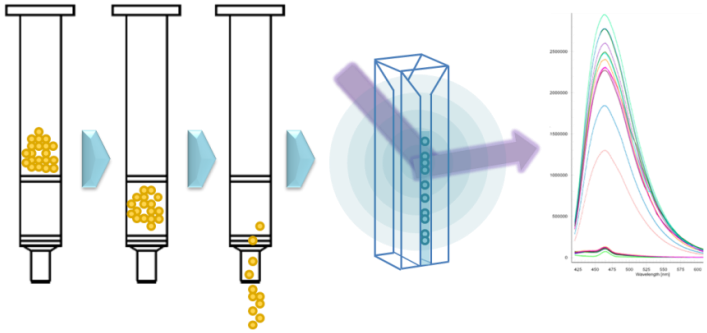

HIGHLIGHTS

- Development of a novel and simple method for determination of graphene quantum dots.
- Preconcentration of graphene quantum dots by solid phase extraction.
- Fluorescence spectroscopy allows fast measurements.
- High sensitivity and great reproducibility is achieved.

1. INTRODUCTION

In the last years, the advances in nanotechnology and the application of a widely variety of engineered nanoparticles in the industry and commercial products such as electronic devices, drugs, cosmetics and foods, make that the human and environmental exposure increase day out[1]. Graphene, a two dimensional one–atom thick with sp^2 hybridization carbon nanoparticles, and graphene family nanomaterials have attracted much attention since the graphene first isolation in 2004, due to their exceptional electronic, mechanical, optical and thermal properties [2, 3]. Recently, graphene quantum dots (GQDs), emerging graphene based luminescent nanoparticles, have become in an object of interest in the scientific community owing to their electronic and optical properties. GQDs are graphene nanosheets smaller than 100nm lateral size and diameters between 3–20nm. These nanoparticles can be as single–, double– or multi–layer [4]. Quantum confinement and edge effect make them exhibit interesting properties such as fluorescent activity, robust chemical inertness, excellent photostability, high biocompatibility and low toxicity [5]. These properties confer it a variety of potential uses in several scopes, mainly, sensors [6] and biosensors [7], bioimaging [8], drug delivery [9] and photovoltaic devices [10]. In spite of the fact that GQDs are defined as low toxic and high biocompatible nanoparticles, there are some works that put into question this features. In vivo studies in

mince revealed that the GQDs were mainly accumulated in liver, spleen, lung, kidney and tumor sites [11]. Otherwise, the theory of lateral dimension explains that the in vivo biodistribution and manifestation of toxicity would be lower as smaller nanomaterial size, so GQDs smaller than 5 nm could be eliminated with urine [12]. Due to the GQDs biosafety issue still been unclear and the increasing production and use of graphene nanomaterials could increase the risk of environmental widespread, methodologies that allow the determination of these nanoparticles should be developed. Nevertheless, at present, there are only a few analytical approaches for this purpose. Some methodologies have been described for carbon nanotubes (CNTs) [13], gold nanoparticles (AuNPs) [14, 15] and, most recently, graphene oxide (GO) [16].

In this work, a simple, rapid and sensitive approach for the determination of GQDs in natural and tap water samples was developed. The interaction of GQDs with the charged sorbent through ionic interactions and their subsequent elution lead to the preconcentration of GQDs. The fluorescence emission of the eluted graphene nanosheets has been used as analytical signal for the quantification of the presence of GQDs. As far as we are concerned, this is the first approach to the determination of graphene quantum dots from environmental and drinking waters.

2. METRIALS AND METHODS

2.1. Reagents and standards

All chemical reagents were of analytical grade and used as received without further purification. Citric acid (≥ 99.0 %), used as precursor in the GQDs synthesis procedure, ammonium acetate (≥ 98.0 %), nitric (≥ 69.0 %) and sulfuric (≥95%) acids were purchased from Sigma–Aldrich (Madrid, Spain). Sodium hydroxide and hydrochloric acid were obtained from Panreac Chemical, SAU (Barcelona, Spain). HPLC-grade methanol (≥ 99.9 %) was purchased from Carlo Erba Reagents (Barcelona, Spain). Single Wall Carbon Nanotubes (SWCNT) were obtained from Shenzhen Nanotech Port Co. Ltd (NTP) (China), with a purity over 90%, an outer diameter of o2 nm, a length of 5–15 mm and a surface area of 500– 700 $m^2 \cdot g^{-1}$. Graphene (avangraphene-2, <6 sheets) was supplied by Avanzare Innovacion Tecnologica SL (Logroño, Spain). Commercial gold nanoparticles (AuNPs), 10 nm sized, were purchased also from Sigma Aldrich. Ultra pure water was obtained from a Milli–Q purification system (Millipore, Madrid, Spain) with a resistivity of 18.2 MΩ/cm and used for the preparation of all solutions.

2.2. Instrumentation

Fluorescence emission spectra were recorded on a PTI QuantaMaster™ spectrofluorometer from Photon Technology International (Barcelona, Spain) equipped with a 75 W xenon short arc lamp and an 814 PTM detection

system. The software FeliX32 was used for data acquisition and instrument control. The excitation and emission slits were both 6 nm wide. All measurements were made at room temperature, using micro quartz cuvettes of 10 mm lightpath.

Fourier transform mid infrared (FT-MIR) spectra were obtained on a Bruker Tensor 27FT-MIR spectrophotometer equipped with a Hyperion 2000 microscope, using KBr pellets.

High-resolution transmission electron microscopy (HRTEM) images were obtained on a JEOL JEM 2010 electron microscope available at the Research Support Service (SCAI) of the University of Córdoba. The instrument has a point-to-point resolution of 0.194 nm and was operated at a medium acceleration voltage of 200 kV.

2.3. Synthesis of GQDs

GQDs were obtained by pyrolysis of citric acid, similarly to that described in [6, 16] using a slightly modify procedure similar to that described by Dong et *al.* [17]. To this end, an amount of 2 g of citric acid was placed in a 10 mL vial and heated at 200 ºC on a thermoblock (JP Selecta, Barcelona, Spain) for 30 min.

During this time, the citric acid changed from a white dust to a dark orange viscous liquid. The resulting liquid was added dropwise to 100 mL of a 0.25M NaOH solution under vigorous stirring. The GQD aqueous solution obtained was kept stirring for 10 min, adjusted to pH 7 with nitric acid and stored at 4 ºC in an amber bottle.

2.4. Functionalization of single–walled carbon nanotubes and graphene.

Carboxylated single–walled carbon nanotubes (c–SWCNTs), graphene oxide (GO) and gold nanoparticles (AuNPs) have been considered in this paper as potential interferences. AuNPs were of commercial origin. C–SWCNTs were prepared by adding 100 mg of SWCNT to 20 mL of a 3:1 H_2SO_4/HNO_3 mixture into a glass flask similar to the procedure described by Lopez–Lorente et al. [13]. The mixture was refluxed for 1 hour. After that, diluted fractions were centrifuged at 10000 rpm for 10 min and washed with ultrapure water. The centrifugation and washing processes were repeated until the supernatant phase stopped having acidic pH. Finally, carboxylated derivates were dried at 60ºC in a heater. The same procedure was performed in order to obtain GO, being diluted fractions of treated graphene centrifuged at 10000 rpm for 20 min, due to the less size of these nanoparticles.

After acid treatment, SWCNTs and graphene posses carboxylic (–COOH) groups on the sidewalls and open ends (in the case of SWCNTs) being negatively charged, which make them highly water soluble.

2.5. Solid Phase Extraction Procedure

50 mg/1mL commercial SAX (Strong Anion Exchange) column (Biotage, Hengoed, United Kingdom) was selected for the SPE extraction of GQDs. SAX is a quaternary amine (functionalized with a chloride counter ion) silica sorbent with an average particle size of 52 μm, 56 Å pore diameter and a surface area of 480 $m^2 \cdot g^{-1}$, packed in a polypropylene column (volume: 1mL; inner diameter: 6mm) and fitted with polyethylene frits. This SAX column was rinsed with 1 mL of ultrapure water, followed by 1mL of 0.1M and 1mL of 15 mM ammonium acetate. Then, 20mL of an aqueous solution containing GQDs at pH 7.0 was passed through the column at a constant flow rate of 1 $mL \cdot min^{-1}$. A daily prepared 0.5 mg/mL GQDs standard aqueous solution was adjusted to pH 7.0 with diluted HNO_3. After loading the sample, the sorbent was dried by passing air through the column. The nanoparticles retained were finally eluted with 0.5mL of 0.25M of NaOH at a flow rate of 0.1$mL \cdot min^{-1}$. The extract obtained was measured directly in a spectrofluorometer.

2.6. Fluorescence measurements

Fluorescence measurements were performed at an excitation wavelength of 380 nm recording the emission between 400 and 600 nm using a PTI QuantaMaster™ spectrofluorometer from Photon Technology International (Barcelona, Spain) equipped with a 75 W xenon short arc lamp and an 814 PTM detection system. The software FeliX32 was used for data acquisition and instrument control. The excitation and emission slits were both 5 nm wide. All measurements were made at room temperature, using a 10 mm lightpath micro quartz cuvette. The extract from the SPE procedure was transferred to the micro cuvette and kept 5 minutes out of the sample compartment in order to the stabilization of GQDs in the alkaline conditions (pH 13.0) of the elution solvent .Then, the fluorescence spectrum was acquired.

2.7. Water sample collection

The drinking water was collected directly from a tap in the lab and the natural spring water samples were collected manually in the surrounding area of Montilla, Córdoba, Spain. All samples were collected in amber glass bottles, which were rinsed 3 times–fold with the sample, filled out of volume and stored at 4ºC. Real samples were filtered through a 0.2 μm nylon filter prior SPE procedure.

3. RESULTS AND DISCUSSION.

GQDs used in this work were surface–pasivated circular nanosheets with averaged diameter of 4.1 ± 0.7 nm, which were characterized by HR–TEM. FT–MIR reveals the presence of namely carboxyl and hydroxyl functional groups which confers them good water stability and solubility. The GQDs obtained by this route were excitation wavelength independent. They exhibit highest fluorescence emission at 474 nm when they were excited at 379 nm. Figure 1 shows (a) HR–TEM images and (b)FT-MIR spectra of GQDs after synthesis.

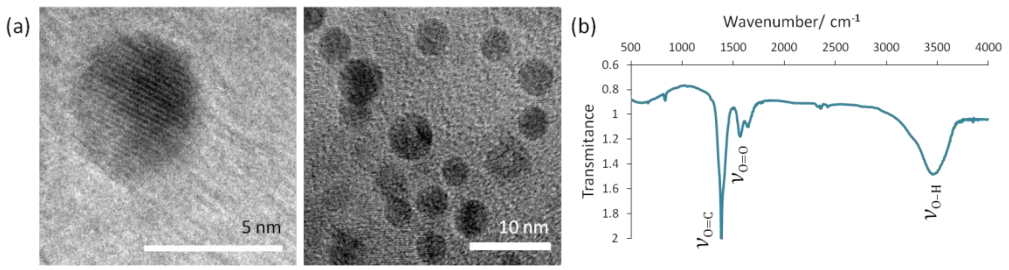

Figure 1. (a) HR–TEM images of GQDs and (b) FT-MIR spectra of GQDs showing the presence of carboxyl and hydroxyl groups.

The GQDs concentration was 4.5 mg·mL^{-1} and the GQDs quantum yield was 4.5 % using quinine sulfate as reference. Functional groups presents only at their edges allow the interaction between GQDs and SPE sorbent.

Figure 2 shows a general scheme proposed for the retention and elution of GQDs mechanisms from aqueous solutions.

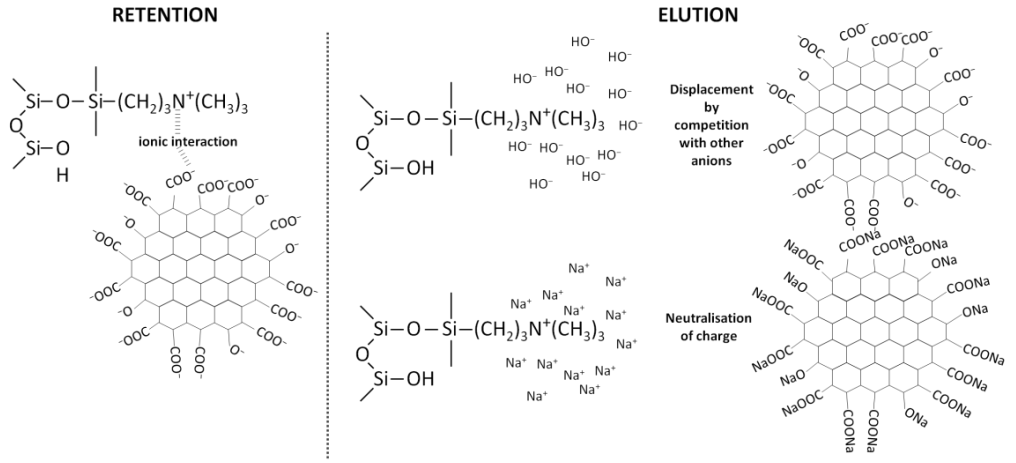

Figure 2. General scheme proposed for the retention and elution mechanisms.

The interaction of the quaternary amine bonded sorbent with the GQDs was strong and therefore quantification of the nanoparticles was possible. Carboxyl and hydroxyl groups, present at the edges of GQDs, interacted with the positive charge of the sorbent through ionic interactions. The quaternary amine kept permanent positive charged across the pH range. Elution by organic solvents did not release the nanoparticles; nevertheless, ultrapure water adjusted to pH 13 accomplished the elution of GQDs from the sorbent by eliminating the charge of the functional groups.

The studies for the optimization of the variables presented below were made in triplicate.

3.1. Optimization of sample volume

The optimum sample loading volume was investigating by passing different volumes of GQDs aqueous solution through the SAX column. The volumes investigated ranged from 1 to 25 mL. All samples were spiked with GQDs at a concentration level of 10mg·L^{-1}. Each studied volume (1, 5, 10, 15, 20 and 25mL) was analyzed milliliter by milliliter in the spertrofluorimeter. As can be seen in Figure 3, the signal of 1mL of GQDs sample after it pass through SAX column was the same as the signal of the ultrapure water and no fluorescence emission was detected after passing 25 mL. So, the loading capacity of the sorbent was high than 0.005mg GQDs/mg of SAX calculated as the ratio between the amount of GQDs in 25mL of sample and the amount of sorbent used for the extraction, 50mg. Under the studied conditions the breakthrough volume was not achieved since the GQDs retention efficiency was observed for increasing sample volumes. As a compromise to achieve good reproducibility, high sensitivity and short analysis times, 20 mL were chosen for all subsequent extractions.

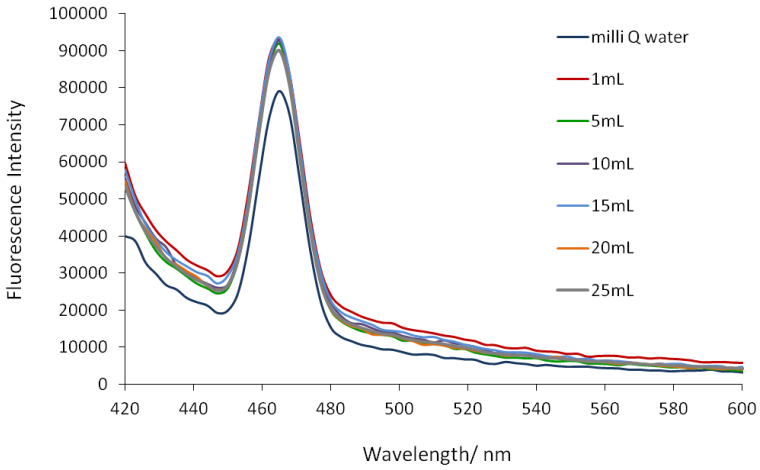

Figure 3. Study of the sample volume passed through the SPE column.

3.2. Optimization of sample pH

In a traditional SPE procedure, sample pH plays an important role since it determines the ionic or molecular form of an analyte and therefore, its interaction with the sorbent. The pKa of a molecular functional group is defined as the pH at which 50% of these groups in solution are charged, and 50% are uncharged. Each pH unit change affects the percentage of charged or uncharged groups by a factor of 10, so it is sensible to perform extractions at a pH at least 2 pH units from the pKa value, to ensure that 99.5% of the functional groups are in the desired state of ionization.

In this paper we used GQDs nanoparticles as analyte and we explore a wide range of pH in order to study their behavior with the sorbent. For this study, 50 mg·L^{-1} GQDs aqueous solution was adjusted a different pH (3, 5, 6, 7, 8, 9, 10, 11and 13) and 1mL of them was passed through the cartridge at a low flow rate to ensure the retention of the nanoparticles. Fluorescence of the solution was measured before and after passing through the column. As can be seen in Figure 4, at low concentrations of GQDs (50 mg·L^{-1}) FL (fluorescence) emission peaked at pH 13, being slightly lower at pH 11 and 9, decreasing at pH 8 and 10 and reducing markedly their emission below neutral pH.

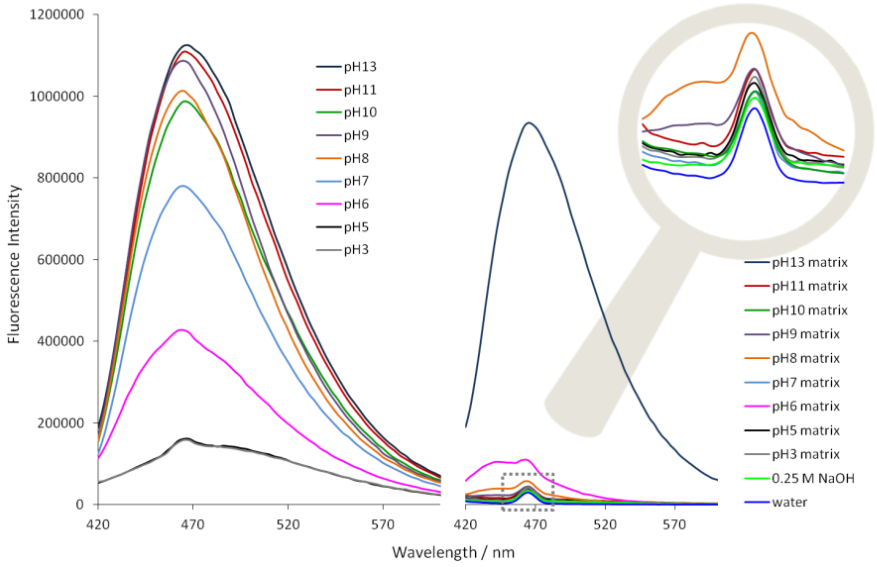

Figure 4. Study of pH for the retention of GQDs by SAX sorbent. GQDs concentration used was 50 mg·L^{-1}. The best retention was achieved with GQDs solution adjusted to pH 7 an 10.

This behavior could be explained due to an aggregation phenomena when GQDs nanoparticles, which exist at low concentration, are pH adjusted. When the concentration of this kind of nanoparticles is high the FL emission follows a different trend [6, 16] peaking at pH 7, decreasing markedly with increasing pH in alkaline media and more gradually in acidic media. Therefore, it can be concluded that GQDs synthesized by bottom–up method using citric acid as carbon precursor are pH–dependent at low and at high concentrations. When GQDs, at low concentration and different pH values, passed through the cartridge it was observed that FL emission was almost equal at pH 13, only 3% of the signal decreased, so interaction with the sorbent had not occurred and retention of GQDs was not achieved. When the sample was passed at pH 6, fluorescence decreased a 78 %. At pH 3 and 5 the signal of the solution passed through the column was reduced a 90% approximately. At pH 8, 9 and 11 fluorescence decreased between 96–98%. The high reduction of the FL emission was reached when sample was passed at pH 7 and 10 with a decrease >99%. Neutral pH was selected for the procedure development taking into account that natural waters usually have a pH between 6.5 and 8.5.

3.3. Optimization of sample flow rate

The sample was passed through the SAX column by using a peristaltic pump. With the purpose of optimizing the flow rate, 20mL of sample were

passed through a conditioned SPE cartridge at different rates: 0.1, 0.25, 0.5, 0.75, 1, 1.25, 1.5 and 2 $mL{\cdot}min^{-1}$. Results showed that no significative differences of the analytical signal were achieved at all studied flow rates. For this reason, and taking into account the manufacturer's specifications, $1mL{\cdot}min^{-1}$ was selected as optimal sample flow rate.

3.4. Optimization of the elution conditions

For the analyte elution six different organic solvents, namely, acetonitrile, ethyl acetate, N,N-Dimethylformamide, dimethyl sulfoxide, methanol and acetone, as well as pH 13.00 adjusted ultrapure water were tested. Methanol and acetone were also tested at pH 3, 5, 7, 10, 12. In all cases 1mL of solvent was passed through the loaded column at a flow rate of $0.1mL{\cdot}min^{-1}$. As a result, no one of the organic solvents tested was able to elute GQDs from the SAX matrix, even those which pH had been adjusted. The best results for the elution of the nanoparticles from the sorbent were achieved by using ultrapure water adjusted to pH 13. Further experiments were performed in order to optimize the eluent volume. With the purpose of achieving a high preconcentration factor with the high recovery, 0.3, 0.4 and 0.5 mL of solvent were tested in the same flow rate ($0.1mL{\cdot}min^{-1}$). Figure 5 shows that 0.5 mL were enough for the elution of 97% of GQDs at least. Considering 0.5 mL as optimal elution volume, the theoretical concentration factor would be 40x.

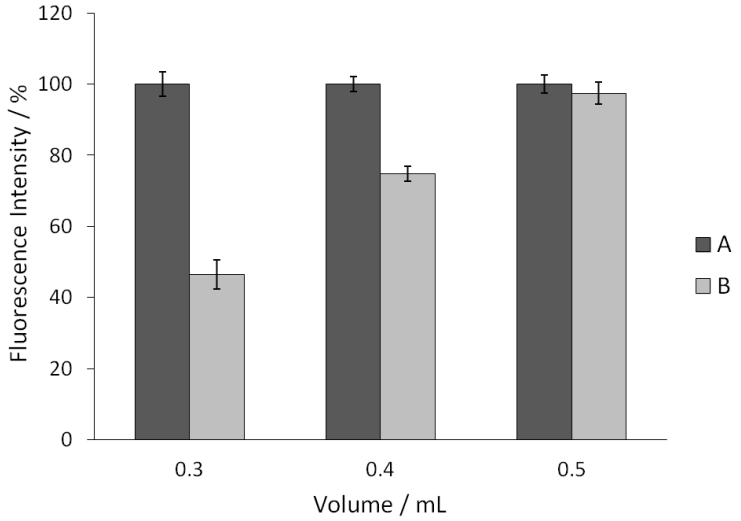

Figure 5. *Study of the elution volume. A) Percentage of fluorescence intensity of the GQDs solution before its pass through the SAX cartridge. B) Percentage of fluorescence intensity of GQDs after elution.*

3.5. Analytical figures of merit

The analytical performance of the proposed method was studied in order to evaluate its usefulness for quantitative analyses. The linearity of the method was then studied using deionized water standards spiked at increasing concentration of GQDs (25–500$\mu g \cdot L^{-1}$) subjected to the above described optimized extraction method. A linear response was obtained in the range of 25–500$\mu g \cdot L^{-1}$ (R^2 = 0.9992) by plotting the FL emission of GQDs in a pH 13 aqueous solution versus the spiked analyte concentration. Each

concentration level was analyzed in triplicate. Error bars depicts the standard deviation of the mean value. The analytical features of the method developed are summarized in Table 1.

The theoretical limits of detection (LOD) and quantification (LOQ) were calculated as $3S_a/b$ and $10S_a/b$, respectively, S_a being the standard error of the intercept and b the slope of de calibration curve (n = 3). The values found were a LOD of 7.5 $\mu g \cdot L^{-1}$ and 25 $\mu g \cdot L^{-1}$ as LOQ. The precision, expressed as relative standard deviation (RSD) in terms of repeatability (n = 5), at a concentration level of 200 $\mu g \cdot L^{-1}$, was 2.85%.

Table 1. Analytical features of the method.

Calibration equation	I= (545723±7037)[GGDs]-(35325±1358)
R^2	0.9992
Lineal range	25-500 $\mu g \cdot L^{-1}$
LOD[a]	7.5 $\mu g \cdot L^{-1}$
LOQ[b]	25 $\mu g \cdot L^{-1}$
RSD[c] (%)	2.85%

[GQDs]: Concentration of GQDs in the aqueous media in $mg \cdot L^{-1}$.
[a]Limit of detection, determined as $(3S_a)/b$, for y=bx+a.
[b]Limit of quantization, determined as $(10S_a)/b$, for y=bx+a.
[c]Relative standard deviation, determined from the average value of five extractions at 200 $\mu g \cdot L^{-1}$ GQDs concentration level.

3.6. Application of the determination of GQDs in real samples.

The feasibility of the proposed method was evaluated by application of the optimized procedure to two real water samples, namely, tap and natural spring water. Despite the fact that no GQDs were expected to be found on them, real samples were spiked with these nanoparticles at two concentration levels, 125 and 375 $\mu g \cdot L^{-1}$, for each one, before performing the recovery studies. In order to avoid interferences from particulate matter, the spiked real samples were filtered through a 0.2μm nylon filter prior to their pass through the SAX column. GQDs passed unhindered through the filter while particles in water were retained. After sample loading and prior to the elution step, 1mL of 15 mM ammonium acetate 20% acetonitrile was passed in order to eliminate interferences from the sample. Relative recovery values were calculated as the percentage of the ratio between the concentration found in spiked samples after performing the extraction procedure and the initially spiked analyte concentration. Table 2 summarizes the GQDs recoveries obtained for the 2 real water samples ranging from 83.75–96.93% and 85.05–99.30% for tap and natural spring water, respectively, with SDs not higher than 6.31%.

Table 2. Recovery study of spiked waters samples.

Type of water	Sample	Added concentration of GQDs ($\mu g \cdot L^{-1}$)	Found concentration of GQDs[a] ($\mu g \cdot L^{-1}$)	Recovery (%)	RSD (%)
Natural Spring Water	1	125	115±7.2	85.1–99.3	6.3
	2	375	351±16.5	86.9–96.5	4.7
Tap Water	1	125	114±5.8	88.1–96.9	5.1
	2	375	337±17.4	84.8–94.9	5.2

[a]Average of five independent spiked samples±CI ($p < 0.05$).

A study of interferences from other nanoparticles that could be presents in natural waters were performed by adding, separately, c–SWCNT, GO and AuNPs (10nm sized) to the GQDs spiked real water samples. For this study, the same procedure as described above for the extraction of GQDs from tap and natural spring water –including a filtration step of the sample prior to their pass through the column and an interference remover step prior to elution– was performed. Real water samples were spiked with 375 $\mu g \cdot L^{-1}$ of GQDs and two different concentrations (375 and 600 $\mu g \cdot L^{-1}$) of c–SWCNT and GO were added to the real sample. AuNPs were tested in concentrations of 185 and 370 $\mu g \cdot L^{-1}$. Prior to pass through the cartridge, prepared real samples were filter by a 0.2 μm nylon syringe filter. As a result c–SWCNT, GO and AuNPs were retained in the filters. Interferences were studied for natural spring water samples. Recoveries obtained are summarized in Table 3. As can

be seen, good recoveries were obtained within the range of 93.81–102.12% for c–SWCNT, 95.62–101.94% for GO and 88.49–99.48% for AuNPs. Each sample was analyzed in triplicate in order to evaluate the precision of the method. The coefficients of variation ranged from 0.98% to 4.84%.

Table 3. Interference study of spiked water samples expressed as % of recovery.

Type of interferent	Sample	Added concentration of interferent ($\mu g \cdot L^{-1}$)	Added concentration of GQDs ($\mu g \cdot L^{-1}$)	Found concentration of GQDs[a] ($\mu g \cdot L^{-1}$)	Recovery (%)	RSD (%)
C–SWCNT	1	375	375	367±17.7	93.8–103.1	4.8
	2	600	375	378±3.7	99.8–101.7	1.9
GO	1	375	375	371±11.8	95.6–101.8	3.2
	2	600	375	373±8.7	97.26–101.9	2.3
AuNPs	1	185	375	349±19.7	88.4–98.9	5.6
	2	370	375	364±8.1	95.16–99.5	2.2

[a]Average of three independent spiked samples±CI ($p < 0.05$).

The results suggest that the proposed method can be used for the extraction, preconcentration and quantification of GQDs in tap and natural spring waters.

4. CONCLUSIONS.

This work presents a novel and very simple and sensitive method for the determination of GQDs in water samples. GQDs are retained in a strong

anion exchange column for their preconcentration being recovered in a water solution and measured in a spectrofluorometer using fluorescence of GQDs as analytical signal for the quantification. A previous clean–up step (filtration through 0.2 μm srynge filter) was incorporated in order to avoid interferences from the particulated matter and from other nanoparticles. The method presents several advantages: i) the preconcentration step is automatic; ii) the analysis time is very short; iii) reduced total solvent consumption; iv) no organic solvent is needed for the elution step, just pH adjusted ultrapure water is used; v) good recovery values are provided.

ACKNOWLEDGEMENTS

The authors wish to thank to the Junta de Andalucía (Project FQM 4801) and to the Ministrey of Economy and Competitiveness for financial support. S. Benítez-Martínez is also grateful to Junta de Andalucía for the award of a Research Training Fellowship.

The authors have declared no conflict of interest.

5. REFERENCES

[1] B.M. Simonet, M. Valcárcel, Monitoring nanoparticles in the environment, Anal. Bioanal. Chem. 393 (2009) 17–21.

[2] K. S. Novoselov, V. I. Fal'ko, L. Colombo, P. R. Gellert, M. G. Schwab, K. Kim, A roadmap for graphene, Nature 490 (2012) 192–200.

[3] H. Brody, Graphene, Nature 483 (2012) S29.

[4] Y. Dong, C. Chen, X. Zheng, L. Gao, Z. Cui, H. Yang, C. Guo, Y. Chi, C. M. Li, One-step and high yield simultaneous reparation of single– and multi–layer graphene quantum dots from CX–72 carbon black, J. Mater. Chem. 22 (2012) 8764–8766.

[5] J. Shen, Y. Zhu, X. Yang, J. Zong, J. Zhang, C. Li, One-pot hydrothermal synthesis of graphene quantum dots surface-pasivated by polyethylene glycol and their photoelectric conversion under near–infrared light, New J. Chem. 36 (2012) 97–101.

[6] S, Benítez–Martínez, M. Valcárcel, Graphene quantum dots as sensor for phenol in olive oil. Sens. Actuators, B 197 (2014) 350–357.

[7] X. Li, S. Zhu, B. Xu, K. Ma, J. Zhang, B. Yang, W. Tian, Self-assembled graphene quantum dots induced by cytochrome c: a novel biosensor for trypsin with remarkable fluorescence enhancement, Nanoscale 5 (2013) 7776–7779.

[8] S. Zhu, J. Zhang, C. Qiao, S. Tang, Y. Li, W.Yuan, B. Li, L. Tian, F. Liu, R. Hu, H. Gao, H. Wei, H. Zhang, H. Sunb, B. Yang, Strongly green-photoluminescent graphene quantum dots for bioimaging applications, Chem. Commun. 47 (2011) 6858–6860.

[9] X. Wang, X. Sun, J. Lao, H. He, T. Cheng, M. Wang, S. Wang, F. Huang, Multifunctional graphene quantum dots for simultaneous targeted cellular imaging and drug delivery, Colloids Surf., B 122 (2014) 638–644.

[10] Y. Li, Y. Hu, Y. Zhao, G. Shi, L. Deng, Y. Hou and L. Qu, An Electrochemical Avenue to Green-Luminescent Graphene Quantum Dots as Potential Electron-Acceptors for Photovoltaic, Adv. Mater., 23 (2011) 776–780.

[11] M. Nurunnabi, Z. Khatun, K. M. Huh, S. Y. Park, D. Y. Lee, K. J. Cho, Y. Lee, In Vivo Biodistribution and Toxicology of Carboxylated Graphene Quantum Dots ACSNano 7(2013) 6858–6867.

[12] Y. Ma, H. Shen, X. Tu, Z. Zhang, Assessing in vivo toxicity of graphene materials: current methods and future outlook, Nanomedicine 9 (2014) 1565–1580.

[13] A. I. López–Lorente, B. M. Simonet, M. Valcárcel, Determination of carboxylic SWCNTs in river water by microextraction in ionic liquid and determination by Raman spectroscopy, Talanta 105 (2013) 75–79.

[14] L. Li, K. Leopold, Ligand-Assisted Extraction for Separation and Preconcentration of Gold Nanoparticles from Waters, Anal. Chem. 84 (2012) 4340-4349.

[15] A. I. López-Lorente, B. M. Simonet, M. Valcárcel, Rapid analysis of gold nanoparticles in liver and river water samples, Analyst 137 (2012) 3528–3534.

[16] S. Benítez–Martínez, A. I. López–Lorente, M. Valcárcel. Graphene Quantum Dots Sensor for the Determination of Graphene Oxide in Environmental Water Samples, Anal. Chem. 86 (2014) 12279−12284.

[17] Y. Dong, J. Shao, C. Chen, H. Li, R. Wang, Y. Chi, X. Lin, G. Chen, Blue luminescent graphene quantum dots and graphene oxide prepared by tuning the carbonization degree of citric acid, Carbon 50 (2012) 4738–4743.

BLOQUE IV

Resultados y discusión

IV.1. INTRODUCCION

En este apartado se trata de dar una visión trasversal de la Memoria hasta aquí expuesta que abarca los artículos publicados o enviados a publicar. Todos y cada uno de ellos tienen también apartados de título semejante, por lo que aquí no se pretende repetir lo ya escrito sino de dar un enfoque complementario al de la estructura de la Tesis, que tiene por esqueleto la consideración como herramientas y/o analitos del grafeno y de algunos de sus derivados más simples, que se resumen esquemáticamente en la Figura IV.1.

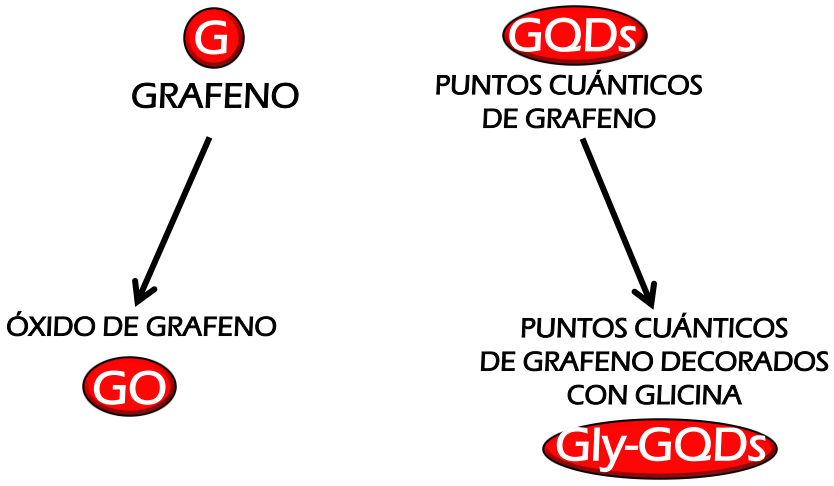

Figura IV.1. Grafeno y derivados involucrados en esta Tesis Doctoral.

Este apartado se va a estructurar de acuerdo con el rol que juegan cada una de estas nanopartículas en los correspondientes procesos analíticos en el marco genérico de la Nanociencia & Nanotecnología Analíticas en la actualidad, que tiene tres facetas, tal como se muestra en la Figura IV.2.

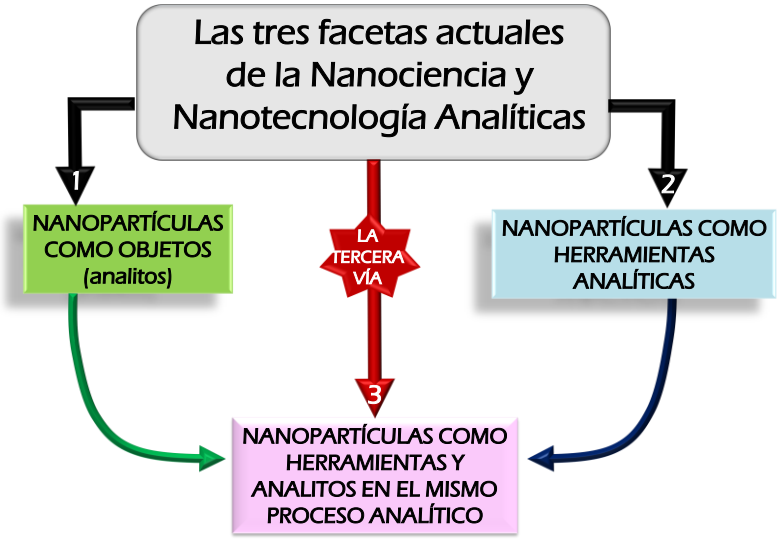

Figura IV.2. Las tres facetas actuales de la Nanociencia&Nanotecnología Analíticas.

La ***primera faceta*** (apartado IV.2) supone la caracterización de las nanopartículas así como su determinación en muestras medioambientales, agroalimentarias, farmacéuticas, cosméticas, etc. Es un gran reto para la Química Analítica ya que solo aproximadamente un 35% de los trabajos

publicados en la Nanociencia & Nanotecnología Analíticas se dedican a este aspecto. Se trata de una faceta crucial dado el crecimiento de las industrias con base nanotecnológica que implica un aumento importante de los productos con nanopartículas o nanoestructurados para su empleo en la sociedad y en la industria así como un incremento relevante de la contaminación ambiental por estas nanopartículas, que son contaminantes emergentes.

La ***segunda faceta*** de la Nanociencia y Nanotecnología Analíticas (apartado IV.3) se centra en la utilización de las nanopartículas y/o material nanoestructurado como herramientas en procesos analíticos buscando su mejora sistemática. Estas nanopartículas pueden actuar como sorbentes en una amplia variedad de técnicas de microextracción, como soportes tanto inertes como activos, como componentes de nanoelectrodos o electrodos nanoestructurados, como fluoróforos y conductores en sensores, como fase estacionaria en HPLC y GC, entre otras funciones. Hay ya cerca de mil artículos indexados en base de datos internacionales en esta temática que supone un 65% aproximadamente de los dedicados a Nanociencia y Nanotecnología Analíticas.

La ***tercera faceta*** de la Nanociencia y Nanotecnología Analíticas (apartado IV.4 de este bloque) se ha puesto en valor recientemente y supone

una combinación sinérgica de las dos anteriores, por lo que la denominamos como "tercera vía". Se trata de desarrollar procesos analíticos para determinar nanopartículas usando como herramientas otras nanopartículas que pueden ser de igual o diferente naturaleza de las herramientas nanotecnológicas. Ambas opciones se han considerado en esta Tesis. Se busca explotar simultáneamente (ver Figura IV.2) las propiedades físico-químicas excepcionales de las herramientas y analitos para aumentar la selectividad, sensibilidad, precisión, recuperación, rapidez, simplicidad y otras características analíticas.

IV.2. DERIVADOS DEL GRAFENO COMO OBJETOS DE ANÁLISIS

La consideración de los materiales nanoestructurados como objeto de análisis deriva del interés por obtener información y conocer su comportamiento físico–químico y estructural y de la cada vez mayor producción a gran escala de este tipo de materiales para su uso industrial y aplicación en productos comerciales. Las atractivas propiedades del grafeno hacen que, además de resultar una herramienta útil en el desarrollo de nuevas metodologías analíticas, sea considerado como un interesante objeto de análisis en muchas áreas de investigación, incluyendo la N&NA, campo en el cual esta faceta ha sido tradicionalmente poco desarrollada.

Los estudios de investigación de esta Tesis Doctoral centrados en la consideración de grafeno y sus derivados como diana para su determinación, estuvieron encaminados hacia la detección y cuantificación de dos formas solubles de grafeno, GO y GQDs, en muestras ambientales.

En este apartado se describirá el método desarrollado para la determinación de GQDs en muestras de agua. A pesar de que la determinación de GO podría encajar también en esta sección, el método será descrito detalladamente en el apartado IV.4., *El grafeno y sus derivados en la*

"tercera vía" de la N&NA, por tratarse de un procedimiento que se fundamenta en el empleo de NPs para determinar otras NPs. Dicho apartado proporciona una nueva visón sobre la N&NA, considerando además de las dos facetas tradicionales, NPs como objeto de análisis y NPs como herramienta para la mejora del proceso analítico, una "tercera vía".

IV.2.1. Determinación de puntos cuánticos de grafeno en muestras de agua

A pesar de la biocompatibilidad y baja citotoxicidad atribuidos a los GQDs desde su aparición, algunos estudios recientes han puesto de manifiesto que los GQDs podrían ser acumulados en hígado, bazo, pulmones, riñones y zonas tumorales. Por otra parte, existen ciertas teorías que afirman que la biodistribución y toxicidad de los materiales nanoestructurados con dimensiones laterales inferiores a 5 nm podría ser baja debido a la eliminación de estos materiales a través de la orina. Todo ello unido a la creciente producción de este nanomaterial hacen que aumente el riesgo de liberación al medio ambiente, haciéndose necesario el desarrollo de metodologías que permitan su detección.

Para la determinación de GQDs en aguas naturales se optó por el empleo de cartuchos de extracción en fase sólida (SPE) de intercambio aniónico fuerte (SAX), que contenían un sorbente empaquetado de sílice

funcionalizada con aminas cuaternarias. La elevada solubilidad en agua de estas NPs se debe a la presencia de grupos funcionales ricos en oxígeno, con predominancia de carboxilos e hidroxilos, los cuales podrían interaccionar con el sorbente, en las condiciones idóneas, y conducir a la retención de los mismos.

Durante la optimización del procedimiento se llevó a cabo el estudio de una serie de variables fundamentales como son el pH, el volumen de muestra, la velocidad a la que pasó la muestra y las mejores condiciones para la elución como tipo de disolvente, volumen de disolvente y velocidad de elución.

Los resultados obtenidos del estudio de pH mostraron que la fluorescencia de los GQDs alcanzó un valor máximo en condiciones muy alcalinas, pH=13, para una concentración de NPs de 50 $mg{\cdot}L^{-1}$. Así mismo se realizó un estudio para evaluar la retención de los mismos, en el sorbente SAX, en función del pH de la muestra acuosa, seleccionándose pH7 como aquel valor al cual la retención fue máxima. pH 10, mostró un comportamiento muy similar, pero dada la naturaleza neutra de la muestra real se seleccionó pH=7. Un volumen de 20mL fue seleccionado para ser pasado a través del cartucho de SPE, en una situación de compromiso para lograr una buena reproducibilidad y una elevada sensibilidad con unos tiempos de análisis aceptables. La velocidad a la que la muestra pasó a través del cartucho

empaquetado fue ajustada a 1ml·min^{-1} mientras que la velocidad a la que los GQDs fueron liberados de la amina cuaternaria fue establecida en 0.1 mL·min^{-1} empleando 500 μL de agua ultrapura ajustada a pH 13, obteniendo de este modo una preconcentración teórica de 40x.

La Figura IV.2.1 ilustra la influencia del pH en la fluorescencia de los GQDs a bajas concentraciones, 50 mg·L^{-1}.

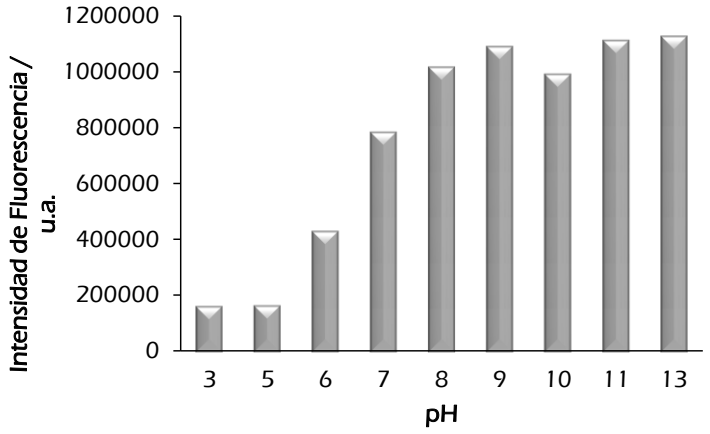

Figura IV.2.1. Comportamiento según el pH de la fluorescencia de los GQDs a un nivel de concentración de 50mg· L^{-1}.

Gracias a la optimización de todas las variables estudiadas pudo definirse el protocolo experimental que permitió la cuantificación de GQDS. En primer lugar, el cartucho SPE SAX fue acondicionado con agua ultrapura y acetato

amónico y, a continuación, 20 mL de muestra acuosa fortificada con distintas cantidades de GQDs se hicieron pasar a través del sorbente empaquetado con un flujo de muestra de 1 $mL{\cdot}min^{-1}$. El cartucho se secó pasando aire a su través y a continuación tuvo lugar la elución previa al análisis fluorimétrico monitorizando la intensidad de emisión. Como ventaja añadida del método de extracción desarrollado hay que resaltar la automatización de la etapa de carga de muestra en el cartucho, que simplificó considerablemente el proceso. En la Figura IV.2. 1 se muestran a modo de ejemplo espectros de GQDs tras su elución del cartucho SPE–SAX

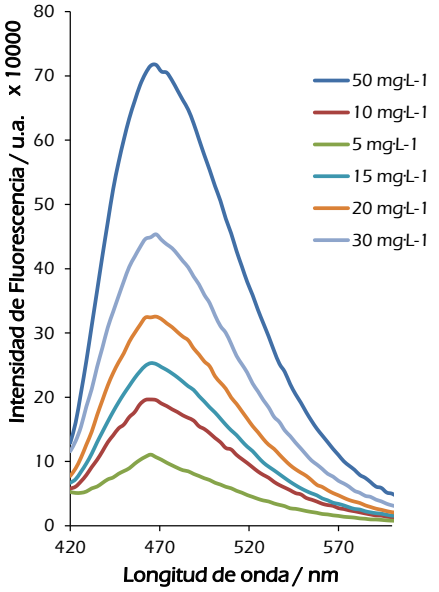

Figura IV.2.2. Espectros de fluorescencia a distintas concentraciones de los GQDs tras ser eluídos del cartucho SAX.

Los resultados obtenidos permitieron dilucidar el mecanismo de retención de los GQDs en cartuchos empaquetados SAX, atribuyéndose éste a las interacciones iónicas que tuvieron lugar entre los grupos funcionales en los bordes de los GQDs y las aminas cuaternarias, con carga positiva, en el sorbente.

El sistema desarrollado resultó ser un método muy simple, rápido y sensible para la detección y cuantificación de GQDs en muestras de agua ambiental y agua de grifo. El límite de detección se situó en 7.5 $\mu g \cdot L^{-1}$. Las recuperaciones obtenidas se situaron siempre en niveles bastante aceptables. La interferencia de otros tipos de nanopartículas como SWCNT, GO y AuNPs fue evaluada pudiéndose concluir que no afectaban a la eficiencia de la extracción de GQDs, confiriéndole al método gran especificad por este tipo de NPs. Así mismo, la metodología propuesta supone la primera aproximación descrita para la determinación de GQDs en muestras de agua, aportando este hecho un valor añadido al trabajo presentado.

IV.3. EL GRAFENO Y DERIVADOS COMO HERRAMIENTAS ANALÍTICAS

Las excepcionales propiedades del grafeno y de los nanomateriales derivados de éste, entre las que merecen ser destacadas su elevada área superficial específica, la presencia de un gran número de sitios reactivos a lo largo de superficie, su habilidad de adsorción y sus propiedades ópticas y de trasporte electrónico, hacen de estas nanoestructuras unas atractivas candidatas para su empleo en el ámbito de la Química Analítica.

A lo largo del periodo experimental de la presente Tesis Doctoral se han desarrollado nuevas metodologías para la mejora de la sensibilidad en la etapa de detección a través del empleo de nanoláminas de grafeno en técnicas como la electroforesis capilar y la espectroscopia Raman por amplificación de superficies. En el primer caso, el empleo de grafeno fue evaluado como fase pseudoestacionaria para la separación de antiinflamatorios no esteroideos (AINEs), siendo añadidas las nanoláminas en el electrolito de separación. En el segundo caso, las nanoláminas fueron empleadas para el desarrollo de un procedimiento analítico basado en la detección mediante espectroscopia Raman, en el que las nanoláminas de grafeno actúan como soporte de nanopartículas metálicas, dando lugar a la

formación de un soporte hibrido utilizado como plataforma para incrementar la sensibilidad de la técnica a través del efecto SERS.

Así mismo, se ha llevado a cabo el diseño de nuevas estrategias para el desarrollo de sistemas sensores basados en derivados de grafeno como son los GQDs. Gracias a las excepcionales propiedades ópticas de estas nanoláminas de grafeno, de reducidas dimensiones laterales, se han desarrollado nanosensores para la detección y determinación de moléculas antioxidantes, de gran interés en el sector agroalimentario, y nanopartículas presentes en productos cosméticos comerciales.

IV.2.1. El grafeno como herramienta analítica

En este apartado se presentan los resultados más relevantes derivados del empleo de nanoláminas de grafeno para la mejora de la sensibilidad en la etapa de detección del proceso analítico. En primer lugar se discutirán las aportaciones más relevantes del empleo de nanoláminas como modificadoras del electrolito de separación en electroforesis capilar y a continuación, se discutirán los hallazgos derivados de la aplicación de estas nanoláminas como sustrato SERS.

Grafeno como fase pseudoestacionaria en electroforesis capilar

La separación de compuestos, neutros o cargados, bajo la acción de un campo eléctrico, se conoce como electrocromatografía. La electroforesis capilar es una modalidad de esta técnica que se conoce desde 1967, en la que los analitos viajan, en el seno de una disolución de electrolito, a través de un capilar de sílice fundida, de unos pocos micrómetros de diámetro interno (50–100μm), para ser separados en función de su relación masa/carga bajo la influencia de un campo eléctrico. De este modo, los analitos se separan según su propia movilidad, llegando al cátodo en primer lugar las moléculas más grandes cargadas positivamente. Las moléculas con carga neutra viajan con el flujo electroosmótico (EOF) y las cargadas de forma negativa alcanzan el detector en último lugar, cuando se trabaja en modo normal. El potencial aplicado hace que los diferentes componentes iónicos de la mezcla se separen en zonas que pueden estar completamente resueltas o parcialmente solapadas.

Para solventar el problema de las especies parcialmente solapadas y la separación de las formas neutras del EOF se han empleado tradicionalmente fases pseudoestacionarias, compuestas por micelas, que interaccionan con los analitos haciendo que estos modifiquen su velocidad de migración. La naturaleza de la fase pseudoestacionaria es de importancia crítica en la

separación, habiendo sido empleadas sustancias como tensioactivos, microemulsiones, proteínas y nanopartículas de distinta naturaleza, entre otros. En los últimos años las CNPs han adquirido importancia en su empleo como modificadores del electrolito de separación, siendo las más usadas los fulerenos y CNTs. La adición de nanopartículas al electrolito supone el mismo efecto que el empleo de micelas, con la ventaja de que las nanoparticulas ofrecen un elevado número de sitios activos que favorecen la interacción con los analitos.

Para que las nanopartículas puedan ser empleadas como fase pseudoestacionaria deben cumplir una serie de requisitos como poseer un tamaño nanométrico, mostrar una superficie con carga residual superficial para formar suspensiones estables, ser capaces de interaccionar con el analito de forma débil y ser compatibles con el sistema de detección usado. Otros aspectos importantes a considerar es la orientación de las nanopartículas dentro del capilar y la agregación de las mismas, que se traduce en un aumento del número de sitios activos, con la consecuente mejora del proceso.

El planteamiento inicial para el desarrollo de una fase pseudoestacionaria compuesta por grafeno se basó en que éste cumplía todos los requisitos resumidos en el párrafo anterior además de no haber sido

descrita su utilización para este fin hasta el momento. Por lo tanto, su efecto en la mejora de la resolución electroforética era desconocido.

En el desarrollo de este trabajo, las nanoláminas de grafeno, fueron añadidas al electrolito de separación, y un pequeño volumen de éste fue añadido tras la inyección del segmento de muestra. Los analitos modelo, fenbufeno, ibuprofeno, ketoprofeno, naproxeno y flurbiprofeno, fueron seleccionados en base a que son un grupo representativo de los antiinflamatorios más utilizados en el cuidado de la salud humana y animal. Éstos suelen encontrarse a menudo en el medio acuático junto con sus metabolitos, considerándose un grupo emergente de contaminantes pues algunos de ellos se utilizan en volúmenes cada vez más grandes, alcanzando cantidades similares a los pesticidas y otros contaminantes orgánicos. Además poseen una estructura aromática que permite su interacción con las láminas de grafeno a través de fuerzas débiles de tipo π–π. El estudio se realizó empleando disoluciones de los analitos en agua ultrapura.

En nuestro caso, la necesidad de emplear una pseudofase deriva de la similar estructura molecular de los AINEs que se traduce en unos tiempos de migración muy similares, que hacen que los picos correspondientes a cada analito en los electroferogramas se solapen, impidiendo de este modo poder

calcular el área de pico correspondiente a cada uno y utilizarla para llevar a cabo la cuantificación de molécula de interés.

La elección de un electrolito adecuado junto con el pH de éste son factores limitantes en electroforesis capilar pues los analitos que se pretenden determinar deben estar ionizados con el fin de facilitar su migración a lo largo del capilar. El rango de pH estudiado fue amplio, encontrándose que cuanto más alcalino era el carácter del electrolito peor fue la resolución de los picos de la mezcla de AINEs. Finalmente el valor de pH elegido como óptimo fue 4.0. Para la elección de este valor se llevaron a cabo una serie de análisis de la mezcla de AINEs empleando el electrolito sin modificar con las nanopartículas, observando cual de los pH estudiados ofrecía mejor separación, sin llegar en ninguno de los casos a resolverse por completo la solapación.

La dispersión de las nanoláminas en el seno de la disolución de electrolito fue examinada de tres formas distintas. En primer lugar se llevó a cabo una agitación manual del electrolito junto con la alícuota correspondiente de la dispersión de grafeno. En segundo lugar, se llevó a cabo la dispersión de las nanoláminas mediante la utilización de un baño de ultrasonidos y en último lugar se aplicó la radiación ultrasónica en el seno de la disolución a través de una sonda. La mayor estabilidad de la dispersión de las láminas de grafeno se consiguió empleando el último procedimiento,

obteniendo así dispersiones del electrolito modificado estables durante más de una semana, y logrando una dispersión más efectiva con un menor tiempo de exposición. La separación de los AINEs fue llevada a cabo con cada dispersión obtenida tras cada tipo de homogeneización, obteniendo una mejora considerable en el ruido de la línea de base, así como un incremento importante en la resolución de los picos y una mejora de la sensibilidad.

Durante el estudio, se emplearon dos tipos de dispersiones de grafeno con el fin de evaluar la influencia del número de láminas en la mejora de la separación. El grafeno–1 contenía mayor cantidad de monocapas y bicapas y el grafeno–2 mayor cantidad de cuatro y más de cuatro capas. Ambas dispersiones de grafeno fueron añadidas al electrolito en diferentes concentraciones, considerándose suficientes para una buena resolución, 1.25 $mg{\cdot}L^{-1}$, en el caso del grafeno–1, y 1.875 $mg{\cdot}L^{-1}$, en el caso del grafeno–2. Para la optimización de esta variable se mantuvieron constantes las optimizadas anteriormente (Acetato amónico, $AcNH_4$, 50 mM a pH 4, 25ºC, +15 kV) y se empleó una concentración fija de AINEs con el fin de poder establecer las comparaciones pertinentes. Gracias a este estudio pudo establecerse el rol del número de láminas de grafeno en la fase pseudoestacionaria, de modo que con una concentración menor de aquel tipo de grafeno que contenía mayor proporción de monocapas y bicapas (grafeno–1) se obtuvo una mejor resolución de los picos que solapaban, atribuyéndose dicha mejora a la

presencia de pocas capas de grafeno y no a la formación de agregados del mismo. El tratamiento con ultrasoidos del electrolito modificado también tuvo sus efectos en el tiempo de migración de los analitos, acortando dicho tiempo en la mayoría de los análisis que se realizaron, en la sensibilidad del método, consiguiendo una mayor definición de los picos, y en el ruido de la línea de base, que mejoró considerablemente debido a la disminución de los agregados. La Figura IV.3.1 muestra una estimación de la concentración de cada fracción de láminas según la cantidad y tipo de grafeno empleado.

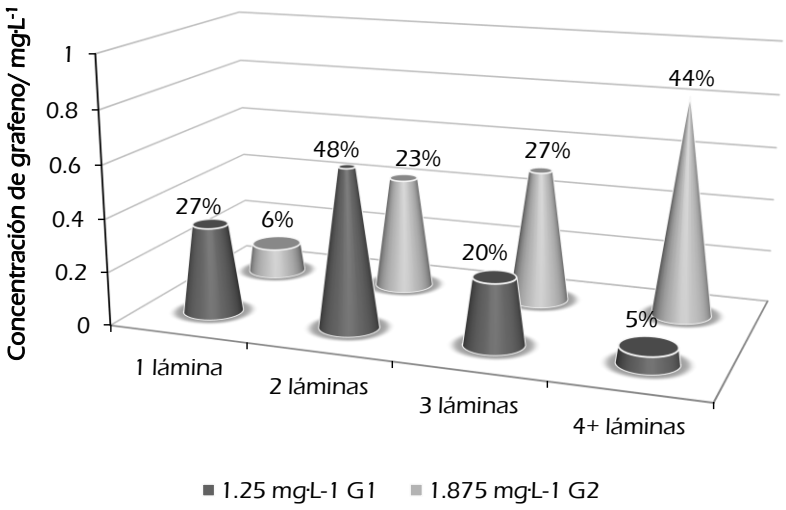

Figura IV.2.1. Estimación de la concentración de cada fracción de láminas según la cantidad y tipo de grafeno empleado.

Puesto que las dispersiones comerciales de grafeno contenían un pequeño porcentaje (2% p/v) del surfactante colato sódico (SC) para hacerlas estables en disolución acuosa, fue necesario evaluar la aportación del mismo al proceso de separación, puesto que la formación de micelas podría dar lugar a la resolución de la solapación de los picos de los analitos por sí misma. Para ello se siguieron dos estrategias diferentes. Una de ellas, consistió en eliminar el tensioactivo aniónico mediante una microextracción líquido–liquido con una etapa posterior de evaporación del disolvente, siendo las nanoláminas aisladas redispersadas en la disolución de electrolito e inyectadas directamente en el sistema. Las láminas en dicha disolución resultaron ser muy inestables precipitando rápidamente en el fondo del vial que las contenía, confirmando de este modo la necesidad de emplear las nanopartículas tal como habían sido suministradas, es decir, en presencia de SC.

En segunda instancia, se evaluó el efecto del SC por si solo en la separación de los AINEs. Para ello, se estudiaron distintas concentraciones de SC en el electrolito de separación y se realizaron los análisis electroforéticos pertinentes. Las concentraciones de colato fueron siempre iguales o mayores a las añadidas junto con el grafeno, pero en ningún caso se alcanzó la concentración micelar crítica (CMC) del SC. Se pudo concluir tras este estudio que el SC no solo no fue capaz de resolver los picos solapados por sí mismos sino que sus efectos apenas fueron observables en los electroferogramas,

confirmando que la mejora en la separación de los AINEs se debió única y exclusivamente a la presencia de nanoláminas de grafeno. La figura IV.2.2 muestra a modo de ejemplo electroferogramas obtenidos durante el desarrollo experimental.

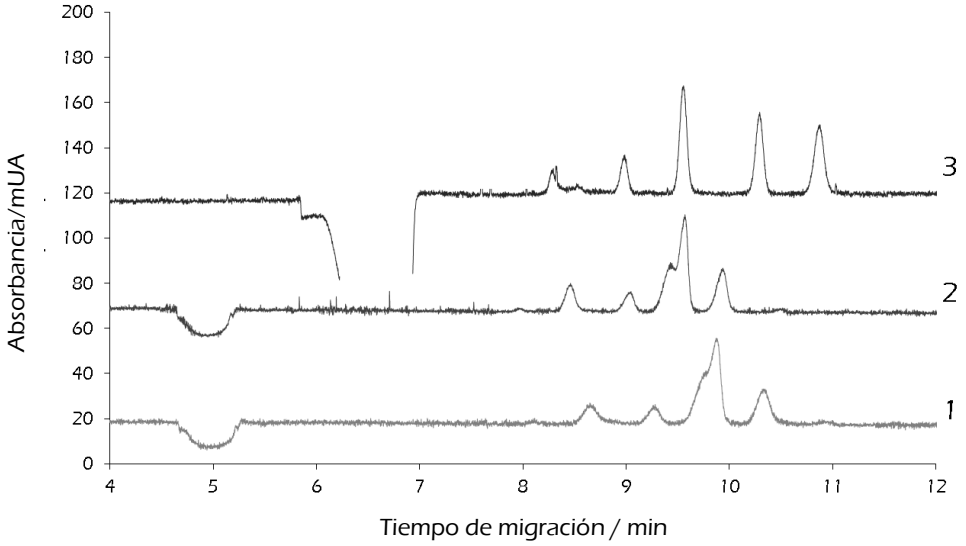

Figura IV.2.2. Electroferogramas de la separación de AINEs. 1) Separación de AINES con electrolito sin modificar, 2) electrolito modificado con 750 mg·L^{-1} de colato sódico y 3) electrolito modificado con 1.25 mg·L^{-1} de nanoálimas de grafeno–1 dispersadas con tratamiento ultrasónico.

Teniendo en cuenta las interacciones que se producen en el sistema, podemos concluir que la estabilización de las nanoláminas dentro del capilar se consigue gracias al tensioactivo presente en la disolución comercial. Se

asume que las moléculas de tensioactivo se adsorben sobre la superficie del grafeno solubilizándolo en el medio acuoso y que los analitos se adsorben sobre la superficie del grafeno mediante el establecimiento de interacciones π–π, modificando estos su coeficiente de reparto y movilidad dentro del capilar, logrando una mejora significativa de la resolución electrocromatográfica. Por otra parte, la inyección de un segmento corto (unos pocos μL en 2 s de inyección) de electrolito modificado tras la inserción del segmento de muestra permitió preconcentrar la muestra obteniendo una mejora de la sensibilidad del método, obteniendo picos más estrechos y mejor definidos.

Resumiendo, el método analítico desarrollado es sencillo y rápido, permitiendo la determinación simultánea de 5 AINEs en un tiempo de análisis corto con el empleo de concentraciones mínimas de grafeno. La reproducibilidad del método fue buena, en lo referente a área de pico y tiempo de migración de cada analito, obteniéndose límites de detección inferiores a 2.37 $mg{\cdot}L^{-1}$. El potencial, eficiencia y uso de ambos tipos de grafeno queda demostrado desde dos puntos de vista: (i) como aditivo del electrolito para la implementación de la resolución y (ii) como herramienta analítica para la mejora de la sensibilidad.

Grafeno como sustrato en Espectroscopia Raman Amplificada por Superficies (SERS)

El efecto SERS se basa en el aumento de la dispersión Raman (o dispersión inelástica) de determinadas moléculas en presencia de nanopartículas metálicas de superficie rugosa, generalmente. La intensidad obtenida cuando la molécula interacciona con la superficie metálica es del orden de 10^5–10^6 veces superior a cuando no se produce el contacto. Existen dos modelos básicos que intentan explicar el incremento de la dispersión Raman: el *modelo electromagnético* (EM) y el *modelo químico o de transferencia de carga* (CM).

El mecanismo EM se origina por un aumento de la intensidad del campo electromagnético de la radiación incidente que llega a la molécula, el cual se ve dispersado por la superficie metálica, siendo mucho mayor cuando entra en resonancia con el pasmón superficial del metal. Depende en gran medida de las características de la superficie metálica y de la distancia entre moléculas y nanopartículas. El modelo CM tiene su origen en mecanismos de transferencia de carga entre las moléculas adsorbidas sobre la nanopartícula metálica y la superficie de la misma. La energía se transfiere al analito, teniendo lugar en éste el proceso Raman y la energía es transferida de nuevo a la nanoestructura metálica que produce la dispersión. La combinación de

ambos mecanismos, con predominancia del modelo electromagnético, puede explicar la generación de este efecto de amplificación.

En los últimos 20 años, el número de publicaciones que explotan el efecto SERS ha crecido exponencialmente en el ámbito de la Química (Figura IV.2.3) debido a la especificidad (efecto de "huella dactilar") y mejora de la sensibilidad que aporta la técnica, resultando una herramienta atractiva para la detección de analitos a niveles traza.

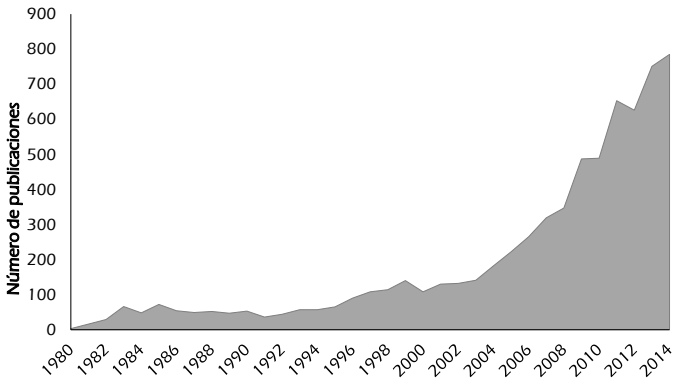

Figura IV.2.3. Evolución del número de publicaciones que emplean el efecto SERS en el campo de la Química (fuente SCOPUS).

Por otra parte, la capacidad de la monocapa de grafeno para generar un incremento en la señal Raman ha sido recientemente descrita, así como el uso de éste y sus derivados (GO y rGO) como sustrato en SERS. Sin embargo, la

amplificación generada por éstos es limitada, habiéndose desarrollado sustratos híbridos de grafeno y nanopartículas metálicas para la mejora de la sensibilidad.

El método analítico propuesto estuvo enfocado a la determinación de metronidazol, un compuesto nitroaromático usado como antibiótico y antiparasitario en el tratamiento de infecciones causadas por bacterias y protozoos en personas y animales. La administración de éste en animales para consumo humano ha sido prohibida por La Comisión Europea y la FDA (Food and Drug Administration, U.S.) debido a su potencial genotoxicidad y propiedades mutagénicas.

El proceso analítico desarrollado para su detección se basó en la obtención de un soporte de multicapas de grafeno combinadas con AuNPs sobre el que se depositó el analito para ser cuantificado. Para ello se depositó una gota de 10 μL de la dispersión comercial de grafeno–2 sobre un cristal de fluoruro cálcico que se mantuvo a una temperatura constante de 50ºC durante todo el procedimiento de deposición. A continuación se llevó a cavo el lavado de la superficie del cristal con 50 μL de metanol seguidos de otros tantos de agua ultra pura, proceso que se repitió una vez más con el fin de eliminar el tensioactivo que acompañaba al grafeno en la dispersión comercial. El procedimiento se repitió hasta depositar un total de 10 gotas de la

dispersión de grafeno con el fin de conseguir una zona con un tamaño suficiente para realizar medidas aleatorias sobre él, con la mayor área posible cubierta por las nanoláminas. A continuación se llevo a cabo la deposición de 300 μL (de 10 en 10 μL) de una disolución de AuNPs sintetizadas a partir de la reducción de ácido tetracloroaúrico con citrato.

Tras la preparación del sustrato hibrido, 1 μL de analito fue depositado en el centro de la superficie de éste con ayuda de una microjeringa Hamilton, cubriendo la muestra toda la superficie del sustrato, pudiendo ser ejecutadas las medidas Raman inmediatamente después.

Los estudios de optimización de las variables involucradas en el proceso de detección condujeron a la investigación de diferentes parámetros con el fin de maximizar el efecto SERS. Éstos fueron: (i) la forma de preparación del sustrato híbrido, (ii) el volumen de la disolución de AuNPs empleado, (iii) el orden de deposición de grafeno, AuNPs y analito, (iv) la influencia de la potencia del láser de excitación, (v) tiempo de adquisión de los espectros y (vi) reusabilidad del sistema. Para el estudio de todos ellos se empleó violeta de metilo, más conocido como cristal violeta (CV) a una concentración de 10^{-4} M, monitorizando los cambios sufridos en la banda correspondiente a 1171 cm^{-1}, una de sus bandas más características. El CV es una sustancia cuyo uso está muy extendido en este tipo de técnicas pues se trata de una molécula muy

activa en Raman debido a su gran simetría. Los resultados mostraron que (i) la deposición de la disolución de AuNPs sobre el grafeno depositado en el cristal de CaF_2 condujo a una distribución de alta densidad de AuNPs de tamaño homogéneo con un elevado número de *hotspots,* es decir, una gran cantidad de AuNPs se distribuyeron sobre toda la superficie del grafeno dando lugar a la creación de numerosos sitos activos en los huecos entre nanopartículas, lugar donde tiene su origen la amplificación de la señal Raman; dicho efecto de amplificación se vio favorecido por la presencia de grafeno, lo que se tradujo en un mayor y más reproducible efecto SERS. (ii)Un volumen 300 μL de AuNPs depositadas sobre grafeno fue considerado como óptimo. (iii)Así mismo el orden de deposición seleccionado fue grafeno en primer lugar, seguido de AuNPs y finalmente analito. (iv) La potencia del láser (785nm) fue ajustada hasta 11mW y (v) el tiempo de adquisición de los espectros fue de 1 s. (vi) Finalmente la reusabilidad del sistema se consiguió lavando la superficie con 10mL de MeOH seguidos de 10 mL de agua, pudiendo reutilizarse 4 veces. La Figura IV.3.4 muestra los espectros SERS tras cada etapa de lavado, observándose claramente como a partir del lavado número 4 la intensidad de la señal comienza a decrecer, no solo en la banda monitorizada sino en todo el espectro. Este efecto fue atribuido al barrido de las AuNPs de la superficie del grafeno después de varias etapas de lavado.

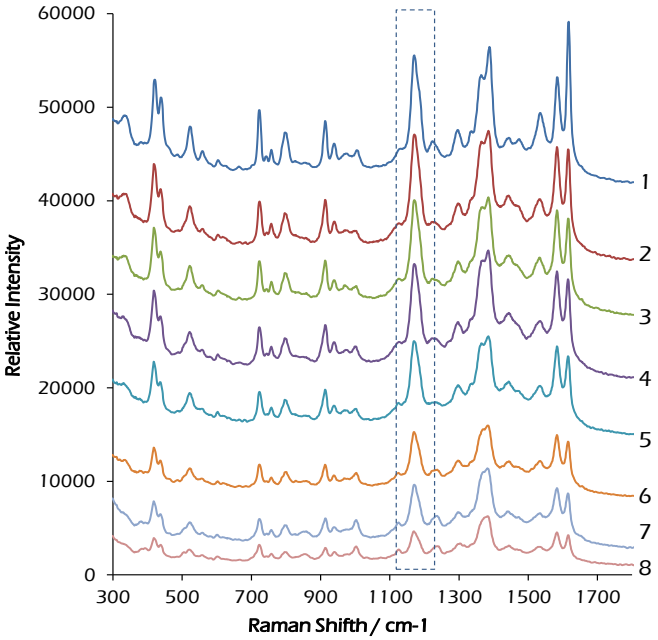

Figura IV.2.4. Espectros SERS de CV tras cada etapa de lavado y nueva deposición de analito.

Una vez optimizadas las variables experimentales se llevó a cabo la determinación de metronidazol registrando los cambios en la intensidad de la banda de 1186 cm^{-1}. Los factores de incremento de la señal Raman fueron 4415 y 124 para CV y metronidazol, respectivamente. Dichos valores son inferiores a los encontrados en la bibliografía, lo que se atribuyó a que, en nuestro caso, solo el mecanismo químico contribuyó a la amplificación de la señal Raman de los analitos. La ausencia del modelo EM pudo deberse a que la longitud de onda de excitación del láser (785 nm) no entró en resonancia

con el plasmón de las AuNPs. En la figura IV.2.5 pueden observarse, a modo ilustrativo, los espectros Raman y SERS del metronidazol.

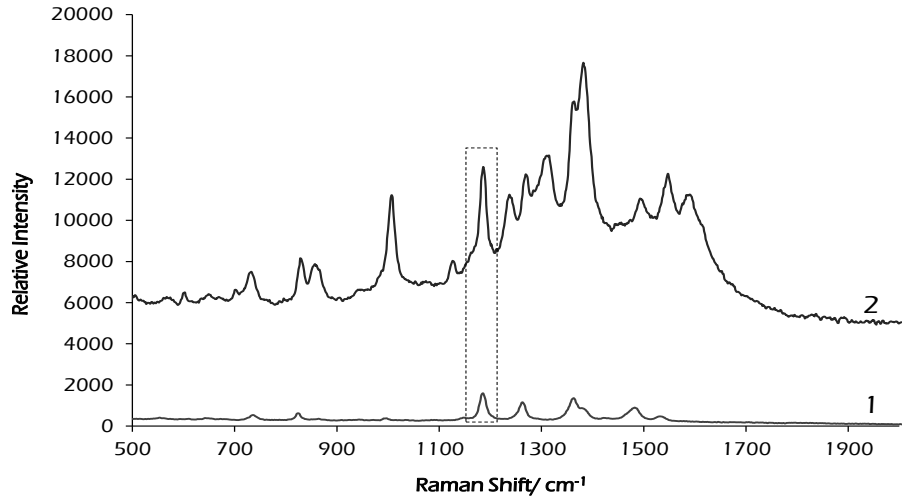

Figura IV.2.5. Espectro Raman del metronidazol a una concentración de 1g·L^{-1} sobre el cristal de CaF_2 (1) y espectro SERS a 30 mg·L^{-1} obtenido con el sustrato híbrido (2).

La amplificación de la señal Raman del espectro del metronidazol en el sustrato híbrido de grafeno–AuNPs fue comparada en sustratos compuestos únicamente por AuNPs y grafeno, manteniendo las mismas condiciones optimizadas para el sustrato híbrido en lo referente a potencia láser, tiempo de integración y volúmenes de las dispersiones de grafeno y AuNPs. Los factores de amplificación obtenidos, para una concentración de 30 mg·L^{-1}, fueron 38 para el sustrato metálico y 0 para el de grafeno.

El método SERS desarrollado a partir de un sustrato hibrido de multicapas de grafeno y AuNPs permitió obtener un límite de detección de 1.1 $mg{\cdot}L^{-1}$. La reproducibilidad del sustrato, expresada como RSD (n=20) fue 7.76 % y la obtenida entre distintos sustratos (n=3) fue de 10.92%. Teniendo en cuenta que la técnica se caracteriza precisamente por una elevada irreproducibilidad de los resultados, debe destacarse que la precisión del método propuesto es bastante aceptable, lo que se atribuyó al empleo de grafeno como sustrato. Comparando los resultados obtenidos con los aportados por investigaciones recientes (10 $mg{\cdot}L^{-1}$)[1], puede concluirse que el modelo híbrido propuesto ha demostrado ser un sustrato apto para la determinación SERS de metronidazol con una elevada sensibilidad.

Además, este trabajo de investigación ha permitido estudiar el efecto SERS de las multicapas de grafeno originado por las AuNPs sobre su superficie. Como todos los alótropos del carbono, el grafeno presenta las bandas D (relacionada con los defectos de la estructura atómica y con el efecto de borde), G (asociada a la vibración en el plano de los átomos de carbono con hibridación sp^2) y G' (sobretono de la banda G relacionado con vibraciones de tipo acústico) características de estos materiales. El factor de ampliación de la señal Raman en esta ocasión fue de 21, comparando las intensidades de las

[1] C. Han, J. Chen, X. Wu, Y. W. Huang, Y. Zhao, Talanta 128 (2014) 293–298.

bandas D (1307 cm^{-1}) y G (1597 cm^{-1}). La banda G' apareció a 2607 cm^{-1}. Factores como el número de láminas y las características del láser de excitación pueden influir en el desplazamiento de estas bandas típicas.

IV.3.2. Los puntos cuánticos de grafeno como herramienta analítica

En este apartado se muestran los resultados más relevantes obtenidos a través del manejo de nuevas formas de grafeno, con propiedades ópticas no observadas en la lámina aislada de grafito, en lo referente a nuevos sistemas nanosensores. A continuación se presentarán los hallazgos más significativos conseguidos en el desarrollo de sistemas sensores basados en GQDs y. Las contribuciones de GQDs funcionalizados como estrategia hacia la mejora de la selectividad podrían encajar perfectamente en este apartado debido al empleo de GQDs como herramienta analitica, pero , sin embargo, serán comentados en la sección IV.4 que se centra en la "tercera via" de la N&NA.

Sensores basados en puntos cuánticos de grafeno

En los últimos años, las propiedades antioxidantes del aceite de oliva se han relacionado con efectos beneficiosos en la salud humana, como la protección contra enfermedades coronarias y la aparición de tumores. Dichas propiedades antioxidantes se encuentran directamente relacionadas con el contenido en polifenoles de este aceite. Investigaciones recientes han puesto

de manifiesto que la presencia de éstos en el aceite disminuye la cantidad de triglicéridos y aumenta el llamado colesterol "bueno", encontrándose, además, una relación inversamente proporcional entre la concentración de polifenoles y la presencia de marcadores de estrés oxidativo.

A pesar de que no existe ninguna metodología oficial para la determinación de polifenoles en aceite de oliva, está ampliamente aceptado el empleo de la técnicas espectrofotométricas combinadas con métodos como el Folin&Ciocalteu, que se sirve del reactivo del mismo nombre para determinar la concentración fenólica a través de la medición de la absorbancia de los extractos coloreados procedentes del aceite de oliva, siendo el contenido fenólico expresado en equivalentes al ácido gálico (GAE). Esta técnica presenta la desventaja de necesitar largos tiempos de incubación que suponen una extensión del tiempo total de análisis.

La espectroscopia de fluorescencia o fluorometría es una técnica en la que las moléculas experimentan un proceso de emisión de radiación luminosa producido por una excitación previa a través de una radiación electromagnética, pasando de un estado vibracional excitado hasta el estado fundamental. Permite obtener mejores límites de detección, mayores intervalos de linealidad en la calibración y mejor selectividad que las técnicas fotométricas.

Basándonos en las propiedades fotoluminiscentes de los GQDs, se llevó a cabo el desarrollo de un sistema sensor para la determinación de polifenoles extraídos del aceite de oliva, a través del registro de la disminución de la fluorescencia (*quenching*) de las nanopartículas inducida por su interacción con los compuestos fenólicos.

En el desarrollo de esta investigación, el extracto del aceite de oliva, evaporado y reconstituido en metanol, se mezcló con un pequeño volumen de una disolución acuosa de GQDs, obtenida a partir de la pirólisis del ácido cítrico. Los analitos modelo, ácido gálico y oleuropeina fueron seleccionados como elementos representativos de la familia de los polifenoles del aceite de oliva. Poseen una estructura compuesta por anillos hexagonales que puede interaccionar con la estructura aromática de los GQDs a través de interacciones de tipo π–π. La determinación del índice de fenoles totales se estudió en distintas muestras de aceite de oliva.

Las metodologías descritas para la extracción de compuestos fenólicos en el aceite de oliva se basan principalmente en extracciones líquido–líquido (LLE) empleando grandes cantidades de disolventes orgánicos. Con el fin de evitar el elevado consumo de éstos, se llevó a cabo una reducción del volumen de muestra (correspondiente a 2 g de aceite) empleando finalmente 2.4 mL de

metanol y 7 mL de hexano entre la etapa de extracción de la fracción fenólica y la etapa de limpieza del extracto.

La extracción se fundamenta en la afinidad que experimentan los compuestos fenólicos polares del aceite de oliva hacia el disolvente orgánico polar usado para su extracción, de modo que éstos pasaran fácilmente a la fase extractante. Durante la extracción, las distintas fases fueron combinadas, con ayuda de un agitador vortex, con el fin de favorecer el paso de la fracción fenólica contenida en la fase apolar (compuesta por aceite y hexano) a la polar (formada por metanol y agua). A continuación se llevó a cabo su centrifugación para favorecer la separación de las fases. Tras la separación de éstas la fase polar fue extraída y la fase apolar fue sometida nuevamente al proceso de extracción. Los extractos metanólicos fueron combinados, calentados suavemente, evaporados bajo una corriente de nitrógeno y reconstituidos para su preconcentración en un volumen de 200 μL. El factor teórico de preconcentración obtenido fue de 10x.

Para el desarrollo de la etapa de detección, se emplearon 200 μL de una disolución de GQDs a pH 10. Además del pH, se estudiaron variables como el disolvente en el que se reconstituyó la fracción fenólica evaporada y la relación de volumen entre muestra y la disolución de NPs. De los disolventes estudiados, el metanol fue el seleccionado para llevar a cabo la reconstitución

del extracto evaporado pues fue el que proporcionó una respuesta rápida del sensor y una señal estable a lo largo del tiempo. La proporción 1/1 entre muestra y disolución de NPs fue seleccionada tras ser la que aportó un mayor quenching de la fluorescencia del GQDs. Una vez optimizadas todas las variables del procedimiento se estudió la influencia de la temperatura en el sistema (Figura IV.3.6), de modo que pudo concluirse que a pesar de que la fluorescencia de los GQDs aumentaba conforme disminuía la temperatura, no se detectaron cambios significativos en los niveles de quenching para las temperaturas estudiadas. El estudio de todas estas variables se realizó empleando disoluciones de ácido gálico a distintas concentraciones.

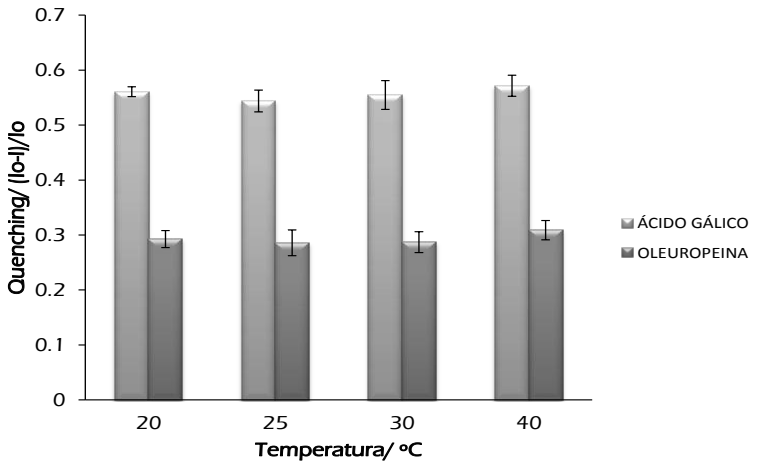

Figura IV.3.6. Estudio de la influencia de la temperatura sobre la sensibilidad del sensor de fenoles totales a través del estudio de los dos analitos modelo, ácido gálico y oleuropeína.

El mecanismo por el cual tiene lugar el quenching de la fluorescencia de los GQDs fue atribuido a la transferencia de carga entre analito y GQD cuando estos se unen para dar lugar a la formación de un complejo en el que los GQDs actúan como donadores y los fenoles como aceptores. La formación del complejo podría justificarse a través de la atracción que experimentan analito y NP mediante el establecimiento de interacciones π–π, dado el carácter aromático de ambos. Por otra parte, teniendo en cuenta el importante papel que juega el pH de la disolución de GQDs en el procedimiento de detección, afectando a los grupos funcionales, hay que contemplar la posibilidad de que, además, ocurran interacciones no covalentes, como puentes de hidrogeno, entre fenoles y GQDs. El mecanismo de transferencia de carga puede justificarse también a través del comportamiento observado con los distintos disolventes orgánicos, empleados en la etapa de optimización de variables, de modo que cuanto mayor es la polaridad del disolvente orgánico, mayor es la atenuación de la fluorescencia lograda, puesto que la transferencia de carga se encuentra más favorecida coincidiendo con los resultados obtenidos en otros trabajos científicos encontrados en la bibliografía en los que se atribuye una transferencia de carga más efectiva cuanto mayor es la polaridad del disolvente empleado.

El método analítico diseñado fue desarrollado a temperatura ambiente y no presentó requerimientos especiales, lo que supone la consecución de un

sistema sensor simple, de respuesta rápida y con una elevada sensibilidad que sirve para profundizar en el conocimiento sobre este derivado del grafeno dentro del ámbito de la Química Analítica. El aceite de oliva usado para la calibración fue aceite de oliva refinado, que se caracteriza por no contener compuestos fenólicos. Las muestras de este aceite fueron fortificadas con los estándares a distintos niveles de concentración. Los límites de detección logrados fueron de 90 y 120 $\mu g{\cdot}L^{-1}$ para ácido gálico y oleuropeína, respectivamente. La reproducibilidad del método y las recuperaciones obtenidas fueron aceptables. Su aplicación para la determinación del índice total de fenoles en aceite de oliva lampante (LOO), virgen (VOO) y virgen extra (EVOO), proporcionó resultados muy satisfactorios, siendo éstos bastante similares a los obtenidos empleando el método clásico Folin&Ciocalteu.

La figura IV.3.5 muestra un gráfico comparativo entre los niveles de fenoles totales determinados por el método propuesto y a través del Folin&Ciocalteu.

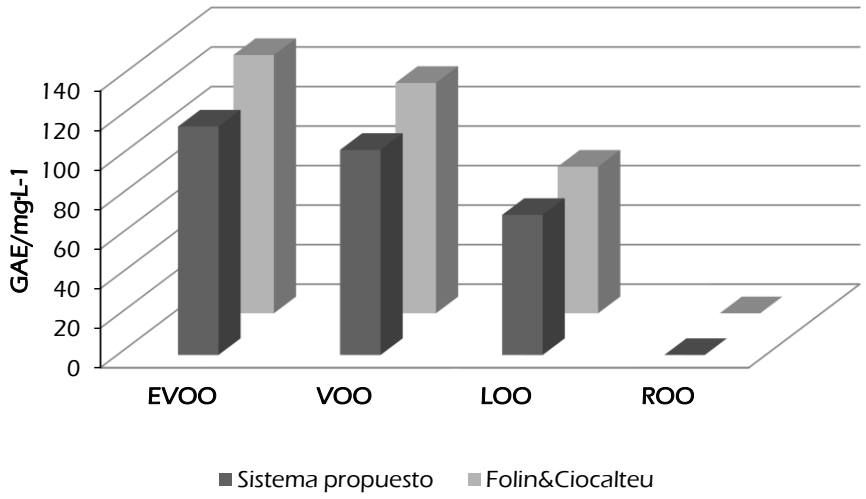

Figura IV.3.5. Comparación entre concentraciones encontradas en las muestras de aceite de oliva mediante el método propuesto y empleando el método clásico Folin&Ciocalteu.

IV. 4. EL GRAFENO Y DERIVADOS EN LA "TERCERA VIA" DE LA NANOCIENCIA Y NANOTECNOLOGÍA ANALÍTICAS

Desde la incorporación de las NPs a la N&NA, han sido dos las formas tradicionales en las que éstas han sido consideradas, bien siendo el objeto del análisis o bien actuando como herramienta en alguna etapa del proceso analítico, como ya hemos indicado en los apartados anteriores de este bloque.

En este apartado se aborda una nueva perspectiva de las NPs en la N&NA, siendo consideradas como analito y como herramienta de forma simultánea en el mismo procedimiento analítico. Las excepcionales características superficiales, reactividad qúimica y propiedades físicas de las NPs les permiten ser explotas de este modo. La Figura IV.4.1 muestra un esquema ilustrativo de los roles de las nanopartículas dentro del proceso analítico.

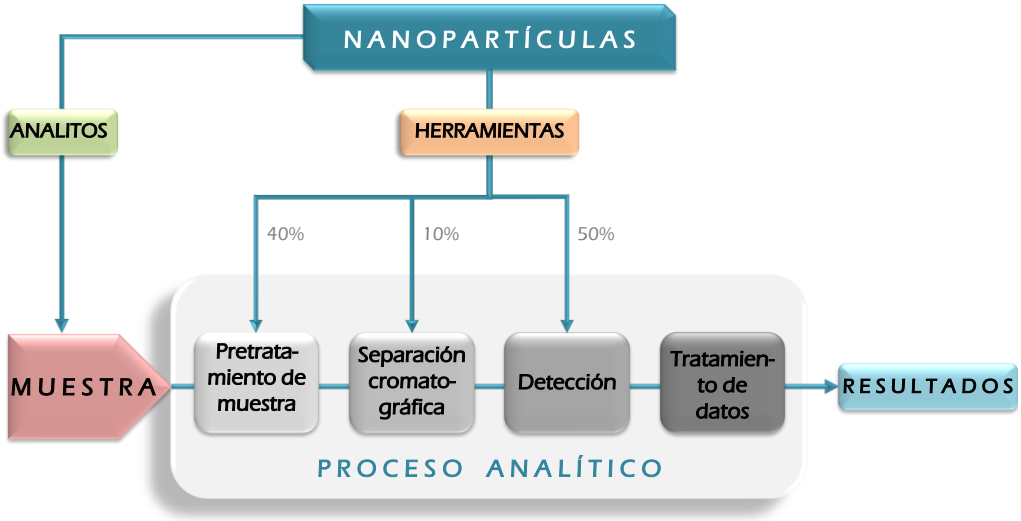

Figura IV.4.1. Esquema Ilustrativo de los roles de las NPs en el proceso analítico.

Los objetivos básicos que persigue esta "tercera vía" de la N&NA son, por una parte, mejorar las propiedades relacionadas con el procedimiento analítico (como son la sensibilidad y la selectividad) a través de los efectos sinérgicos surgidos de la combinación de NPs como herramienta y como analito, y por otra parte, abrir una nueva brecha en la N&NA como consecuencia de la necesidad de establecer nuevas metodologías apropiadas para la mejora de la caracterización y determinación de materiales nanoestructurados de origen artificial.

Esta implicación sinérgica de las NPs dentro del mismo procedimiento analítico hace que surjan diferentes clasificaciones de acuerdo a varios criterios:

- Diferencias entre ambas NPs.
- Papel desempeñado por cada NP.
- Técnica instrumental involucrada en el proceso analítico.
- NP consicerada como referencia.

Atendiendo al primer criterio, que es el que aplica en esta memoria, podemos encontrar:

- *NPs con la misma naturaleza*, como es el caso del capítulo 6, donde se emplean CNPs como analito y como herramienta, siendo además ambas derivados del grafeno.
- *NPs con distinta naturaleza*, como puede observarse en el capítulo 5, empleando NPs de óxidos metálicos como analito y CNPs como herramienta.

A continuación se describen detalladamente las dos estrategias desarrolladas dentro de este nuevo marco de la N&NA. En primer lugar se presentará el método desarrollado para la determinación de GO en muestras ambientales empleando GQDs como herramienta analítica, y a continuación

se detallarán los aspectos más relevantes del sistema sensor de nanopartículas de dióxido de titanio (TiO_2–NPs) basado en el empleo de GQDs, de nuevo como herramienta analítica. En la tabla IV.4.1 se resume brevemente el papel de las NP en cada trabajo experimental.

Tabla IV.4.1. Resumen de la función de las nanopartículas empleadas en los trabajos presentados en esta sección.

CAPÍTULO DE LA MEMORIA	NANOPARTÍCULAS *Herramienta*	NANOPARTÍCULAS *Analito*	MUESTRA
Capítulo 5	GQDs	TiO_2NPs	Cosméticos
Capítulo 6	GQDs	GO	Agua de río

IV.4.1. Determinación de GO en muestras ambientales

El creciente uso de los materiales nanoestructurados y su incorporación a procesos industriales y productos comerciales hacen que aparezcan nuevos problemas analíticos casa día.

El GO, que presenta una estructura compuesta por carbonos con hibridación sp^2 rodeados de carbonos sp^3 y numerosos frupos funcionales que

le confieren una elevada solubilidad y establidad en agua, podria ser considerado un potencial contaminante en las aguas naturales.

Tomando como base la estructura aromática que le confieren al GO los anillos hexagonales de átomo de carbono con hibridación sp^2, se desarrolló un sensor basado en GQDs para la detección de GO, anticipando la posible interacción de ambas NPs a través de enlaces de tipo π–π.

En el desarrollo de esta nueva metodología, el GO contenido en muestras de agua de rio fortificadas fue extraído y preconcentrado mediante el empleo de membranas de celulosa. Tras la etapa de pretratamiento de la muestra. La disolución de GO se puso en contacto con una de GQDs y el quenching de la fluorescencia de éstos últimos fue monitorizado para llevar a cabo la cuantificación de GO.

La etapa de extracción se llevo a cabo pasando un volumen de 5 mL de agua de rio que contenía GO a través de un sistema de filtración que empleaba una membrana de celulosa. El GO quedó retenido en la superficie del filtro, Para eliminar las posibles interferencias de la materia orgánica se pasó un pequeño volumen de NaOH seguido de agua y, a continuación, la membrana se introdujo en 200 μL de agua y se aplicaron ultrasonidos para conseguir la liberación del GO del filtro, logrando una preconcentración teórica de 25 veces. Además del volumen de filtración y elución, del tipo de

membrana y de las condiciones de ultrasonicación, se optimizaron variables como el tamaño del poro de la membrana, eligiendo el 0.2μm para asegurar una completa retención del GO, las condiciones de vacío y la velocidad con la que la muestra fue depositada sobre el sistema de filtración.

En la etapa de detección se emplearon 200 μL de una disolución concentrada de GQDs a pH 7. En la Figura IV.4.2 puede apreciarse el comportamiento de la fluorescencia de los GQDs en presencia de GO en función del pH del medio.

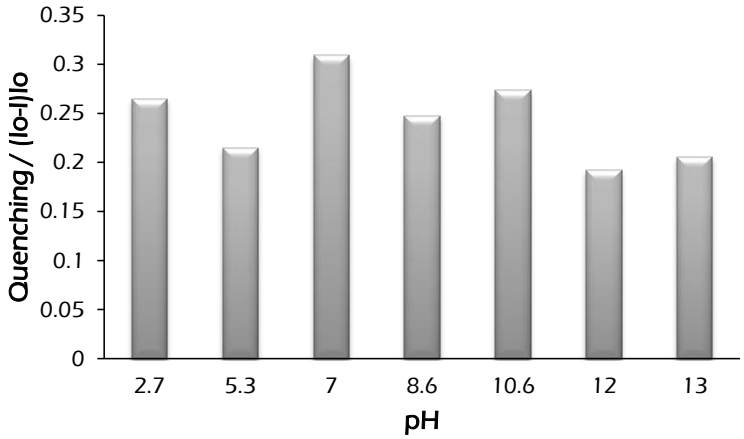

Figura IV.4.2. Comportamiento del quenching de los GQDs en función del pH y en presencia de GO.

Además se optimizaron las variables siguientes: influencia del disolvente en el que se recuperó el GO, seleccionando finalmente agua; Tiempo necesario para la reacción entre ambos tipos de NPs, y dilución de GQDs empleada para el desarrollo del sensor. La figura IV.4.3 muestra la evolución en la señal con respecto al tiempo de reacción estudiado. Para el estudio de todas las variables optimizadas se emplearon disoluciones de GO en agua ultrapura a distintos niveles de concentración.

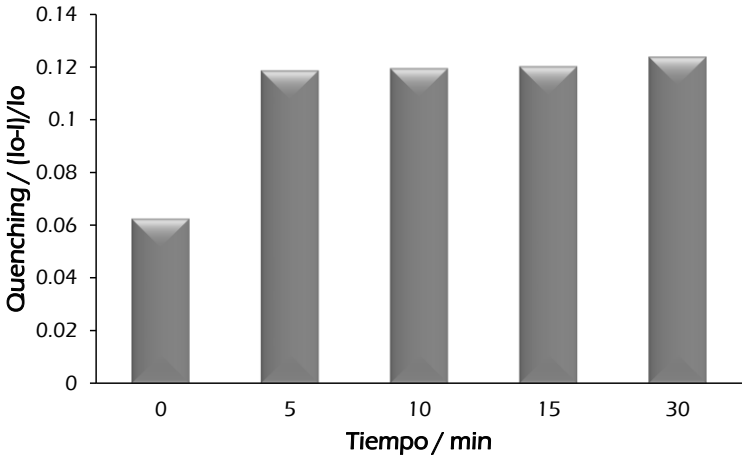

Figura IV.4.3. Evolución del quenching producido por el GO sobre la fluorescencia de los GQDs con respecto al tiempo de reacción. Cinco minutos fueron seleccionados como tiempo de reacción, considerándolos suficientes para obtener una señal estable y reproducible.

Como adelantábamos en apartados anteriores, los abundantes grupos funcionales solamente presentes en el borde de los GQDs le confieren una excelencte solubilidad en agua así como un plano hidrofóbico que les permite interaccionar con la superficie del GO a través de fuerzas de tipo π–π, causando la atenuación de la fluorescencia de los GQDs, que fue empleada como señal analítica en la determinación de GO.

El método propuesto perimió detectar niveles de GO de 35$\mu g \cdot L^{-1}$. La reproducibilidad del método expresada como RDS alcanzó niveles aceptables. El método fue aplicado con éxito a la determinación de GO en agua de rio, obteniendo valores de recuperación comprendidos entre 83.7% y 108.2%.

IV.4.2. Funcionalización de los puntos cuánticos de grafeno como estrategia hacia la mejora de la sensibilidad

La funcionalización de las estructuras de grafeno ha sido un ítem ampliamente estudiado que ha permitido modular las propiedades de estas nanoestructuras. En lo que a los GQDs se refiere, la funcionalización y el dopaje, con moléculas y átomos específicos, ha supuesto un incremento de su rendimiento cuántico (que por lo general es bajo) y el establecimiento de interacciones más especificas entre la molécula diana y los GQDs.

Con el desarrollo de la Nanotecnología, una gran variedad de nanomateriales son aplicados en procesos industriales y productos comerciales de distinto tipo. La incorporación de nanopartículas de dióxido de titanio (TiO_2NPs) a cremas solares es una práctica muy extendida en la actualidad, actuando estas como blanqueante y filtro UV para la piel, gracias al elevado índice de refracción que presentan estas nanopartículas. Pueden llegar a constituir hasta el 25% de la composición de la crema. Actualmente existe cierta controversia entre su peligrosidad sobre la salud humana, habiendo sido catalogados como posibles carcinógenos dentro del grupo 2B por la Agencia Internacional de Investigación contra el Cáncer (IARC). Estas nanopartículas pueden causar daño oxidativo en el ADN, propiciando el desarrollo de cáncer de piel.

Las hipótesis iniciales para el desarrollo de un sistema capaz de detectar TiO_2NPs se basaron en el empleo de GQDs sin modificar, pero la sensibilidad de estos puntos cuánticos hacia las TiO_2NPs resultó ser bastante limitada. Con el fin de conseguir una interacción especifica entre NPs diana y NPs sensores, los GQDs fueron funcionalizados y usados para el desarrollo del sistema de detección.

En el desarrollo experimental de esta investigación, las TiO_2NPs fueron extraídas de distintas cremas solares, y preconcentradas antes de ser puestas en contacto con un pequeño volumen de la disolución de GQDs

funcionalizados. TiO_2NPs comerciales fueron usadas para enriquecer una crema solar que no las contenía, para la optimización y calibración del método analítico planteado.

Para la extracción de las TiO_2NPs se optó por una LLE basada en el empleo de disolventes orgánicos como metanol y n–hexano. Siguiendo el mismo criterio que en el caso de la extracción de la fracción fenólica de los aceites de oliva, el volumen de muestra fue reducido al máximo (0.1g) con el fin de diseñar una extracción más sostenible, empleando unos volúmenes finales de metanol y n–hexano de 2 y 4mL, respectivamente.

En la etapa de separación de las TiO_2NPs de la crema solar, se optó por una LLE asistida por ultrasonidos. Para la etapa de limpieza del extracto se empleó n–hexano que fue mezclado con el extracto de forma manual. Los extractos con las TiO_2NPs se evaporaron bajo una corriente de nitrógeno a 70ºC para favorecer la evaporación. Finalmente fueron reconstituidos en 200 μL de metanol.

En el desarrollo del sensor se emplearon 100 μL de una disolución cuatro veces diluida de GQDs funcionalizados con glicina (gly–GQDs), que se pusieron en contacto con el extracto reconstituido de TiO_2NPs. En la Figura IV.4.4 puede apreciarse el efecto de la presencia de TiO_2NPs sobre la fluorescencia de los gly–GQDs. Se estudiaron variables como el tipo de

nanomaterial fluorescente, el tipo de disolvente para la reconstitución de las TiO_2NPs, el pH de la disolución de gly–GQDs y la concentración de la misma. De los nanomateriales fluorescentes sintetizados solamente los gly–GQDs mostraron ser sensibles a la presencia de nanopartículas de dióxido de titanio. Estas NPs dispersadas en agua ultrapura mostraron una mejor respuesta, en términos de quenching de la fluorescencia de los gly–GQDs, que el resto de disolventes orgánicos estudiados. Sin embargo, el tiempo necesario para alcanzar un valor estable de la señal analítica fue muy largo. El metanol fue seleccionado el disolvente más adecuado en una situación de compromiso entre una sensibilidad aceptable y una respuesta rápida del sensor. El pH de la disolución de gly–GQDs al cual se observó mejor respuesta fue el pH obtenido tras la síntesis. En cuando a la relación entre GQDs funcionalizados (diluidos 4 veces) y muestra se optó por utilizar un ratio de 1:2. En la optimización de estas variables se emplearon dispersiones de TiO_2NPs comerciales que no fueron sometidas al procedimiento de extracción.

En un intento de aclarar el mecanismo por el cual las TiO_2NPs producen la atenuación de la fluorescencia de los gly–GQDs, se atribuyó la interacción entre ambas a la presencia de los aminoácidos. En este modelo, las distintas partes de de los aminoácidos podrían interactuar con la superficie de las TiO_2NPs, de modo que los ácidos carbónicos simples formarían dos enlaces equivalentes entre el oxígeno del grupo carboxilo y los átomos de Ti, mientras

que el protón ácido se disociaría y se uniría a un puente de oxígeno. Por lo tanto, la adhesión a los aminoácidos puede producirse por interacciones de tipo electrostático o puentes de de hidrógeno.

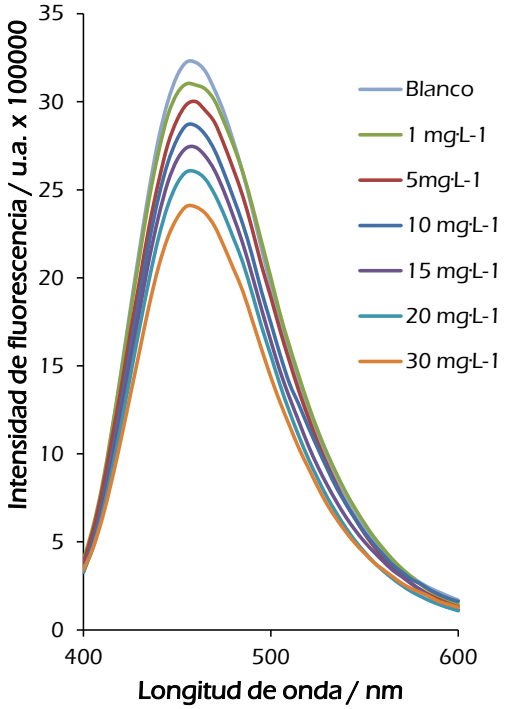

Figura IV.4.4. Efecto de diferentes concentraciones de TiO_2NPs sobre la fluorescencia de los GQDs funcionalizados con glicina.

Para la calibración del método analítico diseñado se utilizaron muestras de cremas solares de bajo nivel de protección que no contenían NPs, que fueron

fortificadas con diferentes cantidades de TiO_2NPs. El método alcanzó unos límites de detección de 1.4 $\mu g \cdot g^{-1}$, con unos valores de precisión (expresados en términos de RSD) y unas recuperaciones bastante aceptables. La metodología desarrollada se aplicó a la determinación de TiO_2NPs en cremas comerciales de distinto factor de protección que las contenían. Los valores hallados se encontraron dentro de los rangos reportados por otros trabajos de investigación que emplean técnicas como fraccionamiento de flujo de campo de plasma inducido acoplado a espectrometría de masas. Por lo tanto puede afirmarse que el sistema sensor desarrollado es adecuado para la determinación de TiO_2NPs de una forma simple, ofreciendo una respuesta rápida, además de una elevada sensibilidad, siendo sostenible con el medio ambiente.

IV.5. MUESTRAS Y ANALITOS EN LOS PROCESOS ANALITICOS DESCRITOS EN LA MEMORIA

A modo recopilatorio se resumen los pares analito-muestra que se han considerado. Así se han involucrado una serie de analitos determinados en matrices de muy diversa naturaleza. La Figura IV.5.1 muestra la relación de sustancias empleadas y la matriz donde se han determinado.

Figura IV.5.1. Analitos y muestras empleados durante el desarrollo experimental de la presente Tesis doctoral.

CONCLUSIONES

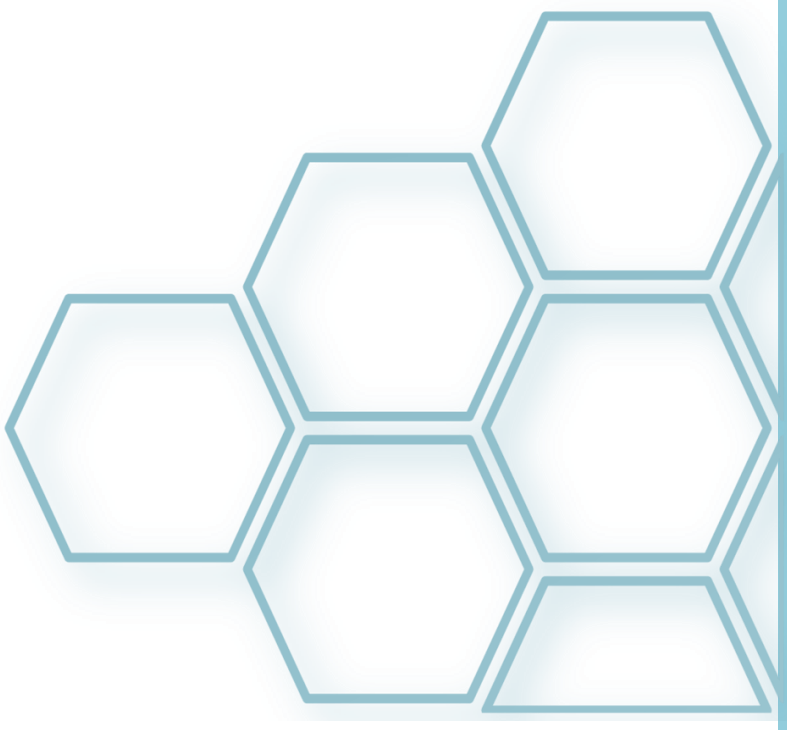

La investigación realizada en la presente Tesis Doctoral se ha centrado en el desarrollo de nuevas estrategias donde el grafeno ha sido explotado como herramienta para la mejora de procesos analíticos. Así mismo, la consideración del grafeno sus derivados como objeto de análisis ha sido uno de los ejes principales de esta Tesis, surgiendo durante la realización de la misma, y derivado de la consideración de estos nanomateriales desde el punto de vista de las dos facetas tradicionales de la N&NA, una nueva perspectiva o "tercera vía" en la que se han desarrollado procedimientos basados en el empleo de NPs derivadas del grafeno para determinar otras NPs. Siguiendo esta clasificación, las conclusiones principales de cada uno de las facetas estudiadas se recogen a continuación.

Derivados de grafeno como objeto de análisis

Los aspectos más relevantes de esta Tesis Doctoral en este sentido han sido los siguientes:

- La consideración de los puntos cuánticos de grafeno como analitos ha permitido desarrollar por primera vez un método simple, rápido y sensible para su determinación en muestras de agua basada en la emisión fluorescente de estas nanopartículas.

- La fuerte interacción de éstos con el sorbente empleado permitió la cuantificación de los mismos, a través de una estrategia sostenible, desarrollada en medio acuoso, con un consumo ínfimo de disolventes orgánicos.

Grafeno como herramienta para la mejora de procesos analíticos

Las principales aportaciones en el empleo de nanomateriales grafénicos como herramientas analíticas involucradas en procesos analíticos son aquellas que implican tres técnicas instrumentales: la electroforesis capilar, la espectroscopia Raman y la fluorimetria, tal como se comenta a continuación:

- Electroforesis capilar.
  - Ha sido evaluado por primera vez rol de las nanoláminas de grafeno como fase pseudoestacionaria en el marco de las separaciones electroforéticos La introducción de estas hojas ultrafinas junto al electrolito de separación condujo a la interacción de estas con los analitos, mejorando la resolución de picos solapados, consiguiendo la perfecta separación de todos ellos.

  - La capacidad de las láminas de grafeno para mejorar la sensibilidad de la técnica fue investigada añadiendo un pequeño

segmento de éstas como pseudofase tras la inyección de la muestra, consiguiendo picos más estrechos y bien definidos.

- Así mismo, el papel del número de láminas de grafeno en la fase pseudoestacionaria fue evaluado. Se consiguieron mejores resultados empleando la dispersión de grafeno que contenía una mayor proporción de monocapas y bicapas, a pesar de que la cantidad de grafeno empleada fue menor. Sin embargo, el tratamiento con ultrasonidos del electrolito modificado con el grafeno de mayor proporción de láminas agregadas permitió su uso como pseudofase de forma satisfactoria, con la ventaja económica que ello supone.

- El procedimiento analítico desarrollado fue muy simple y permitió la separación de cinco compuestos farmacéuticos mediante el empleo de 1.25 $mg{\cdot}L^{-1}$ de grafeno.

- Espectroscopia Raman

  - La capacidad de las multicapas de grafeno para mejorar la sensibilidad en técnicas como la espectroscopia Raman quedó demostrada a través de la creación de un sustrato híbrido formado por grafeno y AuNPs.

- El efecto SERS conseguido con dicho sustrato hibrido alcanzó factores de incremento de la señal de unas 4400 veces y unos valores de reproducibilidad buenos teniendo en cuenta que éste es el principal factor que limita la técnica para ser empleada en análisis cuantitativo.

- El sustrato híbrido desarrollado pudo ser reutilizado 4 veces con una reproducibilidad aceptable.

- El método analítico propuesto permitió la determinación de metronidazol a bajos niveles de concentración sin la necesidad de introducir una etapa previa de tratamiento de muestra.

- <u>Fluorimetría</u>

  - Se demostró la capacidad de los puntos cuánticos de grafeno para actuar como nanosensores fluorescentes permitiendo la detección de la fracción fenólica contenida en aceites de oliva de distintas calidades calidades.

  - Con la introducción de una etapa de preconcentración los niveles detectados fueron comparables con los niveles obtenidos por métodos tradicionales.

Derivados del grafeno en la "tercera vía" de la Nanociencia y Nanotecnología Analíticas

Dentro de esta nueva perspectiva de la N&NA las principales aportaciones han sido las que se resumen a continuación:

- La consideración de los puntos cuánticos de grafeno desde dos perspectivas completamente opuestas, como son su consideración como analito y su empleo como herramienta han dejado patente que el comportamiento y las propiedades fluorescentes de éstos dependen en gran medida del pH del medio y de la concentración de nanopartículas en la disolución.

- El desarrollo de sistemas sensores que emplean como base los puntos cuánticos de grafeno ha permitido la determinación de otras nanopartículas, con la misma naturaleza (GO) y con naturaleza diferente (TiO_2NPs). A la del material sensor.

- La preconcentración de las nanopartículas ha sido un factor importante en ambos casos con el fin de mejorar la sensibilidad.

- Se ha podido demostrar que la funcionalización de los puntos cuánticos de grafeno abre una nueva estrategia hacia la mejora de la selectividad.

- La transferencia de energía ha sido el mecanismo atribuido en el caso de los sensores de puntos cuánticos de grafeno, produciéndose las interacciones entre este sensor y analitos bien por interacciones de tipo π–π, bien por interacciones hidrofóbicas.

- Se han validado casi todas las metodologías propuestas en esta Memoria Doctoral al aplicarlas a muestras reales de diferente naturaleza como matrices medioambientales, agroalimentarias y cosméticas, obteniendo unos buenos resultados.

AUTOEVALUACIÓN CIENTÍFICA

de la Tesis Doctoral

La experiencia adquirida a lo largo de la etapa formativa de esta Tesis Doctoral ha permitido evaluar de forma objetiva el trabajo presentado en esta Memoria. Además de las aportaciones más relevantes que se ponían de manifiesto en el apartado anterior (como el desarrollo de nuevos métodos analíticos, simples, precisos y aplicables, el empleo de metodologías de extracción y preconcentración sencillas, el uso de procedimiento de síntesis de nanomateriales reproducibles, rápidos y económicos, y el bajo consumo global de disolventes orgánicos) también se ha llevado a cabo una evaluación critica. En esta autoevaluación se han tenido en cuenta las carencias y dificultades encontradas a lo largo del periodo experimental, con el fin de planificar futuras investigaciones en este sentido.

A continuación se presentan las principales limitaciones de la investigación desarrollada:

- Los métodos analíticos desarrollados, en dos de los casos presentados (como. El empleo de nanoláminas de grafeno como fase pseudoestacionaria y la utilización de multicapas de grafeno como sustrato híbrido en SERS), no fueron aplicados a muestras reales, por lo que sería conveniente llevar a cabo estudios en matrices complejas.

- Así mismo, en algunos procedimientos desarrollados se llevó a cabo la determinación de un único analito. La ampliación del número de

moléculas diana permitiría en estos casos la consecución de metodologías más universales.

- Los límites de detección podrían haberse mejorado, en algunos casos, introduciendo una etapa de tratamiento de muestra que condujera a su preconcentración y en otros añadiendo una etapa de evaporación o un método de preconcentración más eficaz al empleado. Sin embargo, se optó por priorizar la simplicidad del método propuesto.

- Los límites de detección de nanopartículas derivadas del grafeno estuvieron siempre en niveles del orden de los $\mu g \cdot L^{-1}$ mientras que las predicciones teóricas sitúan estos valores en el rango de $ng \cdot L^{-1}$, en el caso de nanopartículas de carbono en muestras ambientales.

- La reutilización de los cartuchos de SPE en el caso dela determinación de puntos cuánticos de grafeno en muestras de agua, fue estudiada sin éxito, habiéndose conseguido una reducción de los costes del análisis de haberse logrado resultados favorables en este sentido.

- Los factores de preconcentración obtenidos podrían haberse implementado mejorando alguna etapa del proceso analítico.

- En el caso de la detección SERS se podría haber logrado un mayor incremento de la señal Raman si la longitud de onda del láser

empleado hubiese entrado en resonancia con el plasmón superficial de las AuNPs. Sin embargo, pruebas realizadas demostraron que a una longitud de onda de excitación del laser de 532 nm se producían una gran cantidad de interferencias en los espectros por efecto de la fluorescencia generada.

- Las técnicas de caracterización de nanomateriales se centraron en el empleo de técnicas microscópicas (HRTEM, TEM, SEM), así como en FT–MIR y medidas de absorbancia en la región UV/vis. El empleo de otras técnicas complementarias como la espectroscopia Raman, la dispersión de la luz dinámica (DLS, que proporciona información sobre el tamaño hidrodinámico de las nanopartículas y coloides en medio líquido) y la espectroscopia fotoelectrónica de rayos X (XPS, que aporta información cualitativa y cuantitativa de todos los elementos presentes en una superficie a excepción de H y He, permitiendo la obtención de información detallada de la química, organización y morfología de una superficie) habría resultado más interesante esta Tesis Doctoral.

Anexos

Producción Científica

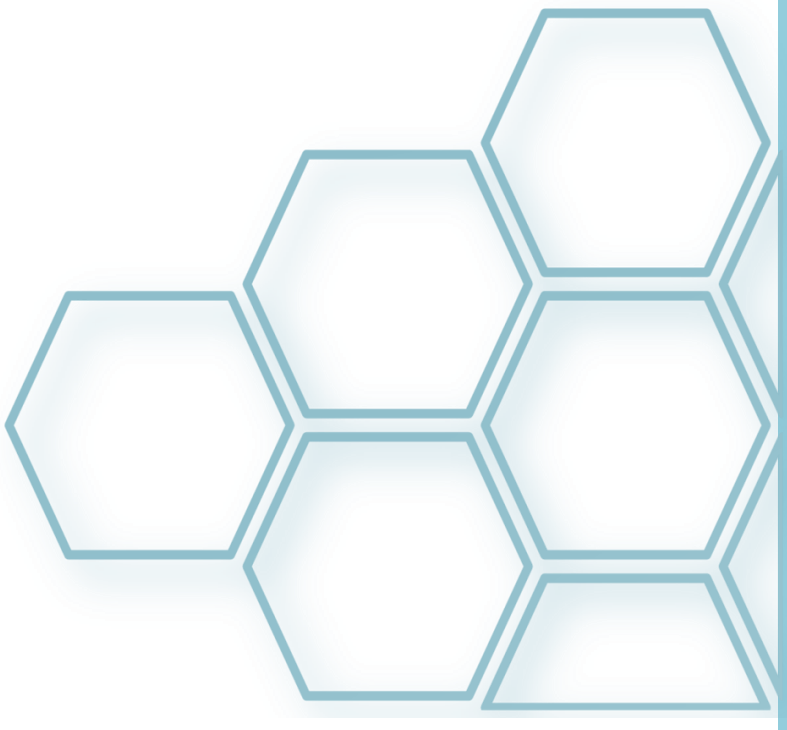

Anexo A

Publicaciones científicas derivadas de la Tesis Doctoral

1. **Graphene nanoparticles as Pseudostationary Phase for the Electrokinetic Separation of Non-Steroidal Anti-Inflammatory Drugs.**

   Sandra Benítez-Martínez, Bartolomé M. Simonet, Miguel Valcárcel

   Electrophoresis 34 (2013) 2561–2567.

2. **Graphene Quantum Dots as Sensor for Phenols in Olive Oil.**

   Sandra Benítez-Martínez, Miguel Valcárcel.

   Sensors and Actuators B 197 (2014) 350–357.

3. **Graphene Quantum Dots Sensor for the Determination of Graphene Oxide in Environmental Water Samples.**

   Sandra Benítez-Martínez, Ángela Inmaculada López-Lorente, Miguel Valcárcel.

   Analytical Chemistry 86 (2014) 12279–12284.

4. **Multilayer Graphene–Gold Nanoparticles hybrid substrate for the SERS determination of metronidazole**

   Sandra Benítez-Martínez, Ángela Inmaculada López-Lorente, Miguel Valcárcel.

   Microchemical Journal.DOI: 10.1016/j.microc.2015.01.006

5. **Fluorescent determination of graphene quantum dots in water samples.**

   Sandra Benítez–Martínez, Miguel Valcárcel.

   En revisión en la revista Analytica Chimica Acta.

6. **Glycine-functionalized graphene quantum dots based fluorescence sensor for the direct determination of TiO_2 nanoparticles.**

   Sandra Benítez-Martínez, Ángela Inmaculada López-Lorente, Miguel Valcárcel.

   En revisión en la revista Analytical Chemistry.

7. **Graphene Quantum Dots in Analytical Science.**

   Sandra Benítez–Martínez, Miguel Valcárcel.

   En revisión en la revista Trends in Analytical Chemistry.

Anexo B

Presentación de comunicaciones a congresos

Comunicaciones orales y posters

1. Comunicación flash y póster

   "Nanoláminas de grafeno como fase pseudoestacionaria en electrocromatografía".

   S. Benítez-Martínez, B.M. Simonet, M. Valcárcel.

   V Workshop Nanociencia y Nanotecnología Analíticas, Toledo (España), Julio–2011.

2. Póster.

   "Electrokinetic Separation of Non-Steroidal Antiinflamatory Drugs by Using Graphene Nanoparticles as Pseudostationary Phase"

   S. Benítez-Martínez, B.M. Simonet, M. Valcárcel

   III Encuentro sobre Nanociencia y Nanotecnología de Investigadores y Tecnólogos Andaluces (NanoUCO), Córdoba (España), Febrero–2011.

3. Póster.

   "Mezclas De Grafeno y Nanopartículas de Oro como Sustrato para SERS".

   Sandra Benítez-Martínez, Bartolomé M. Simonet, Miguel Valcárcel.

   XXIII Reunión Nacional-VII Congreso Ibérico de Espectroscopia, Córdoba (España), Septiembre-2012.

4. Póster.

   "Sustrato Híbrido de Grafeno y Nanopartículas de Oro en Espectroscopia Raman por Amplificación de Superficies (SERS)"

   Sandra Benítez-Martínez, Bartolomé M. Simonet, Miguel Valcárcel.

   IV Encuentro sobre Nanociencia y Nanotecnología de Investigadores y Tecnólogos Andaluces (NanoUCO), Córdoba (España), Febrero–2013.

5. Póster.

   "Graphene Ouantum Dots as Sensor of Phenols from Olive Oil".

   Sandra Benítez-Martínez, Miguel Valcárcel.

   VI Workshop Nanociencia y Nanotecnología Analíticas, Alcalá de Henares (España), Julio–2013.

6. Póster.

   "Total phenols in olive oil sensor based on graphene quantum dots".

   Sandra Benítez-Martínez, Miguel Valcárcel.

   Trends in Nanotechnology International Conference (TNT2013), Sevilla (España), Septiembre-2013.

7. Póster.

"Graphene Quantum Dots sensor for the determination of Graphene Oxide in environmental water samples".

Sandra Benítez-Martínez, A.I. López–Lorente, Miguel Valcárcel.

V Encuentro sobre Nanociencia y Nanotecnología de Investigadores y Tecnólogos Andaluces (NanoUCO)

Anexo C

Pósters

ELECTROKINETIC SEPARATION OF NON-STEROIDAL ANTIINFLAMATORY DRUGS BY USING GRAPHENE NANOPARTICLES AS PSEUDOSTATIONARY PHASE

S. Benítez-Martínez, **B.M. Simonet, M. Valcárcel**
Departamento de Química Analítica, Universidad de Córdoba
Edificio Anexo C3, Campus de Rabanales, 14071Córdoba.
E-mail: ga1meobj@uco.es

Since the development of the capillary electrophoresis several pseudostationary phases (PSPs) have been described in order to improve resolution. Recently, the use of carbon nanoparticles (CNP) has supposed many benefits in this field thanks to their properties.
Graphene is a flat monolayer of carbon atoms tightly packed into a two-dimensional (2D) honeycomb lattice. One of the factors that makes graphene so attractive is its low energy dynamics of electrons with atomic thickness. It is a semiconductor with zero band gap and high carrier mobility and concentration and shows nearly ballistic transport at room temperature. These unusually electronic properties make graphene one of the most promising candidate materials for future nanoelectronic applications.

OBJETIVE: to study the advantages of the use of graphene as pseudostationary phase in EKC separations

TYPES OF GRAPHENE USED IN THIS WORK

GRAPHENE	Type 1	Type 2
Single Layer Content	27%	6%
Double Layer Content	48%	23%
Triple Layer Content	20%	27%
4+ Layer Content	5%	44%

GENERAL PROPERTIES OF GRAPHENE

-High thermal and electrical conductivity.
-High elasticity and hardness.
-High resistivity.
-High resistance.
-Light.
-Supports ionizing radiation.
-Metallic behavior. Graphene behaves as surface gap semiconductor or semimetal of small overlap.
-Pronounced ambipolar electric field effect.
-Quantum Hall effect, whereby the conductivity perpendicular to the current takes discrete values, or quantized. Quantization implies that the conductivity of graphene can never be zero.
-Klein paradox. The probability of electron transmission is always equal to 1.
-Low Joule effect.
-Electrons move on graphene like Dirac fermions.
-Very dense and almost transparent . Not even the helium atom can pass through it.

ANALYTES: NON-STEROIDAL AINTI-INFLAMAMATORY DRUG

1. Fenbufen
2. Ibuprofen
3. Naproxen
4. Ketoprofen
5. Flurbiprofen

Derivates of Arylpropyl Group

EXPERIMENTAL

Graphene were obtained from a commercial source as dispersion in 2% (w/v) of sodium cholate.
Comparisons were performed using a BGE: $AcNH_4$ 50 mM pH = 4.0 + 6.25 ppm graphene
Detection: λ = 210 nm Sample injection: 10 s at 50 mbar
Voltage: 15 KV

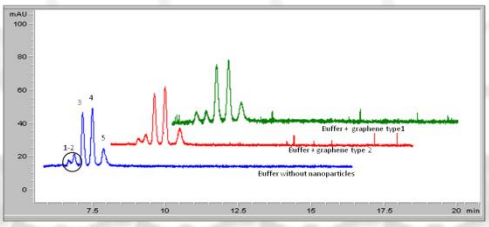

BGE: $AcNH_4$ 50 mM pH = 4.0

EFFECT OF NP's CONCENTRATION

Major quantity of graphene in the buffer produce better separation of peaks, but also higher migration times.

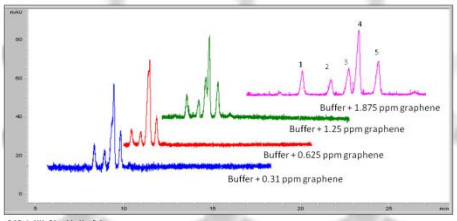

BGE: $AcNH_4$ 50 mM pH = 5.0
GRAPHENE TYPE 2

pH EFFECT

In this study we found that a low pH in the modify buffer produces an erlier electrophoretic separation of analytes for both graphene types.

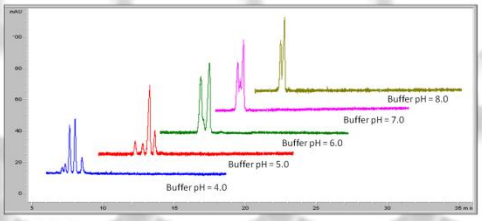

BGE: $AcNH_4$ 50 mM
GRAPHENE TYPE 2

ANALYTICAL FEATURES

ANALYTE	FENBUFEN		IBUPROFEN		NAPROXEN		KETOPROFEN		FLURBIPROFEN	
GRAPHENE	Type1	Type2	Type1	Type2	Type1	Type2	Type1	Type2	Type1	Type2
SLOPE	0.652	1.2929	6.9989	8.7746	18.116	21.09	15.396	18.447	18.111	23.806
INTERCEPT	27.098	30.794	5.4742	10.257	-2.0808	11.558	-1.1615	2.6081	14.889	5.3142
EQUIPMENT REPEATABILITY (RSD%)	6.62	0.85	8.64	6.83	5.99	8.87	10.68	8.48	13.87	10.61

CONCLUSIONS

•Graphene has a great potential to improve separation of organic compound such as non-steroidal anti-inflammatory drugs derivates of arylpropyl group.
•The highest resolution and low migration time were obtained with individual graphene sheets.
•The migration time increase when increasing the number of graphene sheets in the nanoparticle.
•Compared with other nanoparticles, graphene allows higher resolution enhancement and they are more soluble and easy to prepare.

NANOLÁMINAS DE GRAFENO COMO FASE PSEUDOESTACIONARIA EN ELECTROCROMATOGRAFIA

S. Benítez-Martínez, B.M. Simonet, M. Valcárcel
Departamento de Química Analítica, Universidad de Córdoba
Edificio Anexo C3, Campus de Rabanales, 14071Córdoba.
E-mail: qa1meobj@uco.es

V Workshop NyNA 2@11

Desde el desarrollo de la electroforesis capilar han sido muchas las fases pseudoestacionarias que se han utilizado con el fin de mejorar la resolución de las separaciones. En este campo se han ensayado un gran numero de nanoparticulas entre las que destacan las de carbono.
En los últimos años el grafeno ha despertado un gran interés en la comunidad científica, sobre todo desde la concesión del Premio Nobel en Física 2010 a los investigadores Andre Geim y Konstantin Novoselov por sus trabajos sobre este nanomaterial.
El grafeno está compuesto por átomos de carbono con hibridación sp^2 en la que lo átomos se distribuyen en una red con forma de panal de abeja con una nube de electrones deslocalizada sobre su superficie. Posee de 1 – 10 láminas. Presenta excepcionales propiedades ópticas, magnéticas, térmicas y mecánicas.

OBJETIVOS

- Evaluar el empleo de grafeno como fase pseudoestacionaria
- Evaluar la forma de preparar el buffer de separación
- DESARROLLAR UN MÉTODO FIABLE PARA LA DETERMINACIÓN DE AINEs

TIPOS DE NANOLÁMINAS EMPLEADAS

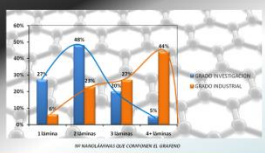

ANALITOS

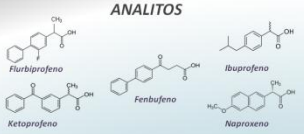

EXPERIMENTAL

1. Separación de los AINE's empleando Buffer AcNH4 50 mM a diferentes pH's → pH óptimo = 4.0 → El SC por si sólo no es capaz de separar los picos → 2. Estudio de la concentración de colato en el buffer

3. Estudio de la concentración óptima de nanoláminas de grafeno → $[grafeno]_{optimo} = 1.875\ mg{\cdot}L^{-1}$ → Se recomienda DISPERSIÓN EN ULTRASONIDOS → 4. Separación de los AINE's empleando Buffer Ac NH4 50 mM pH = 4.0 modificado con nanoláminas de grafeno disperso en ultrasonidos

RESULTADOS MÁS RELEVANTES

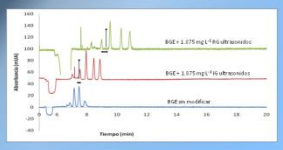

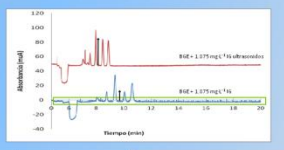

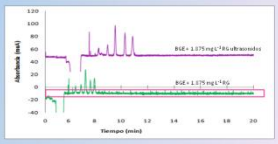

BGE: AcNH4 50 mM pH=4.0
IG: grafeno en grado de industrial
RG: grafeno en grado de investigacion
SC: colato de sodio

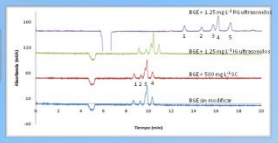

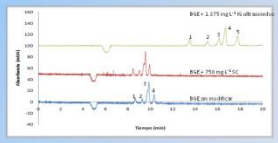

CONDICIONES EXPERIMENTALES	
Tiempo Inyección	10s muestra 2s buffer
Presión Inyección	50 mbar
Longitud del Capilar	48 cm
Voltaje	+15 KV
Temperatura	25 ºC

PROPIEDADES ANALÍTICAS

	LOD ($mg{\cdot}L^{-1}$)	LOQ ($mg{\cdot}L^{-1}$)	R^2	% RSD ÁREA PICO 10 $mg{\cdot}L^{-1}$	% RSD ÁREA PICO 20 $mg{\cdot}L^{-1}$	% RSD TIEMPO MIGRACIÓN 10 $mg{\cdot}L^{-1}$	% RSD TIEMPO MIGRACIÓN 20 $mg{\cdot}L^{-1}$
AcNH4 50 mM pH = 4.0							
Fenbufeno	1,32	4,39	0,9969	4,84	8,79	7,29	9,15
Ibuprofeno	1,99	6,65	0,9947	0,77	2,04	1,11	0,91
Naproxeno	2,37	7,92	0,9971	4,29	2,19	4,99	2,34
Flurbiprofeno	2,63	8,76	0,9928	2,91	7,47	1,33	1,46
Ketoprofeno	1,10	3,68	0,9987	1,67	2,35	0,60	0,70
AcNH4 50 mM pH = 4.0 + 1.875 mg·L⁻¹ grafeno IG							
Fenbufen	1,96	6,53	0,9982	7,21	5,82	1,94	4,68
Ibuprofen	0,68	2,27	0,9995	7,08	5,88	2,00	4,97
Naproxen	0,36	1,21	0,9997	7,46	9,04	2,49	5,38
Flurbiprofen	0,36	1,2	0,9999	7,74	8,58	2,61	5,78
Ketoprofen	0,19	0,63	0,9998	9,3	10,85	2,85	6,21
AcNH4 50 mM pH = 4.0 + 1.875 mg·L⁻¹ grafeno IG dispersado en ULTRASONIDOS							
Fenbufen	0,94	3,14	0,9980	6,41	8,68	1,35	1,20
Ibuprofen	0,56	1,88	0,9997	6,05	3,3	1,41	1,18
Naproxen	0,22	0,73	0,9999	3,18	3,82	1,47	1,32
Flurbiprofen	0,29	0,96	0,9999	4,66	1,97	1,64	1,40
Ketoprofen	0,19	0,63	0,9999	2,76	0,75	1,49	1,39
AcNH4 50 mM pH = 4.0 + 1.875 mg·L⁻¹ grafeno RG							
Fenbufen	1,12	3,73	0,9993	2,25	11,33	1,14	0,88
Ibuprofen	0,91	3,04	0,9995	1,08	4,65	1,00	0,29
Naproxen	2,21	7,37	0,9972	1,94	2,71	1,06	0,28
Flurbiprofen	0,71	2,38	0,9995	5,01	3,39	1,12	0,24
Ketoprofen	0,59	1,98	0,9996	10,04	4,01	1,09	1,26
AcNH4 50 mM pH = 4.0 + 1.875 mg·L⁻¹ grafeno RG dispersado en ULTRASONIDOS							
Fenbufen	7,23	24,1	0,9940	5,29	5,61	3,62	1,19
Ibuprofen	1,86	6,19	0,9967	6,82	4,21	3,77	0,77
Naproxen	0,67	2,23	0,9996	3,75	3,96	3,99	0,31
Flurbiprofen	0,56	1,86	0,9997	2,62	3,17	4,42	0,96
Ketoprofen	0,68	2,27	0,9995	5,24	1,87	4,64	0,98

CONCLUSIONES

El empleo de nanoláminas de **GRAFENO** en el buffer de separación supone una gran **MEJORA** en la separación de AINE's mediante **EKC**.

Se ha demostrado esta mejora a pesar de encontrarse el grafeno en presencia de colato. De forma que se produce un **INCREMENTO** de la **RESOLUCIÓN** y **SENSIBILIDAD** sin afectar significativamente a la **ESTABILIDAD DE LA LINEA DE BASE.**

La correcta **DISPERSIÓN** de las nanoláminas de grafeno es un factor crucial en el proceso, obteniéndose los mejores resultados sometiendo al grafeno a un proceso de **SONICACIÓN**, es decir, obteniendo picos mejor resueltos, con más sensibilidad y líneas de base con menos ruido.

La modificación del BGE con estas nanoláminas nos ha permitido separar dos picos que no se resolvían sin emplear grafeno, además de aumentar hasta 6 veces los valores del límite de detección para los analitos estudiados.

Los resultados obtenidos han demostrado que las nanoláminas de grafeno permiten aumentar la resolución electroforética en 3-5 órdenes de magnitud en el caso de la separación de antiinflamatorios no esteroideos.

De igual modo han supuesto una mejora sustancial de la precisión, siendo la reproducibilidad tanto del área de pico como del tiempo de migración claramente mejor en presencia de las nanoláminas de grafeno.

Tras el estudio de nanoláminas de grafeno de diferente distribución podemos concluir que cuanto menos láminas presenta el sistema se produce una mayor interacción con el analito y un mayor efecto positivo sobre la separación electroforética, pudiendo trabajar a menores concentraciones de la fase pseudoestacionaria.

MEZCLAS DE GRAFENO Y NANOPARTICULAS DE ORO COMO SUSTRATO PARA SERS

S. Benítez-Martínez, B.M. Simonet, M. Valcárcel
Departamento de Química Analítica, Universidad de Córdoba
Edificio Anexo C3, Campus de Rabanales, 14071Córdoba.
E-mail: ga1meobj@uco.es

XXIII REUNIÓN NACIONAL – VIII CONGRESO IBÉRICO ESPECTROSCOPIA CÓRDOBA 2017 (XXIII RNE – VIII CIE)

La Espectroscopia Raman por Amplificación de Superficies, más conocida como SERS , ha adquirido gran importancia en los últimos años en muchos y variados campos de investigación debido a que proporciona información estructural de la muestra combinándola con el efecto de huella dactilar. El grafeno también ha adquirido una gran importancia en los últimos años debido a la peculiaridad de sus propiedades eléctricas, ópticas, magnéticas, mecánicas y térmicas. Recientemente se ha demostrado la capacidad del grafeno de una sola capa para actuar como sustrato SERS amplificando el espectro Raman de moléculas adsorbidas sobre su superficie. En este trabajo, se estudia la capacidad de nanopartículas de grafeno (≈ 4 láminas) depositado en un sustrato y combinado con nanopartículas de oro como sustrato activo en SERS

OBJETIVOS

- DEMOSTRAR LA CAPACIDAD DEL GRAFENO MULTICAPA, COMBINADO CON NANOPARTICULAS DE ORO, PARA ACTUAR COMO SUSTRATO EN SERS
- DESARROLLAR UNA FORMA ALTERNATIVA, RÁPIDA Y EFICAZ PARA PREPARAR EL SUSTRATO SERS
- MEJORAR LA REPRODUCIBILIDAD DE LAS MEDIDAS

PROCEDIMIENTO

1. Deposición de una microgota de grafeno sobre una placa de CaF_2 (calentada a temperatura suave(50 – 60 ºC).
2. Eliminación del tensioactivo en el que se encuentran dispersas las nanoláminas de grafeno mediante lavados con MeOH y agua ultrapura.
3. Deposición de una microgota de grafeno sobre la anterior y lavado del tensioactivo nuevamente. Este paso se repitió hasta depositar 10 microgotas de grafeno totales.
4. Adicion de las AuNP's sobre el grafeno a temperatura suave (50 – 60 ºC).
5. Adición de 1 µL de analito.

Imágenes del sustrato GF-AuNP: a) objetivo 20x b) objetivo 50x.

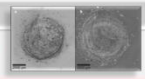

MEDIDAS RAMAN

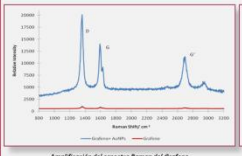

Amplificación del espectro Raman del Grafeno

Comparación entre sustratos: GF – AuNP's y AuNP's
A1: Espectro SERS del sustrato GF – AuNP's
A2: Espectro SERS del metronidazol sobre GF – AuNP's
B1: Espectro SERS del sustrato AuNP's
B2: Espectro SERS del metronidazol sobre AuNP's

CONDICIONES EXPERIMENTALES	Tiempo de integración	Potencia láser	λ (nm)	Número de acumulaciones	Tipo de objetivo
	1 s	10%	785	3	50x

ESTUDIO DE VARIABLES

Efecto de las nanoparticulas de oro

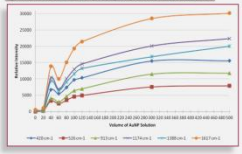

En el estudio del volumen óptimo de nanopartículas de oro que deben depositarse sobre el grafeno se llegó a la conclusión que este debía **ser 40 µL** de disolución. El estudio se llevó a cabo utilizando Violeta Cristal como molécula modelo.

Efecto del orden de deposición de grafeno, NP de oro y analito sobre la señal SERS

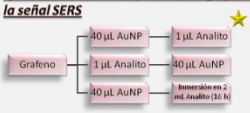

Estas tres aproximaciones no muestran diferencias significativas en los espectros Raman obtenidos. Sin embargo el primer caso resultó ser más reproducible y más rápido en cuanto a la preparación del sustrato. Por estos motivos fue elegido como el orden óptimo

Reutilización del soporte

Para conseguir la reutilización del soporte se llevó a cabo el lavado del mismo de cuatro formas diferentes:

- Pasando 5 mL MeOH (cada 0.5 mL) + 5 mL H_2O ultrapura (cada 0.5 mL)
- Pasando 10 mL MeOH (cada 0.5 mL) + 10 mL H_2O ultrapura (cada 0.5 mL)
- Inmersión del soporte en 5 mL de MeOH (2 h) + lavado posterior con 5mL H_2O ultrapura
- Inmersión del soporte en 10 mL de MeOH (4 h) + lavado posterior con 5mL H_2O ultrapura

Se recomienda la inmersión en 5 mL de MeOH durante dos horas con lavado posterior con 5 mL de agua ya que se produce menor arrastre de las nanopartículas de oro

COMPARACIÓN DE GRAFENOS EN EL SUSTRATO

Distribución de láminas

El soporte GF – AuNP's fue construido con dos tipos distintos de grafeno. La diferencia entre ellos entre ellos radica en la distribución de nanoláminas.

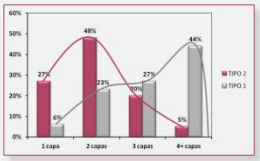

Espectros SERS

Comparación entre sustratos GF – AuNP's con diferentes tipos de grafeno.

A) Espectro SERS del metronidazol sobre el sustrato formado por grafeno tipo 1 y AuNP.
B) Espectro SERS del metronidazol sobe el sustrato formado por grafeno tipo 2 y AuNP.

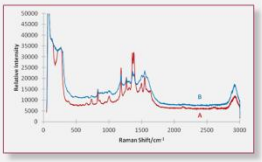

CONDICIONES EXPERIMENTALES	Tiempo de integración	Potencia láser	λ (nm)	Número de acumulaciones	Tipo de objetivo
	1 s	10%	785	3	50x

PROPIEDADES ANALÍTICAS

El sustrato SERS ha sido evaluado en términos de sensibilidad, límites de detección (LOD), cuantificación (LOQ) y precisión. La señal analítica empleada ha sido la intensidad Raman a 1186cm^{-1} para el **metronidazol**.
La recta de calibrado se realizó a partir de la intensidad Raman del pico seleccionado frente a la concentración de metronidazol. El intervalo lineal se encuentra comprendido entre 1 – 50 mg·L^{-1}. La reproducibilidad del sustrato ha sido calculada llevando a cabo 5 medidas independientes a 20 y 50 mg·L^{-1} . De forma adicional la reproducibilidad se ha calculado a 100 mg·L^{-1} dentro de la mismo muestra y entre muestras y la RSD obtenida fue 4.3 y 16.8 % respectivamente.

Sy/x	b ± Sb	a ± Sa	LOD (mg·L^{-1})	LOQ (mg·L^{-1})	RSD (50 mg·L^{-1})	RDS (20 mg·L^{-1})
167.3	407.44 ± 3.69	1240.63± 103.83	0.76	2.54	7.37	6.37

CONCLUSIONES

- La combinación de grafeno multicapa y nanopartículas de oro como sustrato SERS resulta ser un método útil para la determinación de metronidazol.
- Cuando el grafeno forma parte del sustrato SERS provoca un aumento en la señal Raman del analito del orden de tres veces con respecto al empleo de solamente AuNP's .
- El empleo de grafeno proporciona una gran estabilidad y una elevada reproducibilidad al soporte generado.
- El soporte SERS desarrollado es reutilizable y puede utilizarse durante 5 ciclos.

SUSTRATO HÍBRIDO DE GRAFENO Y NANOPARTÍCULAS DE ORO EN ESPECTROSCOPIA RAMAN POR AMPLIFICACIÓN DE SUPERFICIES (SERS)

S. Benítez-Martínez, B.M. Simonet, M. Valcárcel
Departamento de Química Analítica, Universidad de Córdoba
Edificio Anexo C3, Campus de Rabanales, 14071Córdoba.
E-mail: ga1meobj@uco.es

IV Workshop NANOUCO

La Espectroscopia Raman por Amplificación de Superficies, más conocida como SERS , ha adquirido gran importancia en los últimos años en muchos y variados campos de investigación debido a que proporciona información estructural de la muestra combinándola con el efecto de huella dactilar. El grafeno también ha adquirido una gran importancia en los últimos años debido a la peculiaridad de sus propiedades eléctricas, ópticas, magnéticas, mecánicas y térmicas. Recientemente se ha demostrado la capacidad del grafeno de una sola capa para actuar como sustrato SERS amplificando el espectro Raman de moléculas adsorbidas sobre su superficie. En este trabajo, se estudia la capacidad de nanopartículas de grafeno (≈ 4 láminas) depositado en un sustrato y combinado con nanopartículas de oro como sustrato activo en SERS

OBJETIVOS

- DEMOSTRAR LA CAPACIDAD DEL GRAFENO MULTICAPA, COMBINADO CON NANOPARTICULAS DE ORO, PARA ACTUAR COMO SUSTRATO EN SERS
- DESARROLLAR UNA FORMA ALTERNATIVA, RÁPIDA Y EFICAZ PARA PREPARAR EL SUSTRATO SERS
- MEJORAR LA REPRODUCIBILIDAD DE LAS MEDIDAS

PROCEDIMIENTO

1. Deposición de una microgota de grafeno sobre una placa de CaF_2 (calentada a temperatura suave(50 – 60 ºC).
2. Eliminación del tensioactivo en el que se encuentran dispersas las nanoláminas de grafeno mediante lavados con MeOH y agua ultrapura.
3. Deposición de una microgota de grafeno sobre la anterior y lavado del tensioactivo nuevamente. Este paso se repitió hasta depositar 10 microgotas de grafeno totales.
4. Adicion de las AuNP's sobre el grafeno a temperatura suave (50 – 60 ºC).
5. Adición de 1 µL de analito.

Imágenes del sustrato GF-AuNP: a) objetivo 20x b) objetivo 50x.

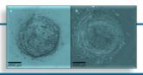

MEDIDAS RAMAN

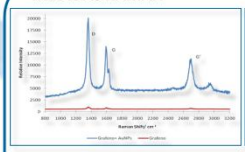

Amplificación del espectro Raman del Grafeno

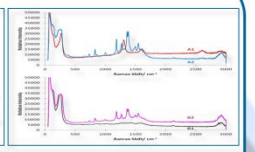

Comparación entre sustratos: GF – AuNP's y AuNP's
A1: Espectro SERS del sustrato GF – AuNP's
A2: Espectro SERS del metronidazol sobre GF – AuNP's
B1: Espectro SERS del sustrato AuNP's
B2: Espectro SERS del metronidazol sobre AuNP's

CONDICIONES EXPERIMENTALES	Tiempo de integración	Potencia láser	λ [nm]	Número de acumulaciones	Tipo de objetivo
	1 s	10%	785	3	50x

ESTUDIO DE VARIABLES

Efecto de las nanopartículas de oro

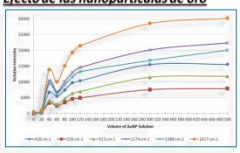

En el estudio del volumen óptimo de nanopartículas de oro que deben depositarse sobre el grafeno se llegó a la conclusión que este debía ser 40 µL de disolución. El estudio se llevó a cabo utilizando Violeta Cristal como molécula modelo.

Efecto del orden de deposición de grafeno, NP de oro y analito sobre la señal SERS

Estas tres aproximaciones no muestran diferencias significativas en los espectros Raman obtenidos. Sin embargo el primer caso resultó ser más reproducible y más rápido en cuanto a la preparación del sustrato. Por estos motivos fue elegido como el orden óptimo

Reutilización del soporte

Para conseguir la reutilización del soporte se llevó a cabo el lavado del mismo de cuatro formas diferentes:

- Pasando 5 mL MeOH (cada 0.5 mL) + 5 mL H_2O ultrapura (cada 0.5 mL)
- Pasando 10 mL MeOH (cada 0.5 mL) + 10 mL H_2O ultrapura (cada 0.5 mL)
- Inmersión del soporte en 5 mL de MeOH (2 h) + lavado posterior con 5mL H_2O ultrapura
- Inmersión del soporte en 10 mL de MeOH (4 h) + lavado posterior con 5mL H_2O ultrapura

Se recomienda la Inmersión en 5 mL de MeOH durante dos horas con lavado posterior con 5 mL de agua ya que se produce menor arrastre de las nanopartículas de oro

COMPARACIÓN DE GRAFENOS EN EL SUSTRATO

Distribución de láminas

El soporte GF–AuNP fue construido con dos tipos distintos de grafeno. La diferencia entre ellos entre ellos radica en la distribución de nanoláminas.

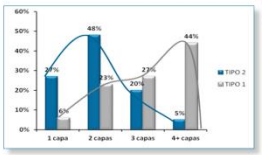

Espectros SERS

Comparación entre sustratos GF – AuNPs con diferentes tipos de grafeno.

A) Espectro SERS del metronidazol sobre el sustrato formado por grafeno tipo 1 y AuNP.
B) Espectro SERS del metronidazol sobe el sustrato formado por grafeno tipo 2 y AuNP.

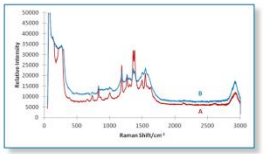

CONDICIONES EXPERIMENTALES	Tiempo de integración	Potencia láser	λ [nm]	Número de acumulaciones	Tipo de objetivo
	1 s	10%	785	3	50x

PROPIEDADES ANALÍTICAS

El sustrato SERS ha sido evaluado en términos de sensibilidad, límites de detección (LOD), cuantificación (LOQ) y precisión. La señal analítica empleada ha sido la intensidad Raman a 1186cm⁻¹ para el metronidazol.
La recta de calibrado se realizó a partir de la intensidad Raman del pico seleccionado frente a la concentración de metronidazol. El intervalo lineal se encuentra comprendido entre 1 – 50 mg·L⁻¹. La reproducibilidad del sustrato ha sido calculada llevando a cabo 5 medidas independientes a 20 y 50 mg·L⁻¹. De forma adicional la reproducibilidad se ha calculado a 100 mg·L⁻¹ dentro de la misma muestra y entre muestras y la RSD obtenida fue 4.3 y 8.02 % respectivamente.

Sy/x	b ± Sb	a ± Sa	LOD (mg·L⁻¹)	LOQ (mg·L⁻¹)	RSD (50 mg·L⁻¹)	RDS (20 mg·L⁻¹)
167.3	407.44 ± 3.69	1240.63 ± 103.83	0.76	2.54	4.64	4.99

CONCLUSIONES

- La combinación de grafeno multicapa y nanoparticulas de oro como sustrato SERS resulta ser un método útil para la determinación de metronidazol.
- Cuando el grafeno forma parte del sustrato SERS provoca un aumento en la señal Raman del analito del orden de tres veces con respecto al empleo de solamente AuNP's.
- El empleo de grafeno proporciona una gran estabilidad y una elevada reproducibilidad al soporte generado.
- El soporte SERS desarrollado es reutilizable y puede utilizarse durante 5 ciclos.

GRAPHENE QUANTUM DOTS AS SENSOR OF PHENOLS FROM OLIVE OIL

S. Benítez-Martínez, M. Valcárcel
Analytical Chemistry Department, University of Córdoba
Annex building C3, Campus of Rabanales, 14071Córdoba.
E-mail: ga1meobj@uco.es

VI Workshop N&NA 2013

Graphene has aroused great interest in the scientific community since it was isolated for the first time in 2010. Graphene consists in carbon atoms, with sp^2 hybridization, arranged in a honeycomb lattice with a delocalized electron cloud on its surface. It can be considered graphene if it had from 1 to 10 sheets. It presents exceptional optical, magnetic, thermal and mechanical properties.
Graphene Quantum Dots (GQDs), or Graphene Quantum Disks, is an emerging carbon-based nanomaterial with sheets smaller than 100 nm. GQDs exhibit special properties such as low toxicity, high fluorescent activity, robust chemical inertness and excellent photostability, due to quantum confinement and edge effect.

OBJECTIVES

- TO DEVELOP A RAPID AND SENSITIVE SENSOR FOR PHENOLICS COMPOUNDS EXTRACTED FROM THE OLIVE OIL
- TO STABLISH DIFFERENCES IN THE FLORESCENCE PROFILE OF DIFFERENTS TYPES OF OLIVE OIL

SYNTHESIS OF GQD [1]

Citric acid was heated at 200 ºC for 30 minutes and dissolved in 10 mg·mL^{-1} NaOH aqueous solution obtaining a homogeneous solution. GQDs emit blue light (474nm) when they are excited from 365 to 420 nm, the maximum emission being at 404 nm excitation. Quantum yield of GQD was 4.9 % at working conditions (pH 10.00, λexc = 404 nm) selecting quinine sulfate as standard. Nanoparticles obtained are nanosheets of 2.8–4.5 nm of diameter and flat circular shape, which have been characterized by HR-TEM. MIR spectra show the presence of carboxyl and hydroxyl groups.

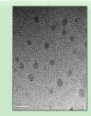

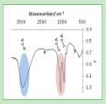

EXTRACTION OF PHENOLS FROM OLIVE OIL [2]

A liquid-liquid extraction (LLE) was carried out to extract the phenolic fraction from olive oil.

1. 1 mL of n-hexane and 2 mL of MeOH:water (60:40) were added to 2 g of olive oil
2. The mixture was agitated in a Vortex for 2 minutes and centrifuged at 4000 rpm during 10 min
3. The methanolic phase was extracted and the procedure was repeated twice
4. The extracts were collected and cleaned with 2 mL of n-hexane for three times
5. The extract containing the phenolic fraction was evaporated at 40 ºC under N_2 stream
6. Phenols were redisolved in 200 µL of MeOH (preconcentration factor =10), mixed with 200 µL of GQD solution and measured in a spectrofluoremeter

Absolute recoveries obtained were better than 73.4%, for galic acid, and 80.5% for oleuropein, in spiked oil samples.

STUDY OF VARIABLES

GQD EXCITATION WAVELENGTH

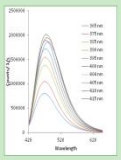

The highest fluorescence emission (474 nm) was achieved with a excitation wavelength of 379nm.

pH OF MAXIMUN EMISSION FLUORESCENCE

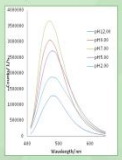

The pH was studied in the range between pH 2.00–12.00, finding the maximum florescence at pH 7.00

pH OF MAXIMUN FL QUENCHING

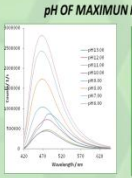

pH of fluorescence Quenching was also studied for Gallic Acid at 100 m· L^{-1} between pH 6.00 and 13.00. The maximum fluorescence quenching was found at pH 10.00

SAMPLE – NANOPARTICLES VOLUME RATIO

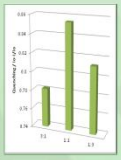

The volumes of GQD solution and sample were studied in three different ratios, 3:1, 1:1 and 1:3. The maximum florescence quenching was achieved by using 1:1

TYPE OF SOLVENT

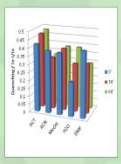

Acetone (ACT), acetonitrile (ACN), methanol (MeOH), water (H_2O) and N-N'-dimetilformamide (DMF) were studied as solvent for the reconstitution of the phenolic fraction extracted from olive oil. GQD solution was at pH 10.00, in 1:1 ratio. MeOH brought good FL quenching and show the best stability over time.

PROFILE OF REAL SAMPLES

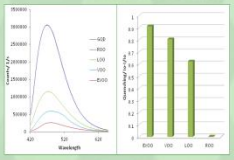

ROO: Refined Olive Oil
LOO: "Lampante" Olive Oil
VOO: Virgin Olive Oil
EVOO: Extra Virgin Olive Oil

ANALYTICAL FEATURES

GQD as sensor has been evaluated in terms of sensitivity, limits of detection (LOD), quantification (LOQ) and precision for two different types of phenols, gallic acid (simple phenol) and oleuropein (polyphenol), commonly presents in Spanish olive oil.
Calibration curve were constructed by plotting the fluorescence quenching versus added concentration of gallic acid and oleuropein in spiked ROO samples. The linear range was found between 0.05 - 3 mg·L^{-1} for gallic acid and 0.1 – 3 mg·L^{-1} for oleuropein.
Reproducibility of the proposed method was evaluated carrying out five independent measures of each analyte.

MODEL ANALYTE	$S_{y/x}$	b ± S_b	a ± S_a	R^2	LOD (mg·L^{-1})	LOQ (mg·L^{-1})	% RDS (n=5) (at 1 mg·L^{-1})
Gallic acid	0.0064	0.053 ± 0.002	-0.0027 ± 0.0037	0.9901	0.21	0.68	0.96
Oleuropein	0.01	0.1 ± 0.003	0.003 ± 0.0053	0.9919	0.15	0.52	0.26

CONCLUSIONS

GQDs have been used for the first time as sensor of phenols extracted from olive oil giving rise a rapid, sensible and selective analytical method.

The pH of GQDs solution have been proved to be a very important factor in the reaction with the phenolic fraction. as well as type of solvent, for the reconstitution of phenols after the extraction procedure ,and the nanoparticles concentration.

Excitation wavelength is important to achieve the highest fluorescence intensity, but it has been shown that the maximun emission wavelength is excitation – independent.

Low limits of detection and quantification for gallic acid and oleuropein were achieved with a high reproducibility.

EVOO shows more fluorescence quenching than VOO , LOO and ROO as expected.

[1] Y. Dong, J. Shao, C. Chen, H. Li, R. Wang, Y. Chi, Xiaomei Lin, G. Chen. *"Blue luminiscent graphene quantum dots and graphene oxide by tuning the carbonization degree of citric acid"*, Carbon, 50, 4738-4743, 2012.
[2] F.M. Pirisi, P. Cabras, C.Faiqui, M. Migliorini, M. Muggelli. *"Phenolic compounds in virgin olive oil. 2. Reappraisal of the extraction, HPLC separation and quantification process"*, Food Chemistry, 48, 1191-1196, 2000.

TOTAL PHENOLS IN OLIVE OIL SENSOR BASED ON GRAPHENE QUANTUM DOTS

S. Benítez-Martínez, M. Valcárcel
Analytical Chemistry Department, University of Córdoba
Annex building C3, Campus of Rabanales, 14071Córdoba.
E-mail: qalmecbj@uco.es

In the last years, graphene, a one-atom thick layer composed by carbon atoms arranged in a honeycomb lattice with sp^2 hybridization and with a delocalized electron cloud on its surface, has attracted much attention in the scientific community since their first isolation in 2004, due to their exceptional electronic, mechanical and thermal properties.

Recently, Graphene Quantum Dots (GQDs), an emerging luminescent carbon-based nanomaterial, are attracting more and more attention due to their optical and electronic properties. GQDs are defined as graphene sheets with lateral size smaller than 100 nm in single, double and multilayer, as their diameters are mainly distributed in a range between 3-20 nm. It exhibits other special properties such as low toxicity and biocompatibility, high fluorescent activity, robust chemical inertness and excellent photostability, due to quantum confinement and edge effect.

As it is well known, the antioxidant potential of olive oil depends on its phenolic compounds content. In recent years, this antioxidant capability has been the subject of considerable interest due to its benefits on human health (protection against coronary heart diseases and tumors, among others) as well as its influence on the olive oil stability and shelf live .

OBJECTIVES

- TO DEVELOP A INEXPENSIVE RAPID AND SENSITIVE SENSOR FOR PHENOLICS COMPOUNDS EXTRACTED FROM THE OLIVE OIL
- TO STABLISH DIFFERENCES IN THE FLORESCENCE PROFILE OF DIFFERENTS TYPES OF OLIVE OIL

Synthesis of GQD [1]

Citric acid was heated at 200 °C for 30 minutes and dissolved in 10 mg·mL^{-1} NaOH aqueous solution obtaining a homogeneous solution. GQDs emit blue light (474nm) when they are excited from 365 to 400 nm, the maximum emission being at 474 nm excitation. Quantum yield of GQD was 4.9 %, at working conditions (pH 10.00, λexc = 379 nm), selecting quinine sulfate as standard. Nanoparticles obtained are nanosheets of 2.8-4.5 nm of diameter and flat circular shape, which have been characterized by HR-TEM. MIR spectra show the presence of carboxyl and hydroxyl groups.

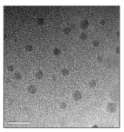

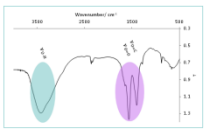

Extraction of phenols from olive oil [2]

A liquid-liquid extraction (LLE) was carried out to extract the phenolic fraction from olive oil.

1 mL of n-hexane and 2 mL of MeOH:water (60:40) were added to 2 g of olive oil

The mixture was agitated in a Vortex for 2 minutes and centrifuged at 4000 rpm during 10 min

The methanolic phase was extracted and the procedure was repeated twice

The extracts were collected and cleaned with 2 mL of n-hexane for three times

The extract containing the phenolic fraction was evaporated at 40 °C under N_2 stream

Phenols were redisolved in 200 µL of MeOH (preconcentration factor =10), mixed with 200 µL of GQD solution and measured in a spectrofluoremeter

Absolute recoveries obtained were better than 73.4%, for galic acid, and 80.5% for oleuropein, in spiked oil samples.

Study of Variables

GQD excitation wavelenght

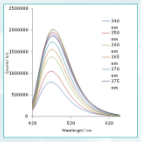

The maximum fluorescence emission (474 nm) independent was achieved with a excitation wavelength of 379 nm.

pH of maximun fluorescence emission

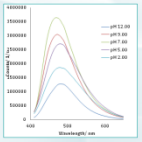

The pH was studied in the range between pH 2.00-12.00, finding the maximum florescence at pH 7.00.

pH of maximun FL quenching

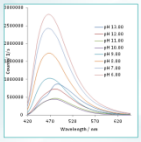

pH of fluorescence Quenching was also studied for Gallic Acid at 100 m· L^{-1} between pH 6.00 and 13.00. The maximum fluorescence quenching was found al pH 10.00.

sample-nanoparticles volume ratio

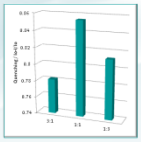

The volumes of GQD solution and sample were studied in three different ratios, 3:1, 1:1 and 1:3. The maximum florescence quenching was achieved by using 1:1

type of solvent

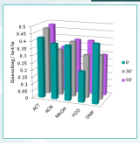

Acetone (ACT), acetonitrile (ACN), methanol (MeOH), water (H_2O) and N-N'-dimetilformamide (DMF) were studied as solvent for the reconstitution of the phenolic fraction extracted from olive oil. GQD solution was at pH 10.00, in 1:1 ratio. MeOH brought good FL quenching and show the best stability over time.

profile of real samples

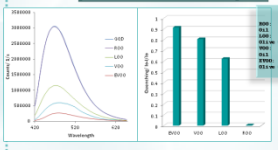

Analytical Features

GQD as sensor has been evaluated in terms of sensitivity, limits of detection (LOD), quantification (LOQ) and precision for two different types of phenols, galic acid (simple phenol) and oleuropein (polyphenol), commonly presents in Spanish olive oil.

Calibration curve were constructed by plotting the fluorescence quenching versus added concentration of gallic acid and oleuropein in spiked ROO samples. The linear range was found between 0.5 - 3 mg·L^{-1} for gallic acid and 0.1 - 3 mg·L^{-1} for oleuropein.

Reproducibility of the proposed method was evaluated carrying out five independent measures of each analyte.

MODEL ANALYTE	Sy/x	b ± Sb	a ± Sa	R^2	LOD (mg·L^{-1})	LOQ (mg·L^{-1})	% RDS (n=5) (at 1 mg·L^{-1})
Gallic acid	0.0064	0.053 ± 0.002	−0.0027 ± 0.0037	0.9901	0.21	0.68	0.96
Oleuropein	0.01	0.1 ± 0.003	0.003 ± 0.0053	0.9919	0.15	0.52	0.26

Conclusions

GQDs have been used for the first time as sensor of phenols extracted from olive oil giving rise a rapid, sensible and selective analytical method.

The pH of GQDs solution have been proved to be a very important factor in the reaction with the phenolic fraction as well as type of solvent, for the reconstitution of phenols after the extraction procedure ,and the nanoparticles concentration.

Excitation wavelength is important to achieve the maximum fluorescence(FL) intensity. It has been shown that the maximum emission wavelength is excitation-independent but not the FL intensity.

Low limits of detection and quantification were achieved with a high reproducibility for galic acid and oleuropein.

EVOO shows more fluorescence quenching than VOO , LOO and ROO as expected.

[1] Y. Dong, J. Shao, C. Chen, H. Li, R. Wang, Y. Chi, Xiaomei Lin, G. Chen. *"Blue luminiscent graphene quantum dots and graphene oxide by tuning the carbonization degree of citric acid"*. Carbon, 50, 4738-4743, 2012.
[2] F.M. Pirisi, P. Cabras, C.Falqui, M. Migliorini, M. Muggelli. *"Phenolic compounds in virgin olive oil.2. Reappraisal of the extraction, HPLC separation and quantification process"*, Food Chemistry, 48, 1191-1196, 2000.

Graphene Quantum Dots sensor for the determination of Graphene Oxide in environmental water samples

Sandra Benítez-Martínez, Ángela I. López-Lorente, Miguel Valcárcel

Analytical Chemistry Department, University of Córdoba. Córdoba. E-mail: ga1meobj@uco.es.

Abstract

• A simple and sensitive approach for the preconcentration and determination of graphene oxide (GO) in environmental samples by using fluorescent graphene quantum dots (GQDs) is proposed.

Preconcentration of GO on a cellulose membrane

Ultrasound assisted elution

Fluorimetric analysis of the quenching effect produced on the GQD

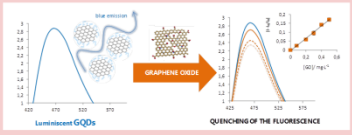

Experimental section

SYNTHESIS OF GQDs

• GQDs were obtained by pyrolysis of citric acid. 2 g of CA was placed in a vial and heated at 200 C until the citric acid changed to a dark orange liquid. Then it was added dropwise to a NaOH solution under stirring. The pH was adjusted to 7 and stored at 4°C.

SYNTHESIS OF GO

•GO was prepared by adding 100 mg of graphene to 20 mL of a 3:1 H_2SO_4/HNO_3 mixture into a glass flask and refluxed for 1 hour. After that diluted fractions were centrifuged at 10000 rpm for 20 min and washed with water until the supernatant phase stopped having acidic pH. Finally, carboxylated derivates were dried at 60°C in a heater.

1 PRECONCENTRATION

(a) Filtration of 5 mL solution on acetate cellulose membrane (Millipore filtration system)

(b) 1 mL 0.25 M NaOH solution.

(c) 1 mL ultrapure water.

2 ELUTION

200 µL ultrapure water. Ultrasound irradiation.

3 FLUORESCENT MEASUREMENT

Emission between 420 and 650 nm.
200 µL GQDs pH 7 + 200 µL sample solution

Characterization of GQDs

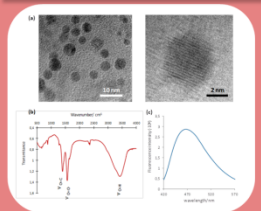

(a) HTEM images of the synthesized GQDs with an average diameter of 3.6 ± 0.9 nm, (b) FT-MIR spectra of GQDs showing the presence of carboxyl and hydroxyl groups and (c) fluorescence spectrum of GQDs which showed blue emission at 474 nm upon excitation at its maximum of 379 nm with a 4.5% of photoluminiscent quantum yield at working conditions calculated using quinine sulfate as standard.

Selection of conditions and mechanism

➡ The abundant hydrophilic edges as well as the hydrophobic plane in the GQDs confer them the ability to interact with GO through π-π stacking interactions leading to a decrease of fluorescence –quenching- which was employed as analytical signal to quantify the presence of GO in the aqueous samples.

➡ It cannot be dismissed that the analyte binding may also occurs by non-covalent interactions between the functional groups of the nanomaterials.

SELECTED CONDITIONS	
0.2 µm pore-size acetate of cellulose membrane	40 s ultrasound elution
5 mL filtration volume	pH 7
0.2 mL elution volume	5 min mixture time
Eluent solvent: water	λ_{max} exc 379 nm

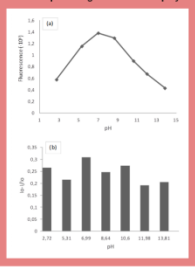

(a) Effect of pH on the fluorescence of GQDs, (b) influence of pH of the GQD solution on the quenching response of the sensor. pH 7 was selected for further experiments.

Analytical features

The fluorescence response of GQD to increasing concentrations of GO was assayed under the above described optimal conditions. The analytical signal –relative fluorescence response (I0-I)/I0- was plotted against GO concentration for standard solutions.

Calibration equation	$(I_0-I)/I_0 = (0.35\pm0.01)[GO]-(0.004\pm0.004)$
R^2	0.9940
Linear range	0-500 µg L^{-1}
LOD[a]	35.008 µg L^{-1}
RSD[b] (%)	5.16%

[GO]: Concentration of GO in the aqueous media in mg·L^{-1}.
[a] Limit of detection, determined as $(3S_b)b_1$ for y=bx+a.
[b] Relative standard deviation, determined from the average value of five measurements of 5 mL 200 µg·L^{-1} GO.

Application to river water samples

In order to demonstrate the accuracy of the proposed method, a recovery test of the analysis of spiked river water samples was also carried out. After the filtration of the sample through the membrane 1 mL of a 0.25 mol·L^{-1} NaOH solution and 1 mL of ultrapure water were passed through in order to eliminate the interference of the organic matter retained in the membrane.

River water sample	Added concentration of GO (mg·L^{-1})	Found concentration of GO[a] (mg·L^{-1})	Recovery (%)	RSD(%)
1	0.2	0.19±0.02	83.7-100.4	8.9
2	0.3	0.30±0.02	93.6-107.7	7.4
3	0.4	0.39±0.03	94.5-108.2	7.6

[a]Average of three independent spiked samples±CI (p < 0.05).

Conclusions

I. A simple and sensitive GQD-based sensor has been developed for the determination of graphene oxide.

II. The interaction of graphene oxide with GQDs through hydrophobic π-π stacking of the GO with the aromatic network at the GQDs surface leads to a decrease –quenching- of the fluorescence of GQDs

III. The procedure has been applied for the determination of GO in environmental river water samples. In such case a clean-up step was necessary in order to remove the interfering organic matter.

IV. In this work, the two facets of analytical nanoscience & nanotechnology are covered. NPs are considered both objects of analysis (GO) and analytical tools (GQDs) improving the detection.